Vol. 281, No. 1, September 1, 1993

ISSN 0003-2670

ANALYTICA CHIMICA ACTA

An international journal devoted to all branches of analytical chemistry

ELSEVIER

ANALYTICA CHIMICA ACTA

Scope. *Analytica Chimica Acta* publishes original papers, preliminary communications and reviews dealing with every aspect of modern analytical chemistry. Reviews are normally written by invitation of the editors, who welcome suggestions for subjects. Preliminary communications of important urgent work can be printed within four months of submission, if the authors are prepared to forego proofs.

Submission of Papers

Americas

Prof. Harry L. Pardue
Department of Chemistry
1393 BRWN Bldg, Purdue University
West Lafayette, IN 47907–1393
USA

Tel:(+1-317) 494 5320
Fax:(+1-317) 496 1200

Computer Techniques

Prof. J.T. Clerc
Universität Bern
Pharmazeutisches Institut
Baltzerstrasse 5, CH-3012 Bern
Switzerland

Tel:(+41-31) 654171
Fax:(+41-31) 654198

Prof. Sarah C. Rutan
Department of Chemistry
Virginia Commonwealth University
P.O. Box 2006
Richmond, VA 23284-2006
USA
Tel:(+1-804) 367 1298
Fax:(+1-804) 367 8599

Other Papers

Prof. Alan Townshend
Department of Chemistry
The University
Hull HU6 7RX
Great Britain

Tel:(+44-482) 465027
Fax:(+44-482) 466410

Prof. Willem E. van der Linden
Laboratory for Chemical Analysis
Department of Chemical Technology
Twente University of Technology
P.O. Box 217, 7500 AE Enschede
The Netherlands
Tel:(+31-53) 892629
Fax:(+31-53) 356024

Prof. Paul Worsfold
Dept. of Environmental Sciences
University of Plymouth
Plymouth PL4 8AA
Great Britain

Tel:(+44-752) 233006
Fax:(+44-752) 233009

Submission of an article is understood to imply that the article is original and unpublished and is not being considered for publication elsewhere. *Anal. Chim. Acta* accepts papers in English only. There are no page charges. Manuscripts should conform in layout and style to the papers published in this issue. See inside back cover for "Information for Authors".

Publication. *Analytica Chimica Acta* appears in 16 volumes in 1994 (Vols. 281–296). *Vibrational Spectroscopy* appears in 2 volumes in 1994 (Vols. 6 and 7). Subscriptions are accepted on a prepaid basis only, unless different terms have been previously agreed upon. It is possible to order a combined subscription (*Anal. Chim. Acta* **and** *Vib. Spectrosc.*).
Our p.p.h. (postage, packing and handling) charge includes surface delivery of all issues, except to subscribers in the U.S.A., Canada, Australia, New Zealand, China, India, Israel, South Africa, Malaysia, Thailand, Singapore, South Korea, Taiwan, Pakistan, Hong Kong, Brazil, Argentina and Mexico, who receive all issues by air delivery (S.A.L.–Surface Air Lifted) at no extra cost. For Japan, air delivery requires 25% additional charge of the normal postage and handling charge; for all other countries airmail and S.A.L. charges are available upon request.

Subscription orders. Subscription prices are available upon request from the publisher. Subscription orders can be entered only by calendar year and should be sent to: Elsevier Science Publishers B.V., Journals Department, P.O. Box 211, 1000 AE Amsterdam, The Netherlands. Tel: (+31-20) 5803 642, Telex: 18582, Telefax: (+31-20) 5803598, to which requests for sample copies can also be sent. Claims for issues not received should be made within six months of publication of the issues. If not they cannot be honoured free of charge. Readers in the U.S.A. and Canada can contact the following address: Elsevier Science Publishing Co. Inc., Journal Information Center, 655 Avenue of the Americas, New York, NY 10010, U.S.A. Tel: (+1-212) 6333750, Telefax: (+1-212) 6333990, for further information, or a free sample copy of this or any other Elsevier Science Publishers journal.
Advertisements. Advertisement rates are available from the publisher on request.

US mailing notice – Analytica Chimica Acta (ISSN 0003-2670) is published biweekly by Elsevier Science Publishers (Molenwerf 1, Postbus 211, 1000 AE Amsterdam). Annual subscription price in the USA US$ 3035.75 (subject to change), including air speed delivery. Second class postage paid at Jamaica, NY 11431. *USA Postmasters*: Send address changes to Anal. Chim. Acta, Publications Expediting, Inc., 200 Meacham Av., Elmont, NY 11003. Airfreight and mailing in the USA by Publication Expediting.

ANALYTICA CHIMICA ACTA

An international journal devoted to all branches of analytical chemistry

(Full texts are incorporated in CJELSEVIER, a file in the Chemical Journals Online database available on STN International; Abstracted, indexed in: Aluminum Abstracts; Anal. Abstr.; Biol. Abstr.; BIOSIS; Chem. Abstr.; Curr. Contents Phys. Chem. Earth Sci.; Engineered Materials Abstracts; Excerpta Medica; Index Med.; Life Sci.; Mass Spectrom. Bull.; Material Business Alerts; Metals Abstracts; Sci. Citation Index)

VOL. 281 NO. 1 CONTENTS SEPTEMBER 1, 1993

(Continued overleaf)

Contents (continued)

ANALYTICA CHIMICA ACTA
VOL. 281 (1993)

ANALYTICA CHIMICA ACTA

An international journal devoted to all branches of analytical chemistry
Revue internationale consacrée à tous les domaines de la chimie analytique
Internationale Zeitschrift für alle Gebiete der analytischen Chemie

Anal. Chim. Acta, Vol. 281 (1993)

ELSEVIER, Amsterdam–London–New York–Tokyo

0003-2670/93/$06.00

Analytica Chimica Acta, 281 (1993) 1
Elsevier Science Publishers B.V., Amsterdam

Editorial
Analytical Biotechnology

Biotechnology is virtually certain to have a major impact on the large-scale production of pharmaceuticals and other biologically active substances. In the same way that analytical chemistry has played an indispensable role in more traditional approaches to chemical manufacturing processes, it will also be critical to the successful development and exploitation of production processes based on biotechnology. As with more traditional areas, analytical methods will impact biotechnology in many ways ranging from quality control on starting materials through optimization, monitoring and control of reactor conditions to quality control of primary products and monitoring of byproducts.

In considering the impact of analytical chemistry on biotechnology, it is important to identify both similarities to and differences from more traditional types of processes. Similarities will be reflected in several ways, including the functional processes involved as well as some of the specific methodologies. The functional processes will be essentially the same as in more traditional areas; they will include sampling, sample processing, chemical reactions and physical changes, separations, measurements, data processing and statistical evaluation. Many of the methodologies will be the same; examples include discrete and continuous-flow sample-processing methods, chromatographic and electrophoretic separation methods, electrochemical, spectrophotometric and luminescence measurement methods and equilibrium- and kinetic-based data-processing options.

Principal differences will result from the different types of chemical matrices and chemical reactions involved. Matrices will of course be biological in nature and will most likely not be homogeneous. Biochemical processes including enzymatic, immunochemical and nucleic acid reactions will predominate. These differences will require innovations in all the functional processes and analytical methodologies mentioned above. Some typical innovations that have already begun to impact on the area are unsegmented continuous-flow sample-processing systems, biosensors, capillary electrophoresis, DNA probes, and amplification via polymerase chain reactions.

Clearly, progress toward and ultimate implementation of approaches to large-scale production will simultaneously draw upon the traditional strengths of analytical chemistry and present many new challenges to the discipline. The Editors and Publisher of *Analytica Chimica Acta* are eager to participate in this challenge by publishing results of research on all aspects of the subject. Because the chemistry associated with biotechnology and the analytical tools and methodologies used to monitor that chemistry are so intimately related, it is not possible to pursue one independently of the other. Accordingly, we at ACA are interested in both the chemical and instrumental aspects of analytical biotechnology. This is reflected not only in regularly submitted papers but also in papers published or in press from Anabiotec Symposia held during 1990 and 1992 and plans to publish papers from Anabiotec 94 to be held in North America. We invite scientists doing research related to all aspects of analytical biotechnology to submit manuscripts for publication in *Analytica Chimica Acta*.

Harry L. Pardue

Analytica Chimica Acta, 281 (1993) 3–11
Elsevier Science Publishers B.V., Amsterdam

Sensitive detection of pesticides using a differential ISFET-based system with immobilized cholinesterases

A.M. Nyamsi Hendji, N. Jaffrezic-Renault, C. Martelet [1] and P. Clechet
LPCI, URA CNRS 404, Ecole Centrale de Lyon, BP 163, 69131 Ecully Cedex (France)

A.A. Shul'ga, V.I. Strikha and L.I. Netchiporuk
Semiconductor Physics Department, Kiev State University, 64 Vladimirskaya St., Kiev 252017 (Ukraine)

A.P. Soldatkin
Institute of Molecular Biology and Genetics, Academy of Sciences of the Ukrainian SSR, 150 Zabolotny St., Kiev 252143 (Ukraine)

W.B. Wlodarski
Royal Melbourne Institute of Technology, Victoria University of Technology, Melbourne (Australia)

(Received 18th December 1992; revised manuscript received 2nd March 1993)

Abstract

Organophosphorus pesticides were determined using a simple biosensor design. Enzymatic membranes prepared by cross-linking with BSA were deposited on a sensor chip consisting of two identical pH-FETs working in the differential mode (ENFET with enzyme, REFET without enzyme). Acetyl- and butyrylcholinesterase membranes were tested using acetyl- and butyrylcholine chloride as substrates. The decrease in the substrate steady-state response caused by exposure of the biosensor to pesticides [diisopropyl fluorophosphate (DFP), trichlorfon, paraoxon-methyl] was used to estimate the enzyme inhibition. The optimized parameters for the measurement procedure were determined and the detection limits were found to be 10^{-12} M for DFP and 10^{-6} M for paraoxon-methyl and trichlorfon.

Keywords: Biosensors; Enzymatic methods; Cholinesterases; Ion-sensitive field effect transistors; Organophosphorus pesticides; Pesticides

Pesticides are one of the principal classes of environmental pollutants. The organochlorine insecticides (DDT, aldrin, lindane, etc.) used in the past have been progressively replaced with organophosphorus compounds. The latter show low environmental persistence but have a high acute toxicity [1]. Regulations are now being strictly enforced in Europe with a maximum concentration of 1 μg l^{-1} for individual pesticide residues in drinking water [2]. Therefore, the development of methods for the rapid inexpensive on-line monitoring of water and food products is of special interest.

Biosensors are useful for this purpose [3,4]. Being a combination of a biological material with a sensing device (transducer), they have great

Correspondence to: A.M. Nyamsi Hendji, LPCI, URA CNRS 404, Ecole Centrale de Lyon, BP 163, 69131 Ecully Cedex (France).
[1] Present address: LTDS, URA CNRS 855, Ecole Centrale de Lyon, BP 163, 69131 Ecully Cedex (France).

versatility of design and a wide range of applications [5]. Thus, for the detection of pesticides, biosensors using enzymes [6–9], antibodies [10–13], microorganisms [14–17] and chemoreceptors [18] have been designed. Among transducers, ion-selective electrodes (ISEs) [7,8,11], amperometric electrodes [17,18], ion-sensitive field effect transistors (ISFETs) [9,18–20], piezoelectric crystals [13], optical fibres [21], fluorimetric devices [4] and bulk wave (BW) and surface acoustic wave (SAW) piezoelectric transducers [22] have been used or proposed.

From the results reported, two biological techniques for the detection of organophosphorus pesticides seem to be promising for use with integrated microsensors: immunoassay and immobilized enzyme probes [23,24]. So far the latter method has been developed more extensively as it is generally simple and practicable.

The basic action of organophosphorus compounds and carbamates is associated with their ability to inhibit acetylcholinesterase (AcChE) and butyrylcholinesterase (BuChE) by phosphorylating the serine OH group in the active site of the enzyme:

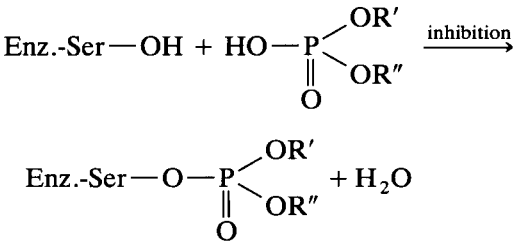

(1)

Normally AcChE and BuChE hydrolyse acetylcholine chloride and butyrylcholine chloride according to the following reactions:

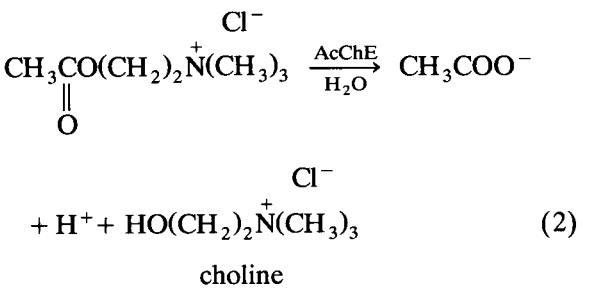

choline (2)

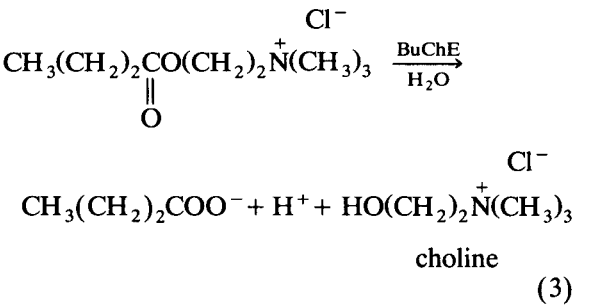

choline (3)

One of the resulting products, H^+, can be easily detected by the transducer and the decrease in the concentration of the enzymatic reaction product caused by enzyme inhibition can be related to pesticide concentration.

The inhibition of immobilized enzyme is almost permanent and the activity is not restored spontaneously except after long periods of time. The resulting enzyme–phosphorus bond after the inhibition reaction in Eqn. 1 cannot be broken by water, but partial recovery of the activity can be obtained by using nucleophilic reagents such as oximes. Pyridine-2-aldoximide methiodide (PAM-2) and hydroxylamine are known as the most effective antidotes for cholinesterase inhibitors [24].

There are some approaches to estimating inhibition levels [25] that involve different experimental procedures. The pesticide determination is usually carried out via enzyme inhibition in the presence of an inhibitor and subsequent activity measurements. These approaches are based on the equation for the percentage free enzyme inhibition (i):

$$i = [I]/([I] + K_i) \quad (4)$$

where K_i is the biomolecular inhibition constant and [I] is the concentration of inhibitor.

A special procedure of enzyme immobilization involving cross-linking with glutaraldehyde vapour has been used. It leads to a thin membrane with high specific activity of the enzyme.

In this work a systematic study of the kinetic parameters of the enzyme activity and of its inhibition was performed, based on the use of ISFET detection of H^+. Under the defined optimum conditions, the detection limits for different organophosphorus pesticides [diisopropyl fluo-

rophosphate (DFP), trichlorfon and paraoxon-methyl] were determined.

EXPERIMENTAL

Materials

Butyryl cholinesterase (BuChE) (pseudo-cholinesterase, EC 3.1.1.8) from horse serum, 255 U mg^{-1}, acetyl cholinesterase (AcChE) (true cholinesterase, EC 3.1.1.7) from electric eel, type VI-S, 225 U mg^{-1}, acetylcholine chloride (AcChCl) and butyrylcholine chloride (BuChCl) were obtained from Sigma (La Verpillière, France), bovine serum albumin (BSA) from Boehringer Mannheim (Meylan, France) and 25% glutaraldehyde (GA) solution from Fluka (Buchs, Switzerland). Diisopropyl fluorophosphate (DFP), dimethyl (2,2,2-trichloro-1-hydroxyethyl)phosphonate (trichlorfon) and the regenerating agent pyridine-2-aldoximide methiodide (PAM-2) were purchased from Sigma and paraoxon-methyl from Riedel-de Haën (Seelze, Germany). Phosphate buffer (KH_2PO_4) and PBS (product No. P-4417, phosphate-buffered saline tablets) were provided by Merck (Darmstadt, Germany) and Sigma, respectively. Other reagents were of analytical-reagent grade.

Sensor chip

Sensor chips were produced at the Microdevices Research Institute (Kiev, Ukraine). Two identical pH-FETs were micromachined on the same p-Si wafer having dimensions 3 × 10 mm, as shown in Fig. 1. The channel dimensions were 7 × 250 μm. Double-layer SiO_2 (70 nm) and Si_3N_4 (150 nm) was used as the gate insulator. The sensor chip was attached to a Sital (fused silica) support and was bound to the aluminium conductors. Then the contact pads of the sensor were encapsulated with epoxy resin (see Fig. 1). The sensor chip works with non-isolated substrate and is insensitive to light.

Measurement scheme

A specially developed ISFET amplifier was used for measurements; the device was designed to work in the so-called constant-charge mode for

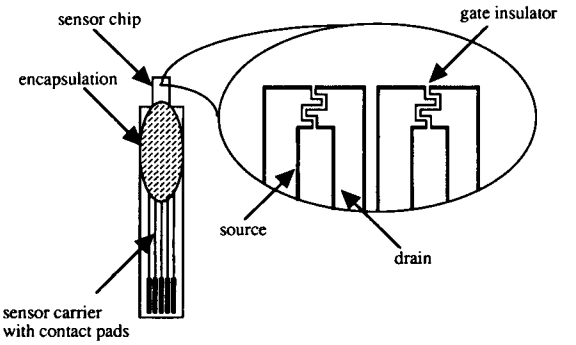

Fig. 1. Sensor chip design.

one or two ISFETs, which means that the drain-source voltage, V_{ds}, and drain current, I_d, were constant. The output signal was the source voltage, V_s, of the ISFET while the reference electrode was earthed. The output signal of a single ISFET can be written as

$$V_s = -V_{gs}(pH) - \phi_{RE} \quad (5)$$

where V_{gs} is a function of the transistor design and of the pH value at the insulator/electrolyte interface and ϕ_{RE} is the potential of the reference electrode.

If two ISFETs are working in this mode, at pH_1 and pH_2, the difference between their output signals, ΔV/s, becomes independent of the reference electrode potential:

$$\Delta V_s = V_{gs_2(pH_2)} - V_{gs_1(pH_1)} \quad (6)$$

and for identical ISFETs can be about zero. This is why differential measurements are widely accepted for determination of the biological substances by means of ENFETs. Nevertheless, a noble metal pseudo-reference electrode was used in differential set-up to supply a gate voltage of nearly constant value [26].

Two pH-FETs of the sensor chip, modified as described below, were connected to the ISFET amplifier (Fig. 2) and the measurements were carried out at $V_{ds} = 1$ V and $I_d = 0.5$ A. The output differential ΔV_s signal was registered with a Linear recorder (Linear Instruments, Reno, NV).

Enzyme immobilization

Before the enzymatic membrane deposition, the chips were treated with a concentrated sul-

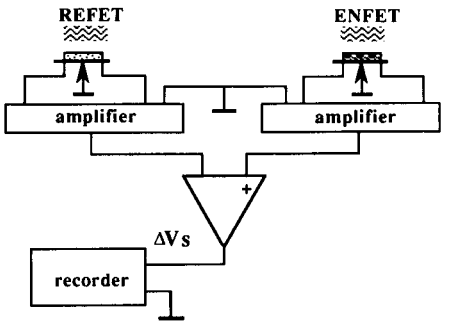

Fig. 2. Sensor chip incorporated in the measurement scheme.

phuric acid–chromic acid mixture (10 min), then washed in a stream of doubly distilled water (10 min) and dried at 70°C (2 h). For ENFET preparation the method reported previously was employed [27]. First, 50–100 mg ml^{-1} solutions of enzyme and BSA in 20 mM phosphate buffer (pH 7.4) were prepared. The average enzyme amount in the deposit is around 2 U. Second, a small drop of each solution was deposited on the sensitive area of one of the pH-FETs. The same membrane with enzyme replaced with BSA was formed on the REFET surface. Then the sensor was placed in saturated vapour of glutaraldehyde for 30 min to achieve complete polymerization of the biomembrane and subsequently dried at room temperature for 1 h.

Measurement of enzyme activity, inhibition and reactivation

All measurements were carried out at 25°C. The sensitive part of the sensor was immersed in the stirred buffer solution (volume of the reactive vessel = 1 ml) and an appropriate amount of 2 M AcChCl (or BuChCl) solution in the buffer was added to obtain the required final AcChCl (or BuChCl) concentration. A change in proton concentration produces by the enzymatic reaction in Eqn. 1 or 2 occurs at the ENFET surface and the corresponding change in the differential output voltage is considered to be a measure of the enzymatic membrane activity.

The reaction vessel and sensor chip were washed three times with buffer solution after each measurement and the "zero" line was set on the recorder.

For pesticide analysis the measurement procedure involved the following steps: the response for a 20 mM substrate concentration was recorded and used as a reference; the sensor was washed and dipped in pesticide solution in the buffer (without stirring) for 10–30 min; and the excess of the pesticide solution was removed with a buffer stream and the enzymatic activity was determined as described above. The percentage of the residual membrane activity was calculated by direct comparison with its initial activity. The enzyme inhibition is also a function of the incubation time and the treatment of the sensor with the pesticide solution was continued for up to 60 min.

To reactivate the inhibited enzyme, a method proposed by Tran-Minh [24] was employed. The sensor was immersed for 10–60 min in a stirred reactivation solution. The latter was diluted 100-fold with a PBS-saturated solution of PAM-2 (1×10^{-6} M PAM-2). Nevertheless, the reactivated membranes were not used again in order to ensure uniform initial conditions in the inhibition study. After equilibration with a pesticide solution, the membrane was mechanically removed, the silicon nitride surface was washed with the sulphuric–chromic acid mixture and recoated with enzyme.

RESULTS AND DISCUSSION

Testing of the enzyme membranes

Some preliminary experiments were performed to establish the optimum conditions for the use of ENFETs.

In the "ageing" test, calibration graphs of V_s versus substrate concentration were constructed at different times after the first immersion of the BuChE biosensor in buffer solution and the conservation of membrane activity was estimated. The test was performed in (a) 2.5 mM KH_2PO_4 buffer, (b) 10 mM KH_2PO_4, (c) 10 mM KH_2PO_4 buffer + 150 mM NaCl and (d) PBS. It was found that within the first 2 h the membrane activity decreased to 70–85% (solutions a–d) of the initial value. This may be associated with a leakage of non-cross-linked enzyme from the membrane.

The activity then remained stable for at least 3 days if the biosensor was stored in solutions c and d at 4°C and occasionally used for more than 50 cycles of activity measurements. In solutions a and b a decrease in activity of about 10% was observed under the same conditions of storage.

The effects of pH, buffer concentration and salt concentration were studied in order to obtain the maximum V_s values and thus to decrease the measurement errors. The BuChE biosensor response can be changed substantially by varying the buffer concentration and the pH (see Fig. 3a and b). No significant influence of salt (such as NaCl) was observed up to the concentration that is usual in physiological liquids (Fig. 3). Taking into account the pH dependence of the sensor response, a standard PBS was chosen for the experiments because its pH value is fixed near 7.4. All further measurements were done in the PBS after equilibration for 2 h.

All these results were obtained using BuChE membranes but they were the same for AcChE. Under the chosen experimental conditions the drift of the output signal (V_s) was less than 1 mV h^{-1}, the response time was about 1 min (see Fig. 4), and reproducibility of repeated measurements was within 1 mV for both BuChE and AcChE biosensor. The calibration graphs for the AcChE-FET and BuChE-FET presented in Fig. 5 are the averages for fourteen AcChE and sixteen BuChCl membranes. It was possible to produce effective cholinesterase sensors by this technique, although the individual membranes differed in response within ±25% of the average.

Enzyme inhibition study and pesticide determination

The choice of an appropriate substrate concentration is important in enzyme inhibition studies. The percentage inhibition was evaluated from the response of the active and inhibited forms of the enzyme. Hence all the enzyme has to take part in the reaction that corresponds to the saturation part of the calibration graph.

Measurements of BuChE inhibition were performed for different substrate concentrations. Reproducible inhibition values were obtained at BuChCl concentrations above 10 mM. From these results, a substrate concentration of 20 mM was chosen for further experiments.

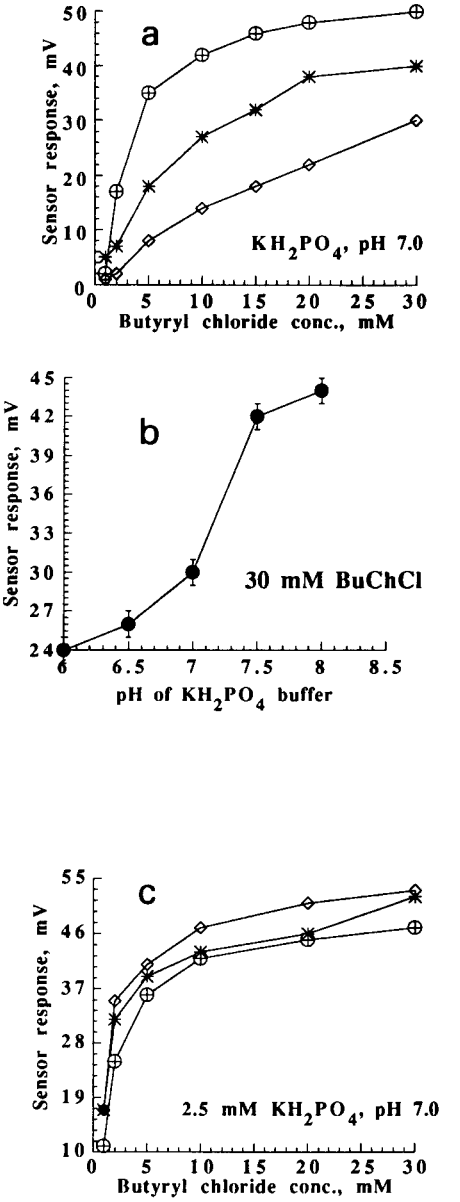

Fig. 3. Response of the butyrylcholinesterase biosensor. (a) Versus buffer concentration: ⊕ = 2.5; ∗ = 5; ◇ = 10 mM. (b) Versus buffer pH. (c) Versus salt concentration: ⊕ = +150 mM NaCl; ∗ = +40 mM NaCl; ◇ = without NaCl.

The dependence of enzyme inhibition of the DFP concentration and incubation time was investigated. It can be seen in Fig. 6 that the

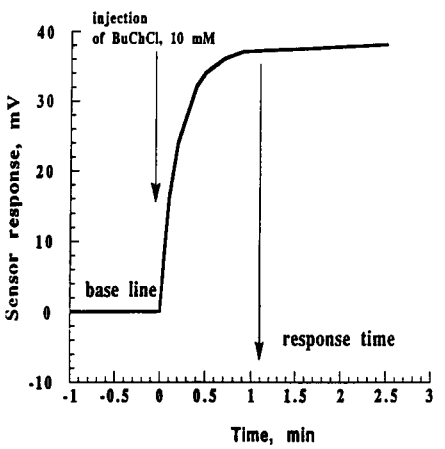

Fig. 4. Typical response of cholinesterase biosensors.

percentage inhibition of immobilized enzyme is not directly proportional to the incubation time. The inhibition curves were replotted versus logarithm of pesticide concentration using the incubation time as a parameter (Fig. 7). The percentage inhibition was nearly proportional to the logarithm of DFP concentration.

As inhibition is dependent on incubation time for the same inhibitor concentration, it is difficult to obtain exact values of inhibition constants for ChE. However, it is clear from Figs. 6 and 7 that BuChE is more selective than AcChE for DFP.

The following requirements were formulated for the pesticide determination procedure: decreasing in initial activity $\geq 10\%$ as the detection limit; sufficiently large dynamic range; and practicable incubation time. Further measurements of enzyme inhibition with paraoxon and trichlorfon (Fig. 8) were performed with an incubation time of 20 min.

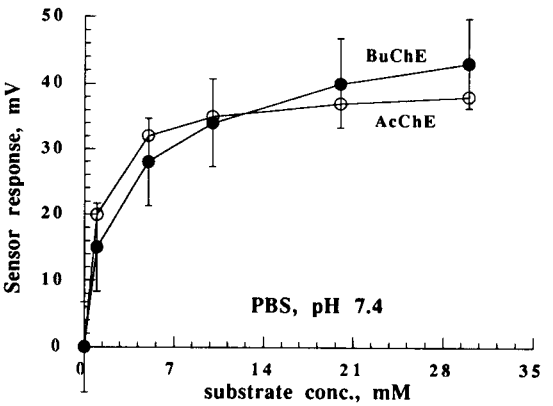

Fig. 5. Calibration graphs for cholinesterase biosensors.

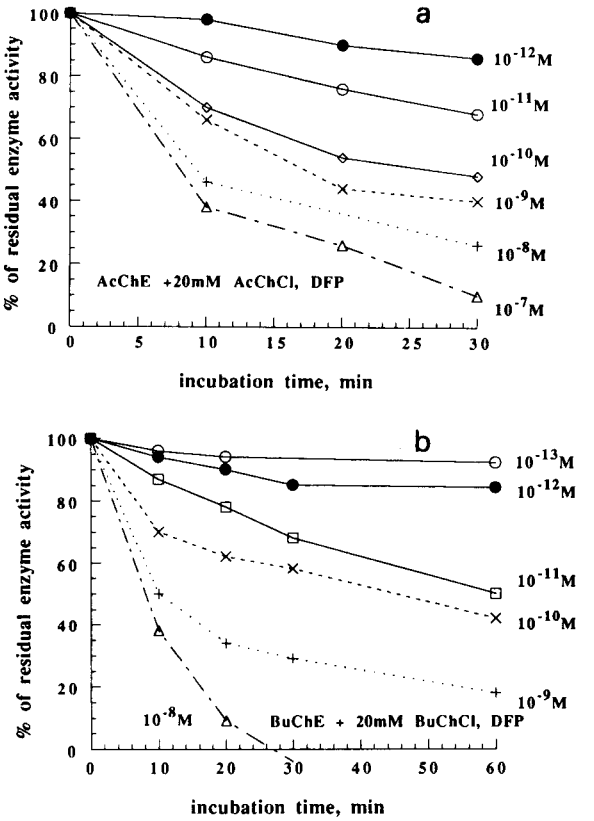

Fig. 6. Inhibition curves for cholinesterase biosensors: (a) acetylcholinesterase; (b) butyrylcholinesterase.

The results obtained for the determination of the pesticide compounds are summarized in Table 1. The detection limits for the compounds examined (from 250 mg l^{-1} to 20 ng l^{-1}) show that the proposed sensors are suitable for monitoring presence of pesticide in water samples.

There is no significant difference in the inhibition level of the cholinesterases, but the small difference that does exist can be developed for more specific multi-sensing of organophosphorus compounds. Unfortunately, the reproducibility and accuracy of these biosensors depend on the characteristics of the enzymatic membranes: thickness, enzyme concentration, adhesion, lifetime, etc.

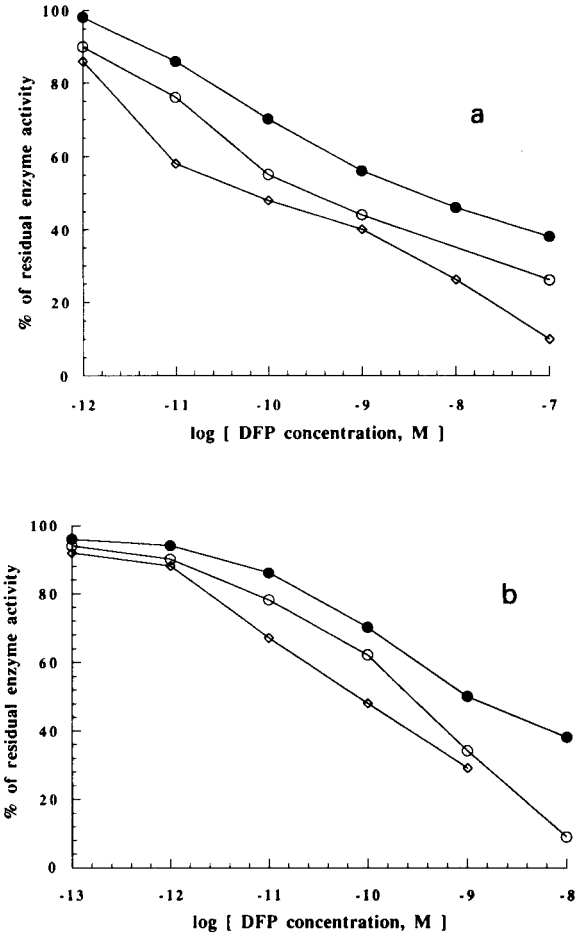

Fig. 7. Dependence of residual enzyme activity on the inhibitor (DFP) concentration for (a) acetylcholinesterase and (b) butyrylcholinesterase. Incubation time = (●) 10, (○) 20 and (◇) 30 min.

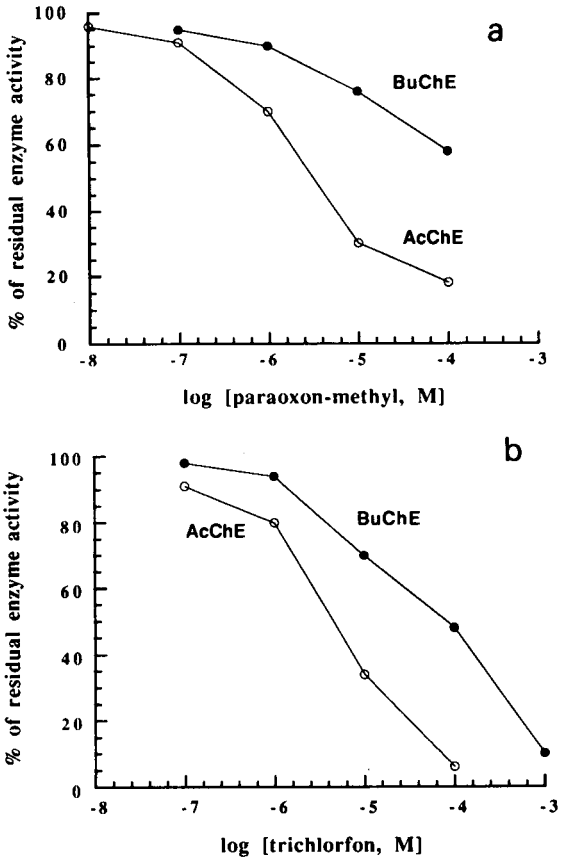

Fig. 8. Calibration graphs for (a) paraoxon-methyl and (b) trichlorfon.

Reported studies differ considerably in the enzyme immobilization techniques and and in the inhibitor used [5,7–9,17,19,21,28,29]. Only for some of the results presented here were similar experimental conditions found in the literature. Thus, DFP has been detected at levels of 10^{-6} and 10^{-8} M using BuChE in gelatin [19] and dialysis [9] membranes, respectively. For paraoxon-methyl, a detection limit of 5 $\mu g\ l^{-1}$

TABLE 1

Analytical characteristics of biosensors for the determination of pesticides

Pesticide	AcChE membrane			BuChE membrane		
	Detection limit		Dynamic range (M)	Detection limit		Dynamic range (M)
	$\mu g\ l^{-1}$	M		$\mu g\ l^{-1}$	M	
DFP	0.0002	10^{-12}	10^{-12}–10^{-7}	0.0002	10^{-12}	10^{-12}–10^{-8}
Paraoxon-methyl	25	10^{-7}	10^{-7}–10^{-4}	250	10^{-6}	10^{-6}–10^{-4}
Trichlorfon	24	10^{-7}	10^{-7}–10^{-4}	240	10^{-6}	10^{-6}–10^{-3}

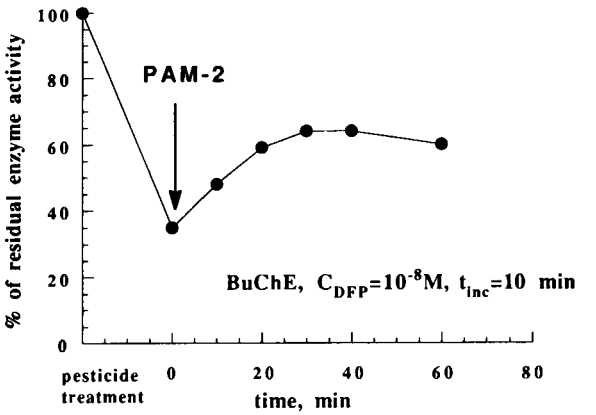

Fig. 9. Typical curve for regeneration of inhibited enzyme.

was obtained [8] with BuChE immobilized on nylon net. However, no complete comparison can be made because of the different measurement conditions used.

Regeneration of inhibited enzyme

Only partial enzyme regeneration was achieved in these experiments. In Fig. 9 a typical curve for regeneration of the inhibited enzyme is shown.

The highest regeneration percentage was 30–40% of the initial activity, hence the latter was completely recovered only in cases of low inhibition. In addition, the regeneration was a maximum after 30 min of PAM-2 treatment, then a decrease in biosensor response was observed. It was assumed that prolonged treatment with PAM-2 may affect the characteristics of the membrane. Further investigations are in progress.

Conclusion

Cholinesterase ENFETs were prepared by cross-linking of the enzyme with BSA on a pH-ISFET. Differential measurements were performed between an ENFET and a REFET. The inhibition effect of organophosphorous pesticides (DFP, paraoxon-methyl and trichlorfon) was measured at a substrate concentration of 20 mM. The detection limit of DFP was 10^{-12} M and those of paraoxon-methyl and trichlorfon were 10^{-6} M. The enzyme regeneration was found to be 60% of its initial activity. Most of the pesticide sensors reported here show a very high sensitivity suitable for the detection of toxic species. Further studies needed in order to make these pesticide biosensors tools for quantitative pesticide analysis.

REFERENCES

1 J.W. Moore and E.A. Moore, Environmental Chemistry, Academic, New York, 1983, pp. 423–438, 449–465.
2 Verordnung uber Trinkwasser und uber Wasser fur Lebensmittelbetriebe (Trinkwasserverordnung–TrinkwV), Bundesgesetzblatt, Bonn, 1986, Teil 1, p. 760.
3 I. Karube and E. Tamiya, Pure Appl. Chem., 59 (1987) 545.
4 H.Y. Neujahr, Biotechnol. Genet. Eng. Rev., 1 (1984) 167.
5 P. Kramer and R.D. Schmid, in W. Gopel, J. Hesse and J.N. Zemel (Eds.), Sensors, Vol. 3, VCH, Weinheim, 1992, p. 1013.
6 I. Karube, Enzyme Technol., 7a (1987) 686.
7 G. Palleschi, M. Bernabei, C. Cremisini and M. Mascini, Sensors Actuators, B7 (1992) 513.
8 H. El Yamani, C. Tranh-Minh, M.A. Abdul and D. Chavane, Sensors Actuators, 15 (1988) 193.
9 Z.-Y. Yuan, T.-M. Zhu, S.-Y. Li, X.-S. Ji, D.-Y. Li and W.B. Wlodarski, 1st World Biosensor Congress, Singapore, Abstracts, 1990, p. 275.
10 D.L. Buch and G.A. Rechnitz, Anal. Lett., 20 (1987) 1781.
11 D.L. Buch and G.A. Rechnitz, Anal. Lett., 21 (1988) 1947.
12 P. Kramer and R.D. Schmid, presented at GDCh-Tagung Fachgruppe Wasserchimie, 1990.
13 J. Ngeh-Ngwainbi, P.H. Foley, S. Kuan Shia and G.G. Guilbault, J. Am. Chem. Soc., 108 (1986) 5444.
14 I. Karube, Microbial Sensors for Process and Environmental Control (ACS Symposium Series, No. 309), American Chemical Society, Washington, DC, 1986, p. 330.
15 I. Karube and S. Suzuki, Biotechnology, 83 (1963) 625.
16 D.M. Rawson, A.J. Willmer and A.P.F. Turner, Biosensors, 4 (1989) 299.
17 D.M. Rawson, A.J. Willmer and M.F. Cardosi, Toxicity Assessment, 2 (1987) 325.
18 C. Dumschat, H. Müller, K. Stein and G. Schwedt, Anal. Chim. Acta, 252 (1991) 7.
19 Y. Vlasov, A. Bratov, S. Levichev, and Y. Tarantov, Sensors Actuators, B4 (1991) 283.
20 J.L. Marty, K. Sode and I. Karube, Electroanalysis, 4 (1992) 249.
21 F.F. Bier, W. Stöcklein, M. Böcher, U. Bilitewski and R.D. Schmid, Sensors Actuators, B7 (1992) 509.
22 W.B. Wlodarski, presented at the Fourth Conference on Control Engineering, Brisbane, 1990.
23 P. Kramer, W. Stocklein and R.D. Schmid, Wasser, 73 (1989) 345

24 C. Tran-Minh, Ion-Sel. Electrode Rev., 7 (1985) 41.
25 J.W. Leyden, Enzyme and Metabolic Inhibitors, Academic, New York, 1963, Vol. 1, p. 863.
26 H. Perrot, N. Jaffrezic-Renault, N.F. De Rooij and H. van den Vlekkert, Sensors Actuators, 20 (1989) 293.
27 A.A. Shul'ga, V.I. Strikha, S.V. Patskovski, S.V. Dzydevich, A.V. El'skaya, A.P. Soldatkin and O.A. Bubryak, Biosensors' 92, Geneva, Elsevier Adv. Technol., Oxford, 1992, p. 81.
28 P. Skladal and M. Mascini, Biosensors Bioelectron., 7 (1992) 335.
29 U. Wollenberger, K. Setz, F.W. Scheller, U. Löffler, W. Göpel and R. Gruss, Sensors Actuators, B4 (1991) 257.

Analytica Chimica Acta, 281 (1993) 13–18
Elsevier Science Publishers B.V., Amsterdam

Detection of human T-lymphocytes with a piezoelectric immunosensor

Bernd König and Michael Grätzel

Institut de Chimie Physique II, Ecole Polytechnique Fédérale de Lausanne, CH-1015 Lausanne (Switzerland)

(Received 26th January 1993; revised manuscript received 9th March 1993)

Abstract

A reusable piezoelectric immunosensor was developed for the detection of purified human T-lymphocytes and of T-lymphocytes in whole human blood. Three different methods for immobilization of anti CD 3 gp M_r 19000–29000 antibody on the gold electrode of the immunosensor were tested. Coating the electrode with polyethyleneimine gave the best results in terms of stability, sensitivity and reproducibility. Similar results were observed on coating the electrode with γ-aminopropyltriethoxysilane. The last method, coating the electrode with protein A, gave inferior results. Applying an anti CD 3 gp M_r 19000–29000 antibody layer via polyethyleneimine immobilization on a 10-MHz AT-cut crystal resulted in 5×10^3–4.5×10^5 cells on the surface in a linear frequency change and a long-term stability of 10 weeks when the modified crystal was stored desiccated at room temperature.

Keywords: Biosensors; Immunoassay; Piezoelectric sensing; Blood; Lymphocytes; T-lymphocytes

The cellular and humoral immune reactions of mammalia are mediated by lymphocytes with a common bone marrow stem cell. In early childhood two main groups of lymphocytes are generated, the B-lymphocytes (bursa equivalent proliferation) and the T-lymphocytes (thymus-dependent proliferation). T-lymphocytes are responsible for the cellular immune response. They are found in the cortex of lymph nodes and are well characterized by different in vitro tests, e.g., T-cells can be stimulated by specific antigens such as tuberculin, a common proof in clinical diagnostics. A subpopulation of the T-cells, the so-called T-helper cells, cooperate with B-lymphocytes and induces the production of antibodies. This very important cell type is destroyed by the HIV virus. Another subpopulation of T-lymphocytes is the memory cells. They remember antigens and speed up the immune response during a second infection with the same antigen. Other types are the T-suppressor and the T-effector cells; the latter synthesize lymphokines such as interferon, interleucin and the macrophage-inhibiting factor.

Because T-cells play an important role in the immune system, it is of great interest to determine the number of these cells per unit volume of whole blood. This is generally done by flow cytometry. This technique has two disadvantages, the high costs and the necessity to label the cells before use. A possible alternative is the use of piezoelectric antibody-based biosensors.

Antibody-based biosensors detect the antigen concentration either by indirect competitive and displacement reactions similar to immunoassays or by direct changes in transducer output [1]. An example of the latter type of system is the piezoelectric (PZ) crystal detector for assays both in the gas phase and in solution. PZ devices consist

Correspondence to: B. König, Institut de Chimie Physique II, Ecole Polytechnique Fédérale de Lausanne, CH-1015 Lausanne (Switzerland).

of an oscillating quartz crystal containing an adsorbent on its surface that selectively interacts with the analyte. Adsorption of the analyte (antigen) increases the mass of the crystal and decreases proportionally the resonance frequency of oscillation.

The theoretical basis of piezoelectricity was first postulated by Raleigh in 1885. However, the use of PZ devices was realized only after Sauerbrey [2] derived the frequency-to-mass relationship:

$$\Delta F = -2.3 \times 10^6 F^2 \Delta M/A$$

where ΔF is the change in resonance frequency of the coated crystal, F is the resonance frequency of the crystal, ΔM is the mass increase and A is the area of the coated crystal. The detection limit of this technique is about 10^{-12} g. In 1964, King [3] reported for the first time the use of a PZ crustal as an analytical detector.

Since then, work with these detectors has focused mainly on the use of inorganic and organic coatings for gaseous environmental pollutants (for a recent review, see [4]). As biologically active molecules, such as enzymes and antibodies, have recently, become available in large amounts, a new class of PZ biosensors has been developed the piezoelectric immunosensor.

The general philosophy behind biosensor technology is real-time output, high analyte sensitivity and specificity, simplicity of use and cost effectiveness [5–7]. Therefore, biosensors are being developed for a wide range of applications such as in the food industry, environmental monitoring and processing, biotechnology and clinical diagnostics [8,9]. The piezoimmunosensor system offers many of the properties desired for an ideal immunosensor.

This paper reports the development of a PZ immunosensor for human T-lymphocytes. The strong complexation between the modified gold electrode and anti CD 3 gp M_r 19000–29000 antibody was exploited to construct a reusable immunosensor. The sensor was applied to purified human T-lymphocytes and to T-cells in whole human blood. The sensitivity, long-term stability and reusability of three different immobilization methods are also reported.

EXPERIMENTAL

Materials

Anti-CD 3 gp M_r 19000–29000 antibody was obtained from Flow Laboratories (Allschwil, Switzerland). Human whole blood anticoagulated with calcium citrate was supplied by the Zentrallaboratorium Blutspendedienst of the Swiss Red Cross (Bern). Polyethyleneimine (PEI) and γ-aminopropyltriethoxysilane (APTES), were purchased from Aldrich (Buchs, Switzerland). Nylon wool fibre and lymphoprep separation media were obtained from Polysciences (Warrington, PA). All other reagents and solvents were analytical-reagent grade or better (Fluka, Buchs, Switzerland).

Equipment

The PZ crystals (Universal Sensors, New Orleans, LA) used in this work were AT-cut with a basic resonance frequence of 10 MHz. The crystal consists of a 15×0.2 mm quartz wafer, which is placed between 7.5 mm gold electrodes, mounted in a ceramic holder with a plug. An identical (uncoated) crystal was used as reference to correct for temperature and humidity fluctuations. The crystal frequency was monitored with a PZ 105 immunobiosensor detector (Universal Sensors).

Immobilization procedures

Three different methods of immobilization were employed [10,11].

Immobilization via a thin polyethyleneimine layer. A methanol solution (5 ml) containing 2% PEI was spread at room temperature on the electrode of the crystal for 30 s. After air drying, the crystal was washed four times with methanol to remove unbound material. The crystal was then immersed in aqueous 2.5% glutaraldehyde solution (pH 7) for 40 min and washed with water. Subsequently, 5 μl of a 5 mg ml^{-1} antibody solution were placed on each side of the crystal for 1 h. Unreacted aldehyde groups were blocked by immersing the crystal in a solution of 0.1 M glycine in 20 mM phosphate-buffered saline (pH 7) (PBS). The crystal was subsequently rinsed with PBS and distilled water and dried in air.

Immobilization via a thin silane layer. The crystal was dipped in a 5% solution of APTES in dry benzene for 2 h at room temperature. After vacuum drying at 70°C, the crystal was washed several times with acetone and incubated for 2 h in 2.5% glutaraldehyde (pH 7). Following washing with distilled water, 5 μl of a 5 mg ml^{-1} antibody solution were spread on both sides of the crystal. After drying for 45 min, the crystal was washed with PBS and distilled water and subsequently air dried.

Immobilization via protein A-gold. The PZ crystal was dipped at room temperature for 30 min in 1.2 M NaOH, then washed with distilled water and placed for 15 min in 1.2 M HCl. Following washing with distilled water and ethanol the crystal was dried at 70°C. Then 5 μl of protein A solution (2 mg ml^{-1}, pH 7) were added to the electrodes on both sides of the crystal. After drying, the coated crystal was rinsed with distilled water and 5 μl of a 5 mg ml^{-1} antibody solution were spread over both gold electrode surfaces, dried, washed with PBS and then rinsed with distilled water and dried again.

Purification of T-lymphocytes [12]

To purify human T-lymphocytes, 10–12 ml of anticoagulated blood were added at room temperature to a tube containing 20–25 glass beads (2–3 mm in diameter) and shaken to remove the platelets. The defibrinated sample was diluted twice with 0.9% (w/v) sodium chloride, layered over 5 ml of lymphoprep separation media and centrifuged at 1000 *g* for 15 min. The mononuclear layer was collected with a syringe and passed over a column of loosely packed nylon wool fibre. Under these conditions T-lymphocytes pass through the column whereas B-lymphocytes and granulocytes adhere to the fibres. The concentration of the T-lymphocytes after column chromatography was 1×10^8 cells ml^{-1} (improved Neubauer).

Measurement procedures

ΔF_1, the frequency difference between the coated crystal and the reference crystal, was determined first. The coated crystal was subsequently dipped for 30 min at room temperature in a stirred 1-ml suspension of human T-lymphocytes in PBS or human whole blood containing different numbers (5×10^3–4.5×10^5) of cells. After rinsing with PBS and air drying, the coated crystal was placed in the test chamber and a new frequency difference was measured (ΔF_2). The change in the frequency difference ($\Delta F = \Delta F_2 - \Delta F_1$) was related to the number of cells adsorbed on the crystal.

TABLE 1

Frequency changes (ΔF) due to binding of purified human T-lymphocytes and of T-lymphocytes in whole human blood to the anti CD 3 gp M_r 19000–29000 antibody-modified crystal surface with three different immobilization procedures

Immobilization method	ΔF [a]	
	Purified T-lymphocytes	Whole human blood
PEI	7638 ± 12	8493 ± 19
APTES	7342 ± 14	8502 ± 24
Protein A	6340 ± 11	8084 ± 23

[a] Average of ten experiments ± SEM.

RESULTS

Three different immobilization procedures were tested to fix the anti CD 3 gp M_r 19000–29000 antibody to the gold electrodes. The best results with respect to sensitivity, reusability and stability were obtained with the PEI method (Table 1). The crystal precoated with a thin layer of PEI could be reused eight times without a detectable decrease in sensitivity over a period of 10 weeks when stored desiccated at room temperature (data not shown). Additionally, it provided the most reproducible results, although reproducibility was not a problem even with the other immobilization procedures (Table 1). As shown in Fig. 1, a plot of frequency change versus number of pure human T-lymphocytes is linear from 5×10^3 to 4.5×10^5 cells for this method. An additional study comparing the frequency change of purified T-lymphocytes and of T-lymphocytes in whole human blood showed a 10% increased signal for whole blood, indicating that a slight amount of unspecific material present in the blood

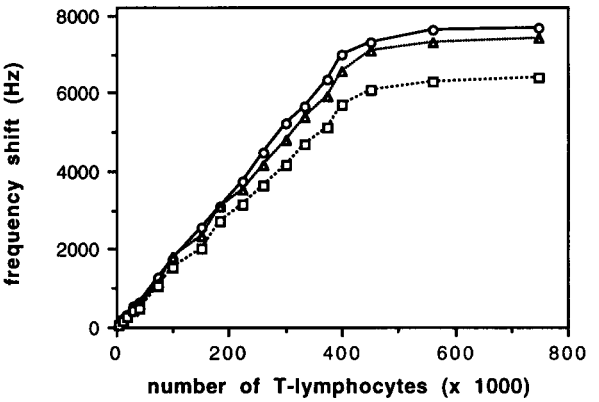

Fig. 1. Comparison of three different immobilization procedures and the relationship between the number of human T-lymphocytes on the crystal and the frequency change of the anti CD 3 gp M_r 19000–29000 antibody-coated crystal. Immobilization via (○) PEI, (△) APTES and (□) protein A. The plots show that the frequency change is linear in the range 5×10^3–4.5×10^5 cells. The number of T-lymphocytes was determined with a standard haemocytometer (improved Neubauer). Each point represents the average of ten experiments with incubation times of 30 min each.

sample adhered to the modified electrode surface (Fig. 2). Imaging the electrodes with stained blood cells indicated that platelets and thymocytes are adsorbed on the surface (data not shown).

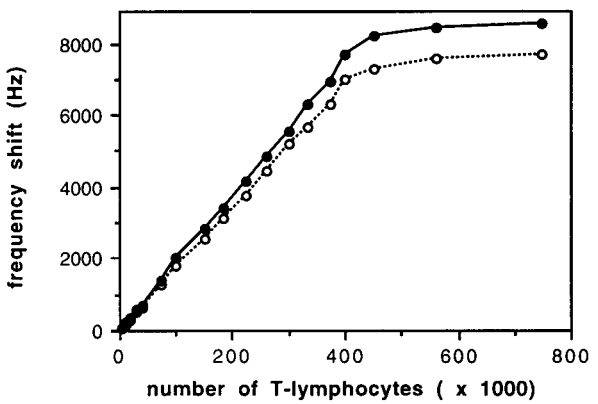

Fig. 2. Comparison of frequency changes with increasing number of (○) purified human T-lymphocytes and (●) T-lymphocytes per ml in whole human blood (PEI immobilization procedure). With whole human blood a 10% increased frequency change is observed owing to unspecific binding of other blood cells, mainly thymocytes and platelets. The number of T-lymphocytes was determined with a standard haemocytometer (improved Neubauer). Each point represents the average of ten experiments with incubation times of 30 minutes each.

Immobilization via APTES led to similar results with a slightly (4%) reduced sensitivity. Also linear from 5×10^3 to 4.5×10^5 cells, the APTES-modified electrode showed a 16% increased frequency change when detecting T-lymphocytes in whole blood samples compared with the results for purified T-lymphocytes (Table 1). The long-term stability of this system was also tested. When stored desiccated at room temperature the modified crystal surface is also stable for 10 weeks and even the number of regenerations (eight times) is identical (data not shown).

Sensors prepared by the third method i.e., immobilization via protein A, gave the most unfavourable results. The smallest frequency change of the three methods tested was observed (17% smaller compared with the PEI method) and the highest interference from unspecifically bound material (28%) in whole human blood (Table 1). Additionally, the crystal could not totally withstand the regeneration step with 8 M urea because of partial desorption of the immobilized antibody of protein A, resulting in a lower reusability (five times). A decreased lifetime of 6 instead of 10 weeks was also observed when the protein A-coated crystal was stored desiccated at room temperature (data not shown).

The crystal surface coated with 5 mg ml^{-1} antibody solution was considered optimum. Up to 5 mg ml^{-1}, the sensitivity of the modified crystal increased with increase in the antibody concentration used for immobilization. Above this concentration, the frequency change was no longer dependent on the antibody concentration (data not shown).

Other important factors affecting the sensitivity of the PZ detection system are the method of regeneration and the time of incubation of the antibody-coated crystal with antigen. Of the three different methods of regeneration tested so far, only a solution of 8 M urea in 20 mM (PBS) removed the bound cells totally. Other dissociating agents such as 0.2 M glycine–HCl (pH 2.8) and 0.2 M ethanolamine (pH 8) did not totally remove the bound T-lymphocytes (data not shown). A disadvantage of all of these methods is that they involve relatively aggressive chemicals that partially desorb the bound antibody. In order

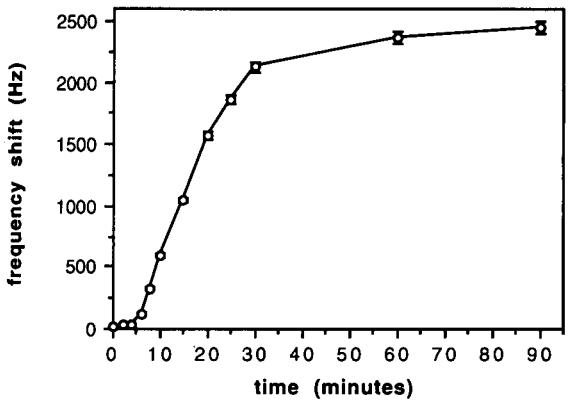

Fig. 3. Correlation between human T-lymphocytes and anti CD 3 gp M_r 19000–29000 antibody reaction time resonance frequency shift (ΔF) for cell concentrations of 1.5×10^5 cells ml^{-1}. After 30 min the antigen–antibody reaction is nearly complete. Each point represents the average of five experiments.

to optimize the second parameter, the crystal was exposed to a solution of 1.5×10^5 T-lymphocytes ml^{-1} for different periods. The results showed that an incubation time of 30 min gives optimum sensitivity (Fig. 3). Prolonged exposure for up to 90 min, did not improve the observed frequency change. Therefore, in all subsequent experiments, a 30-min incubation time was used.

DISCUSSION

This study has demonstrated the successful application of piezoelectric immunosensor technology to detect purified human T-lymphocytes in the range 5×10^3–4.5×10^5 cells bound to the surface of the sensor. T-lymphocyte levels in whole human blood were also determined.

Of the three immobilization procedures employed, attachment of the anti CD 3 gp M_r 19000–29000 antibody to a PEI- or APTES-coated surface gave the best results with regard to stability, sensitivity and reproducibility. This agrees with earlier observations by Prusak-Sochaczewski et al. [10] and recent results with a PZ immunosensor specific for human erythrocytes [9]. Additionally these two methods seems to be superior in specificity to the protein A method, because the smallest number of unspecifically bound blood cells was observed.

This is in contrast to the results of Plomer et al. [13], who obtained the best results with the protein A–gold immobilization procedure. In our hands, however, this method gave the most unfavourable sensor performance. We believe that this is due to the nature of the antigens used here, because blood cells, mainly platelets, generally adhere unspecifically to many surfaces and adsorbed proteins. Owing to the non-homogeneous electrode surface, exposing both hydrophilic and hydrophobic parts, the protein A-derivatized electrodes exhibit an enhanced unspecific interaction with non T-lymphocytic cells contained in the blood. Although it is clear from the supplier's product specification that the antibody used is also specific to thymocytes (about 15%) and not only to T-lymphocytes, the amount of unspecifically adsorbed cells (28%) is about double this value, so that the protein A immobilization procedure cannot be recommended for detecting blood cells. The amount of unspecifically adsorbed cells with the PEI and APTES procedures (10 and 16%, respectively) fits well with the product specification and was supported by imaging the electrodes with stained blood cells. An additional advantage of these two systems is the increased long-term stability of the crystals.

The results reported above demonstrate that a piezoelectric crystal coated with PEI or APTES and CD 3 gp M_r 19000–29000 antibody can be applied to the determination of purified human T-lymphocytes and of lymphocytes in whole human blood. This is very promising, because T-lymphocytes play an important role in the immune system of mammalia. Because in the last decade the number of HIV-positive humans has increased dramatically, the number of blood tests, especially focusing on the number of T-lymphocytes, will also increase. The PZ system seems to be optimum for such tests, because the coating process with the two polymers is simple, cheap and reproducible. However, from the plot of frequency change versus number of T-lymphocytes one can estimate 4.5×10^5 T-lymphocytes as the maximum number of cells bound to the electrode area. Comparison this number with the theoreti-

cal maximum possible number of T-lymphocytes (6×10^5 for an area of 4.4×10^7 μm^2 and a diameter of 8.5 μm for the T-lymphocytes) showed that 75% of the electrode surfaces are occupied with cells. Therefore, better methods for antibody immobilization have to be developed in order to improve the sensitivity, stability and reproducibility of this promising technique of piezoelectric immunosensing.

REFERENCES

1 I. Karube and M. Suzuki, Biosensors, 2 (1986) 343.
2 G.Z. Sauerbrey, Z. Phys., 155 (1959) 206.
3 W.H. King, Anal. Chem., 36 (1964) 1735.
4 G.G. Guilbault and J. Jordan, CRC Crit. Rev. Anal. Chem., 19 (1988) p 1.
5 C.R. Lowe, Biosensors, 1 (1985) 3.
6 A.P.F. Turner, Sensors Actuators, 17 (1989) 43.
7 R.F. Taylor, in D.L. Wise (Ed.), Bioinstrumentation: Research, Developments and Applications, Butterworths, Boston, 1990, p. 355.
8 C. Kösslinger, S. Drost, F. Aberl, H. Wolf, S. Koch and P. Wolas, Biosensors Bioelectron., 7 (1992) 397.
9 B. König and M. Grätzel, Anal. Chim. Acta, 276 (1993) 329.
10 E. Prusak-Sochaczewski, J.H.T. Luong and G.G. Guilbault, Enzyme Microb. Technol., 12 (1990) 173.
11 E. Prusak-Sochaczewski and J.H.T. Luong, Anal. Lett., 23 (1990) 401.
12 S.V. Hunt, in G.G.B. Klaus (Ed.), Lymphocytes—A Practical Approach, IRL, Oxford, 1987, p. 1.
13 M. Plomer, G.G. Guilbault and B. Hock, Enzyme Microb. Technol., 14 (1992) 230.

Analytica Chimica Acta, 281 (1993) 19–24
Elsevier Science Publishers B.V., Amsterdam

Use of tyrosinase for enzymatic elimination of acetaminophen interference in amperometric sensing

Joseph Wang, Najih Naser and Ulla Wollenberger [1]

Department of Chemistry, New Mexico State University, Las Cruces, NM 88003 (USA)

(Received 14th January 1993; revised manuscript received 18th March 1993)

Abstract

An effective enzymatic strategy for eliminating the common acetaminophen interference in amperometric sensing is described. The method relies on the in situ biocatalytic removal of acetaminophen by the surface-bound tyrosinase. Mushroom-containing carbon paste electrodes (rich with tyrosinase) are particularly useful for eliminating contributions from acetaminophen. Various factors affecting the efficiency of the tyrosinase-based elimination capability are explored. Selective biosensing of glucose is accomplished by the coimmobilization of glucose oxidase.

Keywords: Biosensors; Acetaminophen; Enzyme electrode; Tyrosinase

A major challenge for biosensor development is the elimination of interferences. Despite the inherent specificity accrued from the biological recognition process, coexisting compounds may result in an overlapping signal. For example, the amperometric biosensing of glucose is commonly affected by easily oxidizable constituents of the biological fluid, including ascorbic acid, uric acid and acetaminophen.

One useful approach to alleviate the interference problem is to cover the transducer with an appropriate permselective layer [1,2]. For example, the charge discriminative properties of Nafion [3] or Eastman AQ [4] films have been used to minimize interferences from the anionic ascorbic and uric acids. The size exclusion characteristics of cellulose acetate [5] or poly(*o*-phenylenediamine) [6] have greatly facilitated the selective detection of the small, enzymatically-liberated hydrogen peroxide.

An attractive alternative is to use an in situ enzymatic "destruction" (digestion) of interfering substances. For example, the common ascorbic acid interference can be eliminated in the presence of ascorbic acid oxidase (AAO) [7] or an AAO-containing tissue [8]. Similarly, passivation effects due to surface-active proteins can be destroyed utilizing the protease activity of papain [9]. Recently, horseradish peroxidase has been used to effectively catalyze the preoxidation of common oxidizable interferences [10].

This paper describes a new biocatalytic approach for eliminating the current contribution from acetaminophen. The analgesic acetaminophen is one of the most common taken drugs. As a result of its relatively high physiological level and ease of oxidation, acetaminophen greatly influences the biosensing of glucose. The elimination of the acetaminophen interference represents a particular challenge for permselective coatings because it is a neutral and relatively

Correspondence to: J. Wang, Department of Chemistry, New Mexico State University, Las Cruces, NM 88003 (USA)
[1] Present address: Central Institute Molecular Biology, Berlin Buch (Germany).

small molecule. Several successful surface barriers have been shown to effectively exclude all oxidizable interferences with the exception of acetaminophen [10,11]. A dialysis membrane was used successfully for selective detection of hydrogen peroxide in the presence of oxidizable species (including acetaminophen [12]). In the following sections, an effective enzymatic acetaminophen removal is employed utilizing the tyrosinase conversion of acetaminophen to the corresponding quinone.

EXPERIMENTAL

Apparatus

Batch experiments were performed in a 10 ml cell (Model VC-2, Bioanalytical Systems (BAS)). The cell was joined to the working electrode, Ag/AgCl reference electrode (Model RE-1, BAS), and platinum wire auxiliary electrode through holes in its Teflon cover. Voltammetric and amperometric measurements were performed with the EG&G PAR Model 264A and the BAS CV27 analyzers, respectively. The flow injection system was described earlier [13].

The carbon-paste bioelectrodes were prepared by thoroughly hand-mixing the desired amount of the crushed mushroom (usually 0.4 g, from ca. 1 mm below the skin) with 0.7 g mineral oil (Aldrich) and 0.9 g graphite powder (Acheson 38, Fisher). Other compositions of the mushroom containing paste, as well as tyrosinase and glucose oxidase containing pastes were prepared in a similar manner. The latter employed a metalized graphite (3% Pt content, from Aldrich), and contained a 10% (w/w) glucose oxidase. A portion of the modified carbon paste was packed into the end of a 2-mm i.d. glass tube, and its inner end was connected to a copper wire. New surfaces were smoothed on a weighing paper.

Reagents and procedure

All chemicals were reagent grade, and solutions were freshly prepared with doubly-distilled water. The supporting electrolyte was 0.05 M phosphate buffer (pH 7.4). The mushrooms used in this study were purchased from a local grocery store, while acetaminophen, glucose, chlorpromazine, tyrosinase (E.C.1.14.18.1, 2400 U/mg) and glucose oxidase (E.C.1.1.3.4, 138000 U/g) were obtained from Sigma.

Voltammetric measurements were performed in the differential pulse mode by scanning the potential from 0.1 to 0.8 V at a rate of 10 mV/s. Amperometric measurements were carried out by applying the desired working potential and allowing the transient currents to decay to a steady-state value. All measurements were made under air and at room temperature.

RESULTS AND DISCUSSION

Tyrosinase catalyzes the *o*-hydroxylation of monophenols, such as acetaminophen, to the corresponding *o*-quinones [14,15]. Accordingly, we investigated the feasibility of incorporating tyrosinase within the bulk of carbon-paste electrode matrices towards the in situ biocatalytic consumption of this drug. Figure 1 illustrates differential pulse voltammograms for solutions containing increasing levels of acetaminophen 0–4×10^{-4} M, (a–d) as obtained at the bare (A) and tyrosinase-containing (20% w/w) (B) carbon paste electrodes. The well-defined oxidation peaks ob-

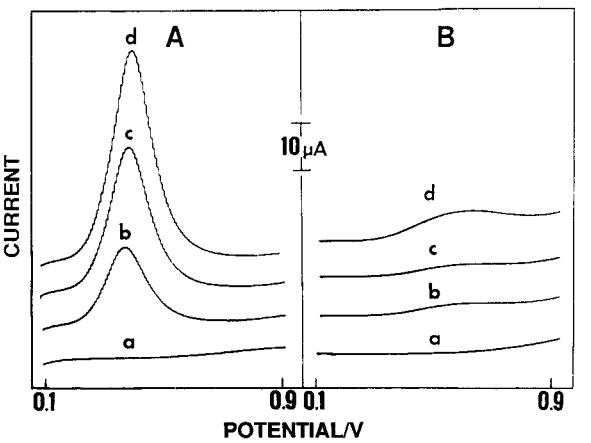

Fig. 1. Differential-pulse voltammograms at the plain (A) and tyrosinase (20% w/w)-containing (B) carbon paste electrodes. (a) Blank solution; (b–d) as (a) but after successive additions of 1×10^{-4} M acetaminophen. Scan rate, 10 mV s^{-1}; amplitude, 25 mV; electrolyte, 0.05 M phosphate buffer (pH 7.4).

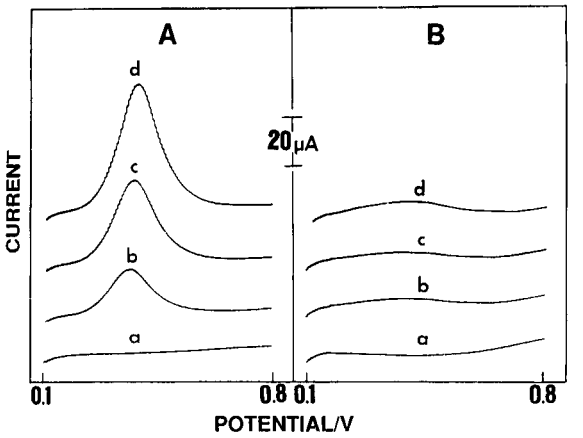

Fig. 2. Differential-pulse voltammograms at the plain (A) and mushroom (20% w/w)-containing (B) carbon paste electrodes. (a) Blank solution; (b–d) as (a) but after successive additions of 1×10^{-4} M acetaminophen. Conditions, as in Fig. 1.

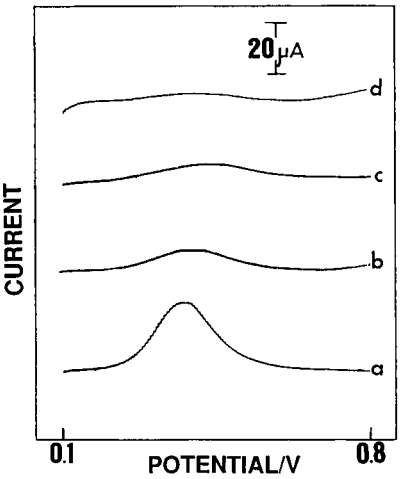

Fig. 3. Effect of the carbon paste composition on the voltammetric response to 2×10^{-4} M acetaminophen. Tissue loading (% w/w): (a) 5, (b) 10, (c) 15 and (d) 20. Other conditions, as in Fig. 1.

served at the unmodified electrode are clearly eliminated at the enzyme-containing surface. Apparently, the tyrosinase rapidly converts the acetaminophen molecules upon their approach to the surface. Such ability to remove the acetaminophen interference depends upon the interferant concentration, as indicated from the very small peak appearing for the higher (4×10^{-4} M) concentration (d). Yet, the magnitude of this peak is only 4% of that observed at the plain carbon paste. Considering the normal (micromolar) physiological level of the drug, this would not pose any selectivity problem. Note also that the presence of tyrosinase or the generation of quinone products do not influence the lower background current inherent to carbon paste electrodes.

An even better elimination efficiency can be accomplished by modifying the carbon paste with

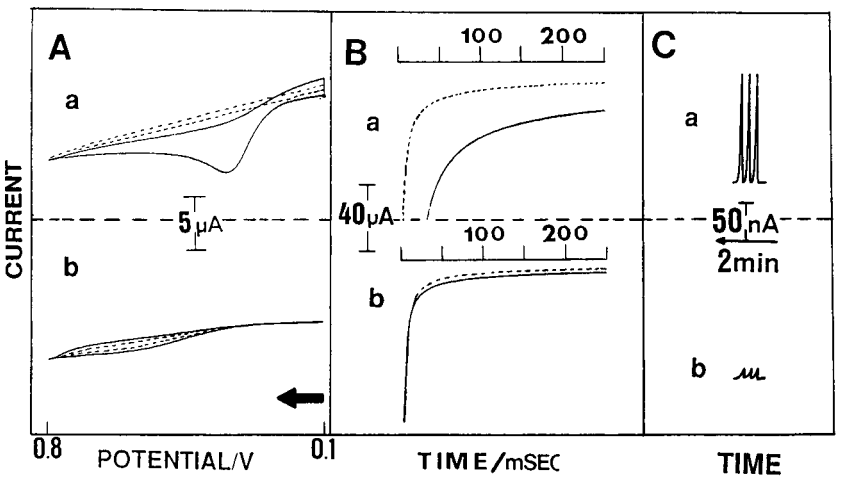

Fig. 4. Cyclic voltammetric (A), chronoamperometric (B) and flow-injection amperometric (C) response to acetaminophen at the plain (a) and mushroom-containing (b) carbon pastes. Dotted lines represent the response of the blank solution. (A) Scan rate, 10 mV s^{-1}; (B) potential step to +0.8 V; (C) operating potential, +0.5 V and flow-rate, 1 ml min^{-1}. Other conditions, as in Fig. 1.

a tyrosinase "rich" plant tissue. Figure 2 displays the differential pulse response of the plain (A) and mushroom-containing (B) carbon pastes for increasing levels of acetaminophen (similar to those employed in Fig. 1). The tissue electrode offers a full suppression of the peaks for these acetaminophen concentrations. The improved elimination capability offered by the tissue is attributed to its high biocatalytic activity. Coupled with the inherent stability of its enzyme, and to its significantly reduced cost, all subsequent work was carried out with tissue-containing electrodes.

The carbon paste sensor configuration actually integrates the tissue "eliminator" with the transducer body. The paste composition has a profound effect upon the removal of the interfering drug. To examine the effect of tyrosinase loading, a series of carbon pastes with increasing tissue contents was prepared. Figure 3 shows differential pulse voltammograms for 2×10^{-4} M acetaminophen at pastes containing 5 (a), 10 (b), 15 (c) and 20% (w/w) (d) mushroom. As expected from the increased biocatalytic activity of the electrode, the acetaminophen response decreases upon increasing the amount of tissue in the paste (with a complete elimination for the 20% loading).

The biocatalytic removal of acetaminophen is influenced also by the measurement technique and its experimental conditions (particularly the time scale and mode of mass transport). Figure 4 displays the cyclic voltammetric (A), chronoamperometric (B) and flow-injection amperometric (C) response to acetaminophen at the plain (a) and mushroom-containing (b) carbon paste electrodes. All three techniques exhibit a well-defined acetaminophen response at the plain carbon paste surface. In contrast, a negligible acetaminophen contribution is observed at the tissue-based electrode, suggesting an effective removal of the drug. Over 95% diminutions of the acetaminophen response is observed for the cyclic voltammetric and chronoamperometric experiments, as compared with a 92% removal of the drug in the flow-injection operation. Such behavior is attributed to the vigorous hydrodynamic conditions of the thin-layer flow cell, as compared to the static conditions characterizing the batch experiments.

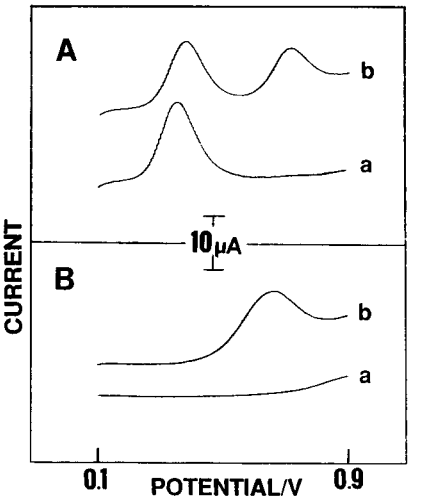

Fig. 5. Differential pulse measurements of chlorpromazine in the presence of acetaminophen at the plain (A) and mushroom-containing (B) carbon pastes. (a) 1×10^{-4} M acetaminophen; (b) same as (a) but after addition of 1×10^{-4} M chlorpromazine. Other conditions, as in Fig. 1.

The stability of the acetaminophen-elimination capability was examined from 40 pulse voltammograms for 2×10^{-4} M acetaminophen over an unbroken 10 h exposure period. The suppression of the acetaminophen peak was maintained during the first 8 h (with a response similar to that of the blank solution). The appearance of a small acetaminophen oxidation peak at the 33rd voltammogram indicated a decreased biocatalytic activity. Renewal of the surface, under these conditions, is not a problem, considering the carbon paste configuration and the low cost of tissue-containing pastes. No apparent difference in the acetaminophen removal was observed when different mushrooms were employed.

Figure 5 demonstrates the selective elimination of acetaminophen in the presence of chlorpromazine. It displays pulse voltammograms for acetaminophen (a) and for a mixture of acetaminophen and chlorpromazine (b), as recorded at the unmodified (A) and mushroom-containing (B) carbon paste electrodes. While two well-defined oxidation peaks are observed at the plain electrode, only a single chlorpromazine response is

observed at the tissue-containing surface. Note also that the chlorpromazine peak is not affected by the tissue modifier. Such ability for an in situ "destruction" of one drug in the presence of a second (co-existing) one holds great promise for pharmaceutical analysis. Indeed, the mushroom bioelectrode was able to completely eliminate the large acetaminophen peak in a voltammogram for a diluted urine sample collected 5 h after a normal (500 mg) acetaminophen dosage (not shown).

The effective elimination of the acetaminophen interference led us to the co-immobilization of tyrosinase and glucose oxidase within the carbon paste matrix. The mixed carbon paste biosensor configuration permits a simultaneous and convenient incorporation of these "eliminating" and "analytical" enzymes (as well as of other modifiers, when needed). Figure 6 (top) shows the amperometric response of the mushroom/glucose-oxidase modified electrode to successive additions of acetaminophen (denoted as A), followed by repetitive injections of glucose (denoted as G). Unlike its well-defined glucose response this modified bioelectrode is not responding to the injections of acetaminophen. In contrast, a large additive response is observed in the absence of the tyrosinase-based elimination capability (bottom). Note also that use of metallized graphite particles [16] greatly facilitates the low-potential (+0.6 V) biosensing of glucose.

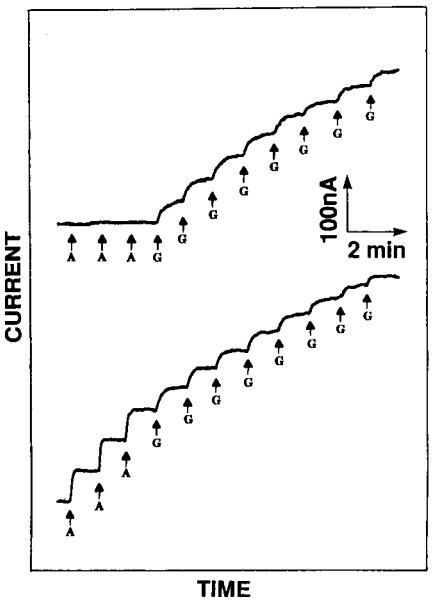

Fig. 6. Amperometric response to 2×10^{-4} M additions of acetaminophen (A), followed by 2×10^{-3} M additions of glucose (G) at the glucose oxidase (bottom) and mushroom/glucose oxidase (top) containing carbon paste electrodes. Operating potential, +0.6 V; stirring rate, 300 rpm; electrolyte, as in Fig. 1. Metallized carbon pastes containing 10% (w/w) glucose oxidase (bottom), as well as 20% (w/w) mushroom (top).

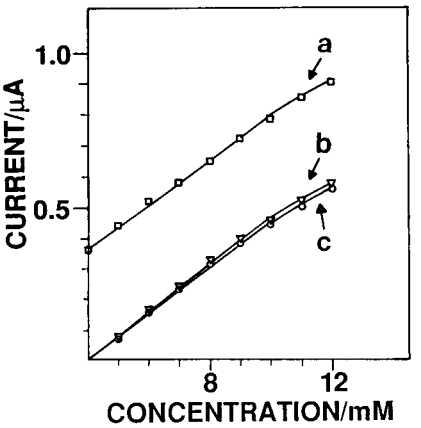

Fig. 7. Calibration plots for glucose in the presence (a,b) and absence (c) of 6×10^{-4} M acetaminophen at the glucose oxidase (a,c) and mushroom/glucose oxidase (b) containing carbon paste electrodes. Conditions, as in Fig. 6.

Calibration plots for glucose (in the presence of acetaminophen, and with or without the mushroom) are shown in Fig. 7 (b and a, respectively). Both exhibit linearity up to 1.1×10^{-2} M glucose with a similar sensitivity (slope of linear portion of 40 nA/mM. However, a large current intercept (of 360 nA), associated with the acetaminophen contribution, is observed in the absence of the tissue "eliminator." Analogous calibration data in the absence of acetaminophen and the mushroom are also shown in Fig. 7c. This plot is nearly identical to that observed in the presence of acetaminophen and the mushroom (compare b and c). The slightly different slope (39 nA/mM) suggests a negligible competition by tyrosinase for the dissolved oxygen. Alternately, it may be attributed to the slightly smaller graphite sensing area (associated with the presence of the mushroom).

In conclusion, we have shown that tyrosinase-containing electrodes can be used for the minimization of the acetaminophen interference. Such tyrosinase-based acetaminophen elimination imparts higher selectivity on amperometric and voltammetric experiments, and expands the scope of biocatalytic schemes for removing interferences. The biological elimination capability is particularly significant considering the difficulty of rejecting acetaminophen by permselective polymeric barriers. The recently published peroxidase-based interferant removal [10] offers an effective acetaminophen elimination but requires an external addition of hydrogen peroxide or a coupled (lactate oxidase) enzymatic reaction. While it should be very attractive for mediator-based enzyme electrodes, it would not be suitable for hydrogen-peroxide based glucose sensing. While the tyrosinase-elimination concept has been illustrated in connection with carbon-paste bioelectrodes, other biosensor configurations should be useful for this task. Preliminary experiments with membrane-based glucose sensors have been very successful (not shown). The enzyme (or tissue) loading and the immobilization scheme must be adjusted to suite the requirement of each particular case (sensor configuration, measurement technique, acetaminophen level, etc.). Coimmobilization of other enzymes (e.g. AAO) should be used for the simultaneous elimination of various interferences.

REFERENCES

1 J. Wang, in P. Edelman and J. Wang (Eds.), Biosensors and Chemical Sensors, ACS Symposium Series No. 487, Washington, DC, 1992, Ch. 10.
2 J. Wang, Electroanalysis, 3 (1991) 255.
3 M. Szentirmay and C. Martin, Anal. Chem., 56 (1984) 1898.
4 J. Wang and T. Golden, Anal. Chem., 61 (1989) 1397.
5 G. Sittampalam and G.S. Wilson, Anal. Chem., 55 (1983) 1608.
6 S. Sasso, R. Pierce, R. Walla and A.M. Yacynych, Anal. Chem., 62 (1990) 1111.
7 G. Nagy, M. Rice and R.N. Adams, Life Sci., 31 (1982) 2611.
8 J. Wang, N. Naser and M. Ozsoz, Anal. Chim. Acta, 234 (1990) 320.
9 J. Wang, L. Wu, S. Martinez and J. Sanchez, Anal. Chem., 63 (1991) 398.
10 R. Maidan and A. Heller, Anal. Chem., 64 (1992) 2889.
11 D. Gindra, Y. Zhang and G. Wilson, R. Sternberg, D. Thevenot, D. Moatti and G. Reach, Anal. Chem., 63 (1991) 1692.
12 G. Palleschi, M. Nabi Rahni, G. Lubrano, J. Ngwainbi and G. Guilbault, Anal. Biochem., 15 (1986) 114.
13 J. Wang and M.S. Lin, Anal. Chem., 60 (1988) 1545.
14 H. Mason, Annu. Rev. Biochem., 34 (1965) 595.
15 G. Payne, W.Q. Sun and A. Sohrabi, Biotech. Bioeng., 40 (1992) 1011.
16 J. Wang, N. Naser, L. Angnes, H. Wu and L. Chen, Anal. Chem., 64 (1992) 1285.

Analytica Chimica Acta, 281 (1993) 25–33
Elsevier Science Publishers B.V., Amsterdam

Development and characterization of an automated flow system for voltammetric analysis

Louise A. Mahoney, John O'Dea and Janet G. Osteryoung

Department of Chemistry, North Carolina State University, Raleigh, NC 27695-8204 (USA)

(Received 21st October 1992; revised manuscript received 16th April 1993)

Abstract

A flow system for voltammetric analysis is described and characterized. This system was designed so that sample manipulation and electrochemical experiments could be performed under automated control. The goal of this work is to expand the practical possibilities for elucidation of the electrochemical behavior of chemical systems. An auxiliary goal is to exploit the potential of flow systems combined with pulse voltammetry for chemical analysis. Once a system has been characterized systematically to establish optimal conditions, voltammograms may be subjected to kinetic analysis. The test system employed here is the reduction and anodic stripping of Pb(II). The accuracy of the sample delivery system was tested by producing calibration curves, which were linear over the range of 0–100% mixing, with correlation coefficients greater than 0.999. The introduction of the sample by means of a sample injector was evaluated along with the effect of the carrier flow-rate on anodic stripping voltammograms. The optimum conditions of 1 ml min^{-1} carrier flow-rate and 150% carrier sweep volume of the loop were determined. Although the flow cell detector is of the wall jet style, the effect of flow-rate on anodic stripping currents is not that of wall jet behavior. The reproducibility of the flow system, for optimum conditions, matched that of the detector for static cell experiments. Finally, the conversion efficiency of the detector was determined to be approximately 1%.

Keywords: Anodic stripping voltammetry; Coulometry; Flow injection; Flow system; Voltammetry; Automation

In any investigation of the electrochemical behavior of a chemical system, one is faced with a number of experimental parameters that may be varied. These include voltammetric parameters, solution conditions, and analyte concentration. Often preliminary experiments need to be performed before the study of electrode kinetics or development of an analytical detection scheme can proceed. The research needed to provide an understanding of the electrochemical response requires significant investment of time and resources for the preparation of solutions and performance of the necessary experiments. Both the expense and the repetitive nature of this type of work usually limit the choice and range of parameters to be varied, often to the serious detriment of the science. Automation of sample handling and experimental execution would allow the electrochemical response to be characterized more efficiently, and thus more thoroughly.

Flow-injection analysis (FIA) has been used routinely since its inception to provide sample handling under automated control [1–7]. FIA involves the injection of a reproducible sample volume into a continuously flowing unsegmented carrier solution, followed by quantitation at the detector [4]. In addition to automated control, FIA offers other advantages. These include convective mass transport, protection of reagents and sample from atmospheric gases and contamina-

Correspondence to: J.G. Osteryoung, Department of Chemistry, North Carolina State University, Raleigh, NC 27695-8204 (USA).

tion, matrix exchange, and increased precision [6]. With automated sample control, concentration of the analyte becomes a practical variable.

A difference between the flow system presented below and FIA is in the detection design. Detection in most FIA applications involves a transient peak-shaped response, characterized by peak height [4]. The transient response is due to the heterogeneous sample profile produced by chemical interaction of the sample plug with a reagent in the carrier solution. Our work more closely resembles the ideas of continuous flow air segmented analysis [8]. This method has been compared to "beakers traveling on a conveyor belt" [4]. The injected sample is homogeneous, and dispersive interactions between the sample plug and carrier solution are minimized. The present flow system does not use air segmentation; instead injection controlled by software provides segmentation of the samples. The "beakers on a conveyor belt" analogy highlights the central purpose of the flow system.

This sample handling system couples the advantages of continuous flow-injection analysis with automated control of experimental operation and data analysis. Unique aspects of this flow system include automated stopped-flow detection with blank subtraction. With these features the voltammetric scan may be performed in quiescent solutions, and the results therefrom can be compared quantitatively with those from experiments performed manually. This is in contrast to systems such as those of Ref. 9 and 10. The latter system convolves the effects of the flow-rate and scan rate into the appearance of the voltammogram. These methods suffer from limitations placed on the detection scheme by the hydrodynamics of the flow system.

An additional advantage of our system over those cited is the coupling of the flow system to square-wave voltammetry. Square-wave voltammetry is a fast technique, a stripping scan requiring less than one second [11]. Attributes of the voltammogram, such as net peak height, position and width, can be determined on-line and are displayed as the experiment progresses. This provides immediate trouble-shooting capabilities. The entire voltammogram is saved digitally and can be analyzed to obtain kinetic parameters for the detection reaction. These parameters can be determined over a range of concentrations down to trace levels due to the sensitivity and rejection of background currents inherent with square-wave voltammetry.

A further advantage of our system is the complete automation of flow system operations. The investigator places the analyte solutions in the reservoirs and with the input of a batch program the system can be run unattended overnight. The results of these experiments are not only the blank-subtracted voltammograms themselves but the analytical data plotted versus the parameter being investigated; thus there is an economy in both experimentation and data analysis.

The accuracy of the sample pump was determined through spectrophotometric measurements using a UV–visible flow cell. The electrochemical detector characterized in this study is a PARC 303A static mercury drop electrode (SMDE), mated to a PARC 420 flow cell. The hydrodynamic regime of this commercial detector is complex and thus not easily described mathematically. Therefore the dependence of signal on experimental parameters cannot be predicted, and this dependence has not been characterized experimentally heretofore. The properties of this detector for flow-injection – stripping experiments were determined with anodic stripping voltammetry and chronocoulometry of lead as a model system.

EXPERIMENTAL

Flow system

The flow system (Fig. 1) consists of a sample pump, a carrier solution pump, a shunt valve, a sample injector valve, and a detector, all controlled by a laboratory mini-computer (DEC PDP 8/e). The sample pump is a Spectra-Physics Model SP8700 ternary solvent delivery system. This system has three gastight bottles whose contents may be mixed by a ternary proportioning valve. The carrier phase pump is an LKB/Bromma 2150 isocratic pump. This pump provides the carrier solution from its reservoir, through the

shunt and sample valves to the detector and out to waste. All solution reservoirs are sparged with helium and all tubing for transport of solutions is stainless steel to eliminate contamination by oxygen.

The shunt valve and the sample valve are Valco EC10W, 10-port, electrically actuated valves. The shunt valve stops the flow of the carrier solution to the system. Stopped flow allows for detection in a quiescent solution. The output of the ternary proportioning valve is introduced to the carrier stream by the sample injector. The carrier solution differs from the sample solution only in that it does not contain the analyte. The carrier solution that precedes the sample plug is analyzed in the same manner as the sample to provide a blank signal to be subtracted from the sample signal. The carrier solution that follows the sample plug sweeps out the sample plug from the cell.

The electrochemical detector is an EG&G PARC Model 303A static mercury drop electrode with a EG&G PARC Model 420 flow cell. This cell contains a housing that fits around the base of the capillary. This housing holds fine bore tubing (0.2 mm i.d.) that directs the output of the sample loop towards the mercury drop of the SMDE. The entire assembly is immersed in a cell containing carrier solution. In all experiments the medium drop size, which has a nominal area of 0.017 cm^2, was used. The analyte solution flows past the drop and fills the cell, which contains also a platinum counter electrode and a saturated calomel reference electrode.

The performance of the ternary sample pump was determined photometrically using a Spectra-Physics Model SP8440 variable-wavelength detector.

Data acquisition software

All the components of the flow system are under computer control. The software provides precise control and timing of the operations of the instruments, allowing them to interact in a manner not possible with manual control. Two software programs were implemented that allow automated electrochemical analysis with square-wave voltammetry or double potential step chronocoulometry. These programs run identical experiments on blank solutions and analyte solutions. In these automated experiments, the value of a parameter of interest is incremented through

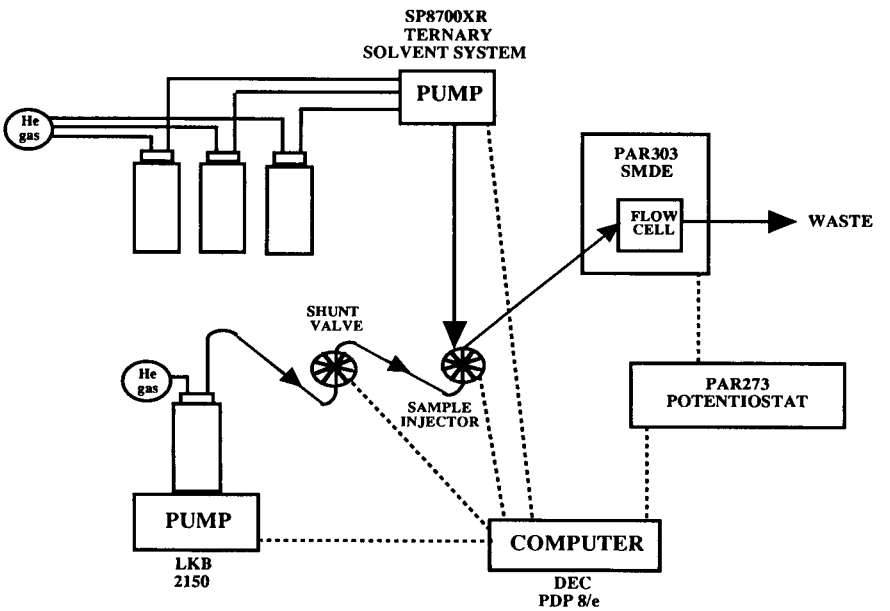

Fig. 1. Flow system: dashed arrows indicate computer control, solid arrows represent fluid path.

a range of values. The automatically adjustable parameters for square- wave voltammetry include: square-wave step height (ΔE_s), square-wave amplitude (E_{sw}), frequency (f), conditioning time and potential for the electrode, carrier flow-rate, and ternary composition established by the sample pump. The parameters available for double-pulse chronocoulometry include: potential and duration of two potential steps, conditioning potential and time for the electrode, carrier flow-rate and ternary composition established by the sample pump.

The square-wave voltammetry program analyzes each voltammogram, after the blank has been subtracted on-line, and determines the value of net peak current, net peak position, and net peak width. These values are plotted against the parameter being incremented, and this output is saved automatically. The program also saves the last voltammogram in the series and the average of all the voltammograms. The chronocoulometry program will automatically save the charge at the end of each pulse and the final chronocoulogram.

Chemicals

A carrier solution 0.05 M in acetic acid and 0.05 M in sodium acetate, pH 4.7, was prepared from glacial acetic acid (99.99 + %) (Aldrich), sodium acetate (99.995%) (Aldrich) and deionized water (Millipore). Lead solutions were obtained from dilution of a 1.0 mM lead nitrate (Fisher Scientific) standard solution in the buffer. Unless otherwise indicated a 10 μM Pb(II) solution was utilized in the experiments. The solution for the photometric calibration of sample proportioning valves was a 10 mM solution of tris(ethylenediamine)cobalt(III) chloride trihydrate (TCT) (prepared according to literature [12]) in deionized water (Millipore).

Characterization of flow system

The ternary solvent mixing system (sample pump) mixes the contents of three bottles through a ternary proportioning valve under microprocessor control. This system can change the mixing ratios among the three bottles by two methods. The initial and final ratio among the bottles can be specified, along with the time needed for the ramp. This method is gradient mixing. The ratios among the bottles can also be changed according to a series of individual concentration ratios input over a period of time. This method is stepwise mixing. The accuracy of these sample delivery methods was determined photometrically.

For the calibration of the proportioning valves, experiments were performed with mixing ratios between bottles containing a 10 mM solution of TCT and water as a diluent. The solution flow-rate was 2.0 ml min^{-1}. The absorbance of the TCT was measured at 335 nm. The absorbance was recorded versus time as the solution flowed through the photometric detector cell. Mixing ratios for gradient and stepwise changes in the concentration of TCT were tested for the three ports of the proportioning valve. The effect of flow-rate on the stepwise change in mixing ratios was also determined for carrier flow-rates in the range 2.0–5.0 ml min^{-1}. After the accuracy of the sample pump was determined, the Model 420 detector was connected to the system and all subsequent experiments were performed under automated software control.

Next the introduction of sample into the carrier solution was characterized. The sample is introduced into the flow system from the ternary sample pump through the injector valve. The sample is loaded into the sample loop, the valve is switched, and the carrier solution moves the sample plug towards the detector. The time needed for the entire plug of sample to pass through the detector region should be given by the ratio of loop size to flow-rate. Due to tailing of the plug and the volume of the connecting tubing (13 μl), this time has to be experimentally determined for all loop sizes and flow-rates. This was done using square-wave anodic stripping voltammetry of 1, 10 and 100 μM Pb(II) solutions. These concentrations were chosen to yield readily measured signals over wide ranges of experimental conditions for the purpose of characterization of the system. They obviously are much higher than those for the practical determination of Pb(II) by anodic stripping. The stripping scan was performed from -0.6 V to -0.2 V. The square-wave parameters of step height, amplitude, and frequency were 5 mV, 25 mV, and 100

Hz, respectively. For the preconcentration of the Pb(II) during the plating step the electrode was held at a potential of −0.6 V. In the automated experiments, the so-called conditioning time, in this case the time between sample injection and the initiation of the voltammetric scan, was incremented from zero seconds to a value at least two times the ratio of volume to flow-rate. Experiments were performed for sample loop volumes of 10, 20, 50, 100, 250, and 500 μl with flow-rates of 0.2, 1.0 and 2.5 ml min^{-1}.

The addition of the shunt valve to this system eliminates the need to analyze the sample in a flowing solution. Therefore flow-rate does not affect directly the square-wave stripping response. The stripping current is determined by the amount of the analyte plated during the deposition step. This dependence of the stripping current on the deposition flow-rate has been described in a number of papers [13–17]. The theoretical dependence expected for wall jet electrode is not often realized in experimental detectors. Thus the effect of the carrier flow-rate on presentation of the sample to the electrode must be empirically determined. In experiments such as anodic or adsorptive stripping, the sample flows past the electrode, which is held at a value of conditioning potential selected to preconcentrate the material at the electrode. The higher the flow-rate the faster this preconcentration step for a given volume injected can be. The carrier solution pump can deliver flow-rates from 0.1 to 5 ml min^{-1}. The effect of flow-rate on sample preconcentration was determined with an automated program that incremented the flow-rate from 0.2 to 3 ml min^{-1}. The value of 3 ml min^{-1} was chosen as the highest value due to instability of the medium mercury drop above this flow-rate. An injection of 100 μl of a 10 μM Pb(II) solution was employed with the electrode held at −0.6 V for 36 s. This conditioning time was sufficient to allow all the material to flow past the electrode at the slowest flow-rates used. A square-wave stripping scan was initiated at the end of the conditioning time.

The reproducibility of a square-wave anodic stripping experiment using the Model 303A was determined for a static cell and for the flow system. The reproducibility in a static cell was determined using a 10 μM Pb(II) solution. The electrode was held at the conditioning potential of −0.6 V in quiescent solution. At the end of a conditioning time of 60 s a square-wave stripping scan was initiated. The experiment was repeated 36 times in the same solution, and each experiment was performed on a different mercury drop. The reproducibility of the flow system was determined using 1, 10 and 100 μM Pb(II) solutions. The conditioning potential was −0.6 V, and the conditioning time was sufficient for all the lead to pass the detector. Experiments were performed for loop volumes of 10–250 μl and flow-rates of 0.2, 1.0 and 2.5 ml min^{-1}. The precision of the measurement was expressed as percent relative standard deviation (% R.S.D.) from the mean of the 16 scans.

Finally the collection efficiency of the flow system with the Model 420/303A detector was determined. The collection efficiency is the ratio of the amount of material converted at the electrode to the amount of material injected into the system. The collection efficiency was determined using solutions of 1.0 and 0.1 mM Pb(II) and the automated chronocoulometry program. The sample was injected into the system, then the potential was stepped to the plating potential of −0.6 V. The charge passed was measured for the entire pulse duration. This experiment was performed for loops of 10, 20, 50, 100, 250, and 500 μl, and for flow-rates of 0.2, 1.0 and 2.0 ml min^{-1}.

RESULTS AND DISCUSSION

The gradient capabilities of the ternary sample pump did not produce a linear dependence of absorbance on concentration. For all ports of the ternary proportioning valve there was a positive deviation in the range of 50% mixing. This method of analyte mixing was not investigated further. All subsequent experiments were performed with discrete, stepwise changes in concentration. Linear dependencies of absorbance on concentration were obtained for the three ports of the ternary proportioning valve at 2.0 ml min^{-1}. The results

TABLE 1

Time required for sample to pass through detector

Loop volume (μl)	Flow-rate (ml min^{-1})	Nominal time (s)	Actual time (s)
10	0.2	3	9
10	1.0	0.6	3
10	2.5	0.24	2
20	0.2	6	15
20	1.0	1.2	3
20	2.5	0.48	2
50	0.2	15	21
50	1.0	3	5
50	2.5	1.2	2
100	0.2	30	36
100	1.0	6	8
100	2.5	2.4	3
250	0.2	75	90
250	1.0	15	21
500	0.2	150	180
500	1.0	30	40

of linear regression for the data for each port are given as the y-intercept (absorbance units) and the correlation coefficient, respectively: port A = -0.0008 ± 0.004, and 0.9999; port B = 0.006 ± 0.001, and 0.9999; port C = 0.0002 ± 0.002, and 0.9999. Linear dependencies for absorbance on concentration were also obtained for flow-rates from 2.0 to 5.0 ml min^{-1}. In all cases, the y-intercept was zero within the accuracy of the line and the correlation coefficients were greater than 0.9995.

The times needed for the samples to pass the detector region are given in Table 1. The automatic program allows conditioning time increments of one second. Thus repetitive measurements with incremented conditioning time are used to identify times after which the peak current no longer increases. For the smallest loops at high flow-rates all the material has passed the electrode in the first few seconds. When using 10- and 20-μl loops a conditioning time of three seconds will ensure that all the material in the loop is being sampled. Extra time is required for these small loops due to the 13-μl volume of the tubing that connects the sample loop to the electrode. For loops larger than 20 μl, a conditioning time of 150% of the ideal time is sufficient.

The effect of flow-rate on the stripping signal is presented in Fig. 2. The stripping signal increases slightly with increasing flow-rate until 1.5 ml min^{-1}, above which it becomes independent of flow-rate. Above 2.5 ml min^{-1} the mercury drops are unstable and can dislodge before the stripping scan is initiated. A flow-rate of 1 ml min^{-1} is a good compromise between time required for an analysis and drop stability.

The design of the Model 420 electrode may be compared with a wall jet configuration. In a wall jet electrode design a jet of solution impinges normally onto an electrode and spreads radially over its surface [13–17]. The theoretical equations relating the current for direct and stripping voltammetry to the flow-rate during deposition have been determined for true wall jet behavior [13–17]. The direct current increases with the 0.75 power of the flow-rate whereas the stripping current decreases with the -0.25 power. Deviations from the predicted wall jet behavior are exhibited by electrode configurations of the wall jet type [16,17]. These deviations are usually attributed to the location of the outlet nozzle within the hydrodynamic boundary layer. The slope of the log–log plot of stripping current vs. flow-rate can have values intermediate between those for various geometries, -0.25 for the wall jet, -0.5

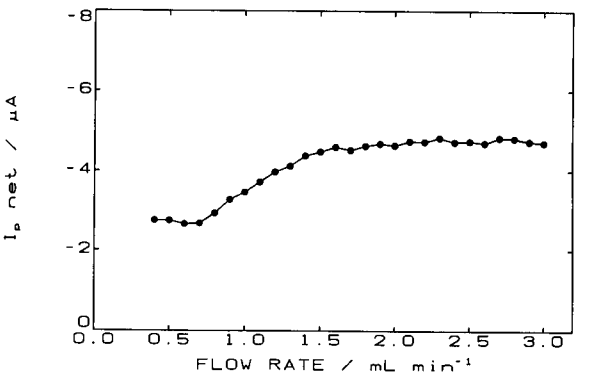

Fig. 2. Flow-rate dependence of peak current. Analyte, 10 mM lead in 0.1 M acetate buffer; 100 μl loop; conditioning time, 36 s; conditioning potential, -0.6 V, $\Delta E_s = 5$ mV; $E_{sw} = 25$ mV; $f = 100$ Hz; $E_i = -0.6$ V; $E_f = -0.2$ V; area = 0.0175 cm^2.

for the disk, and −0.67 for thin-layer electrode behavior. In all cases the slope is negative. Such a plot for the data in Fig. 2 would yield a positive slope. Thus, these equations do not describe the behavior of this electrode system.

The general shape of Fig. 2 was unexpected, but it is not unprecedented [14]. The electrode system in the latter citation is a glassy carbon electrode of wall jet design; however the same increase in current is observed for flow-rates between 0.2 and 0.9 ml min^{-1}. The current decreases with the −0.11 power of flow-rates at higher flow-rates. The instability of the mercury drop at high flow-rates prevented investigation of the PARC 303/420 in this flow region.

The design of the Model 420 flow cell may also be compared with that of the EG&G Model 310 flow cell. The latter was the initial implementation of a flow cell for the EG&G Model 303 SMDE [18]. Flow-injection experiments with normal pulse voltammetric direct detection of Cd(II) yielded flow-rate-independent currents for the regime in which the signal is determined by the pulse width (i.e., sufficiently low flow-rate and long pulse width), but for the regime in which current was controlled by convective mass transport, the signal was proportional to flow-rate [19]. Therefore the comparable stripping signal should be independent of flow-rate, as found here. In our system, the limiting value of current (ca. 4.5 μA, Fig. 2) at higher flow-rates is about that predicted for the peak current for oxidation of Pb(Hg) of the initial uniform concentration corresponding to 1% efficiency (4.0 μA). We return to this point below.

The behavior of the Model 420 is not sensitive to the details of alignments or positioning of the flow cell. That is, routine assembly according to instructions reproducibly yields this result. As response depends only on the flow-rate, this characterization is independent of the particular flow system employed here. Further definition of the hydrodynamics of the Model 420 flow cell is beyond the scope of this work.

The best reproducibility of an anodic stripping peak current of a single quiescent solution in static cell was 0.9% R.S.D. The average precision among a series of eight separate static cell experiments is 1.1% R.S.D. The precision of the static cell, in these experiments, is limited by the reproducibility of the area of the mercury drop. Results obtained for a series of flow cell experiments are presented in Table 2. Results comparable to those from the static cell are obtained for flow-rates of 1 ml min^{-1}. The reproducibility decreases at 2.5 ml min^{-1}, probably due to mechanical instability of the mercury drop. A flow-rate of 1 ml min^{-1} is a reasonable compromise between speed and reproducibility.

TABLE 2

Precision of anodic stripping currents in flow cell

Loop volume (μl)	Flow-rate (ml min^{-1})	%R.S.D.
10	0.2	1.4
	1.0	1.5
20	0.2	1.5
	1.0	0.9
	2.5	4.5
50	0.2	1.2
	1.0	0.9
100	0.2	1.3
	1.0	0.8
	2.5	9.8
250	0.2	1.5
	1.0	1.6

The results of the experiments to determine the collection efficiency of the detector are listed in Table 3. The value of the percent efficiency is the ratio of the number of coulombs for the reduction of Pb(II) from each experiment to the number expected from Faraday's law. In all cases the efficiency was in the range of 1%. This low value of conversion efficiency is typical for "amperometric" detectors [20,21]. The effects of the various flow parameters on current are generally reported for amperometric detectors. We have not found similar reports for effects on collection efficiency.

At a flow-rate of 1 ml min^{-1} the linear flow velocity is about 50 cm s^{-1} and the Reynolds number is about 100. Only under conditions of very low Reynolds number, $Re < 0.5$, does one

TABLE 3

Coulombic efficiency of flow cell [a]

Loop volume (μl)	Flow-rate (ml min^{-1})	Efficiency (%)
10	0.2	0.82 ± 0.01
10	1.0	0.98 ± 0.05
10	2.0	1.09 ± 0.05
20	0.2	0.93 ± 0.01
20	1.0	1.04 ± 0.02
20	2.0	1.15 ± 0.04
50	0.2	0.94 ± 0.01
50	1.0	0.97 ± 0.01
50	2.0	1.03 ± 0.06
100	0.2	0.82 ± 0.07
100	1.0	1.15 ± 0.04
100	2.0	1.27 ± 0.06
250	0.2	0.79 ± 0.12
250	1.0	0.95 ± 0.06
250	2.0	1.02 ± 0.10
500	0.2	0.80 ± 0.05
500	1.0	1.10 ± 0.04
500	2.0	1.0 ± 0.25

[a] Ratio of measured deposition charge to charge equivalent for reduction of all of the analyte in the sample plug.

obtain "creeping flow", that is, flow described by Stoke's law. In the present case, the boundary layer certainly separates from the spherical electrode. One can employ an approximate equation to estimate mass transfer under these conditions [22]:

$$Nu = 2 + 0.6Sc^{1/3}Re^{1/2} \quad (1)$$

where Nu, Sc, and Re are the Nusselt, Schmidt, and Reynolds numbers, respectively. For a flow-rate of 1 ml min^{-1} for this system $Nu = 54$ and the predicted steady state limiting current during the deposition step is 0.39 mA for 10 mM Pb(II). This value leads to coulombic efficiency of 1.2%, which is not unreasonable when compared with the data of Table 3. The data of Table 3 are also consistent with the limiting stripping peak current at higher flow-rates of Fig. 2, as mentioned above.

It may be useful to point out that the deposition charge is obtained from Eqn. 1 by multiplying by the nominal deposition time, $t_d = V_s v^{-1}$, where t_d is the deposition time, V_s is the volume of the sample loop, and v is the volume flow-rate, respectively. Thus Eqn. 1 predicts that stripping peak current and coulombic efficiency should vary as $v^{-1/2}$.

Conclusions

The main goal of this work was to design and characterize an automated sampling handling system that would improve the efficiency of electrochemical studies. A secondary objective was to characterize the PARC Model 303/420 detector. This flow system with its automated experimental parameter adjustment, automated stop flow and blank subtraction and online analysis of the voltammograms, can be used to perform intensive investigation of electrochemical systems without the investment time necessary using manual operations. We have evaluated the accuracy and reproducibility of the system in conjunction with the PARC 303A/420 detector and shown that the uncertainty in the magnitude of the response is dominated by the variation in drop size of the SMDE and is unaffected by detector assembly, the proportioning pump, or the injection system.

The efficiency of the detector is about 1% at a flow-rate of 1 ml min^{-1}. Sensitivity is somewhat larger at higher flow-rates, but transfer of momentum to the drop, resulting in mechanical instability, also is increased. Thus 1 ml min^{-1} is a reasonable compromise between stability, sensitivity and throughput. The stripping peak current does not depend on flow-rate as does a wall jet ($i_p \propto v^{-1/4}$) or a thin-layer detector ($i_p \propto v^{-2/3}$). It is independent of flow-rate at the higher flow-rates, which has some analytical advantage.

Detection with stopped flow provides ideal conditions for medium exchange and for both analytical and physical chemical investigations of chemical species adsorbed or otherwise deposited on the electrode surface.

This work was supported in part by the National Science Foundation under Grants numbers CHE9024846 and CHE9208987, by donations of equipment from EG&G PARC, and by financial support for L.A.M. through an IBM Manufacturing Research Fellowship.

REFERENCES

1 J. Ruzicka and E.H. Hansen, Anal. Chim. Acta, 78 (1975) 145.
2 R. Appelqvist, G.R. Beecher, H. Bergamin, G. den Boef, J. Emneus, Z. Fang, L. Gorton, E.H. Hansen, P.E. Hare, J.M. Harris, J.J. Harrow, N. Ishibashi, J. Janata, G. Johansson, B. Karlberg, F.J. Krug, W.E. van der Linden, M.D. Luque de Castro, G. Marko-Varga, J.N. Miller, H.A. Mottola, H. Muller, G.E. Pacey, C. Riley, J. Ruzicka, R.C. Schothorst, K.K. Stewart, A. Townshend, J.F. Tyson, K. Ueno, M. Valcarcel, J. Vanderslice, P.J. Worsfold, N. Yoza and E.A.G. Zagatto, Anal. Chim. Acta, 180 (1986) 1.
3 J. Ruzicka and E.H. Hansen, Anal. Chim. Acta, 179 (1979) 1.
4 J. Ruzicka, Analyst, 115 (1990) 475.
5 J Ruzicka, Anal. Chem., 55 (1983) 1040A.
6 M. Valcarcel and M.D. Luque De Castro, Flow Injection Analysis, Wiley, New York, 1987.
7 J. Ruzicka and E.H. Hansen, Flow Injection Analysis, Wiley, New York, 1981.
8 L. T. Skeggs, Anal. Chem., 38 (1966) 107.
9 N. Thorgersen, J. Janata and J. Ruzicka, Anal. Chem., 55 (1983) 1986.
10 F. Canete, A. Rios, M.D. Luque De Castro and M. Valcarcel, Anal. Chim. Acta, 211 (1988) 287.
11 J.G. Osteryoung and J.J. O'Dea, in A.J. Bard (Ed.), Electroanalytical Chemistry, Vol. 14, Marcel Dekker, New York, 1986, p. 209.
12 Gmelins Handbook, Vol. 58, Verlag Chemie, Weinheim, 1964, p. 355.
13 J. Yamada and H. Matsuda, J. Electroanal. Chem., 44 (1973) 189.
14 J.M. Elbicki, D.M. Morgan and S.G. Weber, Anal. Chem., 56 (1984) 978.
15 H.B. Hanekamp and H.G. de Jong, Anal. Chim. Acta, 135 (1982) 351.
16 J. Wang and H.D. Dewald, Anal. Chim. Acta, 162 (1984) 189.
17 H. Gunasingham, K.P. Ang, C.C. Ngo and P.C. Thiak, J. Electroanal. Chem., 198 (1986) 27.
18 S. Vohra, Am. Lab., 13 (1980) 66.
19 R. Samuelsson and J. Osteryoung, Anal. Chim. Acta, 123 (1981) 97.
20 D.C. Johnson, S.G. Weber, A.M. Bond, R.M. Wightman, R.E. Shoup and I.S. Krull, Anal. Chim. Acta, 180 (1986) 187.
21 K. Stulik and V. Pacakova, Electroanalytical Measurements in Flowing Liquids, Wiley, New York, 1987.
22 R.S. Brodkey and H.C. Hershey, Transport Phenomena, McGraw-Hill, New York, 1988. p. 599.

Analytica Chimica Acta, 281 (1993) 35–43
Elsevier Science Publishers B.V., Amsterdam

Amperometric and colorimetric enzyme immunoassay for urinary human serum albumin using a plasma-treated membrane

Shigeki Kaku, Setsuko Nakanishi [1] and Kazuo Horiguchi

Research Laboratory, Susumu Co., Ltd., 14 Kamitoba Umamawashi-cho, Minami-ku, Kyoto 601 (Japan)

Masanori Sato

Faculty of Textile Science, Kyoto Institute of Technology, Kyoto (Japan)

(Received 25th January 1993; revised manuscript received 4th March 1993)

Abstract

By water vapour plasma glow discharge treatment, microporous hydrophobic polypropylene film was modified to make it partially hydrophilic. The plasma-treated part was a spot 6 mm in diameter and permeable to water. After treatment with octamethylenediamine and glutaraldehyde, the plasma spot membrane served as a substrate to immobilize proteins such as antibodies or enzymes. Using this membrane, an amperometric enzyme immunoassay system was established to determine human serum albumin (HSA) in urine. The measurable range with this system was from 0.5 to 100 mg l^{-1} HSA in urine, which is suitable for the prognosis of diabetic nephritis. The HSA values in urine samples determined by the present system showed a linear correlation with those obtained by radioimmunoassay ($r = 0.974$). After keeping the antibody-immobilized plasma spot membranes at 4°C for 6 months, the same calibration graph for HSA determination was obtained. In addition, a colour-producing reaction was also performed on the immunoreacted plasma spot membrane. Reflectance spectrometric analysis demonstrated that the colour on the plasma spot membrane itself corresponded to the HSA concentration. The difference in colour between 10 and 100 mg l^{-1} HSA could be visually discerned.

Keywords: Amperometry; Enzymatic methods; UV–Visible spectrophotometry; Human serum albumin; Urine

In geriatric disorders, much attention has to be paid to the possibility of diabetic nephritis. A slightly elevated level of human serum albumin (HSA) in urine can be a diagnostic marker of this disease [1]. The excretion of serum albumin (HSA) in urine at this level (20–100 mg l^{-1}) is defined as microalbuminuria. In diabetic patients with no symptoms of clinical nephropathy, microalbuminuria is possibly of prognostic value [1–4]. The determination of urinary HSA has been done by radioimmunoassay (RIA), while some non-isotopic methods such as enzyme-linked immunosorbent assay (ELISA) [5], measurement of gravimetric changes with a piezoelectric crystal [6], detection of chemiluminescence with a glass fibre [7] and amperometry using an immunoelectrode [8] have been reported. A number of immunosensors and immunoelectrodes have been developed in the past two decades, but only a limited number of them have been applied for the measurement of biological fluids.

Correspondence to: S. Kaku, Research Laboratory, Susumu Co., Ltd., 14 Kamitoba Umamawashi-cho, Minami-ku, Kyoto 601 (Japan).

[1] Present address: Pharmaceutical Basic Research Laboratories, Japan Tobacco Inc., Yokohama, Japan.

A surface modification technique using plasma discharge has been developed. By this technique the hydrophobic surface of a microporous polypropylene film became partially hydrophilic, which could serve as a membrane substrate for the immobilization of proteins. The measurement of insulin in serum [9] and HSA [10] using an enzyme-immunoelectrode with such a plasma-treated membrane has been reported previously. In the previous report on the determination of HSA, a system with a satisfactory range to measure urinary HSA was presented. In this study, this amperometric system was applied to measure HSA in urine samples with a view to clinical assays. The correlation between this system and an RIA system, the specificity for HSA and the stability of the antibody-immobilized plasma spot membrane were examined. The results showed the reliability of this system in clinical application. In addition a colorimetric enzyme immunoassay for HSA was developed by using visual detection.

EXPERIMENTAL

Materials and reagents

Hydrophobic microporous polypropylene film (Celgard No. 2500 from Celanese) (thickness 25 μm maximum pore size 0.04×0.4 μm, porosity 45%) was used as a substrate membrane for the immobilization of proteins. Human serum albumin (globulin free), glucose oxidase (GOD, type VII, from *Aspergillus niger*), bovine serum albumin (BSA, fraction V, RIA grade), human γ-globulin (G-4386), 2-mercaptoethylamine, octamethylenediamine (1,8-diaminooctane), Tween 20 (polyoxyethylene sorbitan monolaurate), concanavalin A (type VII) and phenazine methosulphate (PMS) were obtained from Sigma. *N*-(ϵ-Maleimidocaproyloxy)succinimide (EMCS) and 3-(*p*-iodophenyl)-2-(*p*-nitrophenyl)-5-phenyl-2*H*-tetrazolium chloride (INT) were obtained from Dojindo Labs. Glutaraldehyde (grade for electron microscopy), β-D-glucose and other chemicals of analytical-reagent grade were purchased from Nakalai Tesque.

Rabbit antiserum against HSA was obtained by multiple subcutaneous injection in the back of rabbits with 1 mg of HSA in complete Freund's adjuvant four times during 2 months and boosted using Freund's incomplete adjuvant.

Equipment

Amperometric measurement of GOD activity was performed by using a Yanako p-8 polarograph with a Pt–AgCl electrode (a gift from Horiba). Colorimetric determination was carried out using a spectrophotometer equipped with a cell for reflectance spectrometry (IMUC-7000 multi-channel photodetector; Photal Otsuka Electronics).

Preparation of glucose oxidase-labelled HSA

GOD-labelled HSA was prepared by the maleimide method [11,12]. Details of the procedure have been reported in a previous paper [10]. Briefly, three or four maleimide groups were introduced into a GOD molecule with EMCS. A thiol group was introduced into HSA by treating it with 2-mercaptoethylamine. Both protein solutions were mixed and incubated at 4°C for 2 h. Remaining maleimide groups were blocked by 0.1 M mercaptoethylamine. The conjugate was purified by gel chromatography with Sephadex G-150. A GOD–HSA conjugate free of HSA was obtained by further purification using concanavalin A affinity chromatography. Characterization of the conjugate by gel filtration and gel electrophoresis showed that the binding ratio of GOD to HSA was 1 : 1. The absorbance of this conjugate solution was 0.189 at 280 nm and 0.020 at 450 nm due to GOD. By examination with crossed immunoelectrophoresis and immunoblotting, it was confirmed that the conjugated HSA retained its immunoreactivity as an HSA antigen.

Preparation of antibody-immobilized plasma spot membrane

The Celgard film was produced by biaxial stretching forming a microporous fibrous structure. Intact Celgard film has hydrophobic characteristics, hence water cannot penetrate through the film and no functional groups for immobilization of proteins are present on its surface.

A partial modification of its surface to make it hydrophilic was achieved by plasma treatment. A schematic diagram of the equipment for the plasma treatment is shown in Fig. 1. In a glass bell-jar, two parallel electrodes made of aluminium (area 180 × 180 mm and thickness 1 mm) were placed at a distance of 180 mm. These electrodes were connected to a 5-kHz power supply. Celgard film (180 × 180 mm) was sandwiched between two aluminium masks (180 × 180 mm, thickness 4 mm) which had 64 holes 6 min in diameter, and then it was set in the centre of the two parallel electrodes. These masks with Celgard film were connected to earth. After evacuating to less than 10^{-3} Torr, water vapour was introduced into the bell-jar and glow discharge treatment was carried out at 42 W power for 5 min under a pressure at 0.5 Torr. After this treatment, only the unmasked part 6 mm in diameter could be penetrated by water, because after the plasma treatment only the surface of the spot had become hydrophilic by the introduction of carbonyl groups [9,10]. Observation of its surface after plasma treatment with a scanning electron microscope showed that the micropores had become slightly enlarged [10]. The plasma-treated Celgard film was handled as a whole sheet for further treatment and finally cut into 64 squares just before being attached to the electrode surface for amperometry. Each square contained one spot, hence it was termed a "plasma spot membrane".

After the plasma treatment, the film was dipped into 0.3% (w/v) octamethylenediamine

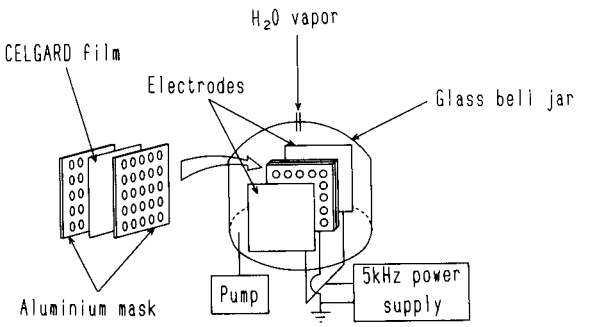

Fig. 1. Schematic diagram of the equipment for plasma treatment.

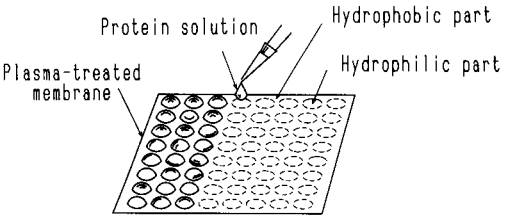

Fig. 2. Immobilization of protein on the plasma spot membrane. The membrane was placed on a table having holes arranged at the same intervals as the spots.

solution for 5 min. It was sandwiched between two sheets of filter-paper in order to remove excess solution and dried in air for 10 min. Subsequently it was immersed in 5% (v/v) glutaraldehyde solution at 4°C overnight. The film was thoroughly washed with distilled water to remove excess of glutaraldehyde. Chemical characterization of its surface during each step of the treatment for the immobilization of proteins by infrared spectrometry has been reported in previous papers [9,10]. After the treatment with octamethylenediamine and glutaraldehyde, the plasma spot membrane had aldehyde groups on its surface. Proteins were immobilized covalently on the surface with these aldehyde groups.

The film was placed on a perforated table having 64 holes 12 mm in diameter and then the protein solution was dropped on each spot as shown in Fig. 2. Outside of the area of the spots the surface remained hydrophobic after pretreatment for immobilization, hence the drops were kept on the spots. A solution of 20 μl of antiserum diluted 150-fold in 0.15 M phosphate-buffered saline (PBS) (pH 7.2) was dropped on each spot and incubated at 4°C overnight. Then, 20 μl of 0.3% (w/v) BSA solution were applied at 25°C for 2 h. After each treatment with protein solution the film was washed with 0.15 M PBS (pH 7.2). All incubations were carried out in a moisture chamber.

Immunoreaction on the plasma spot membrane

A competitive reaction between GOD–HSA and HSA in a given sample was performed on the antibody-immobilized plasma spot membrane as follows.

The standard HSA sample [0, 2, 4, 8, 40, 80 mg l^{-1} in 0.15 M PBS (pH 7.2)] or urine sample containing an unknown amount of HSA was mixed with 20-fold diluted GOD–HSA at a ratio of 1:1 (v/v). Urine samples were mixed directly without dilution. Volumes of 50 μl of the mixtures were dropped on the antibody-immobilized spot membranes and incubated at 25°C for 30 min. The immunoreaction was stopped by washing the membrane with 0.15 M PBS (pH 7.2) containing 0.05% (v/v) Tween 20.

Amperometric determination of HSA

GOD activity fixed on the membrane after the immunoreaction was measured by amperometry using a hydrogen peroxide electrode made of Pt–AgCl (0.65 V was applied) as shown in Fig. 3. The immunoreacted plasma spot membrane was attached to the centre of the Pt electrode with a Teflon ring and immersed in a vessel containing 15 ml of 0.15 M PBS (pH 5.8) with stirring at 450 rpm at 25°C. After adding 0.25 ml of 200 mg ml^{-1} β-D-glucose solution, the current due to hydrogen peroxide generated by the enzymatic reaction was saturated within 30 s. The relative standard deviation (R.S.D.) of the same membrane immobilized with GOD was 3.5% ($n = 50$). The current data obtained were converted into B/B_0 according to the following equation, so that a calibration graph for HSA was obtained:

$$B/B_0(\%) = (I_x/I_0) \times 100$$

where I_x = current given by x mg l^{-1} HSA and I_0 = current in the absence of HSA. The concentration of HSA in unknown samples was determined from this calibration graph.

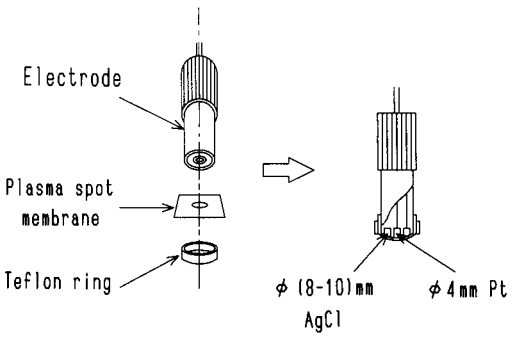

Fig. 3. Design of the H_2O_2 electrode for amperometric measurement with the plasma spot membrane. The membrane was set on the electrode with a Teflon ring. The thin and flexible membrane made good contact with the convex surface of the electrode.

Colorimetric determination of HSA

For colorimetric determination, a GOD immunoenzyme stain [13] was performed on the plasma spot membrane. The substrate solution containing 0.75% (w/v) β-D-glucose, 0.05% (w/v) INT and 0.01% (w/v) of PMS in 0.15 M sodium phosphate buffer (pH 6.8) was prepared each day.

After amperometric measurement of GOD activity, 50 μl of the substrate solution for colorimetry was dropped on the spot and incubated at 25°C for 12 min and then it was washed with 0.15 M PBS (pH 6.8). GOD activity of GOD–HSA fixed on the plasma spot membrane catalysed the decomposition of β-D-glucose to gluconic acid and hydrogen peroxide. PMS worked as a electron carrier and INT was reduced, giving a violet substance that precipitated on to the micropores of the plasma spot membrane. After rinsing with water and drying, colorimetry was performed by measuring the absorbance at 568 nm by reflectance spectrometry with the IMUC-7000 system.

RESULTS AND DISCUSSION

Reproducibility of the immobilization of proteins and amperometric measurement with plasma spot membrane

The main possible factors that might affect the reproducibility of the assay system were the following: (i) distribution of micropores in the intact Celgard film; (ii) reproducibility of the immobilization and immunoreaction processes; (iii) uniformity among the 64 spots in the same film and among different films in different plasma treatment batches; and (iv) accuracy of amperometric measurement.

Concerning (i), the gas permeability of the spot of intact film (6 mm in diameter) was measured. The R.S.D. was 4.6% ($n = 16$).

Concerning (ii) and (iii), the evaluation was done by amperometric measurement of immobilized GOD activity. The immobilization of GOD was effected as follows: the plasma-treated Celgard film was treated with octamethylenediamine and glutaraldehyde. To compare the individual immobilization with batch immobilization, the plasma spot membrane was immersed in the bulk GOD solution. After incubation at 4°C for 8 h, the GOD activity was measured by amperometry. The R.S.D. among the spots was 5.5% ($n = 12$). The individual immobilization by dropping 50 μl of GOD solution on each spot gave an R.S.D. of 7.0% among the 64 spots in the same film. The R.S.D. among plasma-treated films was 8.1% ($n = 12$). As the batch immobilization requires a large volume of protein solution (about 50 ml for one sheet having 64 spots) compared with that required for individual immobilization (3.2 ml for 64 spots), the individual immobilization can be useful for saving valuable reagents such as antibodies.

Concerning (iv), the surface of the H_2O_2 electrode was given a curved shape (radius of curvature $R = 22$ mm). Such a slightly convex surface of the electrode was helpful in ensuring good contact with the thin and flexible plasma spot membrane. The R.S.D. of the amperometric measurement of the same membrane immobilized with GOD was 4.2% ($n = 50$).

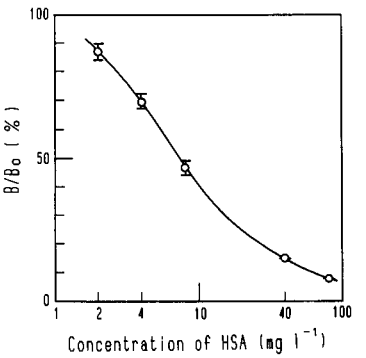

Fig. 4. Calibration graph for human serum albumin measured by amperometry with the plasma spot membrane.

Amperometric determination of HSA

A typical calibration graph for HSA is shown in Fig. 4 with the measurable range of HSA from 2 to 80 mg l^{-1}. In a normal body, the concentration of serum albumin is 1.5–17 mg l^{-1} in 24-h urine [1]. In cases of microalbuminuria the concentration of HSA in urine is 20–100 mg l^{-1}. Hence this measurable range was adequate for the prognosis of diabetic nephritis.

The effect of reaction time on the competitive immunoreaction of HSA or GOD–HSA with antibody immobilized on the plasma spot membrane was examined for reaction times of 5, 10

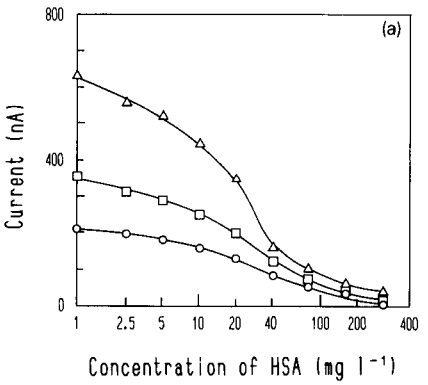

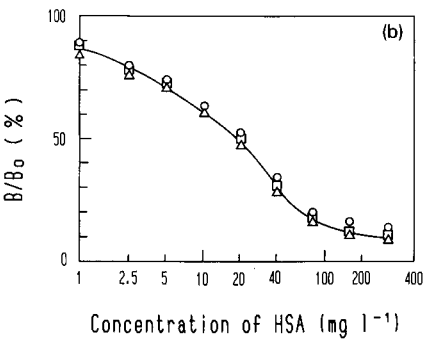

Fig. 5. Effect of competitive immunoreaction time on the calibration graphs for HSA. ○ = 5 min; □ = 10 min; △ = 30 min. Calibration graphs for (a) current vs. concentration and (b) B/B_0 vs. concentration.

TABLE 1

Within-day variation of the amperometric assay of HSA

Urine sample No.	HSA concentration (mg l^{-1})						R.S.D. (%)
	Individual assays [a]					Mean	
1	4.4	4.4	4.1	4.2	4.7	4.4	4.7
2	15.7	15.2	14.6	12.2	11.4	13.8	12.3
3	17.2	16.5	14.6	14.5	15.8	15.7	6.7
4	15.2	15.0	15.8	14.3	16.1	15.3	4.1
5	33.0	33.0	25.3	28.5	28.0	29.6	10.2

[a] Performed in one day.

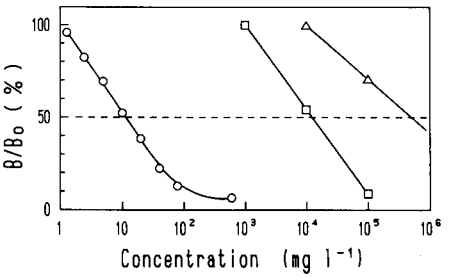

Fig. 6. Calibration graphs for (○) HSA, (□) human γ-globulin and (△) bovine serum albumin. Human γ-globulin and bovine serum albumin did not cross-react with HSA in the present assay system.

and 30 min. Three calibration graphs expressed as amperometric current and B/B_0 vs. HSA concentration are shown in Fig. 5. When the reaction was carried out in a shorter time, the current became lower, but all calibration graphs with B/B_0 were the same. It was possible to carry out the reaction in 5 or 10 min, but the reaction time was fixed at 30 min.

To examine the accuracy of the determination of HSA with this system, 50 pieces of the plasma spot membranes immunoreacted with 10 mg l^{-1} standard HSA sample were measured. The R.S.D. was 7.6%. The measurement of five urine samples was carried out five times on the same day. Five pieces of the plasma spot membrane for each urine sample were used in one assay. The within-day R.S.D.s are given in Table 1. These five different urine samples were also measured every 4 days. The between-day R.S.D.s are given in Table 2; the mean is 6.3%.

Non-specific adsorption in the system was examined by applying GOD–HSA to the plasma spot membranes treated with octamethylenediamine and glutaraldehyde but without antibody. Such membranes gave only 4.4% of the current I_0 given by the usual antibody-immobilized membrane.

The specificity of the system for HSA was tested as follows. Instead of HSA, human γ-globulin or BSA was mixed with GOD–HSA and reacted with anti-HSA antibody immobilized on the plasma spot membrane. After the reaction, GOD activity was measured by amperometry. The curves obtained are shown in Fig. 6. The concentrations at 50% of B/B_0 of human γ-globulin and BSA were 10^4 and 10^6 mg l^{-1}, respectively. Hence the system did not cross-react with human γ-globulin or BSA.

Possible effects of reductive materials on this system were checked by measuring HSA after adding large amounts of creatine or creatinine to the urine sample. Neither a 1000-fold amount of creatine nor a 100-fold amount of creatinine in normal urine interfered with the assay of HSA in this system. A 20-fold amount of ascorbic acid in normal urine also did not affect the assay.

To examine the accuracy of this assay system, a recovery test was carried out by adding HSA solution (2.5, 5.0, 10.0 and 20.0 mg l^{-1}) to two urine samples. The results are given in Table 3. Almost 100% recovery was attained, demonstrating that with the present system HSA could be measured correctly and selectively.

To confirm the reliability of this amperometric system with the plasma spot membrane, urine samples collected from 19 subjects were mea-

TABLE 2

Between-day variations of the amperometric assay of HSA

Urine sample No.	HSA concentration (mg l^{-1})					R.S.D. (%)
	Individual assays [a]				Mean	
1	3.8	4.4	4.7	4.5	4.4	7.7
2	15.5	13.8	17.0	15.8	15.5	7.4
3	15.8	15.7	15.0	17.2	15.9	5.0
4	15.0	15.3	15.8	15.4	15.4	1.9
5	29.0	29.6	34.8	33.5	31.7	7.8

[a] Each performed on a different day.

TABLE 3

Recovery test in the amperometric assay of HSA

Urine sample No.	HSA added (mg l^{-1})	Assay result (mean ± S.D.) [a] (mg l^{-1})	Difference (mean ± S.D.) [a] (mg l^{-1})	Recovery (%)
6	0.0	6.2 ± 0.8	–	
	2.5	8.7 ± 1.3	2.5 ± 1.6	100.0
	5.0	11.3 ± 1.5	5.1 ± 1.7	100.9
	10.0	17.2 ± 4.4	11.0 ± 4.5	106.2
7	0.0	8.6 ± 0.4	–	
	2.5	11.5 ± 0.9	2.9 ± 1.1	103.6
	5.0	14.4 ± 0.5	5.8 ± 0.8	105.9
	10.0	19.0 ± 1.0	10.4 ± 1.1	102.0

[a] $n = 8$.

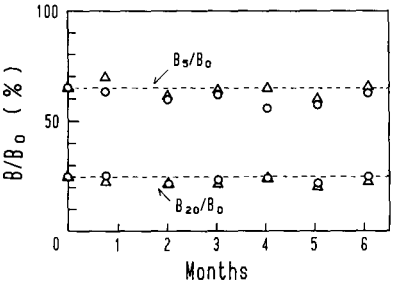

Fig. 7. Stability of calibration graph during storage of the antibody-immobilized plasma spot membrane for 6 months under (○) dry or (△) wet conditions at 4°C. The variations of B_5/B_0 and B_{20}/B_0 are shown.

sured with this system and an RIA system. The present system gave slightly higher value than that obtained by RIA, but good linearity was obtained between the two systems: $y = ax + b$, where $a = 1.58$ and $b = 1.13$ in the low range of HSA (0–5 mg l^{-1}), with regression coefficient $r = 0.903$, and $a = 1.42$, $b = 0.947$ in the high range of HSA (5–80 mg l^{-1}), with $r = 0.974$. The same urine samples were measured with a turbidimetric immunoassay (TIA) system kit (Fujimoto Pharmaceutical), which is one of the few commercially available non-isotopic systems for the determination of HSA. Between the present system and TIA, the results can be correlated by the equation $y = ax + b$ where $a = 0.864$, $b = 3.79$ and $r = 0.969$ in the range of 10–80 mg l^{-1} HSA. For the correlation between values obtained by RIA and TIA, the values by TIA were higher than those by RIA ($a = 1.611$, $b = -2.34$ and $r = 0.991$). Hence the values given by the present system coincided with those obtained by TIA rather than those obtained by RIA. The reason why RIA gave higher values than our system or TIA could not be elucidated.

The stability of the antibody-immobilized plasma spot membrane was tested during storage under wet and dry conditions at 4°C for 6 months. Nine membranes were selected for each test and used to obtain a calibration graph by measuring samples containing 0, 5 and 20 mg l^{-1} of HSA. The variations of B_5/B_0 and B_{20}/B_0 in each test are shown in Fig. 7. Regardless of the humidity during storage, the values of B/B_0 remained stable, hence the antibody-immobilized plasma spot membrane may give a constant calibration graph.

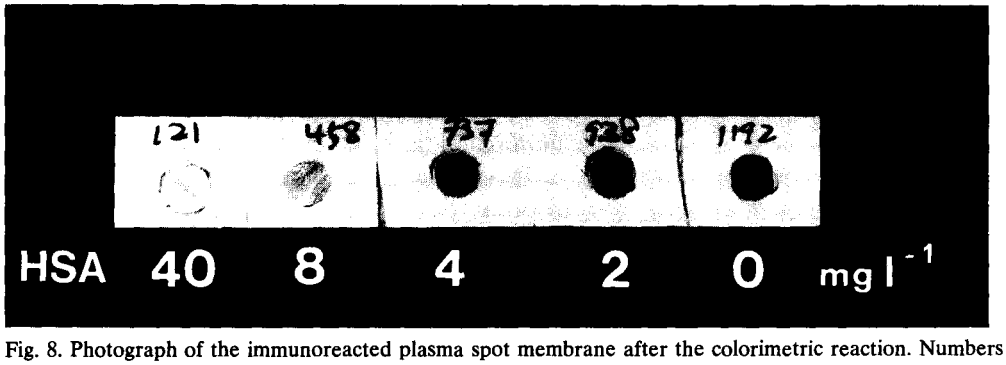

Fig. 8. Photograph of the immunoreacted plasma spot membrane after the colorimetric reaction. Numbers marked on the plasma spot membrane indicate current (nA) measured by amperometry.

Colorimetric assay of HSA

The intact Celgard film was white and the colour did not change during the plasma treatment and the immobilization of proteins. After amperometric determination, the immunoreacted plasma spot membranes were used for colorimetric measurement.

On reaction with the substrate solution including the reagents for colorimetric reaction, the plasma spot membrane changed colour. A photograph of the immunoreacted plasma spot membranes after the colorimetric reaction is shown in Fig. 8. The spots which had reacted with a few mg l^{-1} of HSA were stained deep violet and those which had reacted with high concentrations of HSA became pale pink, scarcely distinguishable from the white colour of the intact Celgard film. WHen the competitive immunoreaction time was 5 or 10 min, the intensity of the colour among the spots was visually indistinguishable.

The stained spots were measured by reflectance spectrometry. The correlation between the current obtained by amperometric measurement of GOD activity and absorbance at 568 nm is shown in Fig. 9. A linear relationship was obtained with a correlation coefficient $r = 0.9723$. The calibration graph obtained for HSA by colorimetry is shown in Fig. 10. Compared with the calibration graph by amperometry, this graph had an inflection point around 20 mg l^{-1}. This is advantageous for checking kidney disorders, because this value corresponds to the threshold for judging whether the kidney functions well or not. This makes it possible to judge visually the change in HSA concentration in urine.

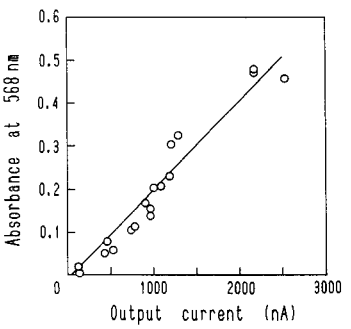

Fig. 9. Correlation between the current obtained by amperometric measurement of GOD activity and absorbance at 568 nm measured by reflectance spectrometry.

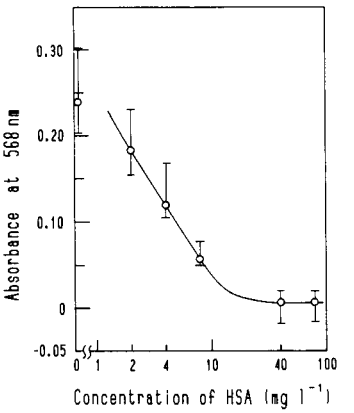

Fig. 10. Calibration graph for HSA by colorimetry.

This coloured substance was fixed by dropping 50 μl of Lillie's neutral buffered formalin solution [100 ml of 37% (v/v) formaldehyde containing 4.0 g of $NaH_2PO_4 \cdot H_2O$ and 12.2 g of $Na_2HPO_4 \cdot 7H_2O$]; the colour was retained for several months. The human eye generally has the highest sensitivity for a change in reddish purple. Other tetrazolium salts (e.g., nitrotetrazolium blue, which formed a blue complex) were also tested, but the colour given by INT was the easiest to distinguish.

In clinical analysis, semi-quantitative analytical methods can serve for screening samples and for checking certain health conditions in the home. Some systems have been introduced, such as test papers for glucose or human chorionic gonadotropin in urine. A test paper for checking proteins in urine is available, but it cannot detect small amounts of HSA selectively in urinary proteins, because it does not depend on the immunoreaction.

This work is a preliminary attempt at a visual colorimetric enzyme immunoassay for small amounts of biological substances. In order to achieve an in situ colorimetric enzyme immunoassay, i.e., where the coloured products can be fixed on the substrate itself, it might be necessary for the substrate to have a large surface area to

retain the coloured product to be detected in a sufficiently homogeneous amount. The coloured area must be contrasted effectively with the colour of the surroundings. Although some problems remain to be solved in the assay system itself, e.g., shortening of the time for immunoreaction, the plasma spot membrane seems to satisfy these requirements.

In conclusion, the plasma spot membrane with a partially hydrophilic part, generated by the treatment with a water vapour plasma glow discharge, is suitable as a substrate for an enzyme immunoassay. The feasibility of an amperometric enzyme immunoassay system using the plasma spot membrane was studied for the measurement of serum albumin in urine. Using the same membrane, a colorimetric enzyme immunoassay system was attempted. The results showed that both systems may be applicable to the clinical assay of microalbuminuria.

We thank Drs. T. Kono, K. Usui, T. Aomi of Horiba (Kyoto) and Dr. M. Nishimura of Shionogi (Osaka) for their collaboration.

REFERENCES

1 U. Di Mario, P. Pietravalle, A. Napoli, S. Morano, M. Mancuso, S. Gambardella and D. Andreani, Horm. Metab. Res., 18 (1986) 689.
2 G.C. Viverti, H. Keen, J.C. Pickup and R.W. Bilous, Acta Endocrinol. (Suppl.), 242 (1981) 59.
3 G.C. Vibeti, R.D. Hill, R.J. Jarret, A. Argyropoulos, U. Mahmud and H. Keen, Lancet, i (1982) 1430.
4 C.E. Mogensen, N. Engl. J. Med., 310 (1984) 356.
5 A. Puri, R. Casburn-Budd, V. Eisen and J.D.H. Slater, Clin. Chem., 31 (1985) 1214.
6 E. Prusak-Sochaczewski and J.H.T. Luong, Anal. Lett., 23 (1990) 401.
7 T. Hara, K. Tsukagoshi, A. Arai and Y. Imashiro, Bull. Chem. Soc. Jpn., 62 (1989) 2844.
8 R. Mattiasson and H. Nillson, FEBS Lett., 78 (1977) 251.
9 S. Kaku, S. Nakanishi and K. Horiguchi, Anal. Chim. Acta, 225 (1989) 283.
10 S. Kaku, S. Nakanishi, K. Horiguchi and M. Sato, Anal. Chim. Acta, 272 (1993) 213.
11 E. Ishikawa, M. Imagawa, S. Hashida, S. Yoshitake, Y. Hamaguchi and T. Ueno, J. Immunoassay, 4 (1983) 209.
12 K. Kusai, I. Sekuzu, B. Hagihara, K. Okunuki, S. Yamauchi and M. Nakai, Biochim. Biophys. Acta, 40 (1960) 555.
13 D.D. Porter and H.G. Porter, J. Immunol. Methods, 72 (1984) 1.

Analytica Chimica Acta, 281 (1993) 45–51
Elsevier Science Publishers B.V., Amsterdam

High speed potentiometric analyzer equipped with an ion-selective electrode detector

Hirokazu Hara, Nobuhiro Ishio and Kazunori Takahashi

Department of Chemistry, Faculty of Education, Shiga University, Otsu, Shiga 520 (Japan)

(Received December 7th 1992; revised manuscript received 15th February 1993)

Abstract

A new type of microcomputer-controlled potentiometric flow-analysis system has been developed. It utilizes the very fast response of an ion-selective electrode when standard and sample solutions alternately flow past the electrode surface at high flow-rates (ca. 2.0 m s^{-1}). The switchover of the solenoid valves for a solution change and the data acquisition are performed by the microcomputer. Regardless of the concentration, it was possible to reduce the analysis time for one sample to 1.2–1.3 s as demonstrated with a solid-state chloride ISE. The repeatability for ten samples of a concentration was within 2% in the concentration range of 10^{-2} mol dm^{-3} to 10^{-4} mol dm^{-3}. This system was applied to the determination of chloride in beverages.

Keywords: Flow system; Potentiometry; Ion selective electrodes; Beverages; Chloride

One of the major subjects for modern analytical chemistry is to develop an analytical method which enables analysis to be performed as rapidly as possible. Flow injection analysis (FIA) seems to be an excellent solution to this problem. For example, Van Staden reported the flow-injection analysis of water using a coated tubular solid-state chloride selective electrode [1], and a sample throughput rate of about 120 h^{-1}. Borzitsky et al. [2] also proposed a fast-response flow cell and achieved a sampling rate of 480 h^{-1} with a chloride selective electrode. Such a high sampling rate is partly due to the very fast response (3–4 s for 95% response [1]) of the ion-selective electrode (ISE).

On the other hand, studies of the dynamic response of ISEs have revealed that some ISEs show a very fast response for an instantaneous change in the ionic concentration at the electrode surface (which is called the activity step method) [3]. Lindner et al. [4] recorded the potential–time curve of an AgI-based iodide-selective electrode using an improved switched wall-jet type measuring system. The response time for the step change in iodide activity from 10^{-2} M to 10^{-3} M was reported to be 100 ms or less [4,5]. The reason for the rapid response is the relatively high linear flow-rates (1.5–3.7 m s^{-1}) at the electrode surface, which contribute to the decrease in the diffusion layer [5]. The rapid response of ISEs has been reported not only on precipitate based electrodes but also on liquid membrane electrodes and ionophore based polymer membrane electrodes [5–7].

In this paper, we tried to develop a new type of flow-analysis system which utilizes the fast response of ISEs. Unnecessary sample dilution, which is often encountered in FIA, could be avoided by flowing directly and alternately with standard and sample solutions across the electrode surface. We labeled this system the high

Correspondence to: H. Hara, Department of Chemistry, Faculty of Education, Shiga University, Otsu, Shiga 520 (Japan).

speed potentiometric analyzer (HSPA) because it enables the determination of individual samples within 1–2 s. A solid-state chloride ISE was used to demonstrate the usefulness of the system for practical applications.

EXPERIMENTAL

Apparatus

A solid-state chloride ISE (Orion 94-17B) was used together with a double-junction type reference electrode (Orion 90-02-00). The outer filling solutions were 1 M potassium nitrate. The potential values were measured with a digital ion meter (Orion 901) and transmitted every 10 ms into a microcomputer (NEC PC9801 DX; CPU 16 bit Intel 80286, 12 MHz) through a digitizer (Autonics, Tokyo; APC204, 12 bit A/D converter). The response time curve was displayed on a CRT and also plotted by an *X–Y* plotter (Roland DG, DX-1100). A programmable I/O interface board having 16 small relay units (I O Data Kiki, Kanazawa; PIO-9042) was used for controlling the switchover of the solenoid valves (MTV-21-M6 and MCV-3R-M6F; Takasago Electronic; Nagoya). The opening or shutting time of the solenoid valves is in the range of 5–20 ms. A roller pump (Cole-Parmer, Chicago, IL; Masterflex 7553–20) equipped with two pump heads and Tygon tubes (1.7 × 4.9 mm) was used to flow the base and sample solutions alternately to the electrode surface. A laboratory made wall-jet type flow-through cell with acrylic resin was used. A dialysis membrane (Viskase, UC 1-7/8, purchased from Sankyo Jyun'yaku, Tokyo) was used to separate the outer chamber of the reference electrode from the solution in the flow cell. Peristaltic pumps (ATTO, SJ1211H and Furue Science, RP/N3) were used to deliver the outer filling solution of the reference electrode at a flow-rate of 13.4 cm^3 min^{-1}.

The major part of the software for data handling and controlling the solenoid valves was coded by the N88 Basic language which was running on Microsoft DOS. Only the part that controls the digitizer, provided from Autonics, was written by an assembler.

Reagents

Distilled water was used for all the sample preparations. A 1 M potassium nitrate solution was added to the sample solution as anionic strength adjuster to make the final concentration of KNO_3 10^{-2} M. A 10^{-2} M solution of the potassium salt of the objective ion was used as a base solution, except in the case of the analysis of beverages (10^{-1} M KCl was used in this case).

Scheme of HSPA

Figure 1 shows the schematic diagram of the HSPA. A base solution first flows across the electrode surface, and when the measured potentials are judged to be stable, the measurement can be started by hitting the space key. Then, the base solution is changed to a first sample by switching the 3-way solenoid valves (SV3). A stabilization part is observed after the rapid increase in the electrode potential. Next the solution is changed to a base solution, causing a rapid decrease in potential and then a return to the initial level. Thus the two changes of the solutions produce one peak, and the height of the peak corresponds to the logarithmic sample concentration. In this study, however, the peak potential rather

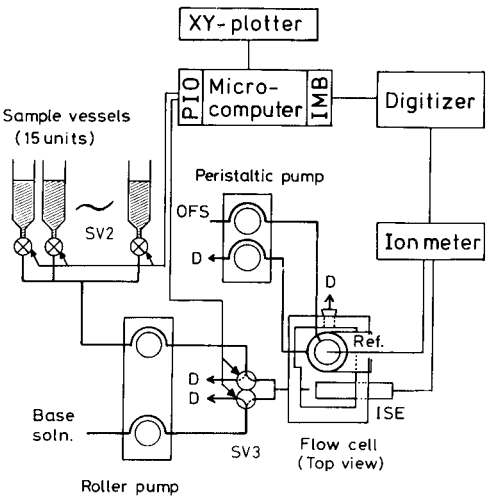

Fig. 1. Schematic diagram of high speed potentiometric analyzer. SV2 = 2-way solenoid valve; SV3 = 3-way solenoid valve; OFS = outer filling solution; D = drain; PIO = programmable I/O interface board; IMB = interface and memory board that is a part of the digitizer.

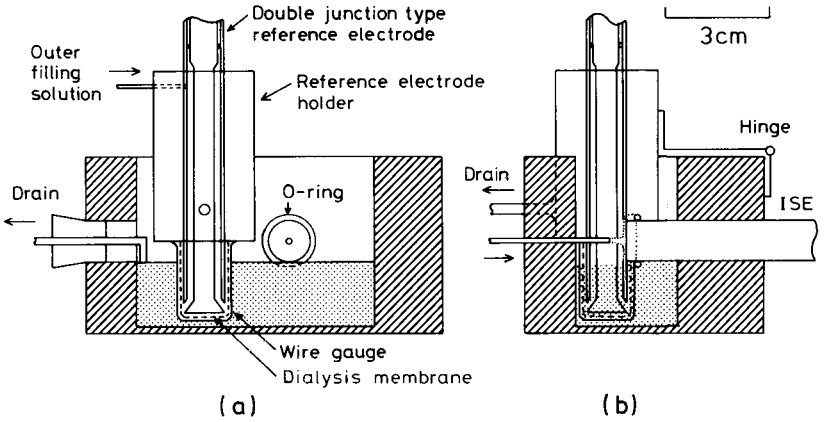

Fig. 2. Flow cell. (a) Front cross sectional view, (b) side cross sectional view. The diameter of the ISE is 1.2 cm.

than the peak height is used for calibration. The curvature of a calibration curve was approximated by the third order Spline function [8].

Figure 2 shows the wall-jet type flow cell with a small water pool. The volume of water in the cell was about 50 cm^3. A base and a sample solution flow across the electrode surface alternately, then flow into a water pool and finally leave through a drain tube connected to another roller pump. The outer filling solution flows into an inner chamber of the reference electrode holder, which is separated by the dialysis membrane. This method may contribute in part to reducing the electrical noise.

Principle of the system

The judgment of whether or not the potentials have become stable is carried out by a microcomputer. The flow chart of the main part of the program is shown in Fig. 3. The basic algorithm is similar to that reported in a previous paper [9], which is termed as a counting method. The occasion which satisfies two conditions, $I > (IC + C1)$ and $D(I) - D(I-1) < C2$, is counted until the number of the count becomes a predetermined value, i.e., C3. The first condition means that the counting should start after the waiting time C1 has passed. The second condition means that the counting should occur if the difference in two successive data points is smaller than the predetermined width C2. The width C2 corresponds to $400 \cdot C2/4096$ mV because a 12 bit A/D converter is used. In this study, these three parameters, C1, C2, and C3,were respectively determined as 50, 5, and 10, unless otherwise noted. These conditions for switching the solenoid valves are effective for solution changes in both directions (i.e., from base to sample and from sample to base). When the switching from sample to base

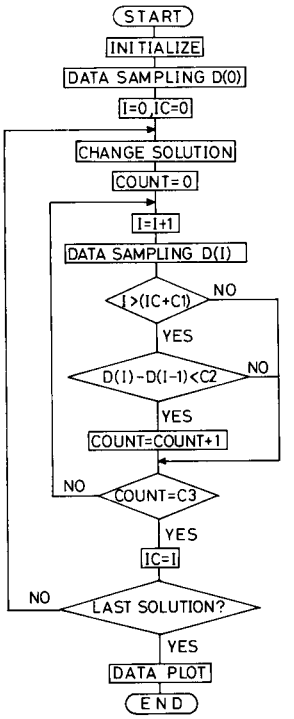

Fig. 3. Flow chart of the main part of the program.

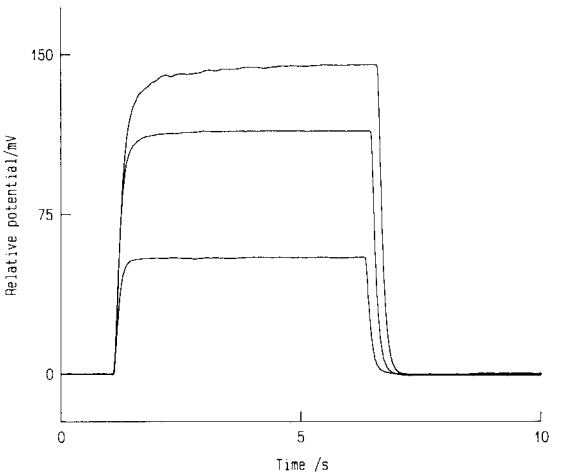

Fig. 4. The dynamic response curve of a chloride ion-selective electrode cell assembly against the concentration change from 10^{-2} M KCl base solution to 10^{-3} M (lower), 10^{-4} M (middle) and 10^{-5} M (upper) KCl solution.

solutions occurs, a sample solution is also changed to a new one by closing the present 2-way valve and opening the next 2-way valve simultaneously.

Analysis of beverages

For the purpose of comparison, both argentimetric and direct potentiometric determination of chloride ion were performed. In order to minimize the interference from the bromide ion etc., the potential just after immersion of the chloride electrode was used for the calculation in the direct potentiometric determination.

RESULTS AND DISCUSSION

Dynamic response behavior of the Cl^- ISE

This system can record the dynamic potential response curves for increasing and decreasing concentrations in a single experiment, if the program is modified to produce the switchover only twice: once from base to sample solution and vice versa. Figure 4 shows the results of the chloride ISE. The switchover of the solenoid valves from base to sample solutions occurred at 1 s, and after the switchover, it took about 90 ms to start the potential change (delay time). The switchover from sample to base solutions was programmed to occur when the condition of $D(I) - D(I-1) <$ 5 exceeded 500 times. The response time from base to sample solutions mainly depends on the sample concentration, while the recovery time from sample to base solution is slightly dependent on the sample concentration and is usually faster than the corresponding response time. This qualitative statement can be quantified by using the value of t_{95}, the time needed for 95% response against the final equilibrium potential, which has been used as a measure of the re-

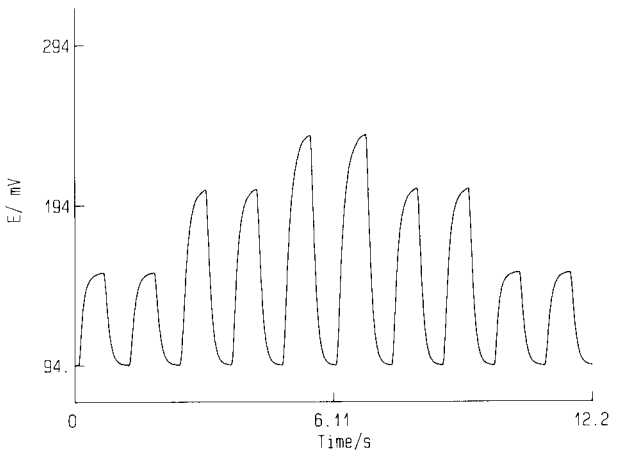

Fig. 5. Potential time response curve for 10^{-3} M, 10^{-4} M and 10^{-5} M potassium chloride standard solutions. Flow-rates of base and sample solutions are 2.2 m/s and 1.9 m/s, respectively. Measured potentials for each peak are 152.6, 152.5, 204.4, 205.1, 238.4, 238.8, 205.4, 205.2, 152.6 and 152.5 mV, respectively.

TABLE 1

Effect of the waiting time, C1, and the number of counts, C3, on the dynamic response for 10^{-3} M, 10^{-4} M and 10^{-5} M standard chloride solutions against a 10^{-2} M base solution

Parameter in Fig. 3	Response [a] time (ms)			Recovery [a] time (ms)			Measuring [a] time (ms)		
	10^{-3}	10^{-4}	10^{-5}	10^{-3}	10^{-4}	10^{-5}	10^{-3}	10^{-4}	10^{-5} [b]
C1 [c]									
30	453	570	695	455	508	515	908	1078	1210
40	503	580	690	500	505	515	1003	1085	1205
50	600	603	655	600	600	600	1200	1203	1255
60	700	703	780	700	700	700	1400	1403	1480
70	800	800	805	800	800	800	1600	1600	1605
C3 [d]									
5	550	558	600	550	550	550	1100	1108	1150
10	600	603	655	600	600	600	1200	1203	1255
20	700	710	755	700	700	700	1400	1410	1455
30	800	805	865	800	800	800	1600	1605	1665

[a] These values were the mean values of four data for 10^{-3} M and 10^{-4} M, and two data for 10^{-5} M taken from the calibration graphs as shown in Fig. 5. [b] Concentration (M) of KCl (every solution contains 0.01 M KNO_3 as an ionic strength adjuster). [c] Variables C3 = 10 and C2 = 5. [d] Variables C1 = 50 and C2 = 5.

sponse time of ion-selective electrodes [10–12]. The values of t_{95} from 10^{-2} M base to 10^{-3},10^{-4}, and 10^{-5} M sample solutions were estimated to be 0.40, 0.56, and 0.99 s, respectively, while the values of t_{95} for 10^{-5}, 10^{-4}, and 10^{-3} M sample solutions to the 10^{-2} M base solution were 0.38, 0.39, and 0.38 s. These values were generally larger than the values reported by Dencks and Neeb [11] (22–330 ms) or Khutsishvili et al [12] (180–210 ms). Though the discrepancy may be ascribed in part to the differences in the measuring conditions, a detailed discussion of this is beyond the scope of this paper.

Characteristics of HSPA

Figure 5 shows the typical potential response curve for standard chloride solutions. The reproducibility of the measured potentials for two successive peaks is usually within 1.0 mV. The reproducibility of the base potentials is also excellent (95.0 ± 0.2 mV) because the concentration of the base solution is as high as 10^{-2} M.

There are some factors which may affect the performance of the HSPA.

First, the effect of the parameters C1 and C3 in Fig. 3 was examined; parameter C2 was kept constant as 5 when the noise level of the response time curve was taken into consideration. Table 1 gives the results. Response time and recovery time are defined as the time needed for the successive switchovers from base to sample and from sample to base solutions, and vice versa. The measuring time is the sum of the response time and the recovery time. If the potential be-

TABLE 2

Effect of flow-rates on the dynamic response for 10^{-3} M, 10^{-4} M and 10^{-5} M standard chloride solutions against a 10^{-2} M base solution

Flow-rate (m/s)		Response time (ms)			Recovery time (ms)			Measuring time (ms)		
Base	Sample	10^{-3}	10^{-4}	10^{-5}	10^{-3}	10^{-4}	10^{-5}	10^{-3}	10^{-4}	10^{-5} [a]
2.2	2.0	600	605	640	600	600	600	1200	1205	1240
1.8	1.7	600	613	655	600	600	600	1200	1213	1255
1.4	1.3	600	628	740	600	600	600	1200	1228	1340
0.91	0.87	613	833	905	600	603	605	1213	1436	1510

[a] Concentration (M) of KCl (every solution contains 0.01 M KNO_3 as an ionic strength adjuster).

TABLE 3

Repeatability for 10 samples of a concentration measured after 3 standard solutions (10^{-3}, 10^{-4} and 10^{-5} M)

$[Cl^-]$		%R.S.D.	%Error	ΔE_{2-5} (mV)	t (s) [b]
Taken	Found [a]				
10^{-5}	$(0.914 \pm 0.0859) \times 10^{-5}$	9.4	−8.6	141.7	16.3
10^{-4}	$(0.972 \pm 0.0184) \times 10^{-4}$	1.9	−2.8	142.1	15.8
10^{-3}	$(1.015 \pm 0.0115) \times 10^{-3}$	1.1	+1.5	140.4	15.7

[a] Mean ± S.D. concentration was calculated with 10^{-2}, 10^{-3}, 10^{-4} and 10^{-5} M potassium chloride standard solutions. [b] Total measuring time for 13 solutions including 3 standard solutions.

comes stable enough to continue counting after the waiting period determined by the value of C1, the response or the recovery time should be given by the sum of C1 and C3 times 10 ms. Actually, this hypothesis was fulfilled in the case of the recovery time except for two cases (C1 = 30 and 40). In these cases, the waiting time is shorter than the time to start counting. The response time depends on the sample concentration more strongly than the recovery time, however, the values of C1 or C3 are more important factors than the sample concentration. Although it is desirable to determine the values to obtain the shortest measuring time, the speed of the sample exchange should also be taken into account. The 2-way valve opens for a new sample at the same time the switchover from the present sample to base solutions occurs, while a new sample continues to flow during the falling part of the response time curve. This means that the recovery time should be long enough for a new sample solution to completely replace the old sample.

Therefore, it is concluded that the values of 50 for C1 and 10 for C2 are suitable for general purposes. The measuring time for one sample in the concentration range of 10^{-2} M to 10^{-5} M can be expected to vary from 1.2 s to 1.3 s.

Second, the effects of the flow-rates on the response characteristics were examined as shown in Table 2. Flow-rates were expressed as the line velocity, which was calculated from the actual flow-rate (148–58.7 cm^3 min^{-1}) and the internal radius of the nozzle (0.6 mm). The response time depended on the flow-rates more significantly as the concentration of the sample became less, however, the recovery time was not affected by

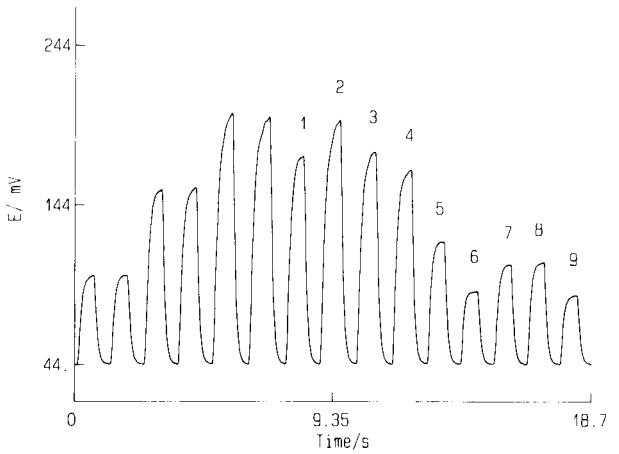

Fig. 6. Analysis of beverages. Nine sample peaks followed the three pairs of peaks for the 10^{-2}, 10^{-3} and 10^{-4} M potassium chloride standard solutions (base solution, 10^{-1} M KCl + 10^{-2} M KNO_3). Flow-rates of base and sample solutions are 2.1 m/s and 2.0 m/s, respectively.

the flow-rate. Thus, the dependence of the measuring time on the flow-rate is not pronounced in the concentration range tested, if the flow-rate is above ca. 110 cm^3 min^{-1}.

Repeatability

Table 3 presents the results of determinations of 10 samples having the same concentration after the measurement of 3 standard solutions. Because the number of sample vessels is restricted to be 15, only one peak was measured for each standard solution. The repeatability is at its worst at 10^{-5} M as judged from the values of the relative standard deviation. One reason for this is that the transient potential which is relatively far from the equilibrium was measured at 10^{-5} M. Another reason is that the complete change of solutions appears to be rather difficult for a time as short as 1.3 s in consideration of the concentration ratio of 1000 fold against the base solution. However, the result appears to be satisfactory at least in the concentration range below 10^{-4} M if the logarithmic character of the ISE sensor is taken into account.

Analysis of beverages

Figure 6 shows the potential response curve for 9 beverage samples after three pairs of peaks for standard chloride solutions (10^{-2}, 10^{-3} and 10^{-4} M). The total measuring time was 18.7 s. Although the sample volume needed for one measurement is theoretically as small as 3 cm^3, it is desirable to fill a sample vessel to at least 5 cm^3 to prevent the inhalation of air bubbles. Table 4 summarizes the results of analyses with three methods. Although the relative error exceeded 10% only for one sample, such a relatively large error is unavoidable for samples having a low concentration of chloride (less than 5×10^{-4} M) during several repeated measurements. For such samples (e.g., 1–4), it may be more desirable to use a 10^{-2} M chloride solution as a base.

The principle of HSPA enables determination of chloride ion concentrations as fast as 1.2–1.3 s for one sample regardless of its concentration level by using the chloride ion-selective electrode as a detector. Of course, this principle can be applied to other ion-selective electrode systems as long as it shows a quick response. Needless to say, care should be taken for the coexistence of interferents, as this system is based on direct potentiometric determination.

TABLE 4

Determination of chloride in beverages

Sample	No. [a]	Titration [b]	$[Cl^-]$ (M) [c]	HSPA	%rel. error [d]
Mineral water	1	4.09×10^{-4}	3.9×10^{-4}	3.8×10^{-4}	−2.6
	2	1.28×10^{-4}	1.2×10^{-4}	1.2×10^{-4}	0.0
	3	3.90×10^{-4}	3.8×10^{-4}	3.3×10^{-4}	−13.2
Soft drink	4	5.90×10^{-4}	5.6×10^{-4}	5.8×10^{-4}	3.6
	5	4.03×10^{-3}	4.0×10^{-3}	4.1×10^{-3}	2.5
	6	1.41×10^{-2}	1.5×10^{-2}	1.5×10^{-2}	0.0
	7	7.84×10^{-3}	7.6×10^{-3}	7.5×10^{-3}	−1.3
	8	6.96×10^{-3}	6.8×10^{-3}	7.2×10^{-3}	5.9
	9	1.65×10^{-2}	1.7×10^{-2}	1.7×10^{-2}	0.0

[a] Number corresponds to that of each peak in Fig. 6. [b] Potentiometric titration with $AgNO_3$. [c] Direct potentiometric determination. [d] (HSPA − DP/DP · 100).

REFERENCES

1 J.F. Van Staden, Anal. Chim. Acta, 179 (1986) 407.
2 J.A. Borzitsky, A.V. Dvinin, O.M. Petrukhin and Yu.I. Urusov, Anal. Chim. Acta, 258 (1992) 135.
3 E. Lindner, K. Tóth and E. Pungor, Dynamic Characteristics of Ion-Selective Electrodes, CRC Press, Boca Raton FL, 1988.
4 E. Lindner, K. Tóth, E. Pungor, T.R. Berube and R.P. Buck, Anal. Chem., 59 (1987) 2213.
5 T.R. Berube, R.P. Buck, E. Lindner, K. Tóth and E. Pungor, Anal. Chem., 63 (1991) 946.
6 T.R. Berube, R.P. Buck, E. Lindner, K. Tóth and E. Pungor, Anal. Lett., 24 (1991) 505.
7 M. Huser, P.M. Gehrig, W.E. Morf, W. Simon, E. Lindner, J. Jeney, K. Tóth and E. Pungor, Anal. Chem., 63 (1991) 1380.
8 H. Hara, Y. Wakizaka and S. Okazaki, Talanta, 34 (1987) 921.
9 H. Hara, A. Motoike and S. Okazaki, Anal. Chem., 59 (1987) 1995.
10 B. Fleet, T.H. Ryan and M.J.D. Brand, Anal. Chem.,46 (1974) 12.
11 A. Dencks and R. Neeb, Fresenius Z. Anal. Chem., 297 (1979) 121.
12 A.N. Khutsishvili, Z.S. Asatiani, E.I. Bondarenko and G.I. Orlova, Elektrokhimiya, 21 (1985) 308.

Analytica Chimica Acta, 281 (1993) 53–62
Elsevier Science Publishers B.V., Amsterdam

Determination of the pK_a values of sparingly soluble substances in water revisited: application to some benzodiazepines

Baltazar de Castro and Paula Gameiro

Departamento de Química, Faculdade de Ciências do Porto, 4000 Porto (Portugal)

José L.F.C. Lima

Departamento de Química-Física, Faculdade de Farmácia do Porto, 4000 Porto (Portugal)

(Received 23rd November 1992)

Abstract

The acid–base behaviour of four benzodiazepines sparingly soluble in water (diazepam, medazepam, chlordiazepoxide and prazepam) was studied by potentiometric and spectrophotometric titrimetry in water. A method was devised to obtain the pK_a values of these substances by potentiometric titrimetry in water-rich water–methanol media [up to 50% (v/v) methanol] by extrapolation to pure water, thus obviating the solubility problems associated with them. The method was found to be accurate and easily applicable, and the results obtained for the pK_a values are identical, within experimental error, with those obtained in water. The operational criteria for applying this methodology are indicated.

Keywords: Potentiometry; Titrimetry; UV–visible spectrophotometry; Acid–base equilibria; Acidity constants; Benzodiazepines

The benzodiazepines are the most widely prescribed minor tranquillizers in current use and they are known to act on the central nervous system (CNS) and to have hypnotic, tranquillizing and anticonvulsant properties [1]. Benzodiazepines act specifically at synapses in which γ-aminobutyric acid (GABA) is a neurotransmitter [2]. Several investigators have found that GABA increases the affinity of benzodiazepine–receptor interactions and conversely that benzodiazepines potentiate the interaction of GABA with its recognition site, suggesting the existence of a close association between the action of GABA and of benzodiazepines [3]. Most neuronal benzodiazepine binding sites are probably coupled to both anion and cation recognition sites [4] and some workers have reported the enhancing effects of several divalent cations on diazepam (7-chloro-1,3-dihydro-1-methyl-5-phenyl-2*H*-1,4-benzodiazepin-2-one) binding sites, suggesting the existence of two different binding sites in the presence of this divalent cation [5,6].

Equilibrium data are of importance in describing and understanding the mechanism of action of benzodiazepines. Further, the effectiveness of drugs depends on their route of administration and on their degree of ionization, and the pK_a value of a drug can be decisive in determining the extent to which it is absorbed by body organs and how it permeates cell membranes. This information is necessary in order to choose the best

Correspondence to: B. de Castro, Departamento de Química, Faculdade de Ciências do Porto, 4000 Porto (Portugal).

conditions for the extraction of drugs and their metabolites from body fluids [7].

The extremely low solubility of benzodiazepines in aqueous solution poses severe limitations on the determination of acidity constants, as few methods are reliable at these low concentrations. A few studies have been reported [8–12], and some results suffer from shortcomings such as no ionic strength control, no indication of the temperature used and, in several instances, determinations carried out solely in mixed solvents.

In this work, the stoichiometric acidity constants of some 7-chloro-1,4-benzodiazepines were determined in water, following the recommendations for the measurement and presentation of biochemical equilibrium data [13], by potentiometric titrimetry (for diazepam, medazepam and chlordiazepoxide) and spectrophotometric titrimetry (for the same drugs and also for prazepam). The values obtained were compared with those reported recently for these compounds [11].

Finally, an accurate and easily applicable method for obtaining acidity constants of substances that are sparely soluble in water, but soluble in water–methanol, is described. The results obtained with this method are shown to be identical, within experimental error, with those obtained by direct titrimetry in pure water, and the operational criteria for its application are defined.

EXPERIMENTAL

Reagents and solutions

Samples of the benzodiazepines were obtained from Laboratórios Bial (diazepam), Hoffman La Roche (medazepam and chlordiazepoxide) and Warner Lambert Portuguesa/Parke Davis (prazepam) and used as received. All other chemicals were purchased from Merck (analytical-reagent grade). All solutions were prepared with doubly deionized water (conductivity less than 0.1 μS cm^{-1}) that was free from carbon dioxide.

Potentiometric pH titrations

All potentiometric measurements and solution additions were carried out in with Crison Model 2002 pH meter and Model 2031 burette controlled by a Philips TC 100 microcomputer coupled to a Unisys PW 300 system for data manipulation. The electrode assembly consisted of a Metrohm 6.0726.100 double-junction AgCl/Ag reference electrode and a Philips GAH 110 glass electrode as indicator. System calibration was performed by the Gran method [14] in terms of hydrogen ion concentration, by titrating solutions of strong acid (0.001 M HCl in water or water–methanol) with strong base (ca. 0.02 M NaOH). A calibration was performed before each run used to determine acidity constants; this calibration also provided a check of the electrode behaviour. All titrations were carried out under a nitrogen atmosphere in a thermostated double-walled glass cell; the temperature was controlled at 25.0 ± 0.1°C and the ionic strength (I) was kept at 0.10 M by use of sodium chloride in all solutions.

pH determinations in water–methanol media. Measurements in water–methanol (water-rich) were carried out using compositions containing up to 50% (v/v) methanol using the following cell (cell 1):

$$\mathrm{Ag}\left|\begin{array}{l}\mathrm{AgCl},\\ \mathrm{KCl_{(sat.)}}\end{array}\right\|\begin{array}{l}\mathrm{NaCl}\\ (0.1\ \mathrm{M})\end{array}\Big\|\underbrace{\mathrm{NaCl\ (0.1\ M),\ H^+}\ (c_{\mathrm{H^+}})}_{\text{sample}}\Big|\begin{array}{l}\text{glass}\\ \text{electrode}\end{array}$$

The potential for this cell is

$$^{s}E = k_1 + k_2 \log(c_{\mathrm{H^+}}\,{}^{s}_{w}\gamma_{H^+}) \qquad (1)$$

where ${}^{s}_{w}\gamma_{\mathrm{H^+}}$, the total transfer activity coefficient (total medium effect), is given by $\log {}^{s}_{w}\gamma^{0}_{\mathrm{H^+}} - \log {}^{s}_{w}\gamma^{0}_{\mathrm{H^+}} + \log {}^{s}_{s}\gamma_{\mathrm{H^+}}$; ${}^{s}_{w}\gamma^{0}_{\mathrm{H^+}}$ is the primary transfer activity coefficient (primary medium effect) and is associated with the change of medium from water to water–methanol; and ${}^{s}_{s}\gamma_{\mathrm{H^+}}$ is the concentration effect (the activity coefficient of hydrogen ion in solvent s referred to the standard state in solvent s) [15]. The term k_1 comprises $^{s}E^{0}_{\mathrm{cell}}$ and the junction potentials, quantities that are constant and independent of solvent composition in this medium [16]; as ${}^{s}_{s}\gamma_{\mathrm{H^+}}$ is invariant when the ionic strength is kept constant (0.1 M in these

experiments), Eqn. 1 can be written as

$$^{s}E = {}^{s}k + k_2 \log c_{H^+} \quad (2)$$

where $^{s}k = k_1 + k_2 \log {}^{s}_{s}\gamma_{H^+} + k_2 \log {}^{s}_{w}\gamma^{0}_{H^+}$: the first two terms are independent of solvent composition and the last is proportional to the transfer Gibbs energy of H^+ from water to water–methanol and hence the only term that is dependent on solvent composition [15]. Plots of the experimental values of ^{s}E versus $-\log c_{H^+}$ obtained in this work yield straight lines with the same slope, but with intercepts at $\log c_{H^+} = 0$, $^{s}k_{exp}$, that are dependent on solvent composition. A plot of $^{s}k_{exp}$ versus ΔG^{0}_{t}, where the latter quantity is the standard molar Gibbs energy of transfer of H^+ from water to water–methanol [17], also yields a straight line at least up to 50% (v/v) methanol. These two observations support the assumptions made above concerning ^{s}k, and provide experimental evidence on the linear relationship between ^{s}E and $-\log c_{H^+}$ for any given solvent composition in the range studied.

This method allows the rapid and accurate determination of c_{H^+} under conditions similar to those used, i.e., cell 1, glass electrode calibration by direction titration (Gran plots) with $c_{H^+} \approx 10^{-3}$ M and titrand concentration $\approx 10^{-3}$ M. Using this approach, it is possible to obtain $-\log c_{H^+}$ for any solution in water–methanol up to 50% (v/v) methanol from the calibration graphs of ^{s}E versus $-\log c_{H^+}$, thus obviating the problems associated with the determination of transfer activity coefficients.

Potentiometric determination of acidity constants

Stock solutions of the benzodiazepines (3.0×10^{-4}–7.0×10^{-4} M) were prepared in water or in water–methanol ($I = 0.1$ M NaCl; $c_{H^+} = 1.0 \times 10^{-3}$ M) and kept in the dark to minimize decomposition. The concentration of benzodiazepines was monitored by checking the compliance of the absorbance at the isosbestic points with the Beer–Lambert law. The experimental data were obtained by titration of the stock solutions with NaOH (ca. 0.02 M; $I = 0.1$ M NaCl) under purified nitrogen. The operational ionic products of water in water and in water–methanol solutions were obtained using the method of Leporati [18]. The calculations were performed with data from at least six independent titrations, each with more than 20 points, using the programs SUPERQUAD [19] and BEST [20].

Spectrophotometric titrations

All UV–visible spectrophotometric measurements were carried out at 25.0×0.1°C in aqueous solutions ($I = 0.1$ M NaCl) using a Shimadzu 265 spectrophotometer equipped with a constant-temperature cell holder. The spectra were recorded over the wavelength ranges 210–410 nm for diazepam, 210–450 nm for medazepam, 210–450 nm for chlordiazepoxide and 210–450 nm for prazepam, all with a slit width of 1 nm. Stock aqueous solutions of the benzodiazepines (2.0×10^{-5}–1.0×10^{-4} M) were prepared and aliquots of strong base or acid were added to 20 cm^3 of the stock solution to adjust $-\log c_{H^+}$ to the desired value; $-\log c_{H^+}$ measurements and system calibration were performed by potentiometry as described previously.

Spectrophotometric determination of acidity constants

The Beer–Lambert law was verified for the experimental conditions employed and the model used (single-step acid–base) was chosen by graphical methods [21,22].

For the particular case of a single-step acid–base titration the Beer–Lambert law may be rewritten as $A_\lambda = l(\epsilon_{\lambda BH}[BH^+] - \epsilon_{\lambda B}[B])$, where A_λ is the absorbance at wavelength λ, $\epsilon_{\lambda B}$ is the molar absorptivity of the neutral form B at wavelength λ and $\epsilon_{\lambda BH^+}$ is that of the ionized species BH^+ at wavelength λ. Combining this equation with the mass balance equations, several linear transformations can be used to determine dissociation constants of a monoprotic acid [22], and the following two were applied in this work:

$$(A_\lambda - A_{\lambda B}) \times 10^{-\log c_{H^+}} = -(1/K_a)A_\lambda + (1/K_a)A_{\lambda BH^+} \quad (3)$$

$$(A_\lambda - A_{\lambda BH^+}) \times 10^{\log c_{H^+}} = -K_a A_\lambda + K_a A_{\lambda B} \quad (4)$$

TABLE 1

pK_a values of benzodiazepines determined by potentiometric and spectrophotometric methods

Benzodiazepine	This work [a]			Literature value	Method	Solvent medium	Temperature (°C)	Ref.
	Potentiometry		Spectrophotometry (water)					
	Water	Water-methanol [b]						
Diazepam	3.58 ± 0.03	3.54 ± 0.05	3.57 ± 0.06	3.3	Spectrophotometry	Water–methanol (95 + 5, v/v)	20	8
				3.17	Spectrophotometry	Water–ethanol (98 + 2, v/v)	25	12
				3.3	Spectrophotometry	Water–ethanol (90 + 10, v/v)	–	10
				3.35	Potentiometry	Water (0.1 M NaCl)	25	11
				3.38	Solubility	Water (0.1 M NaCl)	25	11
Medazepam	6.17 ± 0.03	6.19 ± 0.04	6.21 ± 0.03	6.17	Spectrophotometry	–	37	9
				6.19	Solubility	–	37	9
				6.25	Spectrophotometry	Water–ethanol (90 + 10, v/v)	–	10
				6.20	Spectrophotometry	Water (0.1 M NaCl)	25	11
				6.19	Potentiometry	Water (0.1 M NaCl)	25	11
				6.16	Solubility	Water (0.1 M NaCl)	25	11
Chlordiazepoxide	4.79 ± 0.03	4.82 ± 0.03	4.82 ± 0.03	4.6	Spectrophotometry	Water–methanol (95 + 5, v/v)	20	8
				4.88	Potentiometry	Water (0.1 M NaCl)	25	11
				4.82	Solubility	Water (0.1 M NaCl)	25	11
Prazepam	–	3.21 ± 0.05	3.22 ± 0.04	3.04	Spectrophotometry	Water (0.1 M NaCl)	25	11
				2.94	Solubility	Water (0.1 M NaCl)	25	11

[a] Values determined at 25°C, I = 0.10 M NaCl. Values after pK_a represent scatter [25]. [b] Values obtained by linear extrapolation to pure water. See text for details.

where $A_{\lambda B}$ is the absorbance of the neutral form B at wavelength λ and $A_{\lambda BH^+}$ is the absorbance of the ionized form BH^+ at wavelength λ. The K_a values were obtained by linear regression analysis, and at least four independent titrations, each with ten points and at four different wavelengths, were used.

RESULTS AND DISCUSSION

The major difficulty in obtaining reliable values for the acidity constants of benzodiazepines is due to their low solubility in aqueous solutions and the possible hydrolysis of some benzodiazepines in strongly acidic solutions. These observations explain why most studies have been performed in mixed solvents using UV–visible spectrophotometry, but cannot account for the inadequate description of the experimental conditions given by some workers and for the significant variations of the reported values (see below). In this paper a precise and easily applicable method to evaluate the acidity constants of some benzodiazepines, that can be extended to other systems with low water solubility, is presented.

Potentiometric titrimetry in aqueous solutions is the most precise method for determining equilibrium constants [23], once a model to describe the system adequately has been chosen. It was employed throughout this work in a well defined experimental set-up, albeit pushing the method to its limits as very low concentrations of the titrand were used, to provide stoichiometric pK_a values at $I = 0.1$ M NaCl. Spectrophotometric titrimetry was also used, under similar experimental conditions, to obtain not only precise but also reliable values for the acidity constants of these substances. Determinations of acidity constants were further performed by potentiometric titrimetry in water–methanol media of different composition, and this method revealed a linear relationship between the ${}^s pK_a$ for the benzodiazepines and the amount of methanol in the solvent [up to 50%, (v/v)], thus allowing the pK_a values in pure water to be obtained by linear extrapolation; this method is easily applicable as there is no problem with the solubility of the benzodiazepines and it was shown to be very precise and reliable.

Potentiometric titrations in water

The acidity constants of diazepam, medazepam and chlordiazepoxide (Table 1) were obtained by potentiometry in water by direct base titration of acidic solutions of these benzodiazepines in a pH range where no precipitation occurs. The determinations were performed using benzodiazepine concentrations that were kept below the solubility of the titrand [11] and experimental conditions that prevented hydrolysis from occurring to any significant extension. The ranges of $-\log c_{H^+}$ used were 2.9–3.9 for diazepam, 4.0–6.3 for medazepam and 3.2–5.5 for chlordiazepoxide. The calculated pK_a values were always constant and independent of the titrand concentration used. The possible occurrence of hydrolysis was checked by verifying the constancy of the calculated pK_a values for several independent determinations with the same stock solution during a 48-h period, and by analysing any changes in the NMR spectra of the same stock solution over the same period of time. Hydrolysis was found to occur solely in solutions of diazepam and not before 24 h after preparation; 36 h after preparation, the apparent pK_a value increases ($\Delta pK_a = -0.16$, where ΔpK_a is the difference between the apparent pK_a of diazepam in water before and after hydrolysis) and the NMR spectra exhibit a new band near the original methyl group.

The results obtained in this study support the observation that the greatest source of error in potentiometric determinations is associated with the variability from one titration to another and not with the individual points in each titration [24]. Accordingly, the errors affecting the values of the reported pK_a values are not those given by the computer programs used to calculate them, even when the complete set of data for six titrations is used in a single input for SUPERQUAD. The errors reported in this work were calculated by the method suggested by Albert and Sarjeant [25] in which the errors are calculated as the maximum difference between the logarithm of the average of the antilogarithms of the calculated pK_a values and their individual values. This approach was used throughout this work, including the values determined spectrophotometrically.

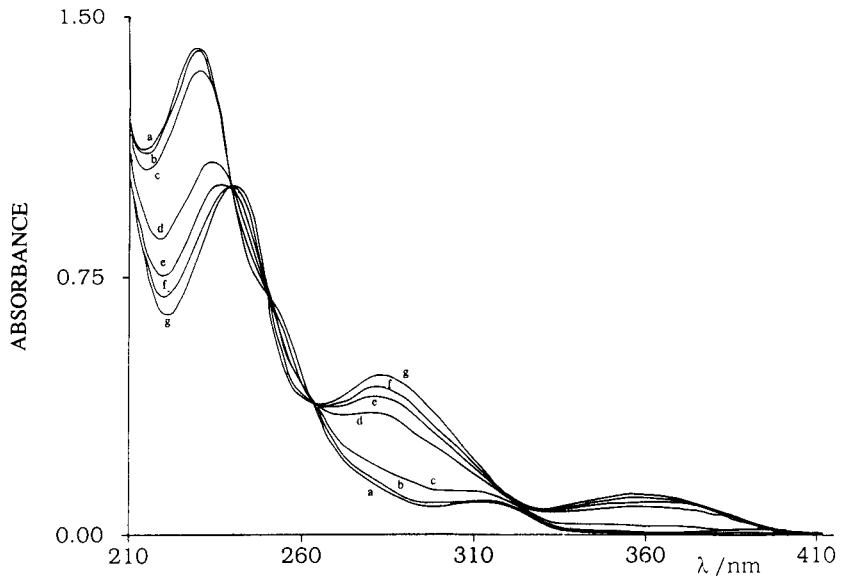

Fig. 1. Dependence of UV–visible spectra of diazepam (3.0×10^{-5} M) in aqueous solution ($I = 0.10$ M NaCl) on values of $-\log c_{H^+}$: (a) 10.31 and 6.42 (both curves are superimposed); (b) 5.77; (c) 4.69; (d) 3.42; (e) 3.01; (f) 2.80; (g) 2.03 and 1.86 (both curves are superimposed).

Spectrophotometric titrations

Independent support for the values of acidity constants determined by potentiometry in water was provided by the good agreement with the values obtained by spectrophotometric titrations (Table 1). Figure 1 shows the type of spectra changes that occur with varying $-\log c_{H^+}$ for a solution of diazepam. It was also possible to determine the acidity constant of prazepam, which is much less soluble (almost insoluble) in water, and thus not amenable to determination by potentiometry in this solvent. The acidity constants were calculated assuming a single-step acid–base titration and further support for the model used was provided by the observed agreement of the calculated and experimental values of $A_{\lambda BH^+}$ and $A_{\lambda B}$.

The low benzodiazepine concentrations used did not allow the extent of hydrolysis to be monitored by NMR spectrometry, but the possibility

TABLE 2

$^{s}pK_a$ values of benzodiazepines in water–methanol media of different compositions

Methanol (%, v/v)	$^{s}pK_a$ of benzodiazepines [a]			
	Diazepam	Medazepan	Chlordiazepoxide	Prazepam
50	2.71 ± 0.05	5.69 ± 0.04	4.19 ± 0.05	2.45 ± 0.05
40	2.87 ± 0.04	5.80 ± 0.04	4.32 ± 0.04	2.62 ± 0.05
30	3.05 ± 0.02	5.89 ± 0.04	4.46 ± 0.02	2.78 ± 0.02
20	3.22 ± 0.03	6.00 ± 0.03	4.59 ± 0.03	2.90 ± 0.02
15	3.31 ± 0.04	6.04 ± 0.03	4.64 ± 0.03	–
10	3.35 ± 0.05	6.09 ± 0.03	4.68 ± 0.03	–
0 [b]	3.54 ± 0.05	6.19 ± 0.04	4.82 ± 0.03	3.21 ± 0.05

[a] Stoichiometric constants. [b] Values obtained by linear extrapolation to pure water. See text for details.

of the occurrence of hydrolysis was checked by monitoring the absorbance of the solutions at several wavelengths during a 48-h period. For diazepam and prazepam, the most acidic of the benzodiazepines studied, only after 24 h did the absorbance of acidic solutions change. The apparent pK_a when calculated with Eqn. 3 after 24 h showed a decrease ($\Delta pK_a = +0.12$); for medazepam and chlordiazepoxide no changes were detected in the electronic spectra over a 48-h period. Under the experimental conditions used it is safe to assert that no hydrolysis took place during pK_a determinations.

Potentiometric titrations in water–methanol media

Such potentiometric titrations were conducted for the four benzodiazepines. Using the values of $-\log c_{H^+}$ determined as described under Experimental, the evaluation of the stoichiometric ${}^{s}pK_a$ was straightforward for any water–methanol composition [up to 50% (v/v) methanol] using either of the computer programs mentioned. The ranges of $-\log c_{H^+}$ used were similar to those of pure water. The values obtained were reproducible but were found to depend on the composition of the titration medium (Table 2), showing that the benzodiazepines become stronger acids on addition of methanol, which is in agreement with what has been observed for charged acids dissociating to neutral bases [26].

This behaviour can be accounted for by noting that the proton acceptor is the water molecule over the full water–methanol composition range [27], that methanol has a higher proton affinity than water and that the effect of the organic molecules when they interact with the aqueous core of proton solvation is to enhance the basicity of the aqueous core by stripping away some of the proton density. Hence the basicity of the water molecules will increase with increase in the methanol fraction and, accordingly, the autoprotolysis constants in the mixed solvent, pK_{SH}, increase with increasing amount of methanol and do so linearly up to 60% (w/w) methanol [28]; this observation can be interpreted to mean that the basicity of the water molecules will increase linearly up to this weight proportion, and hence the ${}^{s}pK_a$ will decrease linearly. In accordance with this explanation, we note that the operational pK_w (pK_{SH}) values determined in this study increase smoothly from pure water to water–methanol (50 + 50, v/v): 1.58 ± 10^{-14} (water), 1.51×10^{-14} (10% methanol), 1.48×10^{-14} (20% methanol), 1.45×10^{-14} (30% methanol), 1.41×10^{-14} (40% methanol) and 1.38×10^{-14} M^2 (50% methanol).

As the stoichiometric constants are defined as ${}^{s}pK_a = -\log([H^+][B]/[HB^+])$ an increase in the basicity of the water molecules will mean a decrease in $[HB^+]$ and an identical increase in [B]. For each benzodiazepine a plot of ${}^{s}pK_a$ as a function of solvent composition (expressed either as volume or as mole fraction) yielded a straight line; the set of points (${}^{s}pK_a$ versus mole fraction) were fitted to a straight line with a correlation coefficient that was never lower than 0.999. Extrapolation of this line to pure water intercepts the ${}^{s}pK_a$ axis at a value that is, within experimental error, identical with the pK_a determined in water, either by potentiometry or by spectrophotometry.

Acidity constants of medazepam, chlordiazepoxide, diazepam and prazepam

Despite the importance of a precise knowledge of acidity constants in pharmacological studies, the values reported in the literature for benzodiazepines show large variations and even in a recent review [29] some of the values quoted are wrong. An extensive literature search revealed only one study carried out in water [11], with most of the studies being conducted by spectrophotometric titrimetry in alcohol media (typically containing 10% or 5% alcohol), often without ionic strength and/or temperature control; it is also important to note that calibration of the glass electrode, necessary to adjust the solution "pH", was done with buffer solutions of unknown ionic strength. Owing to the different methodologies that have been used in the determination of the acidity constants of benzodiazepines, the difficulties and inaccuracies that affect the reported values are due to different causes, and so the

acidity constants of these substances will be analysed by subdividing them into two groups: those which do not undergo hydrolysis and those which are readily hydrolysed. In Table 1, literature values for the pK_a values of benzodiazepines are included.

Medazepam and chloridazepoxide. These are the most soluble of the benzodiazepines studied and are not hydrolysed in aqueous solution under the experimental conditions used in this work. The first reported value for the pK_a of medazepam was 4.4 [8], but this value was soon proved to be wrong and a value of 6.17 was determined by spectroscopy [9]. Neglecting the original value for medazepam, the values reported for the acidity constants of these two benzodiazepines agree well with those obtained in this study (Table 1).

Diazepam and prazepam. These compounds are much less soluble than the previous two, but the main difficulty associated with the determination of their stability constants is related to the possible occurrence of hydrolysis.

Diazepam has been extensively studied and several attempts have been made to determine its pK_a value, with very different results (Table 1). The values obtained by spectrophotometric titrimetry in alcohol media are ca. 3.3, and not very different from the value of 3.35 ± 0.05 determined by potentiometry in this study for water–methanol (90 + 10, v/v) (Table 2).

The literature pK_a values determined in water (0.1 M NaCl; 25°C) for diazepam and prazepam [11] deserve further analysis, as they are about 0.20 lower than those obtained in this study (Table 1). Pfendt et al. [11] used two different methods for pK_a determination for each benzodiazepine that yielded similar results and this observation was used to support the validity of the solubility method developed. The main problem with their method must be associated with the conversion of readings with a combined glass electrode to concentrations of H^+. For the pH region above 3.5, buffer solutions of pH 4.01 and 7.00 were used with no ionic strength adjustment and the equation $pH_{GE} = -\log c_{H^+} + 0.04$ was chosen to relate pH-meter readings (pH_{GE}) with c_{H^+}, and the same equation was also claimed to apply in the pH range 2.0–3.5, based on direct potentiometry of HCl solutions at constant ionic strength (0.1 M NaCl). The main source of error should lie in this latter region as the liquid junction potentials will vary appreciably below $-\log c_{H^+} < 3.0$ [30], and as the activity coefficient of H^+ will change owing to alterations in the titration media [31,32]. The effects of activity coefficients and of junction potential shift the "pH" scale in opposite directions [33], and there is evidence that an equation of the form $pH_{GE} = -\log c_{H^+} +$ constant will only apply in the $-\log c_{H^+}$ range 2.3–7.0 [32], and the actual values of $-\log c_{H^+}$ must be larger than those calculated with equation $pH_{GE} = -\log c_{H^+} + 0.04$, especially in the $-\log c_{H^+}$ range 2.0–3.0. The calculated pK_a values of the more acidic benzodiazepines will then be higher than those reported in [11]. The same error in $-\log c_{H^+}$ will affect in a similar way the pK_a values calculated by the solubility method [11]. For prazepam the pK_a value determined by spectroscopy (3.04) is affected by the use of the Henderson–Hasselbalch equation, which requires a knowledge of the limiting value of $A_{\lambda BH^+}$, which requires solutions with values of $-\log c_{H^+} \approx 1$, a situation where hydrolysis must occur. This situation was recognized by Pfendt et al., who considered this value not to be completely reliable.

Finally, it must be pointed out that in a recent study on pK_a determination by various methods, acidity constants for piretanide and furosemide show that the pK_{a2} values (ca. 4) determined by solubility methods are about 0.2 lower than values obtained by other methods [34].

Conclusions

A review of the recent literature showed that linear extrapolation techniques in mixed solvents were abandoned in favour of solubility methods for the determination of acidity constants of substances that are poorly soluble in water. The difficulties associated with the use of mixed solvents have traditionally been associated with the need to estimate activity coefficients in these media and with the lack of a reasonable theory to perform that estimation, but the lack of ade-

quately defined primary buffers has also played an important role.

This work has shown that when potentiometric titrimetry is performed in water-rich methanolic media and the systems are calibrated directly in concentration, the resulting data allow for an accurate determination of stoichiometric acidity constants. The methodology developed provides a reliable process to determine acidity constants of spring soluble substances in water, as long as they are soluble in water–methanol mixtures, but the following restrictions must be kept in mind. Electrode calibration must be performed before each run, by use of the Gran method, by titrating solutions of constant ionic strength (normally less than 0.15 M) of strong acid with strong base where both concentrations are known. Titrations must be conducted in a medium with the same composition as that where pK_a determinations will be carried out; in this solvent the strong acid and the strong base must be completely dissociated and the strong acid concentration must be ca. 10^{-3} M. Electrode reliability assessment: the Gran plots also provide information on electrode behaviour. Both branches of the Gran function must converge and the values of k_1 and of k_2 (Eqn. 1) must be identical in the acid and basic branches. Solvent media: water–methanol is used, where the methanol content must not exceed 50% (v/v). In water–methanol the glass electrode is stable [35], the liquid junction potentials are constant and independent of solvent composition [16] and the water molecules are the proton acceptors.

The verification of all these criteria has ensured that the linear extrapolation technique does not suffer from most of the problems that have been normally associated with it [25], and linear extrapolation of ${}^{s}pK_a$ determined in water–methanol containing up to 50% (v/v) methanol to pure water always yielded a straight line with an intercept that provided a value of ${}^{w}pK_a$ identical with those determined by direct potentiometry and by spectrophotometry in pure water.

In view of the results obtained, potentiometric titrimetry in water–methanol media is the preferred method for the determination of the acidity constants of substances that are sparingly soluble in water but soluble in water–methanol. The method is rapid, easily applicable and yields very good results.

The authors acknowledge Hoffman-La Roche, Laboratórios Bial and Warner Lambert Portuguesa/Parke Davis for the provision of benzodiazepines. P.G. thanks the Fundação Gomes Teixeira (Porto, Portugal) for a fellowship.

REFERENCES

1 T. Nogrady, Medical Chemistry: a Biochemical Approach, Oxford University Press, New York, 1988, p. 230.
2 E. Roberts, in R.W. Olsen and J.C. Venter (Eds.), Benzodiazepines/GABA Receptors and Chloride Channels: Structural and Functional Properties (Receptor Biochemistry and Methodology, Vol. 5), Liss, New York, 1986, pp. 1–39.
3 J.B. Fischer and R.W. Olsen, in R.W. Olsen and J.C. Venter (Eds.), Benzodiazepines/GABA Receptors and Chloride Channels: Structural and Functional Properties (Receptor Biochemistry and Methodology, Vol. 5), Liss, New York, 1986, pp. 241–259.
4 R.F. Squires, in R.W. Olsen and J.C. Venter (Eds.), Benzodiazepines/GABA Receptors and Chloride Channels: Structural and Functional Properties (Receptor Biochemistry and Methodology, Vol. 5), Liss, New York, 1986, pp. 209–224.
5 S. Mizuno, N. Ogawa and A. Mori, Neurochem. Res., 7 (1982) 1487.
6 S. Mizuno, N. Ogawa and A. Mori, Neurochem. Res., 8 (1983) 873.
7 W.O. Foye, Principles of Medicinal Chemistry, Lea and Febiger, Philadelphia, 1988, pp. 1–35.
8 J. Barrett, W.F. Smyth and I.E. Davidson, J. Pharm. Pharmacol., 25 (1973) 387.
9 G.F. le Petit, J. Pharm. Sci., 65 (1976) 1094.
10 B. Maupas and M.B. Fleury, Analusis, 10 (1982) 187.
11 L.B. Pfendt, D.M. Sladic, T.J. Janjic and G.V. Popovic, Analyst, 115 (1990) 383.
12 P. Seiler and I. Zimmermann, Arzneim.-Forsch., 33 (1983) 1519.
13 International Comission on Biothermodynamics, J. Biol. Chem., 251 (1982) 6879.
14 G. Gran, Analyst, 77 (1952) 661.
15 H. Galster, pH Measurement: Fundamentals, Methods, Applications, Instrumentation VCH, Weinheim, 1991, pp. 18–20.
16 E.P. Serjeant, Potentiometry and Potentiometric Titrations, Wiley, New York, 1984, pp. 409–415.
17 Y. Marcus, Pure Appl. Chem., 62 (1990) 899.
18 E. Leporati, J. Chem. Soc., Dalton Trans., (1988) 953.

19 P. Gans, A. Sabatini and A. Vacca, J. Chem. Soc., Dalton Trans., (1985) 1195.
20 A.E. Martell and R.J. Motekaitis, Determination and Use of Stability Constants, VCH, Weinheim, 1988.
21 J. Polster and H. Lachmann, Spectrometric Titrations: Analysis of Chemical Equilibria, VCH, Weinheim, 1989, p. 33.
22 J. Havel and M. Meloun, in D.J. Leggett (Ed.), Computational Methods for the Determination of Formation Constants, Plenum, New York, 1985, pp. 19–27.
23 F.R. Hartley, C. Burgess and R. Alcock, Solution Equilibria, Horwood, Chichester, 1980.
24 E. Fisicafo and A. Braibanti, Talanta, 35 (1988) 769.
25 A. Albert and E.P. Sarjeant, The Determination of Ionization Constants, Chapman and Hall, London, 2nd edn., 1971.
26 M. Paabo, R.G. Bates and R.A. Robinson, J. Phys. Chem., 70 (1966) 247.
27 E. Pines and G.R. Fleming, J. Phys. Chem., 95 (1991) 10448.
28 E.P. Serjeant, Potentiometry and Potentiometric Titrations, Wiley, New York, 1984, p. 411.
29 L.A. Berrueta, B. Gallo and F. Vicente, J. Pharm. Biomed. Anal., 10 (1992) 109.
30 R.G. Bates, Determination of pH: Theory and Practice, Wiley, New York, 2nd edn., 1973, pp. 26–28.
31 R.G. Bates, Determination of pH: Theory and Practice, Wiley, New York, 2nd edn., 1973, pp. 262–265.
32 M.T.S.D. Vasconcelos and A.A.S.C. Machado, Rev. Port. Quim., 28 (1986) 120.
33 H. Sigel, A. Zuberbühler and O. Yamauchi, Anal. Chim. Acta, 255 (1991) 63.
34 N. Sistovaris, Y. Hamachi and T. Kuriki, Fresenius' J. Anal. Chem., 340 (1991) 345.
35 R.G. Bates, Determination of pH: Theory and Practice, Wiley, New York, 2nd edn., 1973, pp. 372–375.

Analytica Chimica Acta, 281 (1993) 63–70
Elsevier Science Publishers B.V., Amsterdam

Study of cadmium adsorption from iodide media by voltammetry combined with data treatment by deconvolution

Marina Zelić, Ivanka Pižeta and Marko Branica

Center for Marine Research Zagreb, Rudjer Bošković Institute, POB 1016, 41001 Zagreb (Croatia)

(Received 18th February 1993)

Abstract

The Cd^{2+}–I^- system was taken as a model for the investigation of anion-induced adsorption. By additional treatment of voltammetric signals using a deconvolution method, possibilities for new information appeared. Adsorption became evident under conditions where previously it had been only indirectly proved. Practical problems, such as the loss of current–concentration linearity or the appearance of too high peak potential shifts during the determination of stability constants, can be partly overcome by the proposed method.

Keywords: Voltammetry; Adsorption; Cadmium; Deconvolution

The first report [1] on cadmium(II) adsorption from halide media on a mercury surface is more than 60 years old. Later, the phenomenon was studied by double potential step chronocoulometry [2,3], polarography/voltammetry [4–8] and electrocapillary measurements [9], in chloride [2], bromide [3,8,10] or iodide solutions [4–7,9,10]. In all those instances the adsorption of dissolved metal was ascribed to the surface activity of the corresponding free ligand ions [11].

The uncharged species CdI_2 was identified [3,7,12] as the most probable adsorbable complex in iodide media. Its maximum surface concentration (Γ_m) does not exceed 2.2×10^{-10} mol cm^{-2} [5] and even lower values of Γ_m have been reported [10]. According to Flanagan et al. [5], the adsorption process follows a Frumkin isotherm with repulsive interaction.

Correspondence to: M. Zelić, Center for Marine Research Zagreb, Rudjer Bošković Institute, POB 1016, 41001 Zagreb (Croatia).

Accumulation of the electroactive cadmium(II) complex at the electrode surface was confirmed by the appearance of a maximum in normal-pulse polarography (NPP) [6] and peak-height enhancement in differential-pulse polarography (DPP) [4] or square-wave voltammetry (SWV) [7]. Splitting of the reduction signal was not reported.

Simulated DP polarograms [5] indicate that the separation of diffusion and adsorption peaks should be expected if adsorption according to a Langmuir or Frumkin isotherm with attractive interaction takes place. In the case of repulsion, broadening of the signal appears instead.

Most results that have been published were obtained at an ionic strength of 1 mol l^{-1}. In this paper it will be shown that experiments performed at higher electrolyte concentrations ($[NaClO_4] + [NaI] = 4$ mol l^{-1}) can give a more or less pronounced splitting of the cadmium(II) reduction peak in different techniques.

Poorely defined double signals and seemingly "simple" peaks, obtained at different electrolyte

concentrations, were resolved by deconvolution using fast Fourier transforms (FFT) [13,14] in the manner already tested on the Pb^{2+}–Cl^- system [15]. In the present instance, characterized by much stronger adsorption, the method was applied in order to overcome some of the practical problems such as the loss of current–concentration linearity or the appearance of too high peak potential shifts during the determination of complexation constants.

EXPERIMENTAL

All the chemicals used, i.e., $Cd(NO_3)_2$, NaI, $NaClO_4 \cdot H_2O$ and 70% $HClO_4$, were of analytical-reagent grade from Merck (Darmstadt) and Kemika (Zagreb). Solutions were prepared using redistilled water.

All measurements were performed using a PAR 384B polarographic analyser. The instrument was connected to a PAR 303A static mercury drop electrode with a platinum counter electrode and a saturated Ag/AgCl (NaCl) reference electrode. The applied configuration also included a technical computer (HP 9816S) together with a double disk drive (HP 9121D), a graphics printer (HP 82986A) and a six-pen plotter (HP 7475A) [16]. Experimentally obtained curves were saved on a floppy disk for further treatment.

Each series of measurements was performed at a constant ionic strength (1 or 4 mol l^{-1}), maintained with $NaClO_4$, and a constant acidity (0.001 mol l^{-1} $HClO_4$). At increasing ligand concentration the level of dissolved metal was kept constant while titrations with solutions of cadmium(II) were performed at a constant level of dissolved iodide in another series of measurements. The total ligand concentration, $[I]_t$, was always much higher than the total metal concentration, $[Cd]_t$, so the total and free iodide concentrations could be taken as identical.

SWV measurements were performed under the following conditions: initial potential $E_i = -290$ mV, final potential $E_f = -800$ mV, amplitude $a = 24$ mV, frequency $f = 100\ s^{-1}$ and scan increment $e = 2$ mV. When scaning in anodic direction the upper values of E_i and E_f were interchanged.

For obtaining DPP results a drop time of 1 s, a pulse height of 24 mV and a scan increment of 2 mV were selected.

For the titration procedure, room temperature (23 ± 2°C) was adopted. Voltammograms were recorded from solutions previously deaerated with high-purity nitrogen for 10 min.

DATA TREATMENT

The recorded files with experimental curves were transformed from the HP to a DOS environment and all were given the extension .MAT to suit MATLAB [17]. In the deconvolution procedure the following deconvolution function was used:

$$i(E) = \exp(\varphi)/[1 + \exp(\varphi)]^2$$

where $\varphi = (nF/RT)\ (E - E_0)$. All the symbols have their usual meanings, except that n represents the means of changing the width of the deconvolution function and is not restricted to integers; it is one of the parameters of the deconvolution. Other parameters of the deconvolution are the type of filter, cut-off frequency (ω) and length of measured and deconvolution curve (T_0) before the transformation. The details that lead to a successful deconvolution are given elsewhere [14].

The curves after deconvolution had changed their heights owing to the transformation, so they are expressed in arbitrary units. As all the curves are treated in the same way, their relative heights are left unchanged.

For graphical presentation (in three dimensions) of original and deconvoluted curves, the instruction MASH from MATLAB was used. Unfortunately, the figures obtained in such a way can be treated only as qualitative (or semi-quantitative) and not used for quantitative presentations. This is because only the heights and potentials of the corresponding peaks are correctly given. With respect to the third axis, the curves are located as if a constant concentration

increment (on the logarithmic scale) was applied, although this was not the case. However, for qualitative comparison of different series of measurements (before and after deconvolution), performed at different electrolyte concentrations and by means of two electrochemical techniques, even this approach can be useful.

RESULTS AND DISCUSSION

Measurements at a constant iodide concentration

Stability constants of CdI_p complexes at an ionic strength of 1 mol l^{-1} are known ($\log \beta_1 = 1.89$, $\log \beta_2 = 3.3$, $\log \beta_3 = 4.5$, $\log \beta_4 = 5.6$) [18]. Calculation of the distribution of species as a function of the ligand concentration [7] indicates that the surface-active complex CdI_2 will form the highest fraction (ca. 26%) of the total dissolved cadmium(II) if $\log[I^-] \approx -1.3$. Under such conditions adsorption effects should be highly pronounced. Therefore, in the first series of measurements the iodide level was kept constant at 0.059 mol l^{-1} while the cadmium concentration was gradually increased. Over the whole range $[Cd]_t = 1 \times 10^{-6}$–$1.97 \times 10^{-3}$ mol l^{-1} the instrument could detect only one reduction signal whose

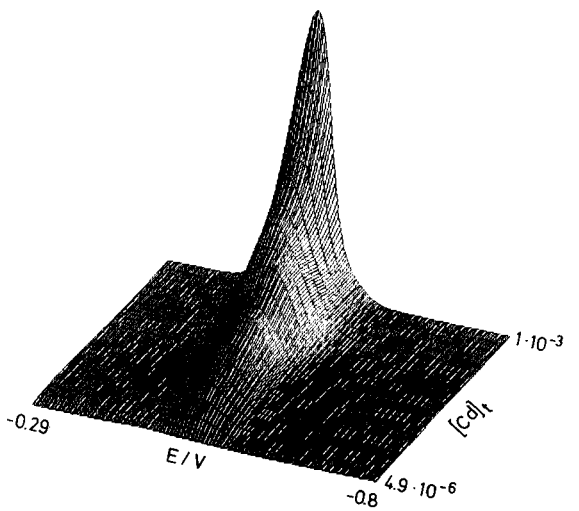

Fig. 1. Square-wave voltammograms of cadmium(II) in iodide medium at increasing metal concentrations (original data). $[I^-] = 0.059$ mol l^{-1}; ionic strength = 1 mol l^{-1}.

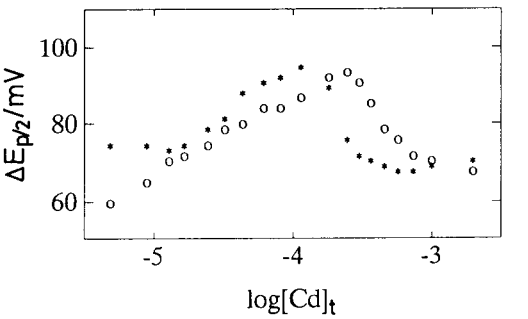

Fig. 2. Change in half-peak width with increasing cadmium(II) concentration for SWV peaks obtained after scanning in (○) cathodic and (*) anodic directions. Other conditions as in Fig. 1.

peak potential shifted positively with increasing metal concentration, especially for $-\log[Cd]_t = 3.62$–3.26 [19]. At higher levels of dissolved cadmium the peak potential reaches a constant value, i.e., its shift with respect to the peak potential, measured in pure perchlorate medium of the same ionic strength, achieves the expected value for the given iodide concentration. It seems that the post-peak is gradually transformed into the main peak without visible splitting of the resulting signal [19].

All SW voltammograms obtained after scanning in the cathodic direction are given in Fig. 1. The change in their half-peak width, together with the corresponding values for anodic peaks, is presented in Fig. 2. The dependence of $\Delta E_{p/2}$ on $\log[Cd]_t$ is a bell-shaped curve, more distorted for cathodic SWV peaks in comparison with the corresponding anodic signals. In both instances, at a chosen iodide level (0.059 mol l^{-1}), it passes through the maximum value of $\Delta E_{p/2} = 94$ mV, but for cathodic peaks it is shifted towards higher metal concentrations for about 0.3 logarithmic units.

At the same time the normalized peak current (i_n), i.e., the ratio between the peak current and the total cadmium concentration, decreases in the way described previously [4] for cadmium(II) DP polarograms at $[I^-] = 0.1$ mol l^{-1}.

Cathodic peaks are much more affected by adsorption than the corresponding anodic signals. However, even in the latter case the effect could not be eliminated completely (Fig. 3A). At lower

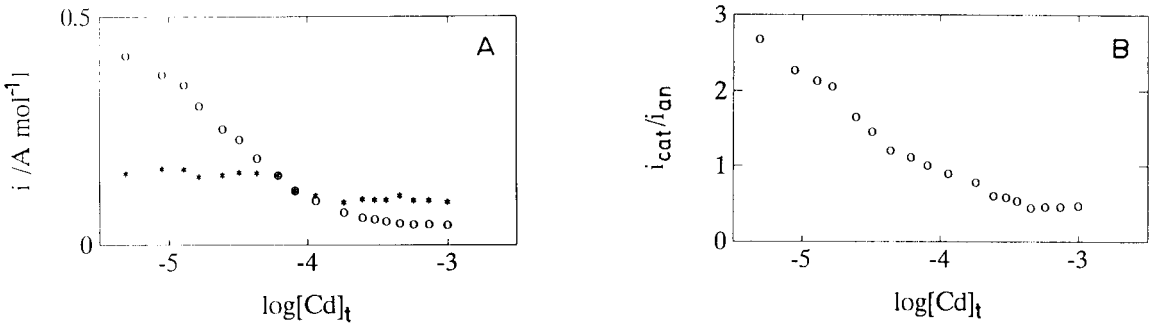

Fig. 3. Changes in (A) the normalized (○) cathodic and (∗) anodic peaks currents and (B) their ratio with increasing metal concentration. Other conditions as in Fig. 1.

metal concentrations (up to $\log[Cd]_t = -4.2$) each cathodic current (i_{cat}) is higher than the corresponding anodic value (i_{an}), although the latter includes some contribution from the metal accumulation at potentials more negative than E_p. In other words, the contribution from adsorption is higher than from anodic accumulation. For $\log[Cd]_t \geqslant -3.9$ the opposite effect appears, i.e., anodic currents become higher than cathodic currents. Between $\log[Cd]_t = -5.3$ and -3.3 the ratio i_{cat}/i_{an} gradually decreases from 2.65 to 0.45 and becomes constant for higher cadmium concentrations (Fig. 3B).

The peak potential at the constant iodide concentration depends on the total metal concentration (Fig. 4), but different values are obtained for cathodic and anodic peaks although in pure perchlorate medium these two values are identical. Qualitatively, the effect can be ascribed to the influence of potential and different (real) cadmium concentrations on the process of interest. Higher (real) metal concentrations near the electrode surface and less pronounced adsorption at more negative potentials are the reasons for the appearance of decreased peak potential shifts of anodic signals at apparently lower $[Cd]_t$ in comparison with cathodic peaks.

Some of the experimentally obtained signals given in Fig. 1 (and also the corresponding anodic peaks) can be resolved into two close peaks (Fig. 5). The point is that such a procedure makes close signals narrower and so better separated [13]. The resulting peaks are probably the main and the post-peak, respectively, but this assump-

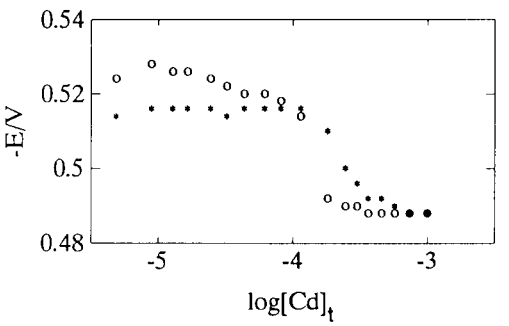

Fig. 4. Dependence of the cathodic (∗) and anodic (○) SW peak potential on cadmium(II) concentration. Other conditions as in Fig. 1.

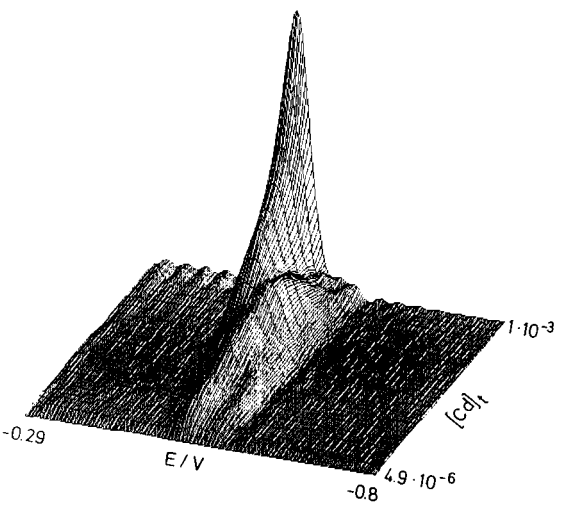

Fig. 5. Deconvoluted square-wave voltammograms from Fig. 1. Parameters of deconvolution: $n = 2$; $\omega = 35/T_0$; $T_0 = 1.024$ V; boxcar filter.

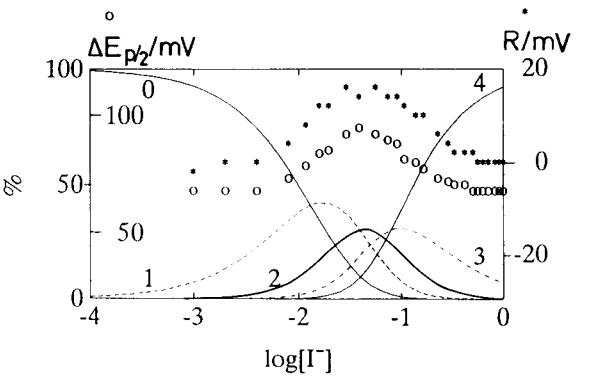

Fig. 6. Dependence of (○) the cathodic half-peak width and (*) the difference (R) between the cathodic and anodic peak potentials on iodide concentration. Distribution of dissolved cadmium(II) among different complexes is given for comparison. Numbers on curves denote p-values of the corresponding CdI_p species.

tion should be proved under different conditions, i.e., at different metal, ligand and electrolyte concentrations.

The appearance of a small, third peak should also be noted. It is, however, in agreement with the results of recent numerical simulations [15] of DPP (not SWV) signals.

Measurements at a constant cadmium concentration

It is well known [19] that anion-induced adsorption of metal ions prevents the successful determination of stability constants by polarographic/voltammetric techniques. In the ligand concentration range in which a surface-active complex constitutes a significant fraction of the total dissolved metal, the measured half-wave or peak potential shifts exceed the values that correspond to complex formation in the aqueous phase.

For measurements at a constant metal concentration, $[Cd]_t = 2 \times 10^{-4}$ mol l^{-1} was chosen because it lies near the maximum of the cathodic curve in Fig. 2. Under such conditions pronounced adsorption and successful resolution of SW voltamograms by deconvolution are expected.

Some of the experimental results are given in Fig. 6. The circle symbols indicate the dependence of the cathodic half-peak width on the ligand concentration. Values obtained at low ($\log[I^-] \leqslant -2.4$) and high ($\log[I^-] \geqslant -0.3$) iodide concentrations are close to the theoretical values [20], whereas inside this range they are significantly higher.

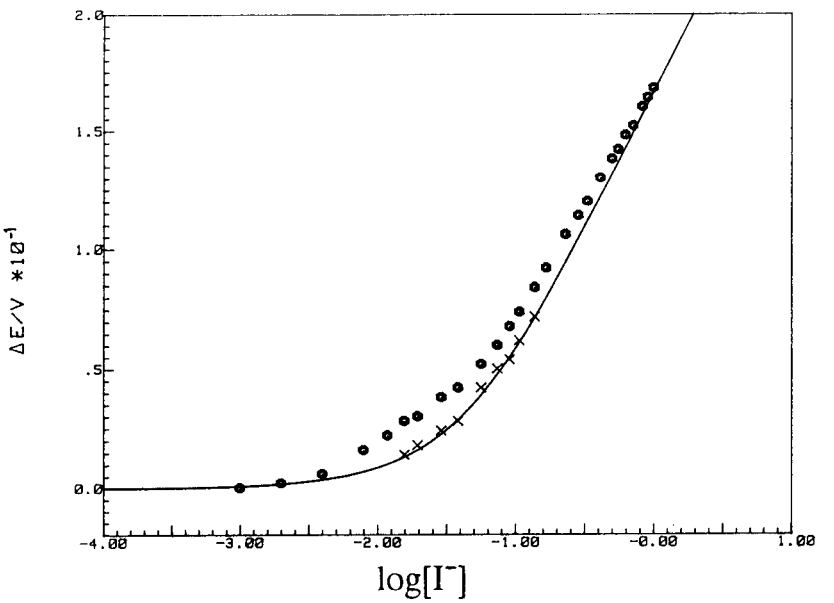

Fig. 7. Dependence of cadmium(II) peak potential shift on iodide concentration. $[Cd]_t = 2 \times 10^{-4}$ mol l^{-1}; ionic strength = 1 mol l^{-1}. (○) Experimental points and (×) shifts of the main wave, obtained by deconvolution, are compared with the expected values (full line).

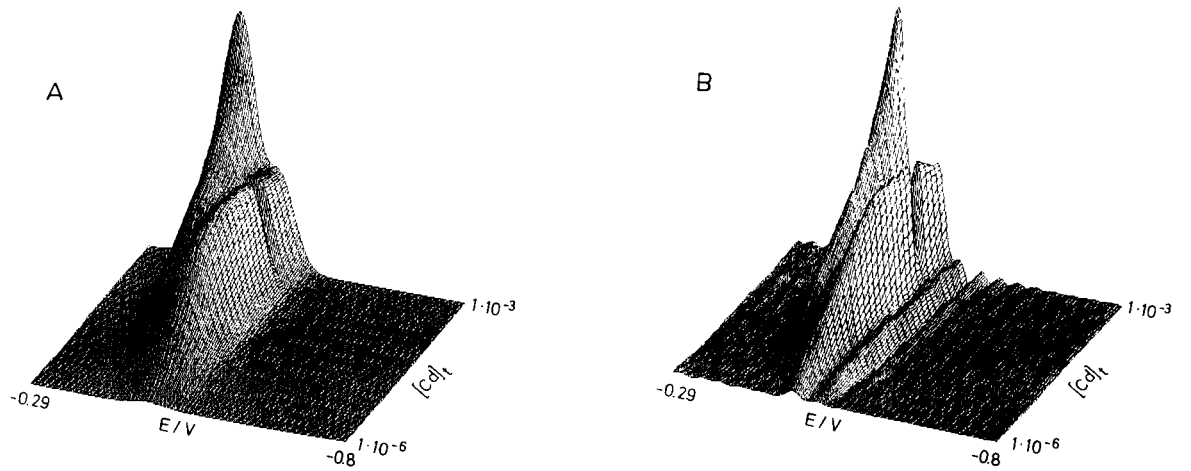

Fig. 8. (A) Original and (B) deconvoluted SW voltammograms of cadmium(II) in iodide medium. $[I^-] = 0.0120$ mol l^{-1}; ionic strength = 4 mol l^{-1}. Parameters of deconvolution: $n = 2$; $\omega = 35/T_0$; $T_0 = 1.024$ V; boxcar filter.

A very similar bell-shaped curve is obtained when the difference (R) between cathodic and anodic peak potentials is plotted as a function of log[I^-] (Fig. 6, asterisk symbols). At high and low ligand concentrations (as above) these values are identical (i.e., $R = 0$) because under such conditions cadmium(II) adsorption is not pronounced. Between them R becomes significant because at the chosen metal concentration cathodic peaks are much more influenced than anodic peaks by adsorption, as follows from Figs. 2 and 4. Both curves in Fig. 6 exhibit a striking similarity with the curve that gives the fraction of the total dissolved cadmium in the form of CdI_2 as a function of log[I^-]. This is surprising because a direct correlation of experimental results with species distribution in solution is usually possible only under conditions where Henry's isotherm is valid [21].

In Fig. 7 the dependence of the SWV peak potential shift (obtained after scanning in cathodic direction) on log[I^-] is given. Points correspond to the experimental values and the full line is the expected curve based on the generally

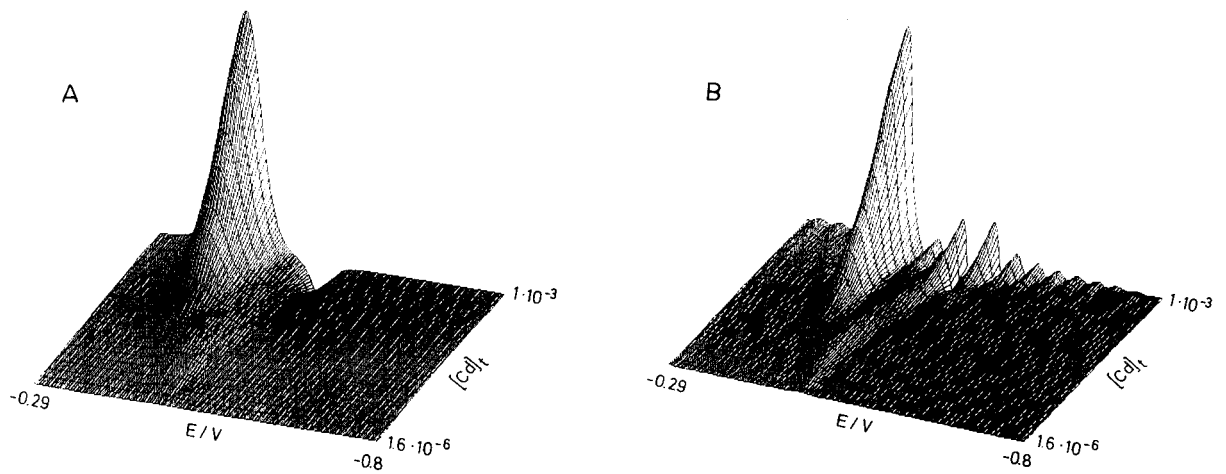

Fig. 9. (A) Original and (B) deconvoluted DP polarograms of cadmium(II) in iodide medium. $[I^-] = 0.0146$ mol l^{-1}; ionic strength = 4 mol l^{-1}. Parameters of deconvolution: $n = 2$; $\omega = 35/T_0$; $T_0 = 1.024$ V; boxcar filter.

accepted stability constants [18]. It is obvious that the measured values are significantly higher than expected, except at very low and very high iodide concentrations. The most important part of Fig. 7 are the crosses located on or near the calculated curve. They reflect the position of the main, i.e., more positive, peak obtained after application of the deconvolution procedure to real square-wave voltammograms. Good agreement of their potentials with the expected values can be observed. Unfortunately, among the 26 voltammograms only 9 could be resolved under the applied conditions, because they fulfil the conditions for successful deconvolution (minimum distance between the peaks and their suitable height ratio).

The upper results can be taken as a proof that the curves obtained after deconvolution are really the main peak and the post-peak (not artefacts of the method or a reflection of some other processes).

Measurements at a high electrolyte concentration ($I = 4$ mol l^{-1})

In more concentrated electrolyte solutions (4 mol l^{-1}), a gradual increase in cadmium concentration at a constant iodide level ($[I]_t = 0.0112$ mol l^{-1}) can give an obvious splitting of the SW reduction signal (Fig. 8A). At first ($[Cd]_t = 10^{-5}$–10^{-4} mol l^{-1}) the reduction peak in SWV loses its symmetry but later a new peak on the anodic side gradually develops. In a narrow metal concentration range ($-\log[Cd]_t = 3.49$–3.37) the instrument recognizes two close signals whose peak potentials are 44–54 mV apart (Fig. 9A). With a further increase in the cadmium level, the adsorption peak diminishes relative to the other.

If the same set of curves is subjected to deconvolution, two close peaks are obtained in a much wider metal concentration range ($-\log[Cd]_t \geqslant 3.75$) (Fig. 8B). The change on the anodic side of the transformed peak appears even at $\log[Cd]_t = -4.90$. However, this can be regarded as a hump or loss of the symmetry but not as a defined peak with a characteristic potential and current.

There is a linear relationship between the height of the main signal, obtained by transformation (i_h), and the total cadmium concentration. All the points are located on the same straight line which can be described by the equation $i_h = 4.67C + 0.26$, with C in mmol l^{-1} and i_h in arbitrary units. Strictly, the condition $[Cd]_t \ll [I]_t$ is not fully satisfied at the highest metal concentration (1.97 mmol l^{-1}), but the departure of the corresponding peak height from the mentioned straight line is less than 2%. The linear relationship between metal concentration and the height of the main peak cannot be observed in Fig. 8B because of the limitation mentioned under Data Treatment.

All the peak potentials of the main peak are located within 4 mV, which seems acceptable taking into account that the lowest possible scan increment in work with the PAR 384B is 2 mV. The upper results can be considered to be satisfactory because they agree with expected results for a diffusion-controlled process.

With the deconvoluted post-peak the situation is slightly different from that expected. The current increases with increasing metal concentration but does not reach a plateau. Instead, it passes through a maximum at $[Cd]_t = 3.5 \times 10^{-4}$ mol l^{-1} and decreases slowly at higher levels of dissolved metal. At the same time, there is a continuous, negative peak potential shift.

The only aspect that remains unclear is the origin of the "gap" in the height of the post-peak (but not of the main peak) appearing at $[Cd]_t = 5.2 \times 10^{-4}$ mol l^{-1} (Fig. 8).

The upper results can be taken as additional proof that the applied deconvolution procedure is applicable to the study of ligand-induced adsorption of metal ions.

Similar dependences of peak height (and peak potential) on the metal concentration at a constant level of the surface-active ligand were also obtained at ionic strengths of 1 mol l^{-1} (SWV measurements) and 4 mol l^{-1} (DPP measurements). Their application in analytical practice can be expected. In other words, deconvolution can help in concentration measurements when, because of adsorption, wide, asymmetric or obviously composite peaks are obtained. After resolution of such signals an unknown concentration can be determined using the linear relationship between the level of dissolved surface-active ana-

lyte and the height of the main, i.e., diffusion-controlled, peak.

With respect to the DPP results, an additional comment should be made. According to the literature data [5], splitting of the reduction signal was not obtained at an ionic strength of 1 mol l^{-1} and also is not to be expected for the adsorption process that follows a Frumkin isotherm with a strong repulsive interaction (in SWV, which is more sensitive to surface processes [20], only the change in the half-peak width could be observed too).

At higher ionic strength (4 mol l^{-1}) the situation is different. The composite character of the cadmium(II) DPP peak (at $[I^-] = 0.0146$ mol l^{-1}) is obvious (Fig. 9A), although the instrument cannot read two different currents and potentials. After the deconvolution procedure, however, two peaks appear (Fig. 9B), although the situation is not so clear as with SW voltammograms. Because of the negative currents on the cathodic side of the peak, deconvolution results in enhanced noise, i.e., two artificial peaks appear. Beside them the adsorption peak is well pronounced.

Additional comparison of the SWV and DPP results (Figs. 8 and 9) indicates a much higher sensitivity of the former towards adsorption processes. A significantly higher ratio between the adsorption and diffusion peaks can be observed. Therefore, if one intends to deconvolute the measured curves and to determine the presence and height of two close peaks, SWV appears to be more appropriate, taking into account that low adsorption peaks in DPP could be masked by noise.

Finally, it remains unclear if the literature statement concerning the type of adsorption isotherm and the appearance of double peaks is generally valid. In other words, it would be interesting to determine whether (and how) an increased electrolyte concentration can change the type of interactions at the electrode surface.

This work was supported by the Ministry of Science, Technology and Informatics of the Republic of Croatia in the frame of the EUREKA–ELANI 37/12 (EUROMAR) project. The authors gratefully acknowledge the Department of Electronic Measurements and Systems of the Faculty of Electronic Engineering Zagreb for the use of MATLAB.

REFERENCES

1 A. Frumkin and F.J. Cirves, J. Phys. Chem., 34 (1930) 74.
2 G. Lauer, R. Abel and F.C. Anson, Anal. Chem., 39 (1967) 765.
3 F.C. Anson and D.J. Barclay, Anal. Chem., 40 (1968) 1791.
4 F.C. Anson, J.B. Flanagan, K. Takahashi and A. Yamada, J. Electroanal. Chem., 67 (1976) 253.
5 J.B. Flanagan, K. Takahashi and F.C. Anson, J. Electroanal. Chem., 81 (1977) 261.
6 J.B. Flanagan, K. Takahashi and F.C. Anson, J. Electroanal. Chem., 85 (1977) 257.
7 M. Zelić and M. Branica, J. Electroanal. Chem., 309 (1991) 227.
8 M. Zelić and M. Branica, Anal. Chim. Acta, 262 (1992) 129.
9 L. Pospišil and R. Volkova, J. Electroanal. Chem., 140 (1982) 367.
10 E. Fatàs-Lahoz, M. Sluyters-Rehbach and J.H. Sluyters, J. Electroanal. Chem., 136 (1982) 59.
11 F.C. Anson, Acc. Chem. Res., 8 (1975) 400.
12 M. Caselli, L. Lampugnani and P. Papoff, J. Electroanal. Chem., 34 (1972) 367.
13 I. Pižeta, M. Lovrić and M. Branica, J. Electroanal. Chem., 296 (1990) 395.
14 I. Pižeta, in preparation.
15 I. Pižeta, M. Lovrić, M. Zelić and M. Branica, J. Electroanal. Chem., 318 (1991) 25.
16 I. Pižeta and M. Branica, J. Electroanal. Chem., 250 (1988) 293.
17 MATLAB for 80836-based MS-DOS Personal Computers, MathWorks, Natic, 1990.
18 R.M. Smith and A.E. Martell, Critical Stability Constants, Volume 4: Inorganic Complexes, Plenum, New York, 1976.
19 M. Zelić and M. Branica, Anal. Chim. Acta, 268 (1992) 275, and references cited therein.
20 M. Lovrić and M. Branica, J. Electroanal. Chem., 226 (1987) 239.
21 M. Zelić, unpublished results.

Analytica Chimica Acta, 281 (1993) 71–84
Elsevier Science Publishers B.V., Amsterdam

Screening of organophosphorus pesticides in environmental matrices by various gas chromatographic techniques

Sílvia Lacorte, Carmen Molina and Damià Barceló

Department of Environmental Chemistry, CID–CSIC, C / Jordi Girona 18–26, 08034 Barcelona (Spain)

(Received 4th January 1993; revised manuscript received 4th March 1993)

Abstract

Gas chromatography with nitrogen–phosphorus detection (GC–NPD) using three different capillary columns, DB-1701, RSL-300 and DB-5, was employed for the identification of 25 organophosphorus pesticides and various transformation products. Spectral information on and typical fragment ions of the different compounds were obtained by gas chromatography–mass spectrometry with electron impact and negative-ion chemical ionization. Clean-up methods involving Florisil, Empore C_{18} extraction discs, C_{18} cartridges and gel permeation chromatography using Bio-Beads S-X3 were evaluated for the isolation of selected organophosphorus pesticides from water and biota samples. Recoveries for water samples varied from 77 to 120% with a relative standard deviation of 2–8% whereas recoveries of 30–130% were obtained with biota samples. Applications are reported for the determination of pyridafenthion in water samples from the Ebro delta (Tarragona, Spain).

Keywords: Gas chromatography–mass spectrometry; Pesticides; Environmental analysis; Waters

Although organophosphorus compounds are not as persistent in the environment as other groups of pesticides, their acute toxicity is of concern and stringent regulations have been implemented in most countries. The European Economic Community (EEC) included many of them, e.g., coumaphos and dichlorvos, in the 76/464 Directive list on pollution caused by certain dangerous substances into the aquatic environment [1]. Similarly, the National Pesticide Survey from the US Environmental Protection Agency (EPA) also included many organophosphorus pesticides and various transformation products (TPs), e.g., ethoprop, stirofos, methyl paraoxon, fenamiphos sulphone and fenamiphos sulphoxide, in its current monitoring programme of drinking water wells throughout the USA [2]. A total of 43 organophosphorus pesticides were included as compounds to be monitored in different commodities within the US EPA [3].

The determination of low concentrations of organophosphorus pesticides in different matrices requires, in addition to highly selective detection techniques, the application of an efficient extraction and clean-up. Although liquid–solid extraction (LSE) procedures are preferred in many laboratories because the disposal of haz-

Correspondence to: D. Barceló, Department of Environmental Chemistry, CID–CSIC, C/Jordi Girona 18–26, 08034 Barcelona (Spain).

ardous and toxic solvents is avoided, many laboratories still use liquid–liquid extraction (LLE) procedures, e.g. the EPA method for the organophosphorus pesticides [2].

As a confirmatory technique, gas chromatography–mass spectrometry (GC–MS) either in the electron impact (EI) or negative ion chemical ionization (NCI) mode, is ideal and it has been applied in various different cases [4–10]. Although GC–MS is the preferred approach to avoid false-positive determinations in environmental analysis, the EPA method for the analysis of organophosphorus pesticides in water samples indicates the use of two different GC columns, usually DB-5 and DB-1701, and MS as an option [2].

Considering the comments made above, it was decided to carry out a systematic study with the following aims: to select 26 organophosphorus pesticides and various TPs that are of importance in the EEC and EPA lists and study their retention times in three different capillary GC columns, DB-1701, RSL-300 and DB-5; to characterize all these compounds by the use of GC–MS with EI and NCI, thus giving their typical characteristic ions; to carry out an extraction and clean-up step in water and biota samples, by the use of LSE with Empore C_{18} extraction discs for water samples and various clean-up techniques such as gel permeation chromatography (GPC) for biota samples; and to apply the analytical methodology developed to analyse spiked and real water samples from the Ebro delta (Tarragona, Spain).

EXPERIMENTAL

Chemicals

Pesticide standards were obtained from Promochem (Wesel, Germany), except for RPA 400629 and vamidothion, which were gifts from Rhône Poulenc Agrochimie (Lyon). Pesticide-grade *n*-hexane, diethyl ether, dichloromethane, acetonitrile and cyclohexane were purchased from Merck (Darmstadt). Ethyl acetate and methanol were obtained from Scharlau (Barcelona). Florisil (60–100 mesh) was purchased from Merck. C_{18} Empore extraction discs and C_{18} cartridges were from J.T. Baker/3M (Deventer, Netherlands) and Bakerbond (6 ml capacity, 40 μm average particle diam., 60 Å), respectively.

Sample preparation

Water samples. Estuarine water samples from the Ebro delta were filtered through a 0.45-μm filter (Millipore) to remove particulate material. Water samples ($n = 5$) of 1 l each were spiked with a mixture of several pesticides to a final concentration of 15 $\mu g\ l^{-1}$. Methanol (0.5 ml) was added to the samples to allow a better extraction. After vigorous shaking the solutions were extracted through C_{18} discs using 40 ml of ethyl acetate as eluting solvent. The fractions were evaporated just to dryness on a rotary evaporator and the residue was dissolved in 1 ml of ethyl acetate. In each instance the amount injected on to the GC column was 1 μl.

Water samples were collected from the Ebro delta in June, 5 days after the area had been treated with organophosphorus pesticides, and in July in three different locations that had been treated 5 days and 3 days before sample collection, and on the same day. These samples were treated as described above.

Biological samples. Red mullet (*Mullus barbatus*) was used to study the efficiency of different clean-up techniques. Fish were freeze-dried and about 2 g of sample were spiked with a mixture of pesticides (azinphos-ethyl, coumaphos, chlorpyrifos, fenamifos, fenchlorphos, fenitrothion, phosmet, pyridafenthion, stirofos) to a concentration between 75 and 100 $ng\,g^{-1}$ of freeze-dried material. The samples were Soxhlet extracted for 18 h with 100 ml of ethyl acetate to remove pesticides from the matrix. The extracts were evaporated just to dryness on a rotary evaporator and the following different clean-up methods were applied.

Clean-up with Florisil. Glass columns (31 cm × 120 mm i.d.) were filled with 7 g of Florisil in *n*-hexane. The Florisil was activated overnight at 300°C, cooled and deactivated with 2% water. The fish extracts were placed at the top of the column and eluted with 60 ml of a mixture of 6, 15, 50 and 100% diethyl ether in *n*-hexane.

Clean-up with C_{18} Empore discs. One disc was placed on the vacuum apparatus and prewashed with 50 ml of ethyl acetate. Sample was added and eluted with 30 ml of the same solvent. The sample was rotary evaporated. As the extract was a viscous fluid, a second filtration with a new disc was necessary to eliminate the lipidic matrix. This procedure was also done using acetonitrile as prewash and eluting solvent.

Clean-up with disposable C_{18} extraction cartridges. The Soxhlet extract was split into three portions and each one (about 0.3 g of lyophilized fish tissue) was filtered through the cartridges. Ethyl acetate was used as prewash and eluting solvent. This protocol was repeated twice more, so ultimately nine cartridges were used to clean-up 1 g of lyophilized sample.

Clean-up with C_{18} Empore discs plus Florisil. A combination of the two techniques mentioned above was used in order to improve the clean-up efficiency. C_{18} filtration of the Soxhlet extract using ethyl acetate as eluting solvent was done prior to Florisil fractionation.

Gel permeation chromatography (GPC). GPC was used to remove the lipid material. Prior to GPC clean-up, the Soxhlet extract was filtered through C_{18} discs with ethyl acetate as eluting solvent in order to remove part of the lipidic matrix. For GPC analysis, a Bio-Beads S-X3 stainless-steel column (450 mm × 10 mm i.d., 200–400 mesh) was used (Bio-Rad Labs., Richmond, CA). The dry extract was diluted with ethyl acetate and aliquots of 150 μl (loop size 160 μl) were introduced on to the column and eluted with dichloromethane–cyclohexane (1 + 1) at a flow-rate of 1 ml min^{-1}. Dump and collection times were determined beforehand by injecting the mixture of standard pesticides. The collection time of pesticide residues was 17–31 min.

In all instances, after each clean-up procedure, the samples were evaporated just to dryness on a rotary evaporator. A 1-μg amount of triphenyl phosphate (TPP) was added to the final extract for quantification. The final extract was dissolved in 1 ml of ethyl acetate prior to injection into the gas chromatograph equipped with a nitrogen–phosphorus detector (GC–NPD). The volume injected on to the GC column was 1 μl and the column used was DB-1701 when the samples were injected into GC–NPD system for recovery studies.

Chromatographic analysis

GC–NPD. Single organophosphorus standards were injected onto a gas chromatograph (HRGC 5300 Mega Series; Carlo Erba, Milan) equipped with a nitrogen–phosphorus detector (NPD-40; Carlo Erba). Three columns were used: a DB-1701 capillary column, 30 m × 0.25 mm i.d., chemically bonded fused phenylcyanopropylmethyl (J&W Scientific, Folsom, CA); a 30 m × 0.25 mm i.d. fused-silica capillary column coated with chemically bonded polyphenylmethylsiloxane FSQT RSL-300 (Alltech, Eke, Belgium) and a 30 m × 0.25 mm i.d. DB-5 capillary column (J&W Scientific).

Helium was used as the carrier and make-up gas. The detector gases were hydrogen and air, and their flow-rates were regulated according to the results given through the simplex optimization of the analytical variables, in this instance air and hydrogen flow-rates in the detector. Because the NPD response depends on the flow-rates of air and hydrogen in the detector, which determine the shape and temperature of the flame and consequently the ionization processes, by changing the flow-rates of air and hydrogen a maximum chromatographic response can be achieved.

The temperatures of the injector and detector were kept at 290°C for all the columns used. The DB-1701 column was programmed from 60 to 90°C at 10°C min^{-1} and from 90 to 280°C at 6°C min^{-1}. The RSL-300 column was programmed from 60 to 90°C at 10°C min^{-1} and from 90 to 310°C at 6°C min^{-1}. In all cases instances the final temperature was held for 3 min and the run time was 40 min. The samples were injected in a split/splitless mode with the septum valve opened for 35 s.

GC–MS with EI. A Hewlett-Packard (Palo Alto, CA) Model 5995 instrument interfaced to a Model 59970C data system was used for GC–EI-MS. A DB-17 fused-silica capillary column coated with 50% phenyl–50% methylpolysiloxane was introduced directly into the ion source of the mass spectrometer. Helium was used as the car-

rier gas at 83 kPa. The column was programmed from 90 to 280°C at 6°C min^{-1}. The ion source and the analyser were maintained at 200 and 230°C, respectively. The splitless mode was used, with the valve opened for 35 s. EI mass spectra were obtained at 70 eV.

The amount of each pesticide injected was 15 ng.

GC–MS with NCI. A Hewlett-Packard Model 5988A gas chromatograph interfaced to an INCOS 500E GC–MS system from Finnigan MAT (San José, CA) data system was used for GC–MS in the NCI mode. A DB-5 column containing 5% phenyl–95% methylpolysiloxane (J&W Scientific) was introduced directly into the ion source. The chromatographic conditions were identical with those described for GC–EI-MS. Methane was used as the reagent gas in NCI at 0.9 Torr. The amount of each pesticide injected was 15 ng.

RESULTS AND DISCUSSION

Qualitative information

GC–NPD. Table 1 gives the retention times (t_R) obtained for 26 organophosphorus compounds (25 pesticides plus TPP, which was used as an internal standard) with three different GC columns. Two of the columns used, DB-5 and DB-1701, and the internal standard, TPP, are recommended by the US EPA when monitoring organophosphorus and organonitrogenous pesticides [11]. When comparing the elution order obtained by the EPA with our results, the elution order matches for both the DB-5 and DB-1701 columns for the commonly characterized compounds: dichlorvos, diazinon, disulfoton, methyl paraoxon, stirofos, fenamiphos and TPP. Stan and Heil [12] also studied organophosphorus pes-

TABLE 1

Retention times of organophosphorus pesticides using three different columns

Pesticide	Peak No.	t_R (min)		
		DB-5	DB-1701	RSL-300
Azinphos-ethyl	24	27.12	34.13	33.12
Chlorpyrifos	11	20.07	25.92	21.67
Coumaphos	23	28.05	36.11	33.64
Demeton	10	23.41	25.86	22.56
Diazinon	4	17.39	19.28	17.68
Dichlorvos	1	8.59	11.18	7.59
Disulfoton	3	19.22	17.53	17.92
Ethoprop	25	15.10	– [a]	14.78
Fenamiphos	17	– [a]	29.29	25.53
Fenchlorphos	6	19.13	24.32	24.69
Fenitrooxon	9	24.22	25.70	– [a]
Fenitrothion	14	19.34	26.44	21.68
Fensulfothion	18	23.18	29.61	27.02
Fonofos	5	17.19	19.42	17.74
Malaoxon	8	24.22	25.59	21.15
Malathion	12	19.53	26.17	21.89
Paraoxon-ethyl	13	19.12	26.44	– [a]
Paraoxon-methyl	7	17.45	24.91	21.37
Parathion-ethyl	15	20.05	27.08	21.98
Phorate	2	16.04	17.50	15.86
Phosmet	22	25.26	35.14	31.03
Pyridafenthion	21	25.26	34.85	30.45
RPA 400629	16	22.44	29.00	20.40
Stirofos	19	21.49	30.26	26.09
TPP	26	– [a]		– [a]
Vamidothion	20	– [a]	30.99	– [a]

[a] Data not available.

ticides; they employed two-dimensional GC with the stationary phases SE-54 and DB-17, which are similar to DB-5 and DB-1701, respectively. The present results also agree with those of Stan and Heil, e.g., parathion-ethyl elutes before malaoxon (with a DB-5 or SE-54 column) whereas the elution order is changed when using DB-1701 or DB-17. The use of a second medium-polarity column such as DB-17 or DB-1701 also avoids co-elution of some compounds, e.g., chlorpyrifos and parathion-ethyl which co-elute on a DB-5 or SE-54 column (see Table 1 and [12]). In this sense, DB-1701 is superior to RSL-300 for these compounds as they also co-elute with the latter column. Finally, vamidothion does not elute from the DB-5 column, similarly to its retention on OV-17 [13]. This could be explained by the polarity and/or thermal stability of this compound, which requires a medium-polarity column such as DB-1701.

GC–MS with EI. Many GC–EI-MS data have been published [5–7,12–20], although in some instances the tentative identification of the different fragment ions was not indicated because common m/z fragments sometimes correspond to different chemical compositions. In addition, the relative abundances of the different ions may vary when different instruments, such as magnetic sectors, quadrupoles or ion traps, are used [7,15]. The most extensive work so far, in which 90 organophosphorus pesticides were studied, was published several years ago [13] and was based on the identification of the compounds by five typical rearrangements ions corresponding to m/z values of 93, 97, 109, 121 and 125. In the present work, the so-called typical fragment ions correspond to a longer list as summarized in Table 2. Various possibilities of tentative ion identification for the same fragment ion, e.g., m/z 97, 109, 127 and 137, are also given. This qualitative information was found to be valuable because it can be used in identifying degradation product of organophosphorus compounds. In this sense, the present work follows a previous study [16] in which exhaustive information on the typical fragment ions for fenitrothion and various decomposition products was reported.

In Table 3 the fragment ions of the 25 organophosphorus pesticides studied are listed. Based on Tables 2 and 3, various comments can be made.

The formation of the typical fragment ions reported in Table 2 will depend on the type of molecule. In this sense it is possible that two compounds will have an ion with the same m/z value, but with different structures. This is the case of organophosphorus pesticides of different classes, e.g., m/z 109 corresponds either to $(CH_3O)_2PO^+$ (dichlorvos, stirofos, fenitrooxon), to $(C_2H_5O)OHPO^+$ (coumaphos, parathion-ethyl) or to $(C_2H_5O)PSH^+$ (fonofos). The rearrangement ion at m/z 97 usually corresponds to $(OH)_2PS^+$, such as for chlorpyrifos, fenitrothion and ethoprop, but in the case of diethyldithiophosphorothioates, RPA, phorate and disulfoton it corresponds to $(SH)_2P$. For all these reasons, it

TABLE 2

Typical fragment ions of organophosphorus pesticides in GC–EI-MS

m/z	Ion	Other possibilities
47	CH_3S^+	
62	CH_3OP^+	
63	CH_3OPH^+	
75	$CH_2SC_2H_5^+$	
77	$C_2H_5OPH^+$	
79	CH_3OPOH^+	
93	$(CH_3O)_2P^+$	
96	$CH_3OP(OH)_2^+$	
97	$(HO)_2PS^+$	$P(SH_2)$
109	$(CH_3O)_2PO^+$	$(C_2H_5O)OHPO^+$, $(C_2H_5O)PSH^+$
121	$(C_2H_5O)_2P^+$	
125	$(CH_3O)_2PS^+$	
126	$(C_2H_5O)OHPSH^+$	
127	$(CH_3O)_2P(OH)_2^+$	$(C_2H_5O)P(OH)_3^+$
137	$(C_2H_5O)(C_2H_5)PS^+$	$(C_2H_5O)_2PO^+$
141	$(C_2H_5O)OHPOS^+$	
142	$(CH_3O)_2POHS^+$	
153	$(C_2H_5O)_2PS$	
157	$(CH_3O)_2PS_2^+$	
158	$(CH_3O)_2PSSH^+$	
169	$(C_2H_5O)_2POS^+$	
171	$(C_2H_5O)_2POHSH^+$	
185	$(C_2H_5O)_2PS_2^+$	

is useful to look at the chemical structures of the different compounds as some of the fragment ions can then be predicted.

The typical fragment ions usually correspond to a class of organophosphorus compounds. In this sense, m/z 109 and 125 are the base peaks for the dimethylphosphates and dimethylphosphorothioates, respectively.

The abundance of $[M]^+$ increases with its ability to sustain a positive charge and is related to the ionization energy, which is lowered for S rather than O. Examples of this case are parathion-ethyl and fenitrothion, which show higher relative abundances of $[M]^+$ than the oxo derivatives (see Table 3).

The chlorinated organophosphorus compounds such as stirofos, dichlorvos, chlorpyrifos and fenchlorphos exhibit as main peaks the corresponding fragment ions with chlorine losses (see Table 3).

Specific fragments which are typical of some compounds are also observed, e.g., McLafferty rearrangement involving proton abstraction by an oxygen of the nitro group indicating the presence

TABLE 3

Fragment ions of organophosphorus pesticides and relative abundances (%) in GC–EI-MS.

Mol. wt.	Pesticide	m/z (relative intensity, %) [main ions]$^+$
345	Azinphos-ethyl	104(19)[$N_2 - C_6H_4$]$^+$, 132(100)[$CH_2 - N_3 - C_6H_4$]$^+$, 160(82)[$CH_2 - N_3 - CO - C_6H_4$]$^+$
349	Chlorpyrifos	97(59), 125(22), 197(100)[$H_2OC_5Cl_3N$]$^+$, 258(37)[M − $(C_2H_4)_2$ − Cl]$^+$, 314(33)[M − Cl]$^+$
362	Coumaphos	89(31), 97(94), 109(100), 125(41), 210(56), 226(49)[$OHC_6H_3C_4H_3O_2$]$^+$, 362(79)[M]$^+$
258	Demeton	109(47), 125(39), 169(100)
304	Diazinon	93(29), 137(100)[OH − C_4H_4 − CH_2 − C − CH − CH_3]$^+$, 152(74)[OH − C_4H_4 − CH_3 − C − $CH(CH_3)_2$]$^+$, 179(98)[C_2H_5O − $C_4H_4N_2$ − CH_3 − C − $CH(CH_3)_2$]$^+$, 199(59), 304(22)
220	Dichlorvos	79(18), 109(100), 185(30)[M − Cl]$^+$
274	Disulfoton	88(100)[C_2H_5 − SCH=CH_2]$^+$, 97(31), 125(26), 147(27), 153(27), 186(25), [M − 88]$^+$, 274(10)[M]$^+$
242	Ethoprop	97(57), 126(48), 139(46)[$SC_3H_7PO \cdot OH$]$^+$, 158(100)[M − C_6H_{12}]$^+$, 200(31)[M − C_3H_6]$^+$
303	Fenamiphos	122(29)[$PO \cdot OH \cdot NHCH \cdot (CH_3)_2$]$^+$, 154(100)[$CH_3S$ − C_6H_3 − CH_3OH]$^+$, 217(54)[260 − C_3H_8]$^+$, 260(30)[M − C_3H_8]$^+$, 288(31)[M − CH_3]$^+$, 303(87)[M]$^+$
340	Fenchlorphos	79(17), 109(28), 125(65), 285(100)[M − Cl]$^+$
261	Fenitrooxon	109(97), 127(20), 244(100)[M − OH]$^+$, 261(12)[M]$^+$
277	Fenitrothion	79(19), 93(18), 109(72), 125(100), 260(37)[M − OH]$^+$, 277(59)[M]$^+$
308	Fensulfothion	97(58), 109(48), 125(81), 139(39), 140(82), 141(64), 153(34), 156(100)[CH_3SO − C_6H_4 − OH]$^+$, 293(84)[M − CH_3]$^+$
246	Fonofos	109(100), 137(57), 246(36)[M]$^+$
314	Malaoxon	99(23)[$(CHCO)_2OH$]$^+$, 109(19), 125(25), 127(100)[$(CH - CO)_2OC_2H_5$]$^+$, 142(16)[MH − 173]$^+$, 173(12)[C_2H_5OOC − CH_2 − CH − $COOC_2H_5$]$^+$, 195(17)[M − CH_3O − CH_3 − $COOC_2H_5$]$^+$
330	Malathion	93(40), 125(85), 127(93)[173 − C_2H_5O]$^+$, 158(43)[173 − CH_3]$^+$, 173(100)[C_2H_5OOC − CH_2 − $CHCOOC_2H_5$]$^+$
275	Paraoxon-ethyl	81(38), 109(100), 127(27), 139(51)[OHC_6H_4 − NO_2]$^+$, 149(66), 220(26)[M − C_4H_7]$^+$, 247(25)[M − C_2H_4]$^+$, 275(27)[M]$^+$
247	Paraoxon-methyl	79(15), 96(41), 109(100), 230(36)[M − OH]$^+$, 247(25)[M]$^+$
291	Parathion-ethyl	97(83), 109(100), 125(49), 139(67)[$HOC_6H_4NO_2$]$^+$, 155(54)[$HSC_6H_4NO_2$]$^+$, 186(29)[M − C_2H_4]$^+$, 291(63)[M]$^+$
260	Phorate	75(100), 97(27), 121(58), 260(20)[M]$^+$
317	Phosmet	77(4), 93(4), 160(100)[CH_2 − N − $(CO)_2$ − C_6H_4]$^+$, 317(2)[M]$^+$
340	Pyridafenthion	77(30), 97(68), 125(47), 188(89)[MH − 153]$^+$, 199(100)[M − 141]$^+$, 204(58)[MH − 137]$^+$, 340(79)[M]$^+$
368	RPA-400629	97(25), 109(24), 121(31), 153(14), 171(100), 215(30)[M − 153]$^+$, 323(11)[M − OC_2H_5]$^+$
366	Stirofos	79(11), 109(100), 331(66)[M − Cl]$^+$
287	Vamidothion	58(13), 60(15), 87(100)[CH_3 − NH − CO − C_2H_5], 109(39), 125(20), 142(39), 145(74)[M − 142]$^+$, 169(26)

TABLE 4

Diagnostic ions of organophosphorus pesticides in NCI mode

m/z	Ion	Group
125	$(CH_3O)_2PO_2$	Dimethylphosphates
141	$(CH_3O)_2POS$	Dimethylphosphorothiolates
153	$(C_2H_5O)_2PO_2$	Dimethylphosphorothionates
157	$(CH_3O)_2PS_2$	Dimethylphosphorodithioates
169	$(C_2H_5O)_2POS$	Diethylphosphorothionates
185	$(C_2H_5O)_2PS_2$	Diethylphosphorodithioates

of CH_3 adjacent to an NO_2 group, for fenitrothion and fenitrooxon. The formation of specific ions for azinphos-ethyl, coumaphos, diazinon and malaoxon also needs consideration and follows reported predictions [14,17], e.g., m/z 179 of diazinon is a result of the migration of an ethyl group from the diethoxy group to the oxygen atom of the moiety with removal of a hydrogen from the isopropyl group either before or after the rearrangement.

From the different compounds reported in Table 3, to our knowledge, RPA and pyridafenthion have not been previously reported in GC–MS. The information reported in this paper is relevant for the latter compound, which has been detected in natural waters by GC with alkali flame ionization detection [21].

GC–MS with NCI. GC–MS with NCI has been demonstrated to be a very selective [as compared with EI and positive-ion chemical ionization

TABLE 5

Typical fragment ions of organophosphorus pesticides and relative abundances (%) in GC–NCI-MS (amount injected 15 ng)

Mol. wt.	Pesticides	m/z (relative abundance, %) [main ions]$^{-\cdot}$
345	Azinphos-ethyl	185(100), 133(4)[$CH_2 - N - CO - C_6H_4$]$^{-\cdot}$
349	Chlorpyrifos	169(23), 212(40)[M – $(C_2H_5O)_2PO$], 313(100)[M – HCl]$^{-\cdot}$
362	Coumaphos	169(6), 225(54)[S – $C_6H_3 - C_4H_3O_2Cl$]$^{-\cdot}$, 362(100)[M]$^{-\cdot}$
258	Demeton	169(15), 187(100)[M – $C_2H_5 - C_3H_6$]$^{-\cdot}$
304	Diazinon	169(100)
220	Dichlorvos	125(100), 134(58)[M – CH_3 – Cl – HCl]$^{-\cdot}$, 170(80)[M – CH_3 – Cl}$^{-\cdot}$
274	Disulfoton	185(100)
242	Ethoprop	199(100)[M – C_3H_7]$^{-\cdot}$
303	Fenamiphos	153(100)[$CH_3S - C_6H_3 - CH_3O$]$^{-\cdot}$
340	Fenchlorphos	141(20), 211(100)[$SC_6H_2Cl_3$]$^{-\cdot}$, 270(54)[M – CH_3Cl]$^{-\cdot}$
261	Fenitrooxon	261(100)[M]$^{-\cdot}$
277	Fenitrothion	141(12), 168(30)[$SC_6H_3NO_2CH_3$]$^{-\cdot}$, 277(100)[M]$^{-\cdot}$
308	Fensulfothion	169(100), 293(8)[M]$^{-\cdot}$
246	Fonofos	109(39)[S – C_6H_5]$^{-\cdot}$;169(100)[$C_2H_5O - C_2H_5PS_2$]$^{-\cdot}$
314	Malaoxon	141(100)
173	Malathion	157(100)
275	Paraoxon-ethyl	275(100)[M]$^{-\cdot}$
247	Paraoxon-methyl	247(100)[M]$^{-\cdot}$
291	Parathion-ethyl	154(100)[$SC_6H_4NO_2$]$^{-\cdot}$
260	Phorate	185(100)
317	Phosmet	157(100)
340	Pyridafenthion	169(40), 340(100)[M]$^{-\cdot}$
368	RPA-400629	169(49), 185(100)
366	Stirofos	125(100)
287	Vamidothion	141(100)

(PCI)] and sensitive technique for the determination of various organophosphorus pesticides [1,4,7,19,22–24]. The molecules of the so-called parathion-like structure offered high sensitivity under the negative-ion conditions owing to the presence of an aromatic moiety together with a nitro group, thus forming a kind of pseudo-acid by electron attachment which stabilizes the negative charge. The compounds studied here include parathion, paraoxon, fenitrothion and fenitrooxon. When this aromatic moiety contains other electron-withdrawing groups, e.g., chlorine atoms, such as for fenchlorphos and stirofos, the stabilization of the negative charge and sensitivity are also enhanced. Around two orders of magnitude higher sensitivity compared with EI have been reported for such compounds [1,7,23]. Demeton, dichlorvos, fenamiphos, fenthion and metamidaphos have been reported to offer better sensitivity under PCI than NCI conditions [23]. This could be explained by their structures, which yield molecules exhibiting high proton affinities and so are better detected using PCI.

Table 4 lists the diagnostic ions of the different organophosphorus pesticides, which are characteristic of the different chemical groups [22]. Table 5 lists the different ions formed by the organophosphorus pesticides. The following general remarks can be made.

The diagnostic ions formed under NCI which are indicated in Table 4 are, in many instances, the base peaks of the different compounds and also, in a few instances, the only spectral information obtained. This is a typical characteristic of MS-NCI of organophosphorus pesticides, so their unequivocal identification should always be carried out in combination with the retention time.

The formation of $[M]^{-\cdot}$ has a 100% relative abundance for the organophosphorus compounds of the so-called parathion group and compounds having an aromatic moiety (with the exception of chlorinated organophosphorus pesticides). This is

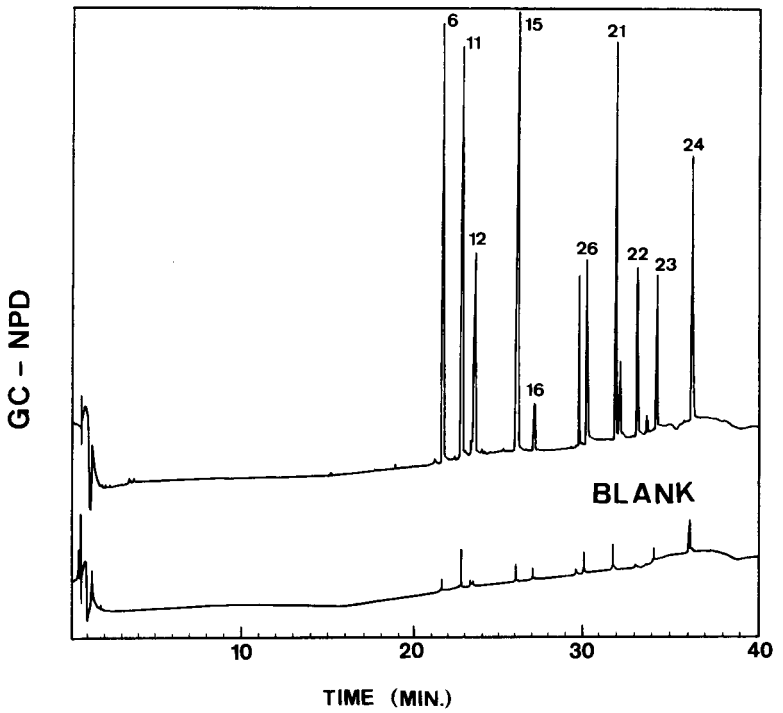

Fig. 1. GC–NPD of Ebro waters spiked with 10–15 $\mu g\ l^{-1}$ of azinphos-ethyl, coumaphos, chlorpyrifos, fenamiphos, fenchlorphos, fenitrothion, phosmet, pyridafenthion and stirofos. A DB-1701 fused-silica column (30 m × 0.25 mm i.d.) was used. Chromatographic conditions as described in text. For peak numbers see Table 1.

due to the fact that $[M]^{-\cdot}$ is fairly stable under NCI conditions when an aromatic moiety exists in the molecule, and is even more important when a nitro group is present.

The chlorinated organophosphorus pesticides with an aromatic moiety have intense or base peaks corresponding to looses of Cl owing to the facility of such processes under NCI conditions. This is the case with fenchlorphos, dichlorvos and chlorpyrifos.

The formation of thiophenolate versus phenolate ions for compounds such as parathion, fenitrothion, coumaphos and fenchlorphos is due to the strong acidity of thiophenolate versus phenolate in the gas phase and there is a transfer from the aromatic moiety from the oxygen to the sulphur atom.

Fenamiphos is not detected under NCI conditions with the amount of compound injected, 15 ng. This is in accordance with expectation for this compound, which should be analysed under PCI conditions [23].

Recovery studies

Water samples. In recent years, instead of using C_{18} silica cartridges [21], an alternative has appeared for the trace enrichment of organic compounds, including pesticides, from water samples. This is also based on liquid–solid extraction (LSE) and concerns the use of membrane extraction discs, which are available in a similar diameter and size to LC solvent filters. Their main advantage over LSE cartridges is the high sampling flow-rate, which facilitates sampling in the field. So far such discs have been tested for the isolation of different groups of compounds, including pesticides, organotin compounds and phthalates from water samples followed by GC and/or LC determination [25–28].

A GC–NPD trace for spiked waters from the Ebro delta with its corresponding blank is shown in Fig. 1. The DB-1701 column allows a good separation of fenchlorphos, fensulfothion, fenitrothion, stirofos, fenamiphos, TPP, pyridafenthion, phosmet, azinphos-ethyl and coumaphos.

The recoveries of the different organophosphorus pesticides and the standard deviations are given in Table 6. Recoveries were calculated in relation to TPP, which is the internal standard proposed by the EPA [11].

TABLE 6

Mean recoveries of organophosphorus pesticides and relative standard deviation of spiked Ebro waters at a level of 10–15 $\mu g\ l^{-1}$ ($n = 5$)

Pesticide	Mean recovery (%)	R.S.D. (%)
Azinphos-ethyl	120	5.6
Coumaphos	108	8.6
Chlorpyrifos	94	4.4
Fenamiphos	77	7.0
Fenchlorphos	91	5.4
Fenitrothion	112	5.3
Phosmet	109	4.4
Pyridafenthion	104	2.3
Stirofos	107	4.5

The recoveries for the different organophosphorus pesticides follow expectation and show general agreement when using C_{18} cartridges [21] or discs [28] with ethyl acetate or acetonitrile as eluting solvent, respectively. The recoveries obtained are within the EPA recommendations (from 70 to 130%) for these levels of detection in water samples. Following the protocol described under Experimental and from the GC traces shown in Fig. 1, a limit of detection (LOD) of ca. 0.1 $\mu g\ l^{-1}$ can be estimated with a signal-to-noise ratio of 3. Such an LOD can be decreased by a factor of five if the final concentration of water samples prior to GC injection is made to 0.2 ml instead of 1 ml.

Biota samples. Methods recommended in literature include typical clean-up with Florisil [5] and GPC [4,10]. However, when the extract contains a high percentage of lipidic matter these techniques give low recoveries and sometimes a combination of two clean-up procedures is needed or the use of solvents of different polarity to improve the clean-up. Relatively new clean-up techniques work with disposable C_{18} cartridges [29] and C_{18} Empore discs, which to our knowledge have never been tested for the clean-up of biota samples. All these methods have been tested using spiked fish samples.

A typical clean-up with Florisil gave very poor results. Lipid interferences appeared in the chro-

matogram, which made quantification impossible. The low recoveries for Florisil can be explained by the fact that the protocol described [5] for bivalve analysis was followed. As fish exhibit a higher lipidic content than bivalves, much more Florisil would be needed in the column to achieve a good clean-up.

A combination of clean-up through C_{18} extraction discs and Florisil fractionation was done. Not all the compounds could be identified, and of those which could be quantified their recoveries were extremely low. These samples were first subjected to GC–EI-MS under full-scan conditions, but no compounds were detected. Only the use of GC–MS with NCI permitted the identification of a few organophosphorus pesticides, confirming the sensitivity and selectivity of this technique. The chromatogram shown in Fig. 2 corresponds to a sample of red mullet spiked with fenchlorphos. Various ions were detected, allowing an unequivocal determination of the compound by three different m/z ions. By the use of GC–NCI-MS under full-scan conditions, it was possible to achieve LODs in the range 3–5 pg (2 ng g^{-1} in the biota samples) with a signal-to-noise ratio of 10, for compounds such as fenchlorphos, fenitrothion, fenitrooxon and pyridafenthion. This corresponds to an LOD approximately two orders of magnitude lower than that for the same compounds using GC–EI-MS. The LOD achieved corresponds to the expected low levels found in biota samples.

Disposable C_{18} cartridges were used to study the recoveries of organophosphorus pesticides, following Gillespie and Wattes [29], who recommended their use for the clean-up of fat extracts.

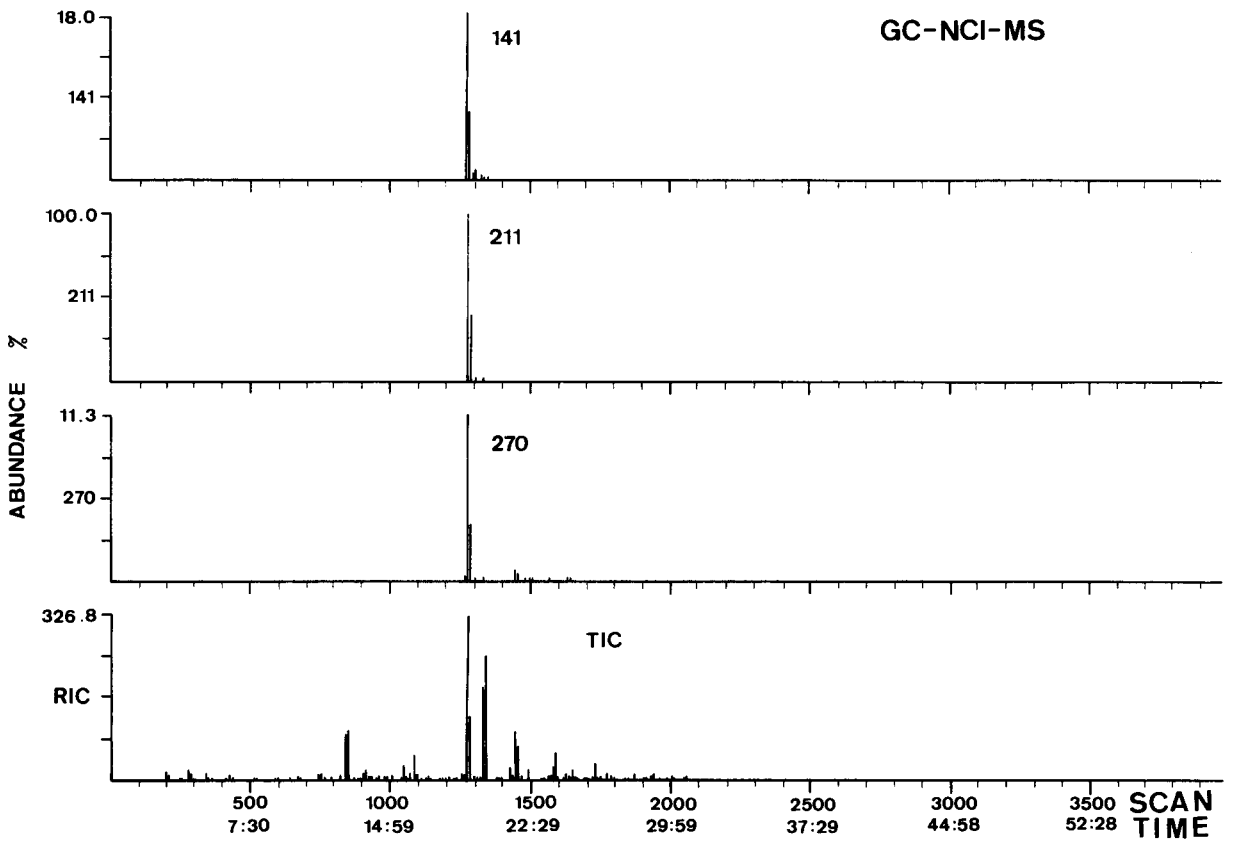

Fig. 2. Total ion current (TIC) and selected ion chromatograms obtained using GC–NCI-MS of spiked fish tissue that contained 75–100 ng g^{-1} of the same organophosphorus compounds as indicated in Fig. 1. Ions monitored correspond to m/z 141, 211 and 270 for fenchlorfos. A DB-5 column was used. Chromatographic conditions as described in text.

TABLE 7

Comparison of mean recoveries (%) of organophosphorus pesticides in fish samples using different clean-up techniques (spike level 0.1 $\mu g\ g^{-1}$ lyophilized tissue)

Pesticide	C_{18} cartridge	C_{18} + GPC	
		Acetonitril	Ethyl acetate
Azinphos-ethyl	104	63	35
Coumaphos	110	81	45
Chlorpyrifos	135	136	92
Fenamiphos	– [a]	30	20
Fenchlorphos	92	132	88
Fenitrothion	– [a]	132	84
Phosmet	– [a]	60	33
Pyridafenthion	106	114	65
Stirofos	92	118	72

[a] Data not available.

The main problem is that nine cartridges were needed instead of the six recommended, probably owing to the high lipidic content of the present samples compared with oily samples such as olives and corn [29]. This method is time consuming and expensive owing to the need to use nine cartridges for each analysis. The recoveries were acceptable for some of the compounds, such as pyridafenthion, azinphos-ethyl, fenchlorphos, coumaphos and stirofos, with recoveries in the range 90–100% (see Table 7). The R.S.D. varied between 7–9% except for compounds with recoveries between 20–45% which exhibit R.S.D. values of 20–25%. Other compounds gave rise to

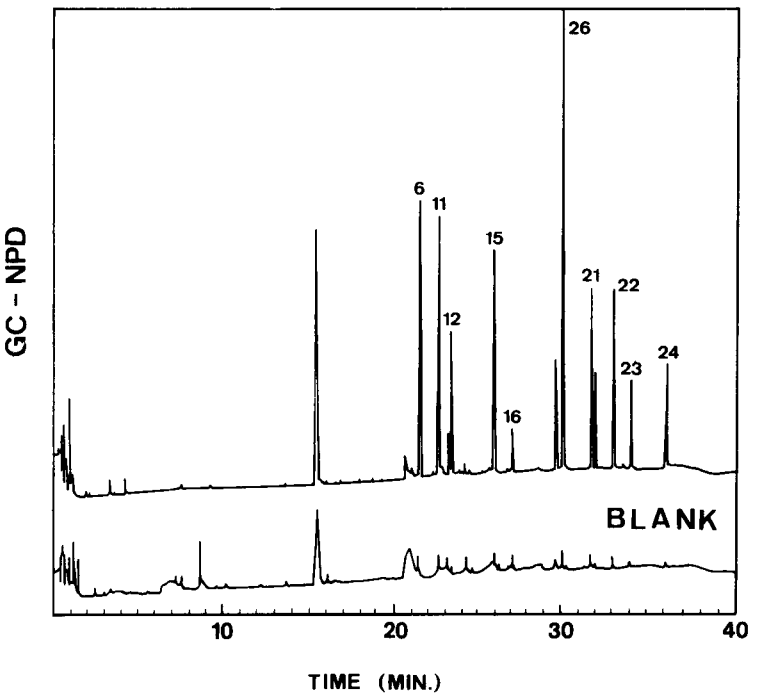

Fig. 3. GC–NPD of fish samples that contained ca. 75–100 ng g^{-1} of azinphos-ethyl, coumaphos, chlorpyrifos, fenamiphos, fenchlorphos, fenitrothion, phosmet, pyridafenthion and stirofos. Clean-up by C_{18} extraction with acetonitrile plus GPC; the GC column used was as in Fig. 1. For peak numbers see Table 1.

difficulties, such as fenamiphos, which could be related to its thermal instability in GC.

A single clean-up with C_{18} Empore discs was tested using ethyl acetate and acetonitrile as eluting solvents. Whereas it was impossible to identify any compound when ethyl acetate was used, satisfactory results were obtained with acetonitrile. For example, for fenchlorphos the recovery was 72%, coumaphos 61%, azinphos-ethyl 42% and pyridafenthion 75%.

GPC is one of the most often used techniques for removing lipidic material from biota samples such as bivalves [5] and fish samples [4–6,30,31]. Bio-Beads S-X3 is the most common stationary phase used when organophosphorus pesticides need to be determined. GPC was combined with C_{18} extraction discs because in previous work [5] it was necessary to combine GPC clean-up with Florisil column chromatography for the isolation of organophosphorus pesticides from bivalves. From experience with C_{18} Empore discs for water analysis [28] and based on a recent paper recommending C_{18} cartridges for the isolation of organophosphorus pesticides from lipid-rich samples [29], it was decided to combine GPC with C_{18} Empore discs. The results are reported in Table 7.

Figure 3 shows an example of this method. The better recoveries obtained with acetonitrile versus ethyl acetate as eluting solvent for organophosphorus pesticides can be related to the behaviour observed for organophosphorus pesticides in their isolation from water samples when using C_{18} Empore discs [28]. When analysing hydrophobic material, such as fish, one can easily overload the active sites of the discs, thus exceeding their capacity for retention of the different compounds, so adsorption of the lipidic material together with the organophosphorus pesticides occurs. In the desorption step, when either ethyl acetate or acetonitrile is added, the organophosphorus pesticides are affected by the

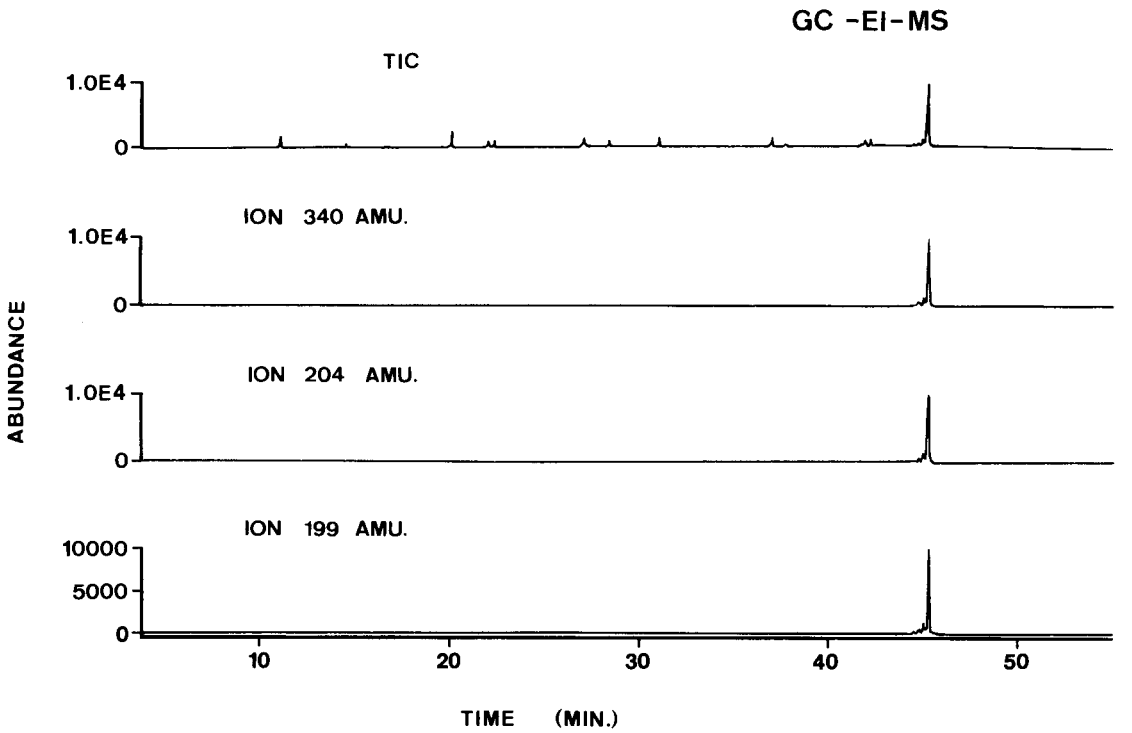

Fig. 4. Total ion current (TIC) and selected ion chromatograms obtained using GC–EI-MS of water samples from the Ebro delta that contained 4 $\mu g\ l^{-1}$ pyridafenthion. Pyridafenthion ions were monitored at m/z values 340, 204 and 199. A DB-17 column was used. Chromatographic conditions as described in text. For peak numbers see Table 1.

solubility of the solvent used. When using ethyl acetate, which has a greater eluting strength than acetonitrile for hydrophobic compounds, the recoveries for the most non-polar organophosphorus pesticides such as fenchlorphos, fenitrothion, stirofos and chlorpyrifos were high and agreed with the values reported for acetonitrile. However, for the most polar organophosphorus pesticides, e.g., phosmet and azinphos-ethyl, the recoveries with acetonitrile were higher, which is related to its capacity to remove relatively polar pesticides from C_{18} discs more efficiently than ethyl acetate.

Environmental levels

Samples of Ebro delta water were analysed during the period of spraying pesticides. Pyridafenthion was found in three different samples for the first time. Confirmatory analyses were made with GC–EI-MS. Figure 4 shows the ion chromatogram corresponding to water samples obtained in June, which contained 4 $\mu g\ l^{-1}$ pyridafenthion. Further sampling was done in July, 5 and 3 days after spraying and on the same day. The concentration found 5 and 3 days after spraying was 9 $\mu g\ l^{-1}$ in both instances. A 62 $\mu g\ l^{-1}$ level of pyridafenthion was found in water samples that had been treated on the same day. These values are much higher than the reported environmental levels, which were generally lower than 0.1 $\mu g\ l^{-1}$ [21].

Conclusions

The identification of 25 organophosphorus pesticides was achieved from their retention times obtained with three GC columns (DB-5, DB-1701 and RSL-300) of different polarity using GC–NPD and from complementary structural information achieved by GC–EI-MS and NCI. Nine of these 25 organophosphorus pesticides of different chemical groups were selected for an isolation and clean-up study in water and biota samples. The use of C_{18} Empore extraction discs was found to be an effective means for the trace determination of these pesticides in natural waters at the 0.02 $\mu g\ l^{-1}$ level. In the isolation of organophosphorus pesticides from biota samples, the combined use of GPC column fractionation and C_{18} Empore discs was an effective means of removing lipidic material from the matrix, and can be recommended. GC–NCI-MS is the best choice for the confirmation of organophosphorus pesticides from biota samples, being a very selective means of detecting levels as low as 2 ng g^{-1} in biota samples of high lipidic content. The technique is very selective and sensitive for organophosphorus pesticides with electron-withdrawing groups, but attention should be paid to certain organophosphorus pesticides for which the technique may not be sensitive enough. For the analysis of real environmental waters recently polluted with pyridafenthion, GC–EI-MS was used. The levels varied from 62 $\mu g\ l^{-1}$ on the same day to 9 $\mu g\ l^{-1}$ 5 days after airplane spraying. At such contamination levels, and following the protocol described in this paper, the use of GC–EI-MS was sensitive enough to achieve its confirmation. Future work will include the investigation of the degradation products of fenitrothion after its application into the channels of the Ebro delta.

This work was supported by the Environment R&D Program 1991–1994 (Commission of the European Communities) on the Analysis and Fate of Organic Pollutants in Water (Contract No. EV5V-CT92-0105). J.T. Baker (Deventer, Netherlands) is thanked for supplying C_{18} Empore extraction discs. S.L. gratefully acknowledges financial support from CICYT (Grant AMB92-0218).

REFERENCES

1 D. Barceló, Trends Anal. Chem., 10 (1991) 323.
2 D.J. Munch and Ch.P. Frebis, Environ. Sci. Technol., 26 (1992) 921.
3 J.P. Hsu, H.J. Schattenberg, III, and M.M. Garza, J. Assoc. Off. Anal. Chem., 74 (1991) 886.
4 D. Barceló, C. Porte, J. Cid and J. Albaigés, Int. J. Environ. Anal. Chem., 38 (1990) 199.
5 D. Barceló, M. Solé, G. Durand and J. Albaigés, Fresenius' J. Anal. Chem., 339 (1991) 676.
6 G. Durand, R. Forteza and D. Barceló, Chromatographia, 28 (1989) 597.

7 G. Durand and D. Barceló, Anal. Chim. Acta, 243 (1991) 259.
8 C. Porte, D. Barceló and J. Albaigés, Chemosphere, 24 (1992) 735.
9 D. Barceló, Analyst, 116 (1991) 681.
10 D. Barceló and J.F. Lawrence, in Th. Cairns and J. Sherma (Eds.), Emerging Strategies for Pesticide Analysis, CRC, Boca Raton, FL, 1992, pp. 127–149.
11 L. Graves, Method 507, Revision 2.0 (1989), Detemination of Nitrogen and Phosphorus Containing Pesticides in Water by Gas Chromatography with a Nitrogen–Phosphorus Detector, U.S. Environmental Protection Agency, Cincinnati, OH, 1989.
12 H.J. Stan and S. Heil, Fresenius' J. Anal. Chem., 339 (1991) 34.
13 J.P.G. Wilkins, A.R.C. Hill and D.F. Lee, Analyst, 110 (1985) 1045.
14 H.J. Stan, B. Abraham, J. Jung, M. Keller and K. Teinland, Fresenius' Z. Anal. Chem., 287 (1977) 271.
15 J.P.G. Wilkins, Pestic. Sci., 29 (1990) 163.
16 G. Durand, M. Mansour and D. Barceló, Anal. Chim. Acta, 262 (1992) 167.
17 N. Damico, J. Assoc. Off. Anal. Chem., 49 (1966) 1027.
18 J.M. Desmarchelier and M.J. Lacey, in F.W. Karasek, O. Hutzinger and S. Saf (Eds.), Mass Spectrometry in Environmental Sciences, Plenum, New York, 1985, pp. 455–474.
19 K.L. Busch, M.M. Bursey, J.R. Hass and G.W. Sovocool, Appl. Spectrosc., 32(1978) 388.
20 A.K. Singh, D.W. Hewetson, K.C. Jordon and M. Ashraf, J. Chromatogr., 369(1986) 83.
21 J.C. Moltó, Y. Picó, G. Font and J. Mañes, J. Chromatogr., 555 (1991)137.
22 H.J. Stan and G. Kellner, Biomed. Mass Spectrom., 9(1982) 483.
23 H.J. Stan and G. Kellner, Biomed. Environ. Mass Spectrom., 18(1989) 645.
24 G. Durand, F. Sanchez-Baeza, A. Messeguer and D. Barceló, Biol. Mass Spectrom., 20 (1991) 3.
25 D.F. Hagen, C.G. Markell, G.A. Schmitt and D.D. Blevins, Anal. Chim. Acta, 236 (1990) 157.
26 A. Kraut-Vass and J. Thoma, J. Chromatogr., 538 (1991) 233.
27 O. Evans, B.J. Jacobs and A.L. Cohen, Analyst, 116 (1991) 15.
28 D. Barceló, G. Durand V. Bouvot and M. Nielen, Environ. Sci. Technol., 27 (1993) 271.
29 A.M. Gillespie and S.M. Walters, Anal. Chim. Acta, 245 (1991) 259.
30 S.M. Walters, Anal. Chim. Acta, 236 (1990) 77.
31 T.E. Horsberg, T. Hoy and O. Ringstad, J. Agric. Food. Chem., 38 (1990) 1403.

Analytica Chimica Acta, 281 (1993) 85–93
Elsevier Science Publishers B.V., Amsterdam

Effect of conformational changes on the reversed-phase chromatographic retention of polyoxyethylenes: quantitative interpretation based on a retention model in combination with molecular mechanics

Tetsuo Okada

Faculty of Liberal Arts, Shizuoka University, Shizuoka 422 (Japan)

(Received 13th January 1993; revised manuscript received 4th March 1993)

Abstract

The reversed-phase chromatographic retention of compounds having polyoxyethylene (POE) as a part of the structure is known to be affected by conformational changes of the POE chains. A modified two-state model, where zig-zag and helix conformers are assumed to be more stable than others, was developed to evaluate the conformational changes and applied to the calculation of the conformational equilibria, the evaluation of the contributions from the stable conformers to the overall retention and the prediction of retention. Molecular mechanics calculation was also used to evaluate the solution behaviour of POE chains.

Keywords: Liquid chromatography; Conformation; Polyoxyethylenes

The separation of polyoxyethylene (POE) oligomers is important in separation sciences and technology, because POE chains play important roles in surface-active agents [1–5], as ligands for hard metal ions [6–10] and recently as conductive polymers [11–13]. Compounds containing POE chains are often polydisperse for both POE and hydrocarbon chains [1,2]. Chromatography is therefore a suitable method for analyses for such compounds, and has been extensively used in a variety of separation modes [14–22]; liquid chromatography [14–20], especially the reversed-phase mode [14–18], is an effective and convenient method, and numerous papers dealing with such separations have been published.

When the distribution of POE chain lengths is of primary interest, understanding the retention behaviour of POE is necessary for the optimization of the separation. Even for separation according to the hydrocarbon chain length, the retention behaviour of POEs should be precisely evaluated because such separations must not be affected by the distribution of POE chain lengths [18,20].

Melander et al. [14] reported irregular retention behaviour of POEs due to the conformational changes of the polymer chains. They attempted to explain this irregular retention behaviour by assuming the presence of two stable rotamers that have different retention abilities, although the chromatographic parameters of each rotamer and thermodynamic parameters for the retention processes were not determined. Chromatography can be an efficient means of probing the solution behaviour of solutes including secondary effects, and conformational changes can also be evaluated using chromatographic data.

Correspondence to: T. Okada, Faculty of Liberal Arts, Shizuoka University, Shizuoka 422 (Japan).

However, no quantitative chromatographic analysis has been applied to clarify the solution behaviour and the irregular retention of POEs. This is due mainly to a lack of the information on the solution behaviours of POEs and partly to insufficient developments of retention models.

Appropriate methods other than chromatography are needed for understanding the conformational changes of POEs. Although nuclear magnetic resonance spectrometry, for example, is efficient, quantitative analyses are difficult for long POE chains. Similarly, Raman spectrometry is not very suitable for the quantitative elucidating of the solution chemistry of POEs with a variety of chain lengths. Therefore, molecular mechanics (MM) calculation, principally developed by Allinger [23], was chosen as a suitable means to study the equilibrium of POE.

In this paper, the retention behaviour of POEs is interpreted using a retention model developed by assuming two stable rotamers, and an attempt is made to reveal the retention mechanisms and the solution behaviour of POEs in combination with the MM calculation. The prediction of separations using this model is also presented.

EXPERIMENTAL

Apparatus

The chromatographic system was composed of a Tosoh CCPM, computer-controlled pump, a Rheodyne injection valve equipped with a 100-μl sample loop, a JASCO 830-RI refractive index detector, a JASCO 875-UV UV detector and a SIC Chromatocoder 12 integator. The separation column, Wakosil 5C8 (a 150 mm $\times$ 4 mm i.d. stainless-steel column packed with octylsilanized silica gel of 5-μm particle size, purchased from Wako), was placed in a thermostated water-bath. The flow-rate was maintained at 1 ml min^{-1}. Unless stated otherwise, experiments were carried out at 25°C.

Reagents

The reagents used were of analytical-reagent grade. Ethylene glycol, diethylene-glycol, triethylene glycol, tetraethylene glycol and polyethylene glycol (PEG) were purchased from Wako. Dialkyl-PEGs were used as solutes to eliminate the effects of terminal hydroxyl groups on the retention and the solution behaviour. Dimethyl-, diethyl- and dibutyl-PEG (MePEG, EtPEG and BuPEG) were synthesized by the reaction of the disodium salts of ethylene glycol (EG), oligo-EG or PEG with an appropriate alkyl bromide or alkyl iodide. Acetonitrile of LC grade and distilled, deionized water were used for the preparation of mobile phases. Mobile phases were used after deaeration. POE samples were dissolved in acetonitrile and diluted with the mobile phase to the appropriate concentration.

Molecular mechanics calculation

Molecular mechanics calculation was performed on an NEC PC-9801VX personal computer using the MM2 force field, which was originally developed by Allinger but translated for PC-9801 series personal computers by Yoshimura [24]. This program was purchased from Science House. MM calculation was carried out for compounds with $n = 1$–9 (where n denoted the number of oxyethylene units). However, because steric energy showed a sudden increase at $n = 5$, results for $n = 5$–9 were omitted and only those for $n = 1$–4 were used for the discussion.

RESULTS AND DISCUSSION

Chromatographic behaviour of POE

Figure 1 shows typical chromatograms of EtPEG and BuPEG. For EtPEG the retention increases with increasing n whereas for BuPEG the retention decreases with increasing n. Longer POEs are usually thought to be more hydrophobic, i.e., POEs having more oxyethylene units are more distributable into an organic solvent. The retention behaviour of EtPEGs is predictable on this basis, but that of BuPEGs is not. Although, in some instances, a decrease in retention with increasing n was explained by a molecular sieve effect from stationary phases [17], the conformational changes of POE chains should be taken

into account to explain this unusual retention behaviour.

Conformation changes of POE chains

Typical stable rotamers of a POE [MePEG ($n = 4$)] are illustrated in Fig. 2. A number of studies have indicated that the *trans* (T) conformer is the most stable one for C–O bonds regardless of the nature of the media [25–31]; it has been reported that a *trans* configuration around the C–O bond is more stable than the *gauche* form by at least 10 kJ mol^{-1} [25], and that this energy difference is too large to be compensated for by the solvation. In contrast, the stability of the *trans* conformer relative to the *gauche* (G) conformer does vary for C–C bonds depending on the nature of the medium, terminal hydrocarbon chains, length of the POE chain, etc. Usually, in the gas phase, an all-*trans* conformer is thought to be the most stable, whereas a helix structure, which is constructed with a succession of TTGTTG along C–O–C–C–O–C–C bonds, becomes more stable with increasing polarity of the solvent. A recent Raman spectroscopic study

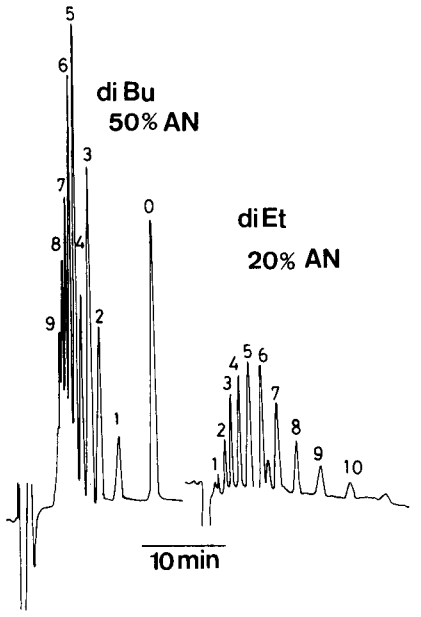

Fig. 1. Typical separation of POE derivatives. Sample: left = BuPEG, right = EtPEG. AN = acetonitrile. Detector, refractive index. Chromatographic conditions are given in the text.

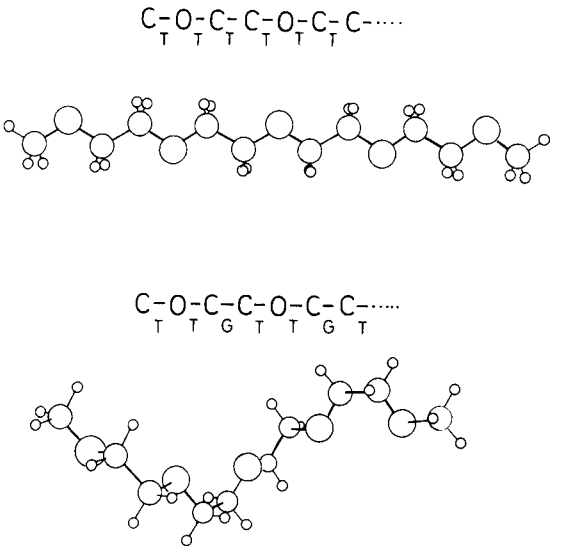

Fig. 2. Illustrations of stable conformers of MePEG ($n = 4$). Top, all-*trans* conformer; bottom, helix structure.

indicated that the preference of the *gauche* conformer is enhanced with dilution of the aqueous solution [29]. In addition, it has been found by hypersonic velocity measurements that the *gauche* conformation is stabilized by the water bridge between oxygen atoms of the oxyethylene units [27].

The MM calculation was carried out for MePEG ($n = 1$) to study the relative stability of the conformers. In this instance, steric energies were calculated for the rotation around the C–C bond by assuming the *trans* conformation for C–O bonds. The results are shown in Fig. 3. Open symbols show the change in steric energies in the gas phase, the specific dielectric constant (ϵ) of which was assumed to be 1.5. The results indicated that the all-*trans* conformer (T–T–T–T–T) is more stable than the *gauche* conformer (T–T–G–T–T) by 3.4 kJ mol^{-1}. This total energy difference agrees well with the 3.8 kJ mol^{-1} reported by Anderson and Karlström [25] using quantum chemical ab initio Hartree–Fock–SCF calculations.

In contrast, the *gauche* conformer becomes more stable than the all-*trans* conformer with increasing ϵ of the media as shown in Fig. 3 by solid circles; the *gauche* conformer is 1.04 kJ

mol^{-1} more stable when $\epsilon = 50$. In the MM2 force field, dielectric constants affect the dipole–dipole interaction, indicating that polar media interact more preferentially with a polar *gauche* conformer.

Figure 4 shows the changes in ΔE (differences in total energies between the all-*trans* and the *gauche* conformer) for MePEG ($n = 1$) and MePEG ($n = 4$) with ϵ. The ΔE values are positive for both compounds in the gas phase, but shift to negative when ϵ becomes large. The absolute ΔE value for $n = 4$ is always larger than the corresponding value for $n = 1$, although the ΔE values for both $n = 1$ and $n = 4$ show similar tendencies with a variation in ϵ. It should be noted that the ΔE values remain almost constant when ϵ becomes larger than 30.

The constancy of the total energies in highly polar media can be explained as follows. According to the calculation procedure based on the classical theory of dielectrics, the energy of the dipolar field in a medium of dielectric constant ϵ_1 can be described by

$$E = \mu^2 X / \left[a^3(\epsilon_0 - 2\alpha X/a^3)\right] \quad (1)$$

$$X = (\epsilon_1 - \epsilon_0)/(2\epsilon_1 + \epsilon_0)$$

where μ is the dipole moment of the solute, ϵ_0 is the dielectric constant in the gas phase, α is the polarizability of the solute and a is the radius of the spherical solute molecule [32,33]. The energy of the quadrupole field is calculated as

$$E = 9XQ/\left[2a^5\epsilon_0(5 - X)\right] \quad (2)$$

$$Q = \sum_{\substack{i,j=x,y,z \\ i \neq j}} \left[4q_{ij}^2 + 3(q_{ij} + q_{ji})^2 - 4q_{ii}q_{jj}\right]$$

where q_{ij} is the component of the quadrupole moment. Both dipolar and quadrupolar equations involve only X as a parameter characterizing the medium. Although there may be arguments that other microscopic parameters characterizing the medium should be involved, these equations have been known to be effective for calculating solvent effects [32–34]. Figure 5 shows changes in ϵ and X in the acetonitrile–water system [35]. In such a high permittivity system, X is almost constant regardless of the concentration of acetonitrile. Therefore, the enthalpic effects of the solvation are not important for the discussion of the conformational equilibrium of POE in polar media. ΔE values for $n = 1 - 4$ obtained with $\epsilon = 1.5$ and 50 are given in Table 1.

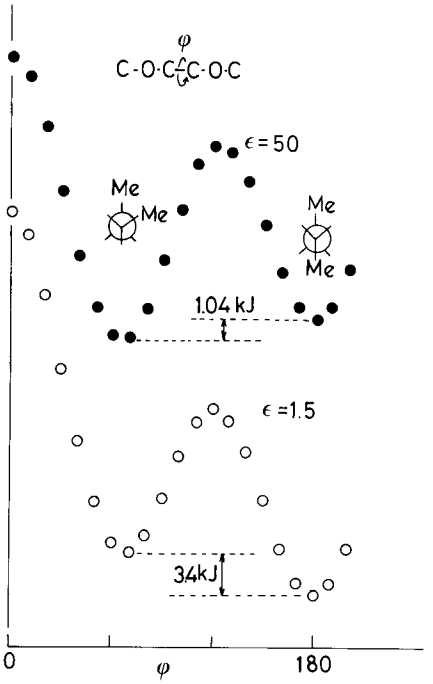

Fig. 3. Changes in steric energy of MePEG ($n = 1$). (○) $\epsilon = 1.5$ (gas phase); (●), $\epsilon = 50$. Steric energies were calculated with the MM2 force field.

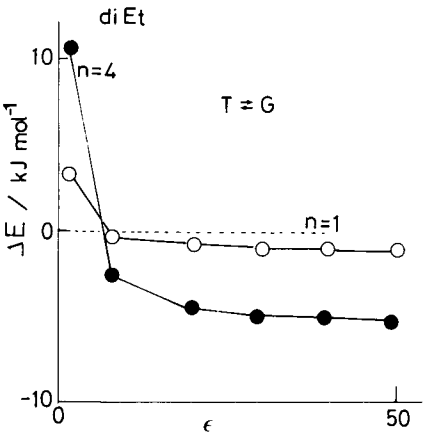

Fig. 4. Changes in ΔE with ϵ. (○) $n = 1$; (●) $n = 4$.

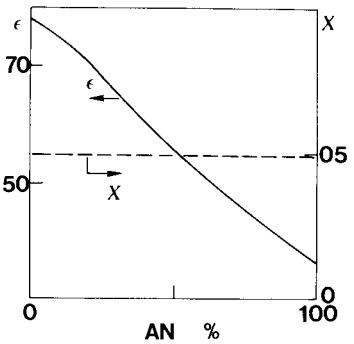

Fig. 5. Changes in ϵ and X with volume percentage of acetonitrile (AN). Data from [35].

The effects of the terminal hydrophobic chains can also be discussed in the same manner. Although the hydrophobic chains basically adopt the all-*trans* extended form, it is known that their conformation affects the POE conformation, and vice versa [28,30]; this influence is not very large, however. The MM calculation was therefore conducted to verify this effect for compounds having various terminal groups. The results are given in Table 2. Although there are slight variations in the resulting values, the differences in ΔE are in general very small.

Interpretation of chromatographic retention

The number of possible conformations of the POE chain increases as the chain becomes longer. Although, as mentioned above, recent spectroscopic measurements have suggested a preference for the *gauche* conformation for the C–C bond, especially in dilute solution, the presence of the *trans* conformer was also implied [29].

TABLE 1

Calculated energy differences between the *trans* and the *gauche* conformers of MePEG ($n = 1$).

n	ΔE (kJ mol^{-1})		K [a]
	$\epsilon = 1.5$	$\epsilon = 50$	
1	3.40	−1.04	1.52
2	5.95	−2.38	2.62
3	8.39	−3.80	4.64
4	10.84	−5.24	8.30

[a] Equilibrium constant at $\epsilon = 50$ obtained by assuming the entropic contribution to be negligible.

TABLE 2

Effect of terminal hydrocarbon chains on ΔE

R [a]	ΔE (kJ mol^{-1})			
	$\epsilon = 1.5$		$\epsilon = 50$	
	$n = 1$	$n = 4$	$n = 1$	$n = 4$
Methyl	3.40	10.84	−1.04	−5.24
Ethyl	3.16	10.47	−1.27	−5.61
Propyl	3.14		−1.30	
Butyl	3.11	11.00	−1.33	
Pentyl	3.11		−1.33	
Hexyl	3.10		−1.34	

[a] Terminal hydrocarbon chain.

Matsuura and Fukuhara [36] reported that GTTG, TTTG, GTGG, TTTT, and TTGG for the C–C–O–C– group were possibly present in an aqueous solution. However, in order to avoid complexity and to facilitate the development of a retention model, it was assumed that GTTG and TTTT (denoted as the *gauche* and the *trans* conformers, respectively) are more stable than the others. Therefore, the contributions from three stable states are taken into account to consider a retention model because two *gauche* conformers (TTG^+TTG^+ and TTG^-TTG^-) exist.

Chromatographic retention can be interpreted according to the following scheme:

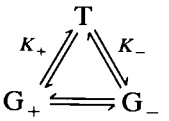

where K_+ and K_- are equilibrium constants. As the free energies of both *gauche* conformers should be identical, the equilibrium constant of $G_+ \rightleftharpoons G_-$ is unity and $K_+ = K_-$. The capacity factor of an oligomer (k) can therefore be described by

$$k = (k_T + k_{G_+}K_+ + k_{G_-}K_-)/(1 + K_+ + K_-)$$
$$= (k_T + 2k_GK)/(1 + 2K) \quad (3)$$

where k_T and k_G are intrinsic capacity factors of the *trans* and the *gauche* conformer respectively, $k_G = k_{G_+} = k_{G_-}$ and $K = K_+ = K_-$. This equation is similar to that proposed by Melander et al. [14] except that their model involves the effects of the *trans* and the meander form, which is considered

to be unstable and unlikely to exist under any conditions because of the great steric hindrance [29].

To analyse the retention data using Eqn. 3, the following relationships were assumed:

$$k_T = k_0 \alpha_T^n \quad (4)$$

$$k_G = k_0 \alpha_G^n \quad (5)$$

where k_0 is the capacity factor of a compound with $n = 0$, whose retention is not affected by the conformational change because this compound contains no oxyethylene units, and α_T and α_G are selectivity factors for the *trans* and *gauche* conformer respectively. If both k_T and k_G are known, K values can be calculated for all oligomers from their capacity factors. In contrast, if K values are available, both k_T and k_G can be calculated.

Theoretical calculations and some experiments have been conducted to elucidate the equilibrium between the *trans* and *gauche* conformers of MePEG ($n = 1$) [25,33,37]. There remain, however, ambiguity and disagreements in the values obtained in polar solvents and, in addition, such values for POEs with $n \geqslant 2$ in polar media have not been reported, to our knowledge. Viti et al. [33], for example, estimated the energy difference between the *gauche* and *trans* conformers of MePEG ($n = 1$) to be 2.8–3.5 kJ mol^{-1} in dimethylformamide using NMR spin–spin coupling measurements. Podo et al.'s dipole moment measurements [37], in contrast, indicated that the difference was 2.2 kJ mol^{-1} in the pure liquid.

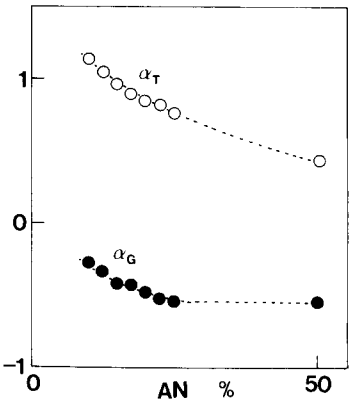

Fig. 6. Changes in α_T and α_G with volume percentage of acetonitrile (AN) in the mobile phase. Samples for the calculation of the selectivity factors were MePEG, EtPEG and BuPEG.

TABLE 3

Comparison of retention times of BuPEG

n	Retention time (min)			
	40% acetonitrile		50% acetonitrile	
	Exp.	Calc. [a]	Exp.	Calc. [b]
0	50.63	50.63	16.44	16.44
1	42.71	43.27	13.99	13.92
2	38.31	37.57	11.37	11.86
3	33.99	33.41	9.99	10.27
4	29.77	30.46	9.05	9.08
5	27.19	28.37	8.17	8.17
6	– [c]	26.84	7.59	7.46
7	– [c]	25.67	7.16	6.90
8	– [c]	24.71	6.79	6.42
9	– [c]	23.90	6.52	6.02

[a] For the calculation, the values $\alpha_T = 1.68$ and $\alpha_G = 0.58$, which were obtained from Fig. 6, were used, [b] $\alpha_T = 1.58$ and $\alpha_G = 0.58$ were used. [c] Retention times were not obtained because of overlapping of peaks.

In this study, the following assumptions were made to solve the above equation: the solution behaviour of POEs is not affected enthalpically by the nature of the media provided that the dielectric constant is kept sufficiently high; hydrocarbon terminal groups hardly influence the solution behaviour of POEs; and though results of the MM2 calculation do not involve the entropic contribution to the equilibria, this contribution can be ignored. These assumptions allowed the calculation of the equilibrium constant from the ΔE values listed in Table 1. The resulting K values are also given in Table 1.

Several retention data were analysed on the basis of the developed model. Logarithms of the resulting selectivity factors (α_T and α_G) are plotted against the concentration of acetonitrile in the mobile phase in Fig. 6. Both α_T and α_G decrease with increasing concentration of acetonitrile. Decreases in capacity (or selectivity) factors with increasing acetonitrile concentration are common phenomena, although usually log k' or log α decreases linearly with the percentage of an organic modifier. It should be noted that

α_T is > 1 whereas α_G is < 1, indicating that for the *trans* conformer the retention increases with increasing n whereas for the *gauche* conformer the retention decreases with increasing n. This is qualitatively understandable because high energies are necessary to transfer the polar and strongly solvated *gauche* conformers from the polar to the less polar stationary phase.

In the above discussion, some assumptions were made. To verify the suitability of these assumptions, the retention times were predicted. The results are given in Table 3. As K values for compounds with $n \geqslant 5$ were not obtained by the present calculation, such values were calculated from the linear relationship between log K and n ($n \leqslant 4$). The predicted chromatograms are depicted in Fig. 7, where chromatograms obtained experimentally are also shown for comparison. Although there is disagreement in the peak heights because no attempt was made to adjust the solute concentration, the predicted capaci factors agrees well with the experimental value suggesting that the present approach is reaso able.

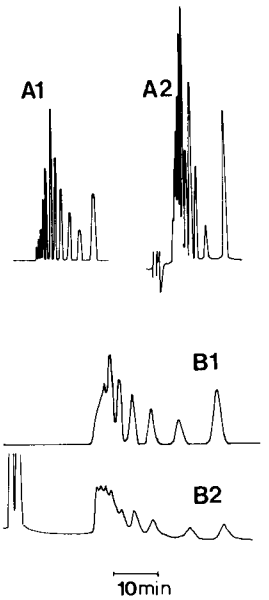

Fig. 7. Comparison of predicted and experimental chromatograms. Sample, BuPEG. A1 shows a predicted chromatogram using 50% (v/v) acetonitrile as mobile phase and A2 shows the actual chromatogram with the same mobile phase. A refractive index detected was used to monitor the elution of POEs in both instances. Similarly, B1 and B2 are the predicted and actual chromatograms with 40% (v/v) acetonitrile as mobile phase. Other chromatographic and calculation conditions are given in the text.

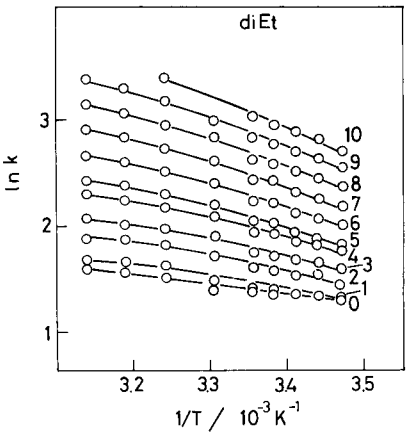

Fig. 8. Van 't Hoff plots for EtPEG.

Contribution of enthalpy

The van 't Hoff plot obtained for the retentic composed of a single retention mechanism usually linear. In contrast, van 't Hoff plots a not linear when the retention involves seconda effects. In the present instance, as the retentic of POE involves conformational changes in bo the mobile and stationary phases, the van 't Hc plots for EtPEG and BuPEG are not linear, shown in Figs. 8 and 9. The overall retention EtPEG is apparently endothermic regardless

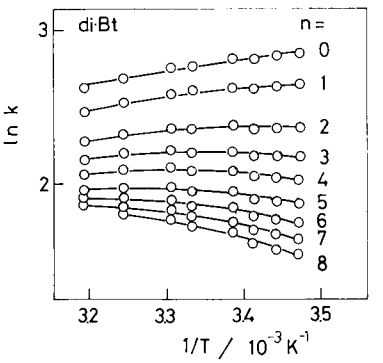

Fig. 9. Van 't Hoff plots for BuPEG.

n, whereas that of BuPEG is endothermic in some instances but exothermic in others.

An apparent ΔH (ΔH_{app}), which can be obtained from the tangent line of a van 't Hoff plot, is derived from Eqn. 3:

$$\Delta H_{app} = -R\,\partial(\ln k)/\partial(1/T)$$
$$= [(k_T\Delta H_T + 2Kk_G\Delta H_G)(1+2K) - 2K(k_T - k_G)\Delta H] \times [(k_T + 2Kk_G)(1+2K)]^{-1} \quad (6)$$

where ΔH_T, ΔH_G and ΔH denote standard enthalpy changes in the retention of the *trans* conformer, that of the *gauche* conformer and that of the equilibrium between these two conformers, respectively.

As shown in Fig. 6, α_T is larger than unity, whereas α_G is smaller than unity, indicating that when n is large enough, the retention of the *gauche* conformer can be ignored. In such a case, ΔH_{app} can be described by the following much simpler equation:

$$\Delta H_{app} = \Delta H_T - 2K\Delta H/(1+2K) \quad (7)$$

Furthermore, if $2K \gg 1$,

$$\Delta H_{app} = \Delta H_T - \Delta H \quad (8)$$

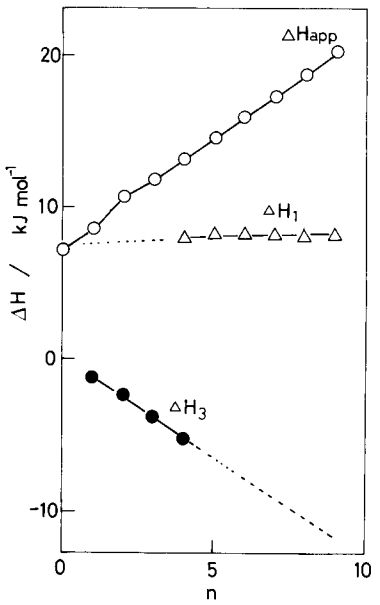

Fig. 10. Variations of ΔH_{app}, ΔH_1 and ΔH_3 for EtPEG.

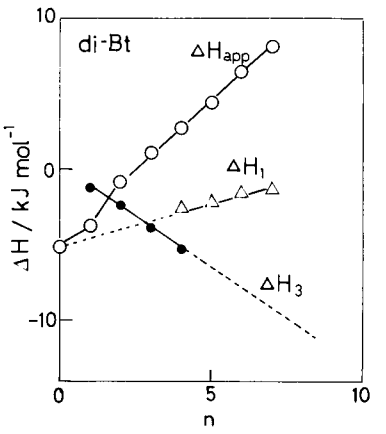

Fig. 11. Variations of ΔH_{app}, ΔH_1 and ΔH_3 for BuPEG.

Since the MM2 calculation provides ΔH, we can estimate ΔH_T according to Eqn. 8. Figures 10 and 11 summarize the results obtained on the basis of eqn. 8. The following parameters, for example, were used for this calculation for Et-PEG ($n = 4$): $K = 8.3$, $k_T = 109$ and $k_G = 0.56$ for 20% (v/v) acetonitrile. These values almost satisfy the above approximations, $k_G \ll k_T$ and $2K \gg 1$. Although ΔH_{app} increases with increasing n for EtPEG and BuPEG, such as tendency is much smaller for changes in ΔH_T.

Conclusion

A modified two-state model involving the conformational changes of POE chains describes well the retention of POE in reversed-phase chromatography. Such an approach and the MM calculation lead to the following conclusions: the *trans* conformer of POEs is less stable than the *gauche* conformer in polar media, particularly for POEs with large n; the conformational changes of POE chains are not enthalpically influenced by terminal hydrocarbon chain lengths; dielectric constants of the media are not an important factor when considering this topic on an enthalpic basis if ϵ is large enough; the *trans* conformer increases in retention ability with increasing n, whereas the *gauche* conformer decreases in retention with increasing n; selectivity factors calculated on the basis of a developed retention model permit the prediction of the retention; and the

present approach makes it possible to calculate the enthalpy changes in the retention process of the *trans* conformer, although the precision of the values obtained depends on that of the MM2 calculation.

These results obviously indicate the problems and limitation involved with the present method. The MM2 force field is capable of calculating enthalpy changes but not entropy changes, although entropy changes are an important factor when discussing the retention and equilibrium of POE chains. In addition, such as calculation has a serious limitation in representing the solution behaviour of the solutes. Hence developments of the theoretical calculations in solution chemistry and efficient experiments to probe the equilibria will be necessary in order to discuss the present topic more precisely. However, despite these limitations, chromatography appears to be an effective means for studying the solution behaviour of solutes including secondary effects. If spectrometric experiments, for example, can elucidate the equilibria of a few POE oligomers having different chain lengths, the present procedure can be appropriately utilized for the determination of the equilibrium constants of other oligomers on the basis of the developed model.

REFERENCES

1 J. Cross, Nonionic Surfactants, Dekker, New York, 1987.
2 M.J. Rosen, Surfactants and Interfacial Phenomena, Wiley, New York, 1978.
3 Y.-P. Zhu, A. Masuyama and M. Okahara, J. Am. Oil Chem. Soc., 67 (1990) 459.
4 N. Suto, T. Imaizumi, J. Tsurubuchi and T. Kuwamura, Yukagaku, 31 (1982) 598.
5 A. Berthod, J. Chim. Phys., 80 (1983) 407.
6 F. Vögtle and E. Weber, Angew. Chem., Int. Ed. Engl., 18 (1979) 753.
7 D.E. Fenton, in G. Wilkinson (Ed.), Comprehensive Coordination Chemistry, Vol. 3, Pergamon, Oxford, 1987, p. 1.
8 K. Ono, H. Honda and K. Murakami, J. Macromol. Sci., Chem., A26 (1990) 567.
9 T. Okada, Macromolecules, 23 (1990) 4216.
10 W. Walkowiak, G.M. Ndip, D.H. Desai, H.K. Lee and R.A. Bartsch, Anal. Chem., 64 (1992) 1685.
11 M.A. Ratner and D.F. Shriver, Chem. Rev., 88 (1988) 109.
12 M. Watanabe, K. Sanui, N. Ogata, T. Kobayashi and Z. Ohtaki, J. Appl. Phys., 57 (1985) 123.
13 G.C. Farrington, H. Yang and R. Huq, Mater. Res. Soc. Symp. Proc., 135 (1989) 319.
14 W.R. Melander, A. Nahum and Cs. Horvath, J. Chromatogr., 185 (1979) 129.
15 G.R. Bear, J. Chromatogr., 459 (1988) 91.
16 P. Jandera, J. Urbanek, B. Prokes and J. Churacek, J. Chromatogr., 504 (1990) 297.
17 K. Noguchi, Y. Yanagihara, M. Kasai and B. Katayama, J. Chromatogr., 161 (1989) 365.
18 M. Kudoh, J. Chromatogr., 291 (1984) 327.
19 T. Okada, Anal. Chem., 62 (1990) 327.
20 T. Okada, J. Chromatogr., 609 (1992) 213.
21 T.L. Chester, J. Chromatogr., 299 (1984) 424.
22 B.E. Richter, J. High Resolut. Chromatogr. Chromatogr. Commun., 8 (1985) 297.
23 U. Burkert and N.L. Allinger, Molecular Mechanics, American Chemical Society, Washington, 1982; Japanese translation, Keigaku Shuppan, Tokyo, 1986.
24 S. Yoshimura, Translated from QCPE 395, MM2–Molecular Mechanics Ver. 2.
25 M. Andersson and G. Karlström, J. Phys. Chem., 39 (1985) 4957.
26 H. Matsuura and K. Fukuhara, Chem. Lett., (1984) 933.
27 H. Matsuura and K. Fukuhara, Bull. Chem. Soc. Jpn., 59 (1986) 763.
28 K. Fukuhara and H. Matsuura, Chem. Lett., (1987) 1549.
29 H. Matsuura, K. Fukuhara, K. Takashima and M. Sakakibara, J. Phys. Chem., 95 (1991) 10800.
30 H. Matsuura, K. Fukuhara, S. Masatoki and M. Sakakibara, J. Am. Chem. Soc., 113 (1991) 1193.
31 D.C.W. Siew, R.P. Cooney and M.J. Taylor, J. Raman Spectrosc., 22 (1991) 183.
32 L. Dosen-Micovic and N.L. Allinger, Tetrahedron, 34 (1978) 3385.
33 V. Viti, P.L. Indovina, F. Podo, L. Radics and G. Nemethy, Mol. Phys., 27 (1974) 541.
34 N.L. Allinger, L. Dosen-Micovic and J.F. Viskocil, Jr., Tetrahedon, 34 (1978) 3395.
35 Nippon Kagakukai, Kagaku Binran, Maruzen, Tokyo, 1984.
36 H. Matsuura and K. Fukuhara, J. Polym. Sci., Part B, 24 (1986) 1383.
37 F. Podo, G. Nemethy, P.L. Indovina, L. Radics and V. Viti, Mol. Phys., 27 (1974) 521.

Analytica Chimica Acta, 281 (1993) 95–101
Elsevier Science Publishers B.V., Amsterdam

Flow-injection determination of traces of potassium by extraction with bis[2-(5′-bromo-2′-pyridylazo)-5-(*N*-propyl-*N*-sulphopropylamino)phenolato]cobaltate(III) and cryptand[2.2.2]

Hiromichi Yamada, Ikuo Kobayakawa, Akio Yuchi and Hiroko Wada

Department of Applied Chemistry, Nagoya Institute of Technology, Showa-ku, Nagoya 466 (Japan)

(Received 12th January 1993; revised manuscript received 25th February 1993)

Abstract

The determination of trace amounts of potassium ion was carried out by liquid–liquid extraction using cobalt(III) 2-(5′-bromo-2′-pyridylazo)-5-(*N*-propyl-*N*-sulphopropylamino)phenolate and cryptand[2.2.2] with a flow-injection system. The determination of potassium ion in the range from tens to several hundred $\mu g\ l^{-1}$ was possible with a sampling frequency of 30 h^{-1}. The detection limit for potassium at a signal-to-noise ratio of 3 was 4.0×10^{-7} M (16 $\mu g\ l^{-1}$). Interferences from alkaline earth and heavy metal ions could be avoided by adding dilithium EDTA to the sample and/or reagent solutions. The results obtained for botanical reference materials were in good agreement with the certified values.

Keywords: Flow injection; Biological samples; Extraction; Potassium

On account of their closed-shell electronic structures, alkali metal ions have only poor coordinating ability. Therefore, for the spectrophotometric determination of alkali metal ions, the ion-pair extraction of crown ether complexes of alkali metal cations, which are caged electrostatically, has been investigated with various hydrophobic counter anions containing a chromophore [1]. If an anion with a high molar absorptivity is available as a counter ion for the ion-pair extraction of an alkali metal complex cation, it is feasible to determine traces of alkali metals spectrophotometrically. It is well known that cobalt(III) complexes are kinetically inert. $Co(PAR)_2^-$ [PAR = 4-(2′-pyridylazo)resorcinol] [1,2] and $Co(5\text{-Br-PAPS})_2^-$ [5-Br-PAPS = 2-(5′-bromo-2′-pyridylazo)-5-(*N*-propyl *N*-sulphopropylamino)phenol] have been successfully used as counter anions. The latter complex anion has the higher molar absorptivity ($\epsilon = 9.8 \times 10^4$ l mol^{-1} cm^{-1}) at 589 nm, which is constant over a wide pH range of at least 1–13. Kasahara et al. [3] employed $Co(5\text{-Br-PAPS})_2^-$ for the extraction and spectrophotometric determination of long-chain quaternary ammonium ions and ternary alkylamines in natural waters.

The extractability of an ion pair has been reported [2,4] to be correlated with the structures of the cation and anion; the combination of a bulky cation and a bulky anion or of a planar

Correspondence to: H. Yamada, Department of Applied Chemistry, Nagoya Institute of Technology, Showa-ku, Nagoya 466 (Japan).

cation and a planar anion result in good extraction. On the other hand, a bulky–planar or planar–bulky combination leads to poor extraction.

In this work, the extraction of potassium cryptate[2.2.2] ($K \cdot cryp^+$) with $Co(5\text{-Br-PAPS})_2^-$ was studied and applied to the determination of traces of potassium in the presence of other alkali metals using a flow-injection system.

EXPERIMENTAL

Reagents

All chemicals were of analytical-reagent grade and used as received unless specified otherwise. Aqueous solutions used were prepared with distilled, deionized water. 2-(5′-Bromo-2′-pyridylazo)-5-(*N*-propyl-*N*-sulphopropylamino)phenol (5-Br-PAPS) sodium salt was purchased from Dojindo Laboratories (Kumamoto, Japan). The lithium salt was prepared as follows: an aqueous solution of 5-Br-PAPS, sodium salt, was passed through a column of cation-exchange resin (Dowex 50W-X12) in the hydrogen form and washed through with distilled water. A solution of 5-Br-PAPS, lithium salt, was obtained by adding equimolar lithium hydroxide to the eluent from the column. An aqueous solution of $Co(III)(5\text{-Br-PAPS})_2^-$ was prepared by mixing cobalt(II) nitrate and 5-Br-PAPS, lithium salt, in a mole ratio of 1:2. A potassium standard solution was prepared by dissolving appropriate amounts of recrystallized potassium nitrate in water. Cryptand[2.2.2] solution was prepared by dissolving Kryptofix 222 (Merck) in water. All aqueous stock solutions were stored in polyethylene bottles. Chloroform was purified by shaking with water just before use.

Apparatus

A Model SA-31 mechanical shaker (Yamato Scientific, Tokyo), a Model 5100 centrifuge (Kubota-Seisakusho, Tokyo), a Shimadzu Model UV-250 UV–visible recording spectrophotometer and a Hitachi-Horiba Model F-5 pH meter were used for the batch method.

The manifold for the proposed flow-injection method is shown in Fig. 1. Two double-plunger

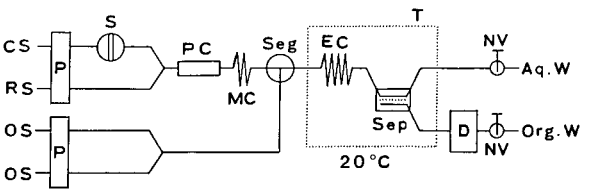

Fig. 1. Schematic diagram for the proposed flow-injection methods. CS = carrier solution (water); RS = reagent solution containing $Co(5\text{-Br-PAPS})_2^-$, cryptand[2.2.2] and LiOH; OS = organic solution (chloroform); P = double-plunger pump; S = six-way injection valve; PC = mini-column packed with Kryptofix 221B polymer; Seg = segmentor; Sep = phase separator; MC = mixing coil; EC = extraction coil; T = thermostat (20°C); D = spectrophotometric detector; NV = needle valve.

pumps (Sanuki Kogyo SRX-3600, Tokyo) were used to propel the carrier and reagent solutions and organic solvent. The segmentor was a commercial T-shaped connector, in which the organic phase (chloroform) is continuously added at right-angles to the aqueous phase flowing straight through. A grooved phase separator (Sanuki Kogyo) with a PTFE porous membrane (Sumitomo Electric Industries, pore size 0.8 μm) was used. The dimensions of the grooves were $10 \times 2 \times 2$ mm (length, width, maximum depth). The extraction coil and phase separator were thermostated in a Coolnics Circulator Model CTE-220 thermostat (Komatsu Solidate, Komatsu) to keep the extraction temperature at 20°C and to prevent the evolution of bubbles in the phase separator. A spectrophotometric detector (S-3250, Soma Kougaku, Tokyo) with a flow-through cell (volume 8 μl, light-path length 10 mm) was used for absorbance measurements. A needle valve restrictor (Gasukoro Kogyo, Tokyo) was placed at each outlet of the aqueous and organic streams. All flow lines were made of 0.5 mm i.d. PTFE tubing.

Procedures

Batch method. A 10-ml volume of chloroform and an equal volume of aqueous solution containing potassium cation, Co(III)-5-Br-PAPS, LiOH and cryptand[2.2.2] were equilibrated in a 40-ml PTFE centrifuge tube by gently shaking for 5 min. This was sufficient for complete equilibration. After phase separation by centrifugation,

the concentration of potassium in the organic phase was determined by measuring the absorbance of the organic phase at 595 nm.

Flow-injection method. The reagent solution consisted of Co(III)(5-Br-PAPS)$_2^-$, cryptand[2.2.2] and LiOH in water. The carrier and organic streams were water and chloroform, respectively. An aliquot of sample solution was injected into the carrier stream via a six-way injection valve (SVM-6M2, Sanuki Kogyo) with a loop and was merged into the reagent stream. After passing through a mini-column (10 cm × 2 mm i.d.) loaded with Kryptofix 221B polymer and the mixing coil, the aqueous stream was merged with the organic stream (pure chloroform) via a T-piece connector. The ion pair formed between potassium cryptate[2.2.2] cation and Co(III)(5-Br-PAPS)$_2^-$ anion was extracted into chloroform in the extraction coil and the absorbance of the chloroform solution passing through the PTFE membrane in the phase separator was measured at 595 nm.

RESULTS AND DISCUSSION

Extraction equilibria

The extraction equilibria for the present extraction systems can be represented as follows:

$$K^+ + \text{cryp} \rightleftharpoons (K \cdot \text{cryp})^+$$

$$(K \cdot \text{cryp})^+ + CoL_2^- \rightleftharpoons (K \cdot \text{cryp}^+, CoL_2^-)$$

$$(K \cdot \text{cryp}^+, CoL_2^-) \rightleftharpoons (K \cdot \text{cryp}^+, CoL_2^-)_o$$

where cryp and CoL_2^- denote the cryptand[2.2.2] and Co(III)(5-Br-PAPS)$_2^-$, respectively, and the subscript o refers to the organic phase. The potassium cryptate is extracted as the 1:1 ion pair $(K \cdot \text{cryp}^+, CoL_2^-)$ into the organic phase. The potassium concentration can then be determined by measuring the absorbance of Co(III)(5-Br-PAPS)$_2^-$ anion in the organic phase which had formed a 1:1 ion pair with the potassium cryptate.

Optimization of the batch method

On the basis of the procedure described above, the conditions for the extraction by a batch method were optimized as follows: the concentrations of Co(III)(5-Br-PAPS)$_2^-$, cryptand[2.2.2], and LiOH were 6×10^{-5}, 6×10^{-4} and 1×10^{-2} M, respectively. Taking into account the extractability and phase separation, chloroform was selected in preference to benzene, toluene, carbon tetrachloride and 1,2-dichloroethane. Cryptand[2.2.2] was the optimum reagent for the ion-pair extraction of potassium with Co(III)(5-Br-PAPS)$_2^-$ anion. On using 18-crown-6, which has a high selectivity for potassium, instead of cryptand[2.2.2] an emulsion appeared near the interface between the organic and aqueous phases. The effect of pH on the extraction was examined by varying the concentration of LiOH from 2×10^{-5} to 7×10^{-2} M.

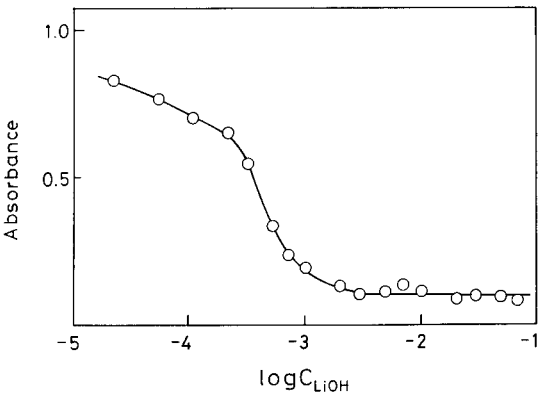

Fig. 2. Effect of LiOH concentration on the reagent blank value (batch method). Aqueous phase, 6×10^{-5} M Co(5-Br-PAPS)$_2^-$, 5×10^{-4} M cryptand[2.2.2], 2×10^{-5}–7×10^{-2} M LiOH; organic phase, chloroform. Absorbance at 595 nm.

The absorbance of the organic phase for the extraction of K^+-free sample solution, that is, the reagent blank value versus the concentration of LiOH, is shown in Fig. 2. As can be seen at LiOH concentrations less than 1×10^{-3} M (pH < 11), the absorbance of the reagent blank was abruptly increased with decreasing LiOH concentration, that is, increasing hydrogen ion concentration in the aqueous phase. This suggests that the Co(III)(5-Br-PAPS)$_2^-$ anion was extracted as the ion pair with the protonated cryptand cation without the potassium cryptate cation. At LiOH concentrations above 0.01 M the absorbance remained approximately constant. Lithium ion was

found not to be extracted under the present extraction conditions. Therefore the extraction was carried out at 0.01 M LiOH (pH 12). For 1×10^{-6} M potassium ion, the optimum concentrations of Co(5-Br-PAPS)$_2^-$ and cryptand[2.2.2], found by varying them in the ranges 2×10^{-5}–1×10^{-4} and 1×10^{-5}–1×10^{-3} M, respectively were 6×10^{-5} and 5×10^{-4} M, respectively. Under these optimum conditions, potassium ions down to 1×10^{-6} M could be determined. However, the calibration graph showed a slight downward curvature with a blank value. The present batch method is a poor for the phase separation and lacks reproducibility. In addition, the batch extraction procedure is tedious. As the extraction rate of potassium with cryptand[2.2.2] and Co(5-Br-PAPS)$_2^-$ was very fast, the extraction was carried out in the flow-injection system to overcome these disadvantages.

Optimization of the flow-injection analysis

The same flow-rates were employed for the carrier, reagent and organic streams. The effects of the flow-rate of each solution on the calibration graph were examined by varying the former from 0.6 to 1.2 ml min^{-1}. As shown in Fig. 3, the slope of the calibration graph increased with increasing flow-rate up to 1.0 ml min^{-1}, but decreased at 1.2 ml min^{-1}. The flow-rate of each stream was therefore selected as 1.0 ml min^{-1}. The ratio of the organic to the aqueous phases was 1:2, and the concentration of the ion pair was approximately doubled by the extraction. Ratios of organic to aqueous phases of 1:3 and 1:1 were gave poorer results than the 1:2 ratio.

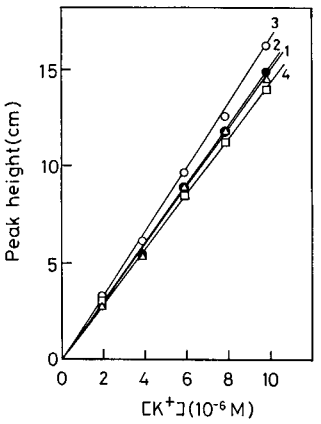

Fig. 3. Effect of the flow-rate of each stream on the slope of the calibration graph. The conditions except for the flow-rate are optimum values. Flow-rate: (1) 0.6; (2) 0.8; (3) 1.0; (4) 1.2 ml min^{-1}.

A 20-cm coil for mixing of the carrier and reagent streams was employed, taking into account the good reproducibility. Fluctuations of baseline absorbance owing to pulsed flow occurred when using a mixing coil shorter than 20 cm. The effects of the extraction coil length on the peak height were examined by varying the length up to 200 cm. As the peak height hardly altered with extraction coils more than 50 cm long, a 50-cm coil was adopted. The mixing and extraction coils were wound in a figure-of-eight fashion.

The peak height increased with increasing sample volume injected up to 230 μl, but only slightly increased at larger volumes. As it was preferable to minimize the sample volume injected, 180 μl was the most suitable for the apparatus employed. The optimum concentrations of LiOH, Co(III)(5-Br-PAPS)$_2^-$ and cryptand[2.2.2] in the reagent stream were examined in the ranges 2×10^{-3}–2×10^{-2}, 2×10^{-5}–1×10^{-4} and 2×10^{-5}–1×10^{-3} M, respectively. The peak height was little affected in this range of the LiOH concentration, whereas the baseline absorbance and noise increased with decreasing LiOH concentration. Taking into account these results, the concentration of LiOH was selected as 0.01 M. The slope of the calibration graph increased with increasing concentration of Co(5-Br-PAPS)$_2^-$ up to 6×10^{-5} M, but hardly increased at higher concentrations. Hence 6×10^{-5} M Co(5-Br-PAPS)$_2^-$ solution was adopted. With concentrations of cryptand[2.2.2] lower than 1×10^{-4} M both the peak height and the slope of the calibration graph were not large enough to permit the exact determination of potassium. In this region the extraction of potassium ion is insufficient and pronounced tailing of the flow signals was observed, whereas at cryptand concentrations of not less than 5×10^{-4} M both the peak height and the slope of the calibration graph were sufficient to ensure an accurate determination. There-

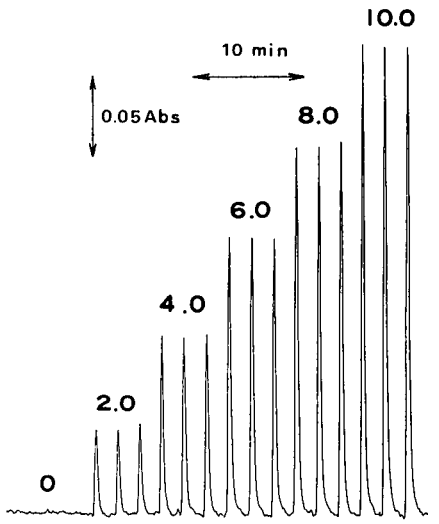

Fig. 4. Flow signals for standard solutions of potassium ion under the optimum conditions. All standard solutions were injected three times each. Values above the peaks are the concentrations of standard potassium solutions (10^{-6} M).

fore, a cryptand[2.2.2] concentration of 5×10^{-4} M was selected for the determination of up to 1×10^{-5} M potassium.

Calibration graph

As shown in Fig. 4, the flow signals for potassium ion show good reproducibility under the above optimum conditions. The calibration graph was linear up to 1×10^{-5} M K^+. The relative standard deviation for sixteen injections of samples of 5×10^{-6} M K^+ (as the nitrate) was 1.6%. The detection limit (signal-to-noise ratio = 3) was 4×10^{-7} M. The sampling frequency of the proposed method was 30 h^{-1}.

Interferences

The effects of the other alkali metal ions on the determination of potassium ion were examined using the proposed batch method. The results are summarized in Table 1 together with the complex formation constants of alkali metal cryptate[2.2.2] and the ionic radii of the alkali metal cations. As illustrated in Fig. 2, lithium ion did not interfere with the determination of potassium ion even when it was present up to 0.07 M. This could be expected from the complex formation constant and the radius of the lithium ion.

TABLE 1

Interferences from other alkali metal ions [a]

Parameter	$[M^+]/[K^+]$ [b]	Li^+	Na^+	K^+	Rb^+	Cs^+
Ionic radius (Å)		0.78	0.98	1.33	1.49	1.65
Log K [5] [c]		2.0	3.9	5.4	4.4	2.0
Recovery (%)	1		104	100	148	108
	5		125		330	108
	10		166		500	107

[a] Cavity size of cryptand[2.2.2] = 1.40 Å. $[K^+] = 5 \times 10^{-6}$ M. [b] Mole ratio. [c] Formation constants for alkali metal ions with cryptand[2.2.2].

On the other hand, sodium and rubidium ions were found to interfere in the determination of potassium ion, as predicted from the values of the formation constants in Table 1. In addition, caesium ion interferes slightly with the determination of potassium ion. However, the interferences from rubidium and caesium are negligible in the determination of potassium ion in natural samples using the present method, because these metal ions, especially caesium, are low in abundance in the natural samples compared with potassium.

Attempts were made to prevent the interferences from sodium and the other metal ions in the proposed flow method. In order to remove sodium ion from the sample, a mini-column packed with Kryptofix 221B polymer was inserted in the flow system as shown in Fig. 1. The dependence of the masking effect for sodium ion of the length of the mini-column is shown in Table 2. When a mini-column not less than 10 cm long was used, the masking effect scarcely varied. Potassium ion was found to be determined with a

TABLE 2

Effect of the length of the mini-column packed with Kryptofix 221B polymer on the masking effect for sodium ion

$[Na^+]/[K^+]$ [a]	Recovery (%)		
	5-cm column	10-cm column	15-cm column
10	108	103	103
20	116	105	105
40	139	110	110

[a] Mole ratio; $[K^+] = 5 \times 10^{-6}$ M.

5% relative error by employing a 10-cm mini-column, even when sodium ion was present in a twentyfold excess over potassium ion. The masking capacity of the mini-column was sufficient to give reliable results for twenty continuous injections of sample solution containing 5×10^{-6} M potassium ion and 1×10^{-4} M sodium ion. In addition, this mini-column can be easily regenerated simply by washing with water.

Interferences from magnesium(II), calcium(II), copper(II) and zinc(II) could be prevented by adding dilithium EDTA to the reagent stream. The addition of 1×10^{-3} M dilithium EDTA to the reagent stream was found to be sufficient to suppress the interferences from these metal ions up to the same level as EDTA in the determination of 5×10^{-6} M potassium ion. On the other hand, potassium in samples containing iron(III) was successfully determined by directly adding dilithium EDTA at a level nearly equimolar with iron(III) to the sample solution at pH < 1 and then adjusting the pH to about 2 prior to its injection into the carrier stream. Heavy and alkaline earth metals other than those noted above can also be expected to be masked in the same manner.

The formation constant of the complex between ammonium ion and cryptand[2.2.2] was estimated to be comparable to that of sodium ion by Szczepaniak and Juskowiak [2]. Hence ammonium cryptate should be also extracted as the ion pair with $Co(5\text{-Br-PAPS})_2^-$ anion using the present extraction systems, and can be predicted to result in a serious error. As, fortunately, in the proposed method potassium cryptate is extracted at high pH (12) in the aqueous phase, the presence of ammonia up to a level comparable to that of potassium ion did not interfere in the determination of 5×10^{-6} M potassium ion. Ammonia in a tenfold greater concentration than potassium ion led to results with significant positive errors.

Application to botanical reference materials

The proposed method was applied to the determination of potassium ion in NIES CRMs No. 1 Pepperbush and No. 7 Tea Leaves botanical reference materials. Acid decomposition of the powdered reference materials was carried out in a domestic microwave oven [6]. This was done for three portions each of Pepperbush and Tea Leaves. The concentration of LiOH in the reagent stream was selected as 0.03 M for the proposed flow-injection method because of the high acidity of these sample solutions prepared by acid decomposition. In the proposed flow-injection method the sample solutions, which were diluted 125-fold compared with those for flame emission spectrometric analysis, were injected to the carrier stream. The results obtained for the respective solutions by the flow-injection method are summarized in Table 3 together with those obtained by flame analysis and the certified values

TABLE 3

Analytical results for certified reference materials

Sample (NIES CRM) [a]	Proposed flow-injection method		Flame emission spectrometry		NIES certified value (mg g^{-1})
	$[K^+]$ (mg g^{-1})	Recovery (%)	$[K^+]$ (mg g^{-1})	Recovery (%)	
No. 1					
Pepperbush	15.6	103	15.6	103	15.1
	15.2	101	15.1	100	
	15.0	99	15.1	100	
No. 7					
Tea Leaves	18.9	102	18.8	101	18.6
	18.9	102	18.8	101	
	18.7	101	18.7	101	

[a] Pepperbush contains Na 106, Rb 75 and Cs 1.2 $\mu g\ g^{-1}$. Tea Leaves contains Na 15.5, Rb 6 and Cs 22 $\mu g\ g^{-1}$.

for the reference materials. All the values agreed closely.

Conclusion

The proposed flow-injection method has the advantages of simple operation, a high sampling rate and high sensitivity. The sensitivity is two orders of magnitude higher than that of flame emission spectrometric analysis and is higher than that achieved with other reported flow-injection methods [7,8]. Interferences from alkaline earth and heavy metals can be easily eliminated by adding dilithium EDTA to the reagent or sample solutions. In addition, the proposed method can be widely applied to the determination of trace amounts of potassium in foods and fertilizers.

The authors thank Dr. Tetsuo Uchida (Nagoya Institute of Technology) for his assistance with the flame emission spectrometric analysis and pretreatment of the certified reference materials.

REFERENCES

1 M. Siroki, Lj. Maric, Z. Stefanac and M.J. Herak, Anal. Chim. Acta, 75 (1975) 101.
2 W. Szczepaniak and B. Juskowiak, Chem. Anal. (Warsaw), 32 (1987) 787.
3 I. Kasahara, M. Kanai, M. Taniguchi, A. Kakeba, N. Hata, S. Taguchi and G. Goto, Anal. Chim. Acta, 219 (1989) 239.
4 M. Yoshio and H. Noguchi, Anal. Lett., 15 (1982) 1197.
5 J.M. Lehn and J.P. Sauvage, J. Am. Chem. Soc., 97 (1975) 6700.
6 H. Isoyama, T. Uchida, K. Oguchi, C. Iida and G. Nakagawa, Anal. Sci., 6 (1990) 385.
7 K. Kina, K. Shiraishi and N. Ishibashi, Talanta, 25 (1978) 295.
8 S. Motomizu and M. Onoda, Anal. Chim. Acta, 214 (1988) 289.

Analytica Chimica Acta, 281 (1993) 103–109
Elsevier Science Publishers B.V., Amsterdam

Automatic continuous-flow determination of paraquat at the subnanogram per millilitre level

Manuel Agudo, Angel Ríos and Miguel Valcárcel

Department of Analytical Chemistry, Faculty of Sciences. University of Córdoba, E-14004 Córdoba (Spain)

(Received 5th February 1993)

Abstract

A flow-through spectrophotometric sensor for the determination of paraquat at the nanogram per mililitre level based on integration of preconcentration, reaction and detection in the flow-cell is proposed. The determination range achieved depends on the sample volume used. Thus, 250 ml of sample provides detection and determination limits of 0.11 and 0.44 ng ml^{-1} paraquat, respectively. The relative standard deviation was $\pm 7.9\%$ for 1.0 ng ml^{-1} paraquat. The potential interference of other pesticides was studied, and the method was used to analyse water samples and study the adsorption of paraquat in different types of soils.

Keywords: Flow system; Paraquat; Soil adsorption; Waters

Paraquat (1,1′-dimethyl-4,4′-dipyridinium) is a herbicide registered for use on terrestrial and aquatic plants whose chemical structure includes a two-fold quaternary ammonium function. It is often used as a selective weedkiller because it is more effective against broad-leaved vegetation than against grasses [1,2]. Paraquat is also a poison that causes heart, kidney and liver diseases. On the other hand, it is strongly adsorbed at the cation-exchange sites clays [3]. Binding is virtually irreversible under natural conditions, especially in montmorillonite. This has adverse agricultural effects because it excludes retention of nutrient cations (mainly ammonium) and oligoelements in soils.

Several methods for paraquat determination have been reported, most of which are either spectrophotometric, polarographic or chromatographic [4–7]; however, none allows accurate monitoring of this compound at the levels established by the European Community Directive on Drinking Water (80/778/EC). The spectrophotometric method most often used for this purpose is based on the reduction of paraquat to a blue radical with alkaline sodium dithionite [8]. In this work we designed a flow manifold integrating preconcentration, reaction, and detection in a sorbent material packed in a flow-cell for the determination of the pesticide. The method relies on the recently developed flow-through sensor technology [9,10] by which reaction (retention) and detection are integrated in a flow-injection system [11,12]. In this case, successive passage of the sample, reagent and eluent through the flow-cell and continuous photometric monitoring of the process provides the analytical information needed to determine the herbicide. The proposed method allows the automatic on-line monitoring of this compound in water, and was applied to study its adsorption by different types of soil.

Correspondence to: M. Valcárcel, Department of Analytical Chemistry, Faculty of Sciences, University of Córdoba, E-14004 Córdoba, Spain.

EXPERIMENTAL

Reagents

Aqueous solutions of 1% (w/v) sodium dithionite (Merck) at pH 12.5 and a saturated solution of ammonium chloride (Merck) were used as reagent and eluent, respectively. A 100 mg l^{-1} aqueous stock solution of paraquat was prepared from 1,1′-dimethyl-4,4′-bipyridylium dichloride (Aldrich). A Dowex 50W-X8-200 cation-exchange resin (Sigma) in its ammonium form was used for retention reaction of paraquat in the flow-cell.

Apparatus

Photometric measurements were made on a Unicam 8625 spectrophotometer connected to a Knauer TY recorder. A Gilson Minipuls-3 peristaltic pump, and Omnifit eight-way valve, a Rheodyne 5041 rotary injection valve, and a Hellma 178.10 QS flow-cell (inner volume 18 μl) were also used.

Manifold and procedure

The manifold initially assayed is depicted in Fig. 1. A single channel was used to drive the water sample, reagent, and eluent to the detector in that order. A switching valve (V_s) allowed the sequence to be controlled. The photometric flow-cell was packed with the cation-exchange resin in the ammonium form. Thus, paraquat in the sample was first retained on the exchange material (preconcentration step). When a preset volume of sample was passed through the flow-cell, V_s was switched in order to introduce the reagent. In this way, reaction took place in the flow-cell (reaction step), and the detector continuously monitored the increase in absorbance. After the reaction was completed, V_s was switched to its third position, thereby allowing the reaction product to be eluted from the exchange resin, which was thus prepared for a new sample by having V_s select the first channel again.

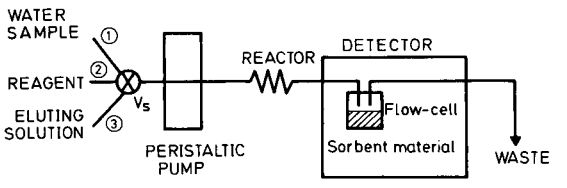

Fig. 1. Manifold for retention–reaction–detection of paraquat in water samples. (1) Sample preconcentration; (2) reaction step; and (3) elution. V_s = Switching valve.

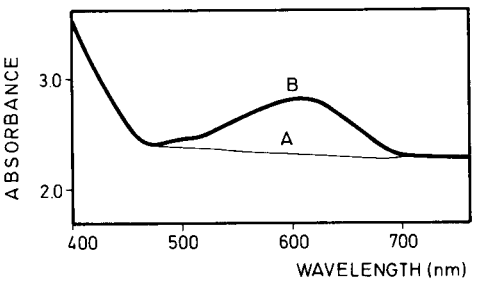

Fig. 2. Visible spectra of the flow-cell packed with the cationic resin in the absence (A) and presence (B) of the retained reaction product of paraquat and dithionite.

RESULTS AND DISCUSSION

Paraquat reacts with dithionite ion to yield a blue compound absorbing at 605 nm. This reaction can be carried out with the paraquat retained on various sorbent materials, onto which the reaction product is also retained. Thus, in preliminary assays, several sorbent materials were tested in order to find the most appropriate for the purpose. Activated glass and aluminum oxide did not retain paraquat at all; C_{18} chromatographic material only retained some analyte at high concentrations of the herbicide, whereas silica gel was unstable in the alkaline medium where the reaction should take place. Cation exchange resins provided the best results, especially Dowex 50W-X8-200. In addition, the visible spectrum of this support packed in the flow-cell was clearly different in the presence and absence of the blue radical bound to the resin (Fig. 2), so integrated retention, reaction and detection was indeed feasible.

As a result of the strong retention of paraquat on this cationic exchange resin, the elution process had to be carefully designed in order to avoid any carry-over. According to Malquori and

Radaelli [13], several cations remove paraquat from clay with a different efficiency (e.g., $NH_4^+ \geq K^+ > Ca^{2+} > Mg^{2+} > Na^+$). Therefore, both these cations and $(CH_3)_4N^+$, which is similar to ammonium ion but features a larger ionic volume, were assayed for removing paraquat from the exchanger. Ammonium chloride proved to be the most efficient for this purpose, but it had to be used at a saturation concentration.

Also, various reductants (ascorbic acid, SnO_2^{2-}, hydrazine, etc.) were tested in order to improve the sensitivity; however dithionite proved to afford the best results. A dithionite concentration at ca. 1% (w/v) provided the maximum possible signal. The pH was another key variable in this reaction, which only takes place in an alkaline medium because of the instability of dithionite in an acidic medium. The sensitivity increased as the pH increased, but a pH of 12.5 was finally chosen in order to avoid rapid deterioration of the pump tubes.

FIA variables

The mixing coil in Fig. 1 was made as short as possible (30 cm × 0.5 mm i.d.), so as to prevent the reaction taking place to any extent in it. The flow-rates of sample, reagent and eluent were also optimized. For the sample stream (preconcentration process) a flow-rate of 2.8 to 3.6 ml min^{-1} provided maximal retention of paraquat in the resin. However, higher flow-rates (up to 4.0 ml min^{-1}) caused no significant decrease in retention and resulted in higher sampling frequencies, so 4.0 ml min^{-1} was finally selected. The optimum flow-rate value for the dithionite stream (reaction step) was 2.2–2.5 ml min^{-1}, while that for ammonium chloride eluent was ca. 4.0 ml min^{-1}. This required the manifold in Fig. 1 to be slightly altered in order to avoid the need to change the drum rotation speed of the pump during the analyses. The manifold depicted in Fig. 3 was finally used, in which V_s selected the water sample or eluent stream (both flowing at 4.0 ml min^{-1}). A second valve (V in Fig. 3) located after the pump switched to the reagent solution (flowing at 2.5 ml min^{-1}) in the detection/determination step. V was a conventional injection valve modified to operate as a switching-diverting valve [14].

Sample preparation

Two major variables were considered in order to increase retention of paraquat from synthetic samples: viz. pH and the ionic strength. The pH of the sample must be higher than 3.5; however, no influence on retention was observed at the normal values of this variable in real samples (from 5–6 to 8–9). On the other hand, the ionic strength played a major role because it affected retention of paraquat on the exchanger adversely; however, a minimum ionic strength was clearly needed in order to prepare synthetic samples with a similar matrix to that of real water samples. Consequently, an ionic strength of 0.05 M in $NaNO_3$ was chosen for all samples. This ionic strength decreased the retention efficiency by ca. 20% relative to samples with an ionic strength of virtually zero (i.e., samples containing the analyte alone).

Determination of paraquat

Various calibration graphs were used depending on the sample volume passed through the flow-cell. Their figures of merit are summarized in Table 1. The proposed method allows paraquat to be determined over a wide range (μg ml^{-1} to

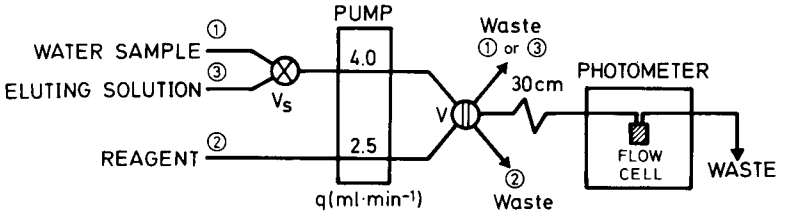

Fig. 3. Manifold for the automatic determination of paraquat under optimal hydrodynamic conditions (see text).

TABLE 1

Features of the determination of paraquat by the proposed method

Sample volume (ml)	Determination range	R.S.D. (%)	Sampling frequency (h^{-1})
1.0	> 0.2 $\mu g\ ml^{-1}$	4.6	10
5.0	0.2 $\mu g\ ml^{-1}$–80 ng ml^{-1}	4.8	15
10	120–40 ng ml^{-1}	5.3	12
25	75–17 ng ml^{-1}	5.8	6
50	24–4 ng ml^{-1}	6.5	4
100	14–1.5 ng ml^{-1}	6.9	2
250	5.5–0.4 ng ml^{-1}	7.9	0.9

ng ml^{-1} levels) by simply selecting the sample volume used. Higher concentrations of paraquat can be determined also by passing lower sample volumes. For that a switching valve is added to the manifold in Fig. 3. An increased sampling frequency is to be anticipated. As a rule, the minimum sample volume must be used in order to increase the sampling frequency, first by reducing the time needed for the preconcentration step, and second by shortening the time required to remove paraquat from the resin. Thus, as the concentration of paraquat in the sample increases, the elution time also increases (hence the sequence of sampling frequency values in Table 1, according to which it did not vary in the same way as the sample volume used). As can be seen, enhanced sensitivity resulted in a dramatically diminished sampling frequency. The authors consider this as the main disadvantage of the proposed method. No significant increase in sensitivity was obtained by using sample volumes above 250 ml, at which the statistic detection limit was 0.11 ng ml^{-1} (Fig. 4). The kinetic profiles of the curves cannot be used for determination purposes because the initial reaction rate is almost the same in all cases. In fact, the recorded effect is not the kinetics of the reaction between paraquat and dithionite (a fast reaction), but the diffusion of the reagent into the exchange resin material where the analyte was fixed. Consequently, only the maximum absorbances of these curves were employed for the determination of paraquat.

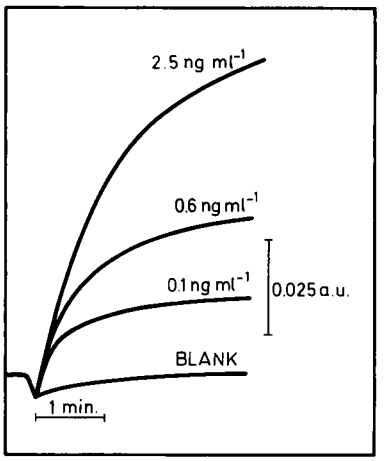

Fig. 4. Absorbance-time recordings obtained for different amounts of paraquat in water samples.

Interferences

A study of the selectivity of this method was carried out by assaying other pesticides. The concentration of paraquat was fixed at 10 ng ml^{-1} in all cases. As shown in Table 2 the maximum tolerated foreign species/paraquat ratio was at least 100:1, except for diquat, which undergoes a similar reaction with dithionite, but with lower sensitivity, especially when the reaction takes place on the support used in this method. Other "polar" pesticides such as propanil, atrazine, simazine and linuron caused no interference.

TABLE 2

Study of pesticide interferences in the determination of paraquat

Foreign species	Maximum tolerated ratio level
Diquat	10
Propanil	> 100
Atrazine	100
Carbaryl	> 100
Carbofuran	> 100
Propoxur	> 100
2-Isopropoxiphenol	> 100
Simazine	> 100
Linuron	> 100
1-Naphthol	> 100

TABLE 3

Results obtained for synthetic water samples

Concentration			
Added (ng ml^{-1})	Found (ng ml^{-1})	Added (ng ml^{-1})	Found (ng ml^{-1})
10	10.6	1	1.4
25	26.1	2	2.1
30	34.4	2.5	2.6
20	20.9	3	2.9
35	37.2	5	4.7

Determination of paraquat in water samples

Paraquat was determined at the nanogram per millilitre level in synthetic samples (see Table 3). The aim here was to test the applicability of the method, particularly in relation to real water samples. None of the natural water samples analysed contained any paraquat, so they had to be spiked with the analyte at different concentrations. The signals provided by these samples were dramatically lower than those for the synthetic samples. This was the result of the presence of calcium and magnesium ions at high concentrations relative to paraquat in the samples. Both cationic ions strongly compete with the analyte for the resin in the retention process. In order to avoid this interference, calcium and magnesium ions were masked with EDTA at pH 9. Thus, 0.4

TABLE 4

Determination of paraquat in real water samples

Type of sample	Paraquat added (ng ml^{-1})	Paraquat found (ng ml^{-1})	Recovery (%)
Tap water	3.0	3.02	100.7
(Córdoba)	0.5	0.46	92.0
Well water	3.0	3.11	103.6
(Villa del Río)	0.5	0.41	82.0
Lake water	3.0	2.71	90.3
(Villa del Río)	0.5	0.38	76.0
River water	3.0	2.65	88.3
(River Guadalquivir, Córdoba)	0.5	0.43	86.0
Rain water	3.0	3.33	111.0
	0.5	0.54	108.0

TABLE 5

Paraquat adsorption by four types of soil

Sample	Type of soil	Total clay content (%)	Total organic matter content (%)	Time	Paraquat concentration (ng ml^{-1})	Adsorption (%)
I	Sandy	19	1.1	0	50	–
				15 min	34	32
				30 min	24	52
				60 [a]	7.8	84
				2 h [a]	5.2	90
				3 h [a]	5.2	90
II	Franco I	33	2.2	0	50	–
				15 min	19.2	61
				45 min [a]	12.6	75
				60 min [a]	9.5	81
				2 h [b]	0.9	98
III	Franco II	41	0.1	0	50	–
				15 min	21.3	57
				45 min [a]	14.8	70
				60 min [a]	10.8	78
				2 h [b]	2.2	95
IV	Clayey	48	1.1	0	50	–
				15 min [a]	12.6	75
				45 min [a]	6.1	88
				2 h [b]	0.7	99

[a] 50 ml of water were taken. [b] 250 ml of water were taken.

g of disodium EDTA salt were added to each sample. The results thus obtained (Table 4) were consistent with those provided by the synthetic samples.

Paraquat adsorption by soils

Paraquat is adsorbed at the cation-exchange sites of clays. Binding is almost irreversible under natural conditions. The pesticide is also adsorbed by humic and fulvic acid. Thus, it is bound within the first centimeters of the soil layer. It has never been detected at a depth < 45 cm [15].

Four different types of soil were studied for adsorption of paraquat, as was the kinetics of this process by using the proposed method for monitoring the paraquat. For these experiments, 20 mg of soil sample were placed into a vessel, then 500 ml of 50 ng ml^{-1} paraquat was added and the mixture was continuously stirred. Periodically 25.0 ml of the supernatant was taken, passed through a PTFE bed packed microcolumn (10 cm $\times$ 2.0 mm i.d.), placed at the start of the sample channel (Fig. 3) and used as a filter, after which the paraquat concentrations was determined. The features of the soil samples used and the changes in the paraquat concentration in the liquid phase with time are shown in Table 5. Several interesting conclusions can be drawn from the results. In all cases, a virtually exponential adsorption–time curve defined the behaviour of the sediments obtained by mixing the soils and the pesticide aqueous solution. Also, equilibrium was reached in about 2 h and resulted in very high adsorption (90% or higher). The total amount of clay in the soils played a major role in the adsorption process, as reflected Fig. 5, which shows two sets of results. The first set corresponds to measurements made 15 min after mixing (Table 5), so the kinetics was main factor (empty circles in Fig. 5). The adsorption efficiency increased with increase in the clay content, as clearly shown for samples I an IV (the total organic matter content of both was 1.1%). However, the amount of organic matter in the soil played a decisive role, as shown by the results obtained for samples II (2.2%) and III (0.1%). For samples with the same amount of organic matter (I and IV), the increase in the clay content

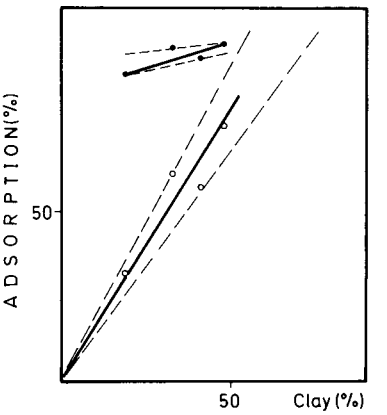

Fig. 5. Adsorption of paraquat by different types of soil (see Table 5) base on the clay content. Empty circles denote measurements made 15 min after mixing 20 mg of soil and 500 ml of aqueous paraquat (50 ng ml^{-1}). Black circles correspond to measurements made at equilibrium (2 h).

defined a linear relationship passing by point (0.0) in Fig. 5. Variations in the organic matter content would result in changes in the slope of this straight line (dashed lines in Fig. 5): the slope increases as the total amount of organic matter increases. When equilibrium is reached (black circles in Fig. 5), such differences decrease dramatically, but the same sequence holds.

Conclusions

The proposed method for the determination of paraquat is characterized by simplicity and automation. Paraquat can be determined at the subnanogram per milliliter level by using an integrated continuous retention–reaction–detection flow approach that is particularly useful for routine analyses, which can be implemented with inexpensive equipment. The method can be extended to the direct determination of other pesticides. On the other hand, the method has a very low throughput and requires large sample volumes for low paraquat concentration.

The CICyT is acknowledged for financial support (Grant No. PB90/0925). M. Agudo is also grateful to the Junta de Andalucía for financial support received in the form of a personal fellowship.

REFERENCES

1 G. Zwing, Pesticides, Plant Growth Regulators and Food Additives, Vol. V, Academic Press, New York, 1967, p. 473.
2 A. Calderbank and S.H. Crowdy, Annu. Rep. Appl. Chem., (1962) 536.
3 L. Torstensson, Weeds Weed Control, 24 (1983) 268.
4 P. Yáñez-Sedeño and L.M. Polo, Talanta, 33 (1986) 745.
5 P. Yáñez-Sedeño, J.M. Pingarrón and L.M. Polo, Mikrochim. Acta, 111 (1985) 279.
6 G.H. Draffen, R.A. Clare, D.L. Davies, G. Hawkasworth, S. Murray and D.S. Davies, J. Chromatogr., 255 (1983) 483.
7 R. Gill, S.C. Qua and D. Moffat, J. Chromatogr., 255 (1983) 483.
8 S.H. Yuen, J.E. Baggness and D. Myles, Analyst, 92 (1967) 375.
9 M. Valcárcel, Analyst, (1993) in press.
10 M.D. Luque de Castro and M. Valcárcel, Trends Anal. Chem., 10 (1991) 114.
11 F. Lázaro, M.D. Luque de Castro and M. Valcárcel, Anal. Chim. Acta, 214 (1988) 217.
12 F. Lázaro, M.D. Luque de Castro and M. Valcárcel, Anal. Chim. Acta, 219 (1989) 231.
13 A. Malquori and A. Radaelli, Italia Agricola, 104 (1966) 35.
14 A. Ríos, M.D. Luque de Castro and M. Valcárcel, J. Automatic Chem., 9 (1987) 30.
15 S. Garrido, private communication.

Analytica Chimica Acta, 281 (1993) 111–118
Elsevier Science Publishers B.V., Amsterdam

Determination of amines by flow-injection analysis based on aryl oxalate–Sulphorhodamine 101 chemiluminescence

Masatoki Katayama, Hideyuki Takeuchi and Hirokazu Taniguchi

Meiji College of Pharmacy, 1-35-23 Nozawa, Setagaya-ku, Tokyo 154 (Japan)

(Received 1st June 1992; revised manuscript received 2nd March 1993)

Abstract

A flow-injection method for amines based on aryl oxalate–Sulphorhodamine 101 chemiluminescence is described. Fifty-five aliphatic, aromatic and heterocyclic amines were studied by the proposed method without a derivatization reaction or expensive apparatus. Twenty-eight amines were detected at levels of 1.0×10^{-10}–4.0×10^{-6} M (signal-to-noise ratio = 3, 20-μl injection) with linear calibration up to 1.0×10^{-4}–1.0×10^{-3} M, respectively. The relative standard deviation ($n = 6$) was 4.8% at 1.0×10^{-6} M triethylamine. The proposed method was applied to the determination of histamine in fish and compared favourably with a liquid chromatographic method using fluorescence detection after derivatization.

Keywords: Chemiluminescence; Flow injection; Amines; Fish; Foods; Histamine

Aryl oxalate chemiluminescence has been reported as one of the most sensitive methods for the determination of hydrogen peroxide [1,2], aromatic hydrocarbons [3], catecholamines [4], amino acids [5], antibodies derivatized by glucose oxidase [6], β-galactosidase [7], chlorophenol [8], steroids [9] and carboxylic acids [10,11] derivatized by fluorescent compounds. In these methods, aryl oxalate was oxidized by hydrogen peroxide in the presence of base (amines were widely used, e.g., imidazole and triethylamine) and a fluorescent compound (sensitizer). Amines have been determined by many other methods. For example, the determination of catecholamines allowed assessments of diseases of the central nervous system [12]. Determination of polyamines gave information about cancer tissues [13]. Many other amines contained in drugs have been reported.

Correspondence to: M. Katayama, Meiji College of Pharmacy, 1-35-23 Nozawa, Setagaya-ku, Tokyo 154 (Japan).

Liquid chromatography (LC) was widely used in those studies because its suitability for biological samples (e.g., serum, plasma and tissue extracts) and selectivity and the inexpensive apparatus involved. However, the poor UV absorptivity of most amines made the determination of small amounts difficult [14]. For sensitive determination by LC, pre- or post-label derivatization reactions were needed for primary and secondary amines [4,5,15–17], but these derivatization reactions could not be applied to tertiary and heterocyclic amines, so sensitive LC methods with photometric and fluorimetric detection after derivatization have not been reported. The development of a sensitive method for the simultaneous determination of tertiary and heterocyclic amines by flow-injection analysis (FIA) and LC would therefore be useful.

In previous papers, we reported a sensitive FIA method for the determination of hydrogen peroxide based on aryl oxalate chemiluminescence with bis[4-nitro-2-(3,6,9-trioxadecyloxycarbonyl)phenyl] oxalate (TDPO) [5,9] and sulpho-

rhodamine 101 in an amine (imidazole)–nitric acid buffer–acetonitrile mixture. This method was more sensitive than other aryl oxalate chemiluminescence methods, and it could detect 3.0×10^{-9} M hydrogen peroxide per 20-μl injection [18]. In this work, this method was applied to the determination of amines, especially tertiary and heterocyclic amines, by FIA. Chemiluminescence detector responses of 55 amines and monitoring of histamine in fish were studied.

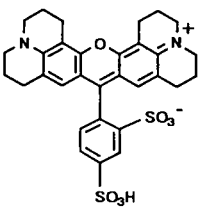

Fig. 1. Sulphorhodamine 101.

EXPERIMENTAL

Reagents and materials

An amine stock standard solution (1.0×10^{-3} M) was prepared by dissolving 1.0×10^{-5} mol amine in 0.1 ml of ethanol and diluting to 10 ml with acetonitrile. Sample solutions were prepared by dilution with eluent [water–acetonitrile (1 + 9)].

Analytical-reagent grade chemicals were used unless indicated otherwise *n*-Hexylamine, diethylamine, diphenylamine, pyrrolidine, piperidine, quinuclidine, piperazine, triethylamine, tributylamine, triethylenediamine, pyrrole, indole, carbazole, imidazole, 2-methylimizadole, 2-ethylimidazole, 1,2-dimethylimidazole, pyrazole, 2-pyrazoline, 1,2,4-triazole, purine, aniline, morpholine, dopamine, tyramine, histamine, pyridine and *o*-phthalaldehyde were purchased from Tokyo Kasei (Tokyo), spermine, spermidine, cadaverine and putrescine from Nacalai Tesque (Kyoto), *N*-ethylmorpholine from Wako (Osaka), amino acids from Ajinomoto (Tokyo) and Tokyo Kasei and TDPO from Wako. Hydrogen peroxide (30%, w/v) was purchased from Mitsubishi Gas Kagaku (Tokyo). Its concentration was determined by titrimetry with potassium permanganate solution. Sulphorhodamine 101 (Fig. 1) was of laser grade (Eastman Kodak, Rochester, NY). Eluents used in the FIA system were of LC grade. Triacetyl cellulose filters SC-40, -50, -52, -54, -56, -58, -60, -62, -64, -66, -68 and -70, which could cut off light under 400, 500, 520, 540, 560, 580, 600, 620, 640, 660, 680 and 700 nm, respectively, were purchased from Fuji Film (Tokyo).

Apparatus

The FIA system is illustrated in Fig. 2. A Shimadzu LC-6A liquid chromatograph (pump 1) (Shimadzu, Kyoto) and a peristaltic pump (pump

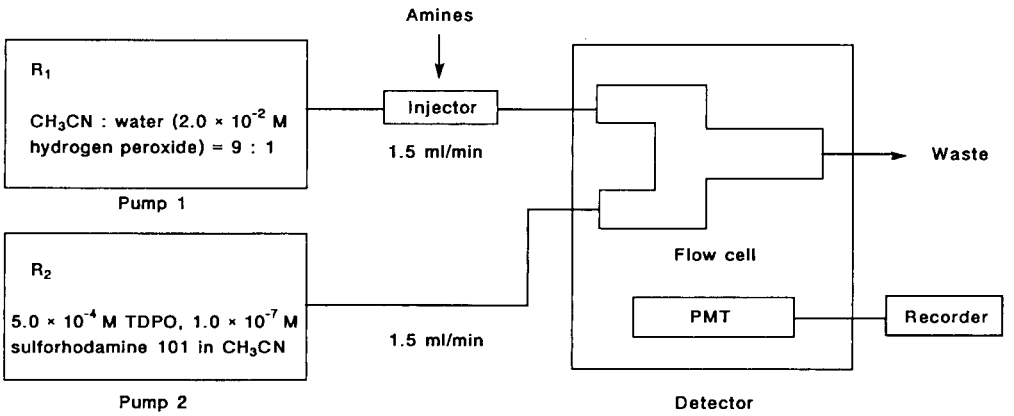

Fig. 2. Schematic diagram of the FIA system. Pump 1, Shimadzu LC-6A; pump 2, Nihon Rikagaku PF-6 (peristaltic pump); detector Niti-On LF-800.

2, PF-6) (Nihon Rikagaku, Tokyo) were used as FIA pumps. Chemiluminescence was observed in a Lumi-flow LF-800 chemiluminescence detector (spiral-type flow cell, volume 160 μl; Niti-On, Funabashi). Eluent R_1 [acetonitrile–water containing 0.02 M hydrogen peroxide (9 + 1, v/v)] was applied at a flow-rate of 1.5 ml min^{-1}. Eluent R_2 (5.0×10^{-4} M TDPO–1.0×10^{-7} M Sulphorhodamine 101 in acetonitrile) was applied at a flow-rate of 1.5 ml min^{-1}. The sample was diluted with eluent R_1 and 20 μl of sample solution were injected into the FIA system.

The LC system for comparison of histamine contents in fish was as described [19,20] and the LC conditions were as follows: pump, Shimadzu LC-6A; analytical column, 7-μm Zorbax ODS (250 × 4.6 mm i.d.) (DuPont, Wilmington, DE); eluent, 0.2 M sodium chloride–methanol (2 + 8), with pH adjusted to 3.0 with 0.1 M hydrochloric acid; column temperature, room temperature (ca. 22°C); detector, Shimadzu RF-535 fluorescence monitor [λ(ex.) 350 nm, λ(em.) 450 nm]; flow-rate, 0.5 ml min^{-1}; and sample volume, 5 μl.

Preparation method for fish sample

Chemiluminescence FIA method. A fish sample was prepared as described [19,20] with some modifications. A 10-g amount of minced tuna fish was extracted with 15 ml of water for 5 min, 20 ml of 10% (w/v) trichloroacetic acid solution were added and the mixture was diluted to 50 ml with water, mixed for 10 min and filtered. This mixture was neutralized with 10% (w/v) sodium hydroxide solution and 10 ml of the neutralized mixture were applied to a Sep-Pak C_{18} ENV plus cartridge. The column was washed with 20 ml of water and the histamine was eluted selectively with 20 ml of 2% (v/v) acetonitrile. Other amines, e.g., cadaverine, were retained on the Sep-Pak C_{18} ENV plus cartridge under these conditions. A 20-μl aliquot of the eluate was injected into the FIA system.

LC method [20]. A 10-g amount of minced tuna fish was extracted with 15 ml of water for 5 min, 20 ml of 10% (w/v) trichloroacetic acid solution were added and the mixture was diluted to 50 ml with water, mixed for 10 min and filtered. The pH of 10 ml of the filtrate was adjusted to 5–7 with 10% (w/v) sodium hydroxide solution and 10 ml of 0.4 M acetate buffer solution were added. This mixture was applied to an ion-exchange column (55 × 10 mm i.d., Amberlite CG-50, Type I, 100–200 mesh) (Rohm and Haas, Philadelphia, PA) and the column was washed with 80 ml of 0.2 M acetate buffer. The histamine was eluted with 15 ml of 0.2 M hydrochloric acid. The eluate was neutralized with 1.0 M sodium hydroxide solution and diluted to 20 ml with water. A 0.2-ml volume of 1.0 M sodium hydroxide solution and 0.1 ml of 1% (w/v) *o*-phthalaldehyde were added to a 1-ml aliquot of the histamine eluate. After 4 min, 0.3 ml of 1.0 M sulphuric acid was added and a 5-μl aliquot of the derivatized histamine eluate was injected into the LC system.

RESULTS AND DISCUSSION

FIA conditions

The FIA conditions (flow-rate, composition of eluent, TDPO concentration, Sulphorhodamine 101 concentration, hydrogen peroxide concentration, injection volume) were examined using 1.0×10^{-5} M triethylamine.

Effect of flow-rate. The flow-rates of eluents R_1 and R_2 were varied from 0.1 to 3.5 ml min^{-1}. The maximum detector response and the lowest limit of detection were obtained with both eluents at a flow-rate of 1.5 ml min^{-1}.

Effect of composition of eluent. It was found that the compositions of the eluents affected the detector response [18]. The water–acetonitrile composition was varied over the range of 1 + 100–1 + 10 (v/v) (Fig. 3). Water–acetonitrile (1 + 20, v/v) gave the highest detector response and the lowest limit of detection.

Effect of TDPO concentration. The TDPO concentration was varied from 1.0×10^{-5} to 5.0×10^{-3} M. As the TDPO concentration was increased, the detector response became higher, but the background noise and the baseline drift also increased. The lowest limit of detection was obtained at 5.0×10^{-4} M TDPO and this concentration was used in eluent R_2.

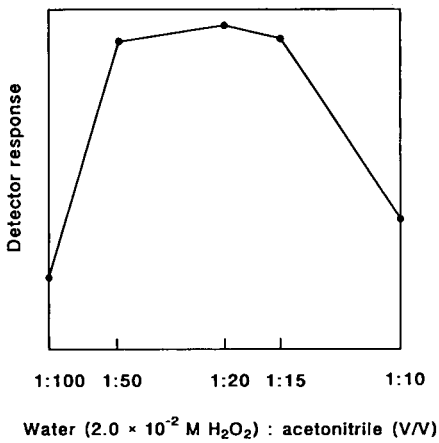

Fig. 3. Effect of volume ratio of water and acetonitrile in FIA eluent. Triethylamine taken, 1.0×10^{-5} M; Sulphorhodamine 101 taken, 1.0×10^{-7} M; TDPO taken, 5.0×10^{-4} M.

Effect of Sulphorhodamine 101 concentration. The concentration of Sulphorhodamine 101 was varied from 1.0×10^{-9} to 1.0×10^{-6} M. As the Sulphorhodamine 101 concentration increased the detector response became higher but the background signal from the eluent was also increased. The limit of detection was lowest at 1.0×10^{-7} M Sulphorhodamine 101 and this concentration was used in eluent R_2.

Effect of hydrogen peroxide concentration. The concentration of hydrogen peroxide was varied from 1.0×10^{-5} to 0.1 M. The detector response increased when the hydrogen peroxide concentration increased. The limit of detection was lowest at 0.02 M hydrogen peroxide and this concentration was selected in eluent R_1.

Effect of injection volume. The injection volume was varied from 5 to 1000 μl. The highest constant detector response was obtained with a 10–80-μl injection of sample solution. The lowest limit of detection was obtained when 20 μl of sample solution were injected, so this volume was adopted.

Construction of pump and effect of damper. In order to decrease the noise in FIA, damping by an LC column and coil have been reported [8,9]. Therefore, two LC columns (7-μm ODS gel, each 250×4.6 mm i.d.) were tested for damping the LC pump and PTFE tubing (3, 5 and 8 m $\times$ 2.0 mm i.d.) were tested for damping the peristaltic pump. The noise reduction was not improved. Therefore, no damping was applied to eluents R_1 and R_2. An LC pump was used as pump 1 and a peristaltic pump as pump 2. When peristaltic pumps were used as both pump 1 and pump 2, the same analytical data were observed, and when LC pumps were used as both pump 1 and pump 2 the same result was also observed. It is intended to develop the proposed FIA system for use with an LC system for amines in foodstuffs in areas polluted by acid rain. The above pump system was adopted.

Effect of noise cut-off filter. Background emissions of aryl oxalate esters at around 450–550 nm have been reported [3,8], and these have an adverse effect on the detection limits. Hence the necessity for a noise cut-off filter at 500–550 nm and a fluorophore that emits long-wavelength light has been reported [8]. In a previous paper, an FIA system for the determination of hydrogen peroxide via aryl oxalate chemiluminescence was reported [18]. Sulphorhodamine 101 was used as a fluorophore that emits long-wavelength light at 600 nm, but no noise cut-off filter was used. In this work, the effect of a noise cut-off filter on the FIA traces was studied. Triacetylcellulose filters were set in front of the photomultiplier tube. A decrease in the detector response was observed

TABLE 1

Effect of noise cut-off filter on the limit of detection (LD)

Filter [a]	LD (M) (S/N = 3) [b]
SC-40	7.0×10^{-7}
SC-50	7.0×10^{-7}
SC-52	7.0×10^{-7}
SC-54	7.0×10^{-7}
SC-56	1.4×10^{-6}
SC-58	3.0×10^{-6}
SC-60	3.0×10^{-4}
SC-62	3.0×10^{-3}
SC-64	3.0×10^{-3}
SC-66	N.D. [c]
SC-68	N.D.
SC-70	N.D.

[a] Triacetylcellulose filters were used; SC-40 cut off the light under 400 nm and the others (SC-50 to -70) cut off the light under 500–700 nm (see text). [b] Hydrogen peroxide taken, 0.02 M; Sulphorhodamine 101 taken, 1.0×10^{-7} M; TDPO taken, 5.0×10^{-4} M. [c] No detector response.

when SC-56 to SC-70 filters were used (Table 1). An SC-54 filter was adopted.

Determination of amines

The detection limits of 55 amines were studied by the proposed FIA method (Table 2). The peaks of cadaverine, histamine and triethylamine are shown in Fig. 4. Primary aliphatic amines, e.g., hexylamine, were detected down to 1.2×10^{-8} M (signal-to-noise ratio = 3, 20-μl injection). Polyamines, e.g., cadaverine, were detected down to 7.0×10^{-10} M. The aromatic amines aniline and diphenylamine were not detected even with an injection of a 0.01 M sample. A secondary aliphatic amine, diethylamine, was detected down to 1.4×10^{-8} M. Cyclic amines, e.g., piperidine, were detected down to 5.0×10^{-7} M. Tertiary amines, triethylamine and tributylamine were detected down to 7.0×10^{-7} M. For a quaternary ammonium salt, e.g., trimethylammonium hydroxide, the detection limit was 8.0×10^{-5} M; trimethylammonium bromide was not detected. The heterocyclic amines, pyrrole, carbazole and indole were not detected. Imidazole, was detected down to at 2.0×10^{-10} M and histamine at 7.0×10^{-10} M. Pyridine was detected down to

TABLE 2

Detection limits of amines using the proposed FIA method

Compound [a]	LD (M) (S/N = 3) [b,c]	Compound [a]	LD (M) (S/N = 3) [b,c]
Hexylamine	1.2×10^{-8}	*N*-Ethylmorpholine	5.0×10^{-7}
Cadaverine	7.0×10^{-10}	Triethylenediamine	4.0×10^{-7}
Putrescine	1.0×10^{-10}	Quinuclidine	1.0×10^{-10}
Spermine	1.0×10^{-10}		
Spermidine	1.0×10^{-10}	Trimethylammonium hydroxide	8.0×10^{-5}
		Trimethylammonium bromide	N.D.
Dopamine	5.0×10^{-10}		
Tyramine	5.0×10^{-10}	Alanine	N.D.
Aniline	N.D.	Arginine	1.5×10^{-6}
		Aspartic acid	N.D.
Diethylamine	1.4×10^{-8}	Glycine	N.D.
Diphenylamine	N.D. [d]	Histidine	2.5×10^{-6}
		Hydroxyproline	N.D.
Pyrrolidine	7.0×10^{-7}	Lysine	4.0×10^{-6}
Piperidine	5.0×10^{-7}	Methionine	N.D.
Piperazine	5.0×10^{-7}	Phenylalanine	N.D.
Morpholine	7.0×10^{-7}	Proline	N.D.
		Serine	N.D.
Triethylamine	7.0×10^{-7}	Tryptophan	N.D.
Tributylamine	7.0×10^{-7}	Tyrosine	N.D.
Pyrrole	N.D.	Sodium hydroxide	N.D.
Carbazole	N.D.	Potassium hydroxide	N.D.
Indole	N.D.	Sodium carbonate	N.D.
Imidazole	2.0×10^{-10}	Sodium hydrogencarbonate	N.D.
2-Methylimidazole	2.0×10^{-10}	Ammonium chloride	N.D.
2-Ethylimidazole	2.0×10^{-10}	Ammonium nitrate	N.D.
1,2-Dimethylimidazole	1.4×10^{-9}	Dipotassium hydrogenphosphate	N.D.
Histamine	7.0×10^{-10}		
1,2,4-Triazole	N.D.	Aqueous ammonia	7.0×10^{-9}
Pyrazole	N.D.		
2-Pyrazoline	N.D.		
Purine	N.D.		
Pyridine	5.0×10^{-7}		

[a] Amines were taken at 1.0×10^{-8}, 1.0×10^{-6} and 1.0×10^{-4} M. [b] LD = limit of detection. [c] Hydrogen peroxide taken, 0.02 M; Sulphorhodamine 101 taken, 1.0×10^{-7} M; TDPO taken, 5.0×10^{-4} M. [d] No detector response.

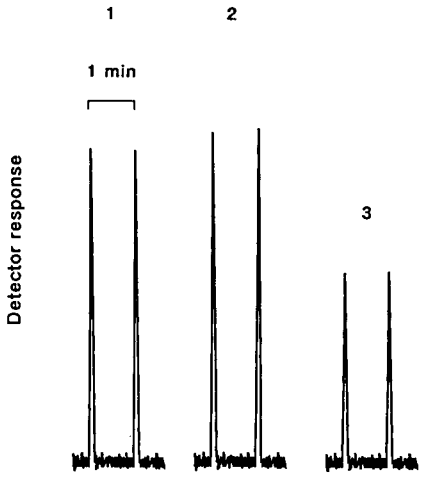

Fig. 4. Chemiluminescence peaks of amines using the proposed FIA system. Hydrogen peroxide taken, 0.02 M; Sulphorhodamine 101 taken, 1.0×10^{-7} M; TDPO taken, 5.0×10^{-4} M. 1 = Cadaverine (5.0×10^{-9} M); 2 = histamine (5.0×10^{-9} M); 3 = triethylamine (1.0×10^{-6} M).

5.0×10^{-7} M. Inorganic base compounds were not detected. However, aqueous ammonia was detected down to 7.0×10^{-9} M.

The upper limit of each amine ranged in concentration from 1.0×10^{-3} to 1.0×10^{-4} M. Consequently, the proposed FIA method appears to be selective and sensitive for aliphatic amines and imidazoles. The detection limits of primary and secondary amines were over 50 times lower than those in other LC methods using fluorescence detection after derivatization with *o*-phthalaldehyde [15], fluorescamine [16] or NBD-Cl [17]. The proposed method showed the same sensitivity as the method using chemiluminescence detection after derivatization with dansyl chloride [4,5] and luminol derivatives [21]. Tertiary amines could not be determined by the above LC method with derivatization, so GC and GC–MS were the only methods available for sensitive determination [22,23]. However, the proposed method is more sensitive than GC or GC–MS and expensive apparatus and derivatization are not required. The proposed method should therefore be useful for the determination of trace amounts of amines in tissues, drugs and foods.

Determination of histamine in fish

Histamine is a biogenic amine that causes an allergy. Biological methods, chemical methods, fluorimetry [24], thin-layer chromatography (TLC) [20] and LC [19,20] have been used for the determination of histamine in seafood. Of these methods, LC with precolumn derivatization was the most sensitive and selective. However, precolumn derivatization required derivatization with *o*-phthalaldehyde, fluorescamine or NBD-Cl [19,20]. In contrast, the proposed FIA method needs no derivatization and is more sensitive than above LC methods. The proposed FIA method was therefore applied to the determination of histamine in raw fish.

Separation of histamine. Histamine in raw fish (tuna) was deproteinized with trichloroacetic acid and extracted selectively using a Sep-Pak C_{18} ENV plus cartridge with 2% (v/v) acetonitrile. Other amines, e.g., cadaverine were retained on the cartridge under these conditions. A 20-μl sample was analyzed using the proposed FIA method.

Recovery test. The recoveries of histamine (5, 50 and 500 mg per 10 g) added to fresh tuna fish samples were 94.0 ± 2.0, 95.8 ± 2.2 and 96.2 ± 1.8% (mean ± S.D., $n = 6$) (Table 3).

Determination of histamine. The FIA peaks for a tuna fish sample is shown in Fig. 5. The results of determinations over a 5-day period are shown in Fig. 6. An increase in histamine was observed up to 3 days. The amount of histamine at 3 days was about 280 mg per 10 g.

TABLE 3

Recovery test on application to the determination of histamine in tuna fish [a]

Expected histamine concentration (mg per 10 g)	Found histamine concentration (mean ± S.D.) (mg per 10 g)	Relative standard deviation (%)
5.0	4.7±0.1	3.4
50.0	47.9±1.1	2.3
500.0	481.1±9.2	1.9

[a] A 10-g tuna fish sample was spiked at the indicated concentration. Average values obtained from six runs.

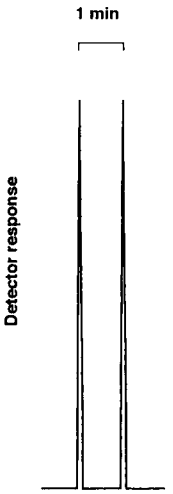

Fig. 5. Chemiluminescence peaks of histamine in a tuna fish sample after standing for 1 day, using the proposed FIA system. Hydrogen peroxide taken, 0.02 M; Sulphorhodamine 101 taken, 1.0×10^{-7} M; TDPO taken, 5.0×10^{-4} M.

Comparison with LC method using fluorescence detection after derivatization. Histamine contents in 100 samples of fish were measured by both the proposed FIA method and the LC method [20]. The correlation coefficient was 0.996 ($n = 100$) and the regression equation was $y = 1.00x - 0.25$, where y and x are concentrations in nM obtained by the FIA and LC methods, respectively. The results demonstrate that the proposed FIA method could be used to determine histamine in foods, biological samples and drugs.

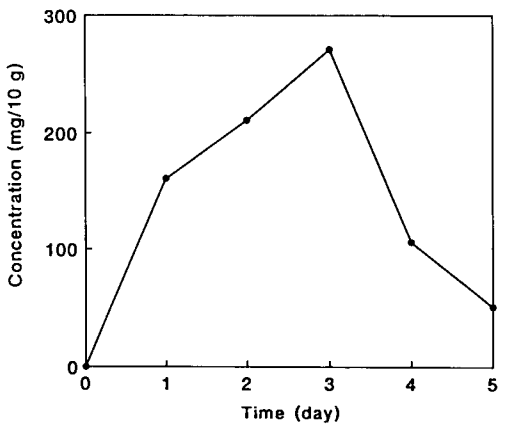

Fig. 6. Variation of the concentration of histamine in tuna fish with time.

Conclusions

The proposed method is simple and can be used to determine 1.0×10^{-10}–1.0×10^{-3} M aliphatic primary, secondary, tertiary and imidazole amines without derivatization. The method can particularly be used to determine amines that show no strong absorbance (e.g., putrescine) and tertiary amines for which derivatization reactions cannot be applied (e.g., triethylamine). The proposed FIA method is therefore superior to other FIA and LC methods with fluorimetric detection after derivatization reactions [15,16], UV detection [14] and chemiluminescence detection [4,5,23], in view of its sensitivity, the simplicity of the apparatus and the lack of a derivatization reaction. Further studies on the application of the method to the determination of biogenic amines (especially polyamines) in food samples are in progress.

REFERENCES

1 P. Van Zoonen, D.A. Kamminga, C. Gooijer, N.H. Velthorst and R.W. Frei, Anal. Chim. Acta, 167 (1985) 249.
2 G. Gübitz, P. Van Zoonen, C. Gooijer, N.H. Velthorst and R.W. Frei, Anal. Chem., 57 (1985) 2071.
3 K.W. Sigvardson and J.W. Birks, Anal. Chem., 55 (1983) 432.
4 S. Kobayashi, J. Sekino, K. Honda and K. Imai, Anal. Biochem., 112 (1981) 99.
5 K. Imai, Y. Matsunaga, Y. Tsukamoto and A. Nishitani, J. Chromatogr., 400 (1987) 169.
6 H. Arakawa, M. Maeda and A. Tsuji, Clin. Chem., 31 (1985) 430.
7 S. Takayasu, M. Maeda and A. Tsuji, J. Immunol. Methods, 83 (1985) 317.
8 P.J.M. Kwakman, J.G.J. Mol, D.A. Kamminga, R.W. Frei, U.A.Th. Brinkman and G.J. De Jong, J. Chromatogr., 459 (1988) 139.
9 K. Imai, S. Higashidate, A. Nishitani, Y. Tsukamoto, M. Ishibashi, J. Shoda and T. Osuga, Anal. Chim. Acta, 227 (1989) 21.
10 M.L. Grayeski and J.K. DeVasto, Anal. Chem., 59 (1987) 1203.
11 M. Tod, M. Prevot, J. Chalom, R. Farinotti, G. Mahuzier, J. Chromatogr., 542 (1991) 295.
12 H. Nohta, E. Yamaguchi, Y. Ohkura and H. Watanabe, J. Chromatogr., 467 (1989) 237.
13 Z. Lu, H. Veening and J.E. Coutant, J. Chromatogr., 540 (1991) 199.

14 B. Björkqvist, J. Chromatogr., 204 (1981) 109.
15 H. Umagat, P. Kucera and L.F. Wen, J. Chromatogr., 239 (1982) 463.
16 T.L. Lee, L. D'arconte and M.A. Brooks, J. Pharm. Sci., 68 (1979) 454.
17 M. Ahnoff, I. Grundevik, A. Arfwidsson, J. Fonselius and B.-A. Persson, Anal. Chem., 53 (1981) 485.
18 M. Katayama, H. Takeuchi and H. Taniguchi, Anal. Lett., 24 (1991) 1005.
19 J.L. Mietz and E. Karmas, J. Food Sci., 42 (1977) 155.
20 Pharmaceutical Society of Japan, Standards Methods of Analysis for Hygiene Chemists, Kanehara Shuppan, Tokyo, 1990, p. 287.
21 A. Townshend, Analyst, 115 (1990) 495.
22 H.S. Knight, Anal. Chem., 30 (1958) 2030.
23 B.J. Gudzinowicz and M.J. Gudzinowicz, Analysis of Drugs and Metabolites by Gas Chromatography–Mass Spectrometry, Vol. 4, Dekker, New York, Basle, 1978, p. 22.
24 Official Methods of Analysis of the Association of Official Analytical Chemists, AOAC, Arlington, VA, 15th edn., 1990, pp. 875, 876, Methods 954.04, 957.07, 977.13.

Analytica Chimica Acta, 281 (1993) 119–127
Elsevier Science Publishers B.V., Amsterdam

Determination of the composition of isomeric mixtures of allylstannanes by means of ^{119}Sn and ^{13}C NMR measurements

Tommaso Carofiglio and Daniele Marton

Dipartimento di Chimica Inorganica, Metallorganica ed Analitica, Università di Padova, Via Marzolo, I-35131 Padua (Italy)

Frauke Lenzmann

Institüt fur Anorganische Chemie und Analitische Chemie, Johannes Gutenberg Universität, D-6500 Mainz (Germany)

(Received 20th October 1992; revised manuscript received 15th February 1993)

Abstract

Allylstannanes of the type $Bu^n_3Sn(C_3H_3)$ (C_3H_3 = allenyl and propargyl) $Me_3Sn(C_4H_7)$, $Bu^n_3Sn(C_4H_7)$, $Ph_3Sn(C_4H_7)$, $Me_2Sn(C_4H_7)_2$ and $Bu^n_2Sn(C_4H_7)_2$ [C_4H_7 = (*E*)-but-2-enyl, (*Z*)-but-2-enyl, and but-1-en-3-yl] were prepared via Grignard reactions as isomeric mixtures whose compositions can be directly determined by ^{119}Sn and ^{13}C NMR spectrometry. The ^{119}Sn and ^{13}C δ-values of all possible isomers together with the isomeric compositions of freshly prepared compounds and after isomerization in dry methanol under reflux are reported. The course of isomerization of some compounds in anhydrous methanol at room temperature or in the presence of Bu_3SnCl was followed by ^{119}Sn NMR spectrometry.

Keywords: Nuclear magnetic resonance spectrometry; Allylstannanes; Organotin compounds

Allyltin compounds with the formulae $R_3Sn(C_4H_7)$ and $R_2Sn(C_4H_7)_2$ [C_4H_7 = (*E*)- and (*Z*)-but-2-enyl, $-CH_2CH{=}CHCH_3$, and but-1-en-3-yl, $-CH(CH_3)CH{=}CH_2$ (α)] are generally synthesized as mixtures containing up to three and six isomers, respectively. Further, systems of the type $R_3Sn(C_3H_3)$ contain both the allenylic and propargylic moieties.

The isomeric composition of freshly prepared mixtures is mainly dictated by the procedure and the work-up adopted for their synthesis [1–6]; once isolated and stored in a freezer (−25°C), their composition remains substantially unchanged for long periods. However, in the presence of polar donor solvents, Lewis bases [4,7–9] or Lewis acids [10–12], isomerization takes place with progressive disappearance of isomers containing the α-moiety. Analogously the propargylic tautomer gradually isomerizes to the more thermodynamically stable allenyl isomer [13].

These compounds are employed in organic synthesis in C–C bond-forming reactions with various electrophiles [14,15]. In order to evaluate the stereochemical outcome of these reactions, it is important to know the isomeric composition of these systems. Consequently, the availability of analytical methodologies that allow the rapid assay of these isomeric mixtures, is necessary.

Chromatographic procedures are inadequate because of the interaction of allylstannanes with

Correspondence to: D. Marton, Dipartimento di Chimica Inorganica, Metallorganica ed Analitica, Università di Padova, Via Marzolo, I-35131 Padua (Italy).

the stationary and mobile phases, which often leads to isomerization and destannylation processes [16]. The best way for the rapid and direct analysis of these mixture is probably by ^{119}Sn NMR spectrometry, a technique now widely used in the organotin field [17–20].

In this paper, the allylstannane systems $Bu^n_3Sn(C_3H_3)$ (**1**), $Me_3Sn(C_4H_7)$ (**2**), $Bu^n_3Sn(C_4H_7)$ (**3**), $Ph_3Sn(C_4H_7)$ (**4**), $Me_2Sn(C_4H_7)_2$ (**5**) and $Bu^n_2Sn(C_4H_7)_2$ (**6**) were analysed using ^{119}Sn and ^{13}C NMR spectrometry. The compositions of these systems were determined either when freshly prepared or after isomerization mediated by methanol or Bu^n_3SnCl.

Analytical data for changes in isomeric composition with time were obtained for systems **2**, **3** and **5** (using methanol as catalyst) and systems **1** and **3** (with Bu^n_3SnCl as catalyst).

EXPERIMENTAL

Equipment

The ^{13}C and ^{119}Sn NMR spectra (22.9 MHz for ^{13}C and 33.35 MHz for ^{119}Sn) were recorded with a Jeol FX 90Q multinuclear spectrometer operating in the Fourier transform mode. Measurements were made in 5-mm tubes. The spectra for systems **1**, **2**, **3**, **5** and **6** were recorded as pure liquids, whereas for system **4** solutions in $CDCl_3$ or *n*-hexane were used (0.2 g ml^{-1}). The ^{13}C and ^{119}Sn NMR chemical shifts (δ) are given with respect to tetramethylsilane (TMS) as internal standard and tetramethyltin (TMT) as external standard. Off-resonance (OFR) and insensitive nuclei enhanced polarization transfer (INEPT) techniques were also employed with the ^{13}C NMR spectra. In order to determine the isomeric composition of the various systems, the gated decoupling technique was used to eliminate the nuclear Overhauser effect (NOE) [21,22], and pulse delays of 30 and 3 s were used in order to avoid partial ^{13}C and ^{119}Sn nuclei saturation, respectively. A good signal-to-noise ratio was obtained after 150 scans for ^{13}C and 20 scans for ^{119}Sn.

Chemicals

All the commercially available chemicals were purified prior to use by standard procedures.

Allylstannanes **1–6** were prepared by Grignard reactions, as described previously [3,11,23,24]. A typical procedure for the system $Bu^n_3Sn(C_4H_7)$ (**3**) is as follows. Crotylmagnesium bromide was prepared by slow addition (45 min) of a solution of crotyl bromide (16.5 g, 0.122 mol) in anhydrous diethyl ether (150 ml) to magnesium turnings (14.9 g, 0.61 mol) covered by diethyl ether. Then, tributyltin chloride (20 g, 0.06 mol) dissolved in 100 ml of diethyl ether was slowly added (60 min) to the Grignard reagent separated from the excess of magnesium. After hydrolysis, the organic layer was separated and distilled to give **3** (15.6 g, 74% yield), b.p. 106–108°C/0.03 mmHg.

Procedures for isomerization

(i) The allylstannane (2 g) was added to dry methanol (3 ml) and refluxed for 30 min. The sample was analysed by NMR spectrometry after removal of the methanol under vacuum;

(ii) The allylstannane (2 g) (**2**, **3** or **4**) was allowed to isomerize in the presence of dry methanol (3 ml) at room temperature. The course of the isomerization was monitored over time by ^{119}Sn NMR spectrometry.

(iii) Compound **1** or **3** was mixed at room temperature with Bu^n_3SnCl in different molar ratios. The progress of the isomerization was monitored with time by ^{119}Sn NMR spectrometry.

RESULTS AND DISCUSSION

System $Bu^n_3Sn(C_3H_3)$ (1)

The ^{119}Sn NMR spectrum of the freshly prepared system shows two well resolved resonance lines at −8.6 and −34.2 ppm in a 25:75 ratio. Isomerization in dry methanol under reflux [procedure (i)] results in almost complete disappearance of the signal at −8.6 ppm. Since the tautomeric equilibrium

$$Bu^n_3Sn(CH_2C{\equiv}CH) \rightleftharpoons Bu^n_3Sn(CH{=}C{=}CH_2)$$

greatly favours the allenylic form [13], the signal at −8.6 ppm corresponds to the propargylic isomer. Hence, the other signal is assigned to the

allenylic isomer. The ^{119}Sn NMR chemical shifts and the isomeric compositions before and after isomerization are given in Table 1 (entries 1 and 2).

The δ^{119}Sn values were used to follow the isomerization of system **1** in the presence of Bu^n_3SnCl [procedure (iii)]. The analytical compositions as a function of time are given in Table 2.

Slow isomerization also takes place in the presence of an equimolar amount of C_2H_5CHO, and after 2 days only the allenylic isomer is present.

Systems $Me_3Sn(C_4H_7)$ (2), $Bu^n_3Sn(C_4H_7)$ (3) and $Ph_3Sn(C_4H_7)$ (4)

The ^{119}Sn NMR spectra of the freshly prepared systems **2–4** show three signals corresponding to the isomers (*E*)-, (*Z*)- and (α)-$R_3Sn(C_4H_7)$ (R = Me, *n*-Bu and Ph) As an example, the ^{119}Sn NMR spectrum of system **2** is shown in Fig. 1.

The recognition of all resonance lines of the relevant carbon atoms 1′, 1, 2, 3 and 4 of the C_4H_7 group (see Scheme 1 and Table 3 for the ^{13}C NMR chemical shifts) in the ^{13}C NMR spectra of each system indicates unambiguously the presence of solely the above three isomers. Their compositions can be determined by integration of the corresponding signals. [It should be noted that the tin σ-bonded carbon atoms of the saturated groups (methyl for system **2** and *n*-butyl for system **3**) give three separated signals, one for each isomer, in the order C(*Z*), C(*E*) and C(α) going from low to high fields. The corresponding δ values are −10.1, −10.5 and −11.5 ppm for system **2** and 9.51, 9.29 and 8.7 ppm for system **3**.]

Assignments of the ^{119}Sn NMR resonance lines related to the isomers (*E*)-, (*Z*)- and (α)-

TABLE 1

δ^{119}Sn values and isomeric compositions of the systems **1–6** freshly prepared and after isomerization in methanol under reflux [a]

Entry	System	Compound	δ^{119}Sn (ppm) [b]	Isomeric composition (%)			
				Initial		After isomerization	
				By ^{119}Sn	By ^{13}C	By ^{119}Sn	By ^{13}C
1	**1**	$Bu^n_3Sn(CH{=}C{=}CH_2)$	−34.2	25	24	98	
2		$Bu^n_3Sn(CH_2C{\equiv}CH)$	−8.6	75	76	2	
3	**2**	(*E*)-$Me_3Sn(C_4H_7)$	−4.3	35	35	46	46
4		(*Z*)-$Me_3Sn(C_4H_7)$	−1.6	43	42	54	54
5		(α)-$Me_3Sn(C_4H_7)$	+4.0	22	23	–	–
6	**3**	(*E*)-$Bu^n_3Sn(C_4H_7)$	−17.8	35	35	39	40
7		(*Z*)-$Bu^n_3Sn(C_4H_7)$	−13.9	38	39	61	60
8		(α)-$Bu^n_3Sn(C_4H_7)$	−17.5	27	26	–	–
9	**4**	(*E*)-$Ph_3Sn(C_4H_7)$	−119.2 [c]	36	35	42	40
10		(*Z*)-$Ph_3Sn(C_4H_7)$	−122.2 [c]	30	28	58	60
11		(α)-$Ph_3Sn(C_4H_7)$	−117.9 [c]	34	37	–	–
12	**5**	(*E*,*E*)-$Me_2Sn(C_4H_7)_2$	−12.6	6	6	15	16
13		(*E*,*Z*)-$Me_2Sn(C_4H_7)_2$	−9.6	13	14	47	45
14		(*Z*,*Z*)-$Me_2Sn(C_4H_7)_2$	−6.8	8	7	38	39
15		(*E*,α)-$Me_2Sn(C_4H_7)_2$	−7.2	23	24	–	–
16		(*Z*,α)-$Me_2Sn(C_4H_7)_2$	−4.3	19	19	–	–
17		(α,α)-$Me_2Sn(C_4H_7)_2$	−3.6	31	30	–	–
18	**6**	(*E*,*E*)-$Bu^n_2Sn(C_4H_7)_2$	−25.6	11	11	18	20
19		(*E*,*Z*)-$Bu^n_2Sn(C_4H_7)_2$	−21.6	38	40	51	49
20		(*Z*,*Z*)-$Bu^n_2Sn(C_4H_7)_2$	−17.8	25	23	31	31
21		(*E*,α)-$Bu^n_2Sn(C_4H_7)_2$	−26.4	9	8	–	–
22		(*Z*,α)-$Bu^n_2Sn(C_4H_7)_2$	−22.0	– [d]	5	–	–
23		(α,α)-$Bu^n_2Sn(C_4H_7)_2$	−22.0	– [d]	12	–	–

[a] Isomerization by procedure (i). [b] Chemical shifts of pure liquid from external TMT standard. [c] NMR measurements in *n*-hexane solution. [d] Undetermined compositions.

TABLE 2

Isomeric composition of the system $Bu^n_3Sn(C_3H_3)$ [a] during isomerization [b] at 25°C mediated by Bu^n_3SnCl [c]

Entry	Time	Isomeric composition by ^{119}Sn NMR (%)	
		Bu^n_3Sn-($CH{=}C{=}CH_2$)	Bu^n_3Sn-($CH_2C{\equiv}CH$)
1	0	25	75
2	5 min	30	70
3	15 min	33	67
4	40 min	34	66
5	26 h	34	66
6	47 h	57	43
7	52 h	60	40
8	71 h	75	25
9	141 h	96	4

[a] C_3H_3 represents allenylic ($-CH{=}C{=}CH_2$) and propargylic ($-CH_2C{\equiv}CH$), groups. [b] See Experimental, isomerization procedure (ii). [c] Molar ratio $[Bu^n_3Sn(C_3H_3)]/[Bu^n_3SnCl] = 0.012$ [0.5 g (1.52 mmol) of $Bu^n_3Sn(CH_3)$ and 0.0058 g (0.018 mmol) of Bu^n_3SnCl].

$R_3Sn(C_4H_7)$ are possible by comparison with the ^{13}C NMR spectra. However, an additional check of these assignments comes from the isomerization of the three components systems by means of procedure (i), which leads to the total disappearance of the (α)-$R_3Sn(C_4H_7)$ isomers. Hence the ^{119}Sn NMR resonance lines of the (α)-$R_3Sn(C_4H_7)$ isomers are further confirmed, together with the other two, because isomerization give rise to mixtures where the (Z)-$R_3Sn(C_4H_7)$ isomer is always the major component [4–7,9].

The ^{119}Sn NMR chemical shifts, together with the isomeric compositions of the systems when freshly prepared and after isomerization determined by ^{119}Sn and ^{13}C NMR measurements, are reported in Table 1 (entries 3–11).

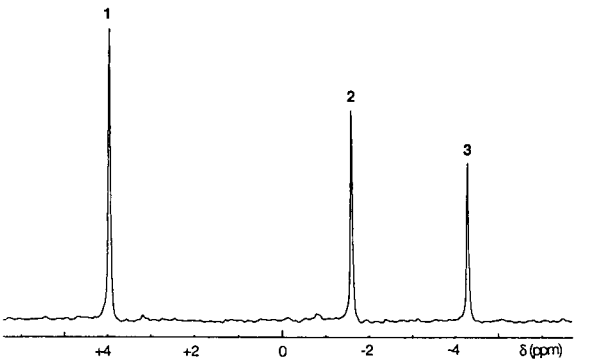

Fig. 1. ^{119}Sn NMR spectrum of the system $Me_3Sn(C_4H_7)$. The signals 1, 2 and 3 correspond to the (α)-, (Z)- and (E)-$Me_3Sn(C_4H_7)$ isomers, respectively.

Measurements at different times revealed that these systems do not change their composition when stored at −5°C [$Me_3Sn(C_4H_7)$, with an initial $E:Z:\alpha$ ratio of 32:43:25, when stored at −5°C shows a ratio of 35:43:22 after 16 days and 34:43:23 after 30 days. $Bu^n_3Sn(C_4H_7)$, with an initial $E:Z:\alpha$ ratio of 35:38:27, when stored at −5°C shows a ratio of 36:39:25 after 34 days]. In contrast, isomerizations take place when these systems are allowed to stand in donor solvents [7,8] or in the presence of Lewis acids [10], leading to mixtures solely of the E- and Z-isomers.

The analysis of systems **2–4** during the isomerization processes can be quickly achieved by means of ^{119}Sn NMR measurements. The compositions of all these systems after isomerization by procedure (i) are given in Table 1 (entries 3–11). The compositions checked during the isomerization processes either by procedure (ii) (systems **2** and **3**) or by procedure (iii) {system **3**; molar ratio $[Bu^n_3Sn(C_4H_7)]:[Bu^n_3Sn(C_4H_7)] = 1:1$} are given in Table 4.

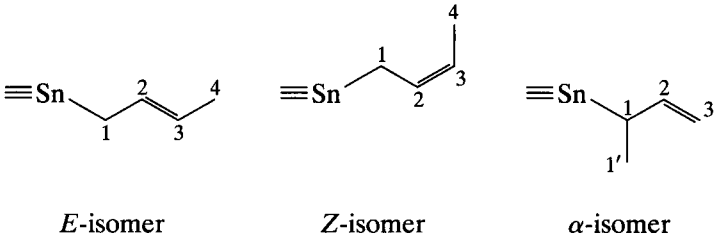

E-isomer *Z*-isomer α-isomer

Scheme 1. Framework of the relevant C_4H_7 carbon atoms.

TABLE 3

$\delta^{13}C$ values of the C_4H_7 [a] group of systems **2**, **3** and **4**

Entry	System	Compound	Carbon atom of the C_4H_7 group [b,c]				
			1	1′	2	3	4
1	**2**	(*E*)-$Me_3Sn(C_4H_7)$	16.0		129.2	120.3	17.8
2		(*Z*)-$Me_3Sn(C_4H_7)$	11.9		128.3	118.4	12.4
3		(*α*)-$Me_3Sn(C_4H_7)$	25.5	15.3	143.1	106.7	
4	**3**	(*E*)-$Bu^n_3Sn(C_4H_7)$	14.3		130.0	120.1	17.9
5		(*Z*)-$Bu^n_3Sn(C_4H_7)$	10.2		129.0	117.8	12.5
6		(*α*)-$Bu^n_3Sn(C_4H_7)$	25.7	15.9	143.7	106.4	
7	**4**	(*E*)-$Ph_3Sn(C_4H_7)$	16.0		127.8	123.1	17.7
8		(*Z*)-$Ph_3Sn(C_4H_7)$	12.0		126.9	121.0	12.6
9		(*α*)-$Ph_3Sn(C_4H_7)$	27.9	16.1	142.5	109.1	

[a] C_4H_7 represents (*E*)- and (*Z*)-but-2-enyl ($-CH_2CH{=}CHCH_3$) and but-1-en-3-yl [$-CH(CH_3)CH{=}CH_2$) (*α*)] groups. [b] Chemical shifts (ppm) from TMS as internal standard. [c] NMR measurements performed with pure liquid for systems **1** and **2** and in $CDCl_3$ solution for system **4**.

Tables 1 and 4 show some interesting points. There is good agreement between the results determined by ^{119}Sn and ^{13}C NMR measurements (see Table 1, compare columns 5 and 6, and columns 7 and 8). The isomerizations provide by means of the metallotropic equilibrium $E \leftrightharpoons \alpha$

TABLE 4

Isomeric compositions determined by means of ^{119}Sn NMR during isomerization of the systems $Me_3Sn(C_4H_7)$ [a] and $Bu^n_3Sn(C_4H_7)$ [a] at 25°C by procedures (ii) and (iii)

Entry	Time	System								
		$Me_3Sn(C_4H_7)$, isomerization procedure (ii) [b]			$Bu^n_3Sn(C_4H_7)$, isomerization procedure					
					(ii) [b,c]			(iii) [d]		
		E(%)	*Z*(%)	*α*(%)	*E*(%)	*Z*(%)	*α*(%)	*E*(%)	*Z*(%)	*α*(%)
1	0	35	43	22	35	37	28	36	39	25
2	2 min	36	51	14						
3	9 min							36	43	21
4	12 min	38	54	8						
5	30 min	48	56	2						
6	45 min	42	58	–						
7	203 min							34	50	16
8	386 min				36	48	16			
9	422 min	41	59	–						
10	470 min							35	57	8
11	1 d				36	56	8	38	62	–
12	3 d	52	48	–						
13	10 d	52	48	–	51	49	–			
14	16 d							39	61	–
15	17 d	55	45	–						
16	27 d							43	57	–

[a] C_4H_7 represents (*E*)- and (*Z*)-but-2-enyl ($-CH_2CH{=}CHCH_3$) and but-1-en-3-ylmethylallyl [$-CH(CH_3)CH{=}CH_2$ (*α*)] groups. [b] 2 g of stannane and 3 ml of anhydrous methanol. [c] Heterogeneous system. [d] 0.5 g (1.44 mmol) of $Bu^n_3Sn(C_4H_7)$ mixed with an equimolar amount of Bu^n_3SnCl (0.47 g, 1.44 mmol).

$\rightleftharpoons Z$ solely mixtures of the E- and Z-isomers. Under the experimental conditions of isomerization by procedure (i), all systems produce E/Z mixtures, in which the the less thermodynamically stable Z isomer predominates ($Z = 54\%$, 61% and 58% for systems **2**, **3** and **4**, respectively; see Table 1, entries 4, 7 and 10) [4,7,8,25]. System **2** isomerizes within 45 min in the presence of methanol at room temperature to give the kinetic mixture $E:Z = 42:58$ (see Table 4, entry 6), similar to that obtained by procedure (i). With a much longer time a slow $Z \rightarrow E$ isomeric interconversion also takes place. After 17 days a mixture having an excess of the thermodynamically more stable E-isomer ($E:Z = 55:45$; see Table 4, entry 15) is obtained. The start of the $Z \rightarrow E$ interconversion is only reached after 10 days with the heterogeneous system $Bu^n_3Sn(C_4H_7)$–MeOH [procedure (ii)] ($E:Z = 51:49$, see Table 4, entry 13); even after 27 days no isomerization of $Bu^n_3Sn(C_4H_7)$ results in the presence of equimolecular Bu^n_3SnCl (see Table 4, entry 16).

Systems $Me_2Sn(C_4H_7)_2$ (5) and $Bu^n_2Sn(C_4H_7)_2$ (6)

The ^{119}Sn NMR spectrum of the freshly prepared system **5** shows six separated signals, which are related to the isomers (E,E)-, (E,Z)-, (Z,Z)-, (E,α)-, (Z,α)- and (α,α)-$Me_2Sn(C_4H_7)_2$. Only five signals are observed in the ^{119}Sn NMR spectrum of **6**. Nevertheless, contemporaneous ^{13}C NMR measurements show the presence of all six isomers in both systems. In particular, six highly diagnostic separated signals are observed in the region of the tin σ-bonded carbon atoms of the saturated organic groups (methyl for system **5** and n-butyl groups for system **6**). By comparing the ^{13}C NMR spectra registered before and after isomerization by means of procedure (i), it has been possible to identify in this region three signals relating to the isomers (Z,Z)-, (E,Z)- and (E,E)-$R_2Sn(C_4H_7)_2$ (e.g., −10.8, −11.2 and −11.5 ppm for system **5** and 10.0, 9.8 and 9.6 ppm for system **6**), in addition to those relating to the other three isomers (Z,α)-, (E,α)- and (α,α)-$R_2Sn(C_4H_7)_2$ (e.g., −12.1, −12.5 and −13.5 ppm for system **5**, and 9.3, 9.2 and 9.0 ppm for system **6**).

The above-assigned orders $\delta_{C-Sn}(Z,Z) > \delta_{C-Sn}(E,Z) > \delta_{C-Sn}(E,E)$ and $\delta_{C-Sn}(Z,\alpha) > \delta_{C-Sn}(E,\alpha) > \delta_{C-Sn}(\alpha,\alpha)$ are based on the arguments in the previous sub-section. In the former sequence, the $\delta_{C-Sn}(E,Z)$ values are between the other two and can be calculated for both systems as an arithmetic average, $\delta_{C-Sn}(E,Z) = [\delta_{C-Sn}(Z,Z) + \delta_{C-Sn}(E,E)]/2$. The calculated values, −11.5 and 9.8 ppm for systems **5** and **6**, respectively, are in very good agreement with those observed. Likewise, in the later series, the $\delta_{C-Sn}(Z,\alpha)$ and $\delta_{C-Sn}(E,\alpha)$ values are between the $\delta_{C-Sn}(Z,Z)$ and $\delta_{C-Sn}(\alpha,\alpha)$ values and $\delta_{C-Sn}(E,E)$ and $\delta_{C-Sn}(\alpha,\alpha)$ values, respectively, and they can be calculated as an arithmetic average, $\delta_{C-Sn}(Z,\alpha) = [\delta_{C-Sn}(Z,Z) + \delta_{C-Sn}(\alpha,\alpha)]/2$ and $\delta_{C-Sn}(E,\alpha) = [\delta_{C-Sn}(E,E) + \delta_{C-Sn}(\alpha,\alpha)]/2$, respectively. The calculated $\delta_{C-Sn}(Z,\alpha)$ and $\delta_{C-Sn}(E,\alpha)$ values (e.g., −12.15 and −12.5 ppm, respectively, for system **5** and 9.45 and 9.3 ppm, respectively, for system **6**) are in good agreement

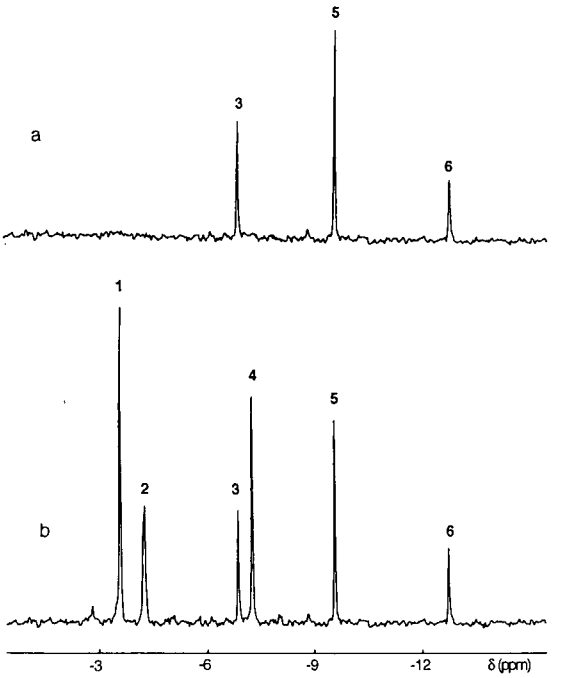

Fig. 2. ^{119}Sn NMR spectra of the system $Me_2Sn(C_4H_7)_2$: (a) after isomerization by procedure (i); (b) when freshly prepared. The signals 1, 2, 3, 4, 5 and 6 correspond to the (α,α)-, (Z,α)-, (Z,Z)-, (E,α)-, (E,Z)- and (E,E)-$Me_2Sn(C_4H_7)_2$ isomers, respectively.

TABLE 5

$\delta^{13}C$ values of the C_4H_7 [a] group of systems **5** and **6**

Entry	System	Compound	Isomeric form	Carbon atom of the C_4H_7 group [b]				
				1	1′	2	3	4
1	**5**	(E,E)-$Me_2Sn(C_4H_7)_2$	E	15.5		129.1	120.7	17.9
2		(E,Z)-$Me_2Sn(C_4H_7)_2$	E	15.7		129.2	120.6	17.9
			Z	11.4		128.3	118.6	12.5
3		(Z,Z)-$Me_2Sn(C_4H_7)_2$	Z	11.8		128.2	118.9	12.5
4		(E,α)-$Me_2Sn(C_4H_7)_2$	E	14.9		124.1	120.8	17.9
			α	26.1	15.7	143.1	106.9	
5		(Z,α)-$Me_2Sn(C_4H_7)_2$	Z	10.8		128.2	118.8	12.5
			α	26.1	15.7	143.1	107.0	
6		(α,α)-$Me_2Sn(C_4H_7)_2$	α	25.9	15.6	143.1	107.2	
7	**6**	(E,E)-$Bu^n_2Sn(C_4H_7)_2$	E	14.5		129.7	120.4	17.9
8		(E,Z)-$Bu^n_2Sn(C_4H_7)_2$	E	14.8		129.7	120.5	17.9
			Z	10.4		128.7	118.2	12.5
9		(Z,Z)-$Bu^n_2Sn(C_4H_7)_2$	Z	10.7		128.9	118.4	12.6
10		(E,α)-$Bu^n_2Sn(C_4H_7)_2$	E	14.0		129.7	120.6	17.9
			α	26.3	15.3	143.5	106.7	
11		(Z,α)-$Bu^n_2Sn(C_4H_7)_2$	Z	10.0		128.7	118.3	12.6
			α	26.3	15.3	143.5	106.8	
12		(α,α)-$Bu^n_2Sn(C_4H_7)_2$	α	26.1	16.1	143.5	107.0	

[a] C_4H_7 represents (E)- and (Z)-but-1-enyl ($-CH_2CH{=}CHCH_3$) and but-1-en-3-yl [$-CH(CH_3)CH{=}CH_2$ (α)] group. [b] Chemical shifts (ppm) from internal TMS standard.

with those observed. These assignments were confirmed by examination of the other carbon regions of the ^{13}C NMR spectra and are the basis for the assignments of the ^{119}Sn NMR resonance lines of all isomers in both systems examined. The ^{119}Sn NMR spectra of both systems regis-

TABLE 6

Isomeric compositions of the system $Me_2Sn(C_4H_7)_2$ [a] during the isomerization process in the presence of methanol at 25°C [b]

Entry	Time	Isomeric composition by ^{119}Sn NMR (%)					
		(E,E)	(E,Z)	(Z,Z)	(E,α)	(Z,α)	(α,α)
1	0	6	13	8	23	19	31
2	2 min	6	15	9	21	19	30
3	7 min	7	25	15	15	14	24
4	13 min	10	41	35	–	4	10
5	22 min	9	44	43	–	–	4
6	29 min	12	46	41	–	–	2
7	360 min	12	46	42	–	–	–
8	1 d	16	46	38	–	–	–
9	5 d	21	50	29	–	–	–
10	10 d	26	52	22	–	–	–
11	18 d	29	51	20	–	–	–
12	25 d	31	51	18	–	–	–
13	33 d	31	51	18	–	–	–

[a] C_4H_7 represents (E)- and (Z)-but-2-enyl ($-CH_2CH{=}CHCH_3$) and but-1-en-3-yl [$-CH(CH_3)CH{=}CH_2$ (α)] groups. [b] Isomerization by procedure (ii).

tered after isomerization show three signals relating to the sole isomers (*E*,*E*)-, (*E*,*Z*)- and (*Z*,*Z*)-$R_2Sn(C_4H_7)_2$, as is also clear from ^{13}C NMR measurements. Figure 2a and b shows the ^{119}Sn NMR spectra for system **5** after and before isomerization, respectively.

The ^{119}Sn NMR chemical shifts of the six isomers of each system are reported in Table 1 together with the isomeric compositions of the system before and after isomerization (entries 12–23). The ^{13}C NMR chemical shifts of the carbon atoms of the C_4H_7 moiety (see Scheme 1) for all isomers are given in Table 5.

In Table 6 are listed the changes in the isomeric composition of **5** with time at room temperature in the presence of methanol [procedure (ii)].

The composition of both the complex systems (**5** and **6**) were completely determined by ^{13}C and ^{119}Sn NMR (see Table 1, entries 12–23). It was only possible to determine the relative amounts of the isomers (*Z*,*α*)-$Bu^n_2Sn(C_4H_7)_2$ and (*α*,*α*)-$Bu^n_2Sn(C_4H_7)_2$ by ^{13}C NMR spectrometry, as both compounds have the same $\delta^{119}Sn$ value of −22.0 ppm (Table 1, entries 22 and 23).

The following observations can be made. In the series (*E*,*E*)-, (*E*,*Z*)- and (*Z*,*Z*)-$R_2Sn(C_4H_7)_2$, the $\delta^{119}Sn$ value of the species (*E*,*Z*)-$R_2Sn(C_4H_7)_2$ is exactly to the arithmetic average of those values of the isomers (*E*,*E*)- and (*Z*,*Z*)-$R_2Sn(C_4H_7)_2$ (see Table 1, entries 12–14 for R = Me, and entries 18–20 for R = Bu^n) The substitution of a *Z*-group with an *E*-group in (*Z*,*Z*)-R_2Sn produces a shift to higher field of −2.8 ppm when R = Me and −3.8 ppm when R = Bu^n. These same $\Delta\delta$ values are found for the system $Me_3Sn(C_4H_7)$ and $Bu^n_3Sn(C_4H_7)$ (see Table 1, entries 3 and 4 when R = Me; entries 6 and 7 when R = Bu^n). The isomerization of the system $Me_2Sn(C_4H_7)_2$ by procedure (i) produces the isomeric mixture (*E*,*E*):(*E*,*Z*):(*Z*,*Z*) = 15:47:38 (see Table 1, entries 12–14). The same isomeric ratio is achieved after 1 day [(*E*,*E*):(*E*,*Z*):(*Z*,*Z*) = 16:46:38; see Table 6, entry 8]. It should be noted that, via procedure (ii), the point of the $Z \rightarrow E$ isomeric interconversion is only reached after 10–18 days (see Table 6, entries 10 and 11). The final isomeric mixture shows an (*E*,*E*):(*E*,*Z*):(*Z*,*Z*) ratio of 31:51:18, which is achieved after a very long time (25–33 days; see Table 6, entries 12 and 13). The formal calculated *E*:*Z* ratio of about 56:44 is the same as the final ratio reached by the system $Me_3Sn(C_4H_7)$ after a long time (*E*:*Z* = 55:45; see Table 4, entry 15). Probably this ratio defines the thermodynamic composition of these systems.

Conclusion

The use of ^{119}Sn NMR spectrometry in the analysis of allylstannanes is very important because it permits rapid and direct determinations of the analytical compositions. As only a few scans and very short times are required, this technique can be successfully employed to analyse complex isomeric systems when slow isomerization processes take place. Studies are in progress in order to verify the applicability of this approach to more complex systems such as $R_{4-n}Sn(C_4H_7)_n$ (*n* = 3 and 4).

The authors are grateful for financial support from the Ministero della Pubblica Istruzione (Rome) and CNR (Rome) under the "Progetto finalizzato per la Chimica Fine". They thank Professor Giuseppe Tagliavini, University of Padua, and Dr. James L. Wardell, University of Aberdeen, for critical reading of the manuscript. One the authors (F.L.) is grateful to the Erasmus Exchange Programme, under the Aberdeen Chemistry Erasmus Network, for financing her stay in Padua.

REFERENCES

1 C. Prevost, M. Gaudemar and J. Honigberg, C.R. Acad. Sci., 230 (1950) 1186.
2 A. Boaretto, D. Marton and G. Tagliavini, J. Organomet. Chem., 297 (1985) 149.
3 E. Matarasso-Tchiroukine and P. Cadiot, C.R. Acad. Sci., Ser. C, 274 (1972) 2118.
4 E. Matarasso-Tchiroukine and P. Cadiot, J. Organomet. Chem., 121 (1976) 155.
5 P. Ganis, D. Marton, V. Peruzzo, and G. Tagliavini, J. Organomet. Chem., 231 (1982) 307.
6 V. Peruzzo, G. Tagliavini and A. Gambaro, Inorg. Chim. Acta, 34 (1979) L263.
7 E. Matarasso-Tchiroukine and P. Cadiot, C.R. Acad. Sci., Ser. C, 2 (1972) 218.

8 J.A. Verdone, J.A. Mangravite, N.M. Scarpa and H.G. Kuivila, J. Am. Chem. Soc., 97 (1975) 843.
9 P.A. Barlett, Tetrahedron, 36 (1980) 3.
10 G.E. Keck, D.E. Abbot, E.P. Boden and E.J. Enholm, Tetrahedron Lett., 25 (1984) 3927.
11 A. Gambaro, D. Marton and G. Tagliavini, J. Organomet. Chem., 210 (1981) 57.
12 A. Boaretto, D. Marton, G. Tagliavini and P. Ganis, J. Organomet. Chem., 321 (1987) 199.
13 G. Guillerm, F. Meganem and M. Lequar, J. Organomet. Chem., 67 (1976) 43.
14 G. Tagliavini, Rev. Si Ge Sn Pb Compd., 8 (1985) 237, and references cited therein.
15 M. Pereyre, J.P. Quintard and A. Rahm, Tin in Organic Synthesis, Butterworths, London, 1977, p. 185.
16 J.R. Behling, J.S. Ng, K.A. Babak, A.L. Campbell, E.E. Sworth and B.H. Lipshutz, Tetrahedron Lett., 60 (1989) 27.
17 R.K. Harris, J.D. Kennedy and W. McFarlane, NMR and the Periodic Table, Academic, London, 1978, p. 342, and references cited therein.
18 E. Matarasso-Tchiroukhine, Can. J. Chem., 62 (1984) 133.
19 J. Otera and T. Yano, Bull. Chem. Soc. Jpn., 58 (1985) 387.
20 M. Pereyre, J.P. Quintard and A. Rahm, Pure Appl. Chem., 54 (1982) 29.
21 C.H. Sotak, C.L. Dumoulln and G.C. Levy, Anal. Chem., 55 (1983) 783.
22 R. Freeman, M.D.W. Hill and R. Kaptein, J. Magn. Reson., 7 (1972) 327.
23 E. Matarasso-Tchirouchine and M.P. Cadiot, Can. J. Chem., 61 (1983) 2476.
24 D. Marton and G. Tagliavini, unpublished results.
25 S. Bank, A. Schriesheim and C.A. Rowe, J. Am. Chem. Soc., 87 (1965) 3244.

Analytica Chimica Acta, 281 (1993) 129–134
Elsevier Science Publishers B.V., Amsterdam

Development of magnesium-selective ionophores

James O'Donnell, Hongbin Li [1], Bruno Rusterholz, Urs Pedrazza and Wilhelm Simon [2]

Department of Organic Chemistry, Swiss Federal Institute of Technology (ETH), Universitätstrasse 16, CH-8092 Zürich (Switzerland)

(Received 5th February 1993)

Abstract

The syntheses of new magnesium-selective ionophores together with selectivity and ^{13}C NMR measurements are presented. Ion-selective electrodes based on the ionophore 1,3,5-tris[10-(1-adamantyl)-7,9-dioxo-6,10-diazaundecyl]-benzene (ETH 5506) showed excellent magnesium selectivity over calcium and potassium. Selectivity coefficients log $K^{Pot}_{MgCa} = -1.9$ and log $K^{Pot}_{MgK} = -3.7$ are observed. The conformational influence of different amide substituents was examined using ^{13}C NMR spectrometry. Two different series of isologue ionophores were studied. In both instances the addition of bulky substituents increased the ionophore selectivity of magnesium.

Keywords: Ion selective electrodes; Ionophores, Magnesium

In recent years, several new ionophores have been discovered that have shown good magnesium selectivities [1–4]. For example, ETH 7025 has been used to good effect in both intra- and extracellular measurements of magnesium activity [4,5]. A search for new ionophores with even better magnesium selectivity has been in progress and the results are presented in this paper.

EXPERIMENTAL

Reagents

The synthesis of ionophore ETH 7025 has already been published [6] and those of ionophores ETH 7160, ETH 3832 and ETH 5506 are presented below (see Fig. 1 for the structures of all the ionophores). The synthesis of the highly lipophilic plasticiser ETH 5373 (see Fig. 2) will be published elsewhere [7]. For all e.m.f. experiments, the aqueous solutions used were prepared with doubly quartz-distilled water and metal chlorides salts of puriss. or p.a. grade (Fluka).

Membrane preparation

The preparation of the membranes has already been fully described [8]. The membranes were composed of 1 wt.% ionophore, 33 wt.% poly(vinyl chloride) (PVC) (high molecular weight; Fluka Selectophore) and 65–66 wt.% plastisicer [either *o*-NPOE (2-nitrophenyl octyl ether, Fluka Selectophore) or ETH 5373]. As the lipophilic anionic site, potassium tetrakis(*p*-chlorophenyl)borate (KTpClPB) (Fluka Selectophore) was added in molar ratios of either 0.40, 0.77 or 1.55 relative to the ionophore.

E.m.f. and selectivity measurements

The membranes were fitted into Philips (Eindhoven, Netherlands) IS-561 electrode bodies. A solution of 0.1 M $MgCl_2$ was used as the inner electrolyte. E.m.f. measurements were carried out at 21 ± 1°C with a free-flowing, free-diffusion liquid-junction calomel reference electrode [9]. The different half-cells are

$$Hg\,|\,Hg_2Cl_2\,|\,KCl(satd.)\,\vdots\,3\ M\ KCl\,\vdots\,sample\ |membrane\,|\,0.1\ M\ MgCl_2\,|\,AgCl\,|\,Ag$$

Correspondence to: J. O'Donnell, Department of Organic Chemistry, Swiss Federal Institute of Technology (ETH), Universitätstrasse 16, CH-8092 Zürich (Switzerland).

[1] On leave from Shanghai University of Technology, 149 Yanchang Road, 200072 Shanghai (China).

[2] Author deceased.

$MgCl_2$ solutions (1×10^{-6}–0.1 M) were used to calibrate the e.m.f. response of the electrode to variations in magnesium activity. The selectivity coefficients were obtained using the separate solution method [10] in 0.1 M metal chloride solutions. Correction of all experimental e.m.f. data by the Henderson formalism [11] allowed for changes in the liquid-junction potential. The necessary activity coefficients have already been published [12]. Details of the e.m.f. measuring equipment can be found elsewhere [13]. The electrodes were conditioned for 50 h in 0.1 M $MgCl_2$.

Lipophilicity measurements

The lipophilicity of each ionophore was determined using thin-layer chromatography on reversed-phase silica plates with an ethanol–water (7 + 3) solvent mixture as described fully elsewhere [14].

NMR experiments

All experiments were conducted at room temperature. Solutions of the pure ionophores were prepared (ETH 7025, 18.2 mg, c = 35 mmol; ETH 7160, 13.5 mg, c = 23 mmol; ETH 3832, 32.7 mg, c = 59 mmol; ETH 5506, 16.6 mg, c = 27 mmol) in $CDCl_3$ (0.6 ml). ^{13}C NMR experiments were performed on a Varian XL300 spectrometer operating at a frequency of 75 MHz. The carbonyl regions of the different ionophores are given in Fig. 3. The carbonyl signals of ETH 7025 (31 mg, c = 60 mmol in 0.6 ml of $CDCl_3$) were assigned using a long-range ^1H–^{13}C connectivity experiment, heteronuclear multiple-bond connectivity (HMBC) [15]. HMBC: (absolute value of spectra); 512 FIDs of 2K data points in ω_2, 160 scans were acquired for each FID; transformed with a sine-squared filter shifted by $\pi/3$ in ω_2 and $\pi/4$ in ω_1 to give a 1K × 0.5K real × real data matrix; performed on a Bruker AMX400 spectrometer using an inverse probe head.

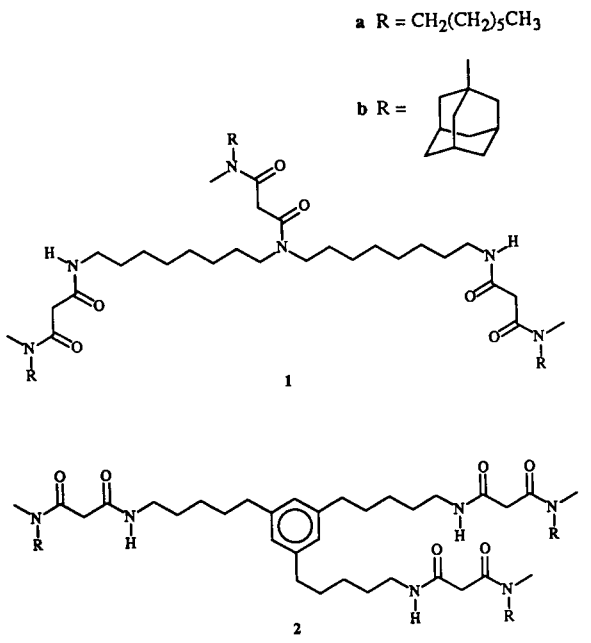

Fig. 1. Structures of the ionophores ETH 7025 (**1a**), ETH 7160 (**1b**), ETH 3832 (**2a**) and ETH 5506 (**2b**).

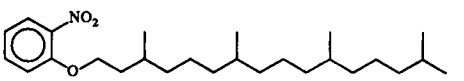

Fig. 2. Structure of the plasticizer ETH 5373.

Synthesis of N-(1-adamantyl)-N',N'-bis(8-{[3-[(1-adamantyl)methylamino]-1,3-dioxopropyl]amino}octyl)-N-methylpropanediamide (ETH 7160)

This ionophore was prepared by the same procedure as for ETH 7025 [6] using malonic acid mono(4-nitrophenyl) ester mono-*N*-(1-adamantyl)-*N*-methylamide (see ETH 5506) instead of malonic acid mono(4-nitrophenyl) ester mono-*N*-heptyl-*N*-methylamide. Analysis: calculated for $C_{58}H_{94}N_6O_6$ (971.42), C 71.71, H 9.75, N 8.65; Found, C 71.59, H 9.47, N 8.36%.

Synthesis of 1,3,5-tris(10-methyl-7,9-dioxo-6,10-diazaheptadecyl)benzene (ETH 3832)

1,3,5-Tris(5-methoxypentyl)benzene. 1-Bromo-5-methoxypentane (39.15 g, 216 mmol), prepared according to [16], was dissolved in diethyl ether (130 ml; Fluka, puriss. p.a.) and added dropwise at 0°C under argon to magnesium grit (5.22 g, 30–55 mesh; Fluka, purum) which was already suspended in diethyl ether (20 ml). The addition was made at such a rate that the solvent was gently boiling. After additional refluxing for 2 h, the reaction mixture was cooled to 0°C and a solution of 1,3,5-trichlorobenzene (13.1 g, 72

mmol; Fluka, purum) in diethyl ether (100 ml) and [1,3-bis(diphenylphosphino)ethane]nickel(II) chloride ($NiCl_2$[dppe]) (0.2 g, Aldrich) were added. The reaction mixture was stirred for 4 h at 0°C. Another portion of $NiCl_2$[dppe] (0.2 g) was then added. The reaction mixture was stirred for 20 h at 0°C and subsequently for 2 days at room temperature. After hydrolysis, by slow addition of dilute HCl–ice, the diethyl ether layer was separated and the solvent evaporated. Unreacted starting materials were removed by high-vacuum distillation and the residue was purified by flash chromatography [silica gel, dichloromethane–hexane–ethyl acetate (6 + 3 + 1)] to give the pure product (12.07 g, 44 mmol, 44.2%).

1,3,5-Tris(5-iodopentyl)benzene. At room temperature, trimethylchlorosilane (37.9 g, 350 mmol; Fluka, puriss.) was added dropwise under argon to 1,3,5-tris(5-methoxypentyl)benzene (22.0 g, 58 mmol) and sodium iodide (52.0 g, 350 mmol; Fluka, puriss. p.a.) which had both been dissolved in CH_3CN (120 ml; Fluka, puriss. p.a.) [17]. After stirring at room temperature for 2 h and refluxing for 4 h, the reaction mixture was quenched with water and dissolved in diethyl ether. The ether layer was then washed with sodium thiosulphate

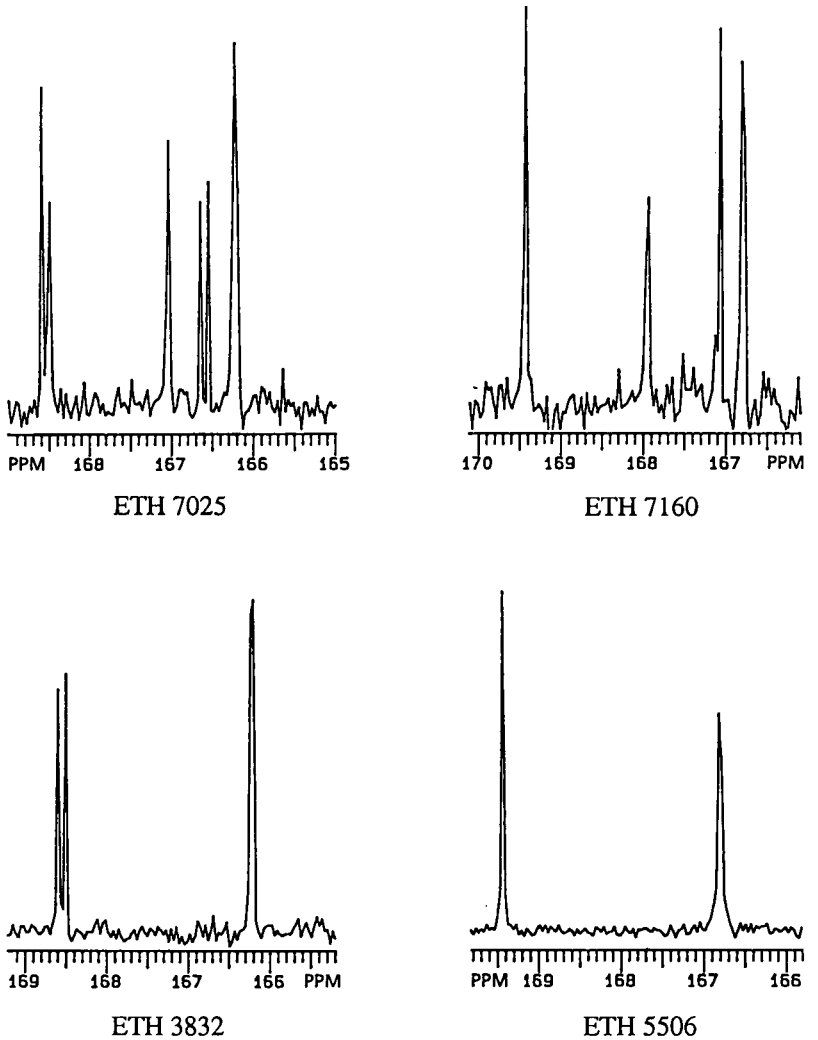

Fig. 3. ^{13}C NMR spectra of the ionophores ETH 7025, ETH 7160, ETH 3832 and ETH 5506.

solution (10%) and brine and dried over $MgSO_4$. Evaporation of the solvent gave 1,3,5-tris(5-hydroxypentyl)benzene. Repeating the same procedure, the 1,3,5-tris(5-hydroxypentyl)benzene was converted into 1,3,5-tris(5-iodopentyl)benzene [17]. The crude product was purified by flash chromatography [silica gel, dichloromethane–hexane (1 + 1)] to give the pure product (36.67 g, 55 mmol, 94.7%).

1,3,5-Tris(5-phthalimidopentyl)benzene. A solution of 1,3,5-tris(5-iodopentyl)benzene (36.0 g, 54 mmol) and potassium phthalimide (60.1 g, 325 mmol; Fluka, purum) in *N,N*-dimethylformamide (150 ml; Fluka, puriss. p.a.) was stirred at room temperature overnight, refluxed for 10 h and again stirred at room temperature overnight. The reaction mixture was then poured into water and extracted with CH_2Cl_2. The organic phase was washed with 0.2 M NaOH and water and dried over $MgSO_4$. The solvent was evaporated and the residue purified by flash chromatography [silica gel, dichloromethane–acetone (9 + 1)] to give the pure product (23.29 g, 32 mmol, 59.5%).

1,3,5-Tris(5-aminopentyl)benzene. A solution of 1,3,5-tris(5-phthalimidopentyl)benzene (23.29 g, 32 mmol) and hydrazine hydrate (14.51 g, 290 mmol; Fluka, puriss. p.a.) in ethanol (600 ml; Fluka, puriss. p.a.) was refluxed for 10 h and stirred at room temperature overnight. After adding water (500 ml), the ethanol was evaporated. The residue was acidified by adding concentrated HCl (10 ml). This solution was refluxed for 24 h and then cooled to 0°C. The precipitate was filtered off and the residue was adjusted to pH 11 by adding 5 M NaOH. This solution was extracted several times with diethyl ether. The organic phase was dried over $MgSO_4$ and the solvent evaporated to give the product (7.31 g, 22 mmol, 67.8%).

1,3,5-Tris(10-methyl-7,9-dioxo-6,10-diazaheptadecyl)benzene. A mixture of 1,3,5-tris(5-aminopentyl)benzene (1.6 g, 4.8 mmol), malonic acid monomethyl ester mono-*N*-heptyl-*N*-methylamide (9.8 g, 42.8 mmol; prepared according to [2]) and 2-hydroxypyridine (4.1 g, 43.1 mmol; Fluka, pract.) was stirred at 100°C under argon for 4 h. The reaction mixture was cooled to room temperature and then poured into CH_2Cl_2 (200 ml). The organic phase was washed several times with water and then dried over Na_2SO_4. The solvent was evaporated and the residue purified twice by flash chromatography (silica gel, dichloromethane and subsequently acetone) to give pure ETH 3832 (0.8 g, 0.86 mmol, 18.0%). Analysis: calculated for $C_{54}H_{96}N_6O_6$ (925.39), C 70.09, H 10.46, N 9.08; found, C 70.14, H 10.25, N 9.01%.

Synthesis of 1,3,5-tris[10-(1-adamantyl)-7,9-dioxo-6,10-diazaundecyl]benzene (ETH 5506)

Malonic acid monomethyl ester N-(1-adamantyl)-N-methylamide. At 0°C, malonic acid monomethyl ester chloride (7.84 g, 57.4 mmol; Fluka, purum) was added dropwise to a solution of *N*-(1-adamantyl)-*N*-methylamine (8.63 g, 52.2 mmol; prepared according to [18]) and triethylamine (5.28 g, 52.2 mmol; Fluka; puriss. p.a.) in diethyl ether (250 ml; Fluka, puriss. p.a.). The reaction mixture was stirred for 30 min at 0°C and subsequently for 16 h at room temperature. The precipitate was then filtered off and the filtrate washed twice with water and once with brine. The organic phase was dried over $MgSO_4$ and then evaporated. The residue was purified by flash chromatography [silica gel, hexane–ethyl acetate (3 + 2)] and recrystallization from hexane to yield the pure product (4.35 g, 16.4 mmol, 31.4%).

Malonic acid mono-N-(1-adamantyl)-N-methylamide. A sample of powdered KOH (1.58 g, 24 mmol; Fluka, purum, > 85%) was added to a solution of malonic acid monomethyl ester *N*-(1-adamantyl)-*N*-methylamide (4.25 g, 16 mmol) in ethanol (150 ml; Fluka, puriss. p.a.). The reaction mixture was stirred for 17 h at room temperature, then acidified with 1 M HCl and extracted twice with diethyl ether. The organic phase was washed twice with water and once with brine, then dried over $MgSO_4$ and evaporated. The residue was purified by recrystallization from hexane–ethyl acetate to yield the pure product (2.4 g, 9.5 mmol, 59.6%).

Malonic acid mono(4-nitrophenyl) ester N-(1-adamantyl)-N-methylamide. *N,N*-Dicyclohexylcarbodiimide (1.9 g, 9.2 mmol; Fluka, puriss. p.a.) was added to a solution of malonic acid mono-*N*-(1-adamantyl)-*N*-methylamide (2.3 g, 9.2 mmol) and 4-nitrophenol (1.28 g, 9.2 mmol; Fluka, puriss.

p.a.) in ethyl acetate (100 ml; Fluka, puriss. p.a.). After stirring the reaction mixture for 3 h at room temperature, another portion of *N,N*-dicyclohexylcarbodiimide (0.85 g, 4.6 mmol) was added. The reaction mixture was stirred again for 3 h, then the precipitate was filtered off. The filtrate was evaporated and the resulting residue was recrystallized from hexane–ethyl acetate to yield the pure product (2.1 g, 5.6 mmol, 61.3%).

1,3,5-Tris[10-(1-adamantyl)-7,9-dioxo-6,10-diazaundecyl]benzene. A solution of malonic acid mono(4-nitrophenyl) ester *N*-(1-adamantyl)-*N*-methylamide (2.0 g, 5.4 mmol) and 1,3,5-tris(5-aminopentyl)benzene (0.6 g, 1.8 mmol; see *ETH 3832*) in tetrahydrofuran (60 ml; Fluka, puriss. p.a.) was stirred for 16 h at room temperature. The solvent was then evaporated and the residue dissolved in CH_2Cl_2 and washed three times with 0.1 M NaOH and once each with water and brine. The organic phase was then dried over $MgSO_4$ and evaporated. The residue was purified twice by flash chromatography [silica gel, dichloromethane–acetone (3 + 2)] to yield pure ETH 5506 (1.35 g, 1.3 mmol, 72.6%). Analysis: calculated for $C_{63}H_{96}N_6O_6$ (1033.49): C 73.22, H 9.36, N 8.13; found, C 72.99, H 9.21, N, 8.05%.

The constitutions of all ionophores were confirmed by ^1H NMR (300 MHz, $CDCl_3$), ^{13}C NMR (75 MHz, $CDCl_3$), IR ($CHCl_3$) and fast atom bombardment mass spectrometric measurements.

RESULTS AND DISCUSSION

All the electrodes showed a Nernstian e.m.f. response to magnesium, that is, an experimental slope of 29.2 ± 0.5 mV at 21°C (theoretical slope = 29.23 mV). The selectivity coefficients of the electrodes for each ionophore with two different plasticisers, *o*-NPOE and ETH 5373, are given in Table 1 and 2.

Selectivity coefficients showing the best magnesium selectivity were obtained with ion-selective electrodes containing membranes with an ionophore to KTpClPB molar ratio of 1.55. These selectivity coefficients are presented here. The ionophores ETH 7025, ETH 7160, ETH 3832 and ETH 5506 showed lipophilicities (log P_{TLC}) of 6.2, 7.1, 7.6 and 8.1 (±1.2), respectively. Both series of ionophores showed an improvement in the Mg^{2+}/Ca^{2+} selectivity on substitution of the heptyl groups by adamantyl groups. With the plasticizer ETH 5373, ETH 5506 shows Mg^{2+} selectivity with coefficients log $K^{Pot}_{MgCa} = -1.9$ and log $K^{Pot}_{MgK} = -3.7$. With *o*-NPOE as plasticizer, log $K^{Pot}_{MgCa} = -1.7$ and log $K^{Pot}_{MgK} = -2.7$ were obtained.

Using ^{13}C NMR the heptyl or adamantyl groups were observed to influence the conformation of the amides about the C–N bond. In ETH 7025, two distinct carbonyl signals were found for the various tertiary amides with different chemical environments, one each for both the *E* and *Z* conformers of the amide. (The spectra are shown in Fig. 3.) The HMBC experiment allowed the assignment of the carbonyl signals. The two sec-

TABLE 1

Selectivity coefficients of the different ionophores with *o*-NPOE as plasticizer

Selectivity coefficient	ETH 7025	ETH 7160	ETH 3832 [a]	ETH 5506
Log K^{Pot}_{MgCa}	−1.0	−1.2	−1.4	−1.7
Log K^{Pot}_{MgSr}	−2.3	−2.3	−2.6	−2.8
Log K^{Pot}_{MgK}	−2.7	−2.0	−3.0	−2.7
Log K^{Pot}_{MgRb}	−1.4	−0.8	−2.1	−1.6
Log K^{Pot}_{MgNa}	−4.2	−4.2	−4.1	−4.4
Log K^{Pot}_{MgLi}	−4.6	−4.3	−4.6	−4.7
Log K^{Pot}_{MgH}	+0.9	+1.9	−1.0	+0.1

[a] See [19] for the optimization of membranes based on this ionophore for physiological measurements.

TABLE 2

Selectivity coefficients of the different ionophores with ETH 5373 as plasticizer

Selectivity coefficient	ETH 7025	ETH 7160	ETH 3832 [a]	ETH 5506
Log K^{Pot}_{MgCa}	−1.3	−1.6	−1.7	−1.9
Log K^{Pot}_{MgSr}	−2.7	−2.8	−2.9	−3.1
Log K^{Pot}_{MgK}	−3.3	−3.1	−3.8	−3.7
Log K^{Pot}_{MgRb}	−2.2	−2.0	−3.0	−2.8
Log K^{Pot}_{MgNa}	−4.5	−4.0	−5.0	−4.7
Log K^{Pot}_{MgLi}	−4.9	−4.4	−5.4	−4.8
Log K^{Pot}_{MgH}	+1.5	+2.3	−0.3	+0.9

[a] See [19] for the optimization of membranes based on this ionophore for physiological measurements.

ondary amide carbonyls have a chemical shift of 166.2 ppm whereas the two neighbouring tertiary amide carbonyls exhibit signals at 168.5 and 168.6 ppm due to the different conformations. The central tertiary amide carbonyl equally shows two signals with chemical shifts of 166.5 and 166.6 ppm, respectively. The sixth and final carbonyl gives a single signal at 167.0 ppm (at the lower temperature of 233 K, this signal was also split in two). At higher temperatures the signals for the different conformations coalesce and a single signal is observed for each tertiary carbonyl group with a similar chemical environment. However, on substituting the heptyl groups with bulky adamantyl groups, only one conformation for each tertiary amide predominates. This explains the loss of two signals in the carbonyl region of ETH 7160. The same effect is again seen when ETH 3832 is compared with ETH 5506. ETH 3832 displays three signals in the carbonyl region. The tertiary amides, all of which have the same chemical environment, again show *E* and *Z* conformers. ETH 5506 exhibits only two signals at 166.8 and 169.4 ppm, which are attributed to the secondary and tertiary carbonyls, respectively. Again with adamantyl groups, only one tertiary amide conformer prevails.

According to previous investigations on the different conformations of the amide bond [20], that isomer which places the bulkyl alkyl groups *trans* to one another about the C–N bond is sterically preferred. Hence the adamantyl group favours that conformation about the amide bond where the bulky group is *cis* to the amide carbonyl and allows a more favourable selectivity of the magnesium cation. The results with ionophores ETH 7160 and ETH 5506 support this particular observation. Ion-selective electrodes based on both ionophores show a clear improvement of the Mg^{2+}/Ca^{2+} and Mg^{2+}/K^{+} selectivities over electrodes with the respective heptyl isologues.

This paper is dedicated to the late Professor Wilhelm Simon, a mentor for us all. Special thanks are due to Dr. Jaun for his technical help and advice and to Professor Pretsch for his thorough perusal of this work and his helpful comments. This work was partly supported by the Swiss National Science Foundation and by Ciba-Corning Diagnostics Co.

REFERENCES

1 M.V. Rouilly, M. Badertscher, E. Pretsch, G. Suter and W. Simon, Anal. Chem., 60 (1988) 2016.
2 M. Müller, M.V. Rouilly, B. Rusterholz, M. Maj-Zurawska, Z. Hu and W. Simon, Mikrochim. Acta, III (1988) 283.
3 K. Suzuki, personal communication, (1992).
4 U.E. Spichiger, R. Eugster, E. Haase, G. Rumpf, P. Gehrig, A. Schmid, B. Rusterholz and W. Simon, Fresenius' J. Anal. Chem., 341 (1991) 727.
5 U. Schaller, U.E. Spichiger and W. Simon, Pflügers Arch., in press.
6 R. Eugster, B. Rusterholz, A. Schmid, U.E. Spichiger and W. Simon, Clin. Chem., in press.
7 R. Eugster, B. Rusterholz, U.E. Spichiger and W. Simon, in preparation.
8 U. Oesch, Z. Brzózka, A. Xu, B. Rusterholz, G. Suter, H. Pham, D.H. Welti, D. Ammann, E. Pretsch and W. Simon, Anal. Chem., 58 (1986) 2285.
9 R.E. Dohner, D. Wegmann, W.E. Morf and W. Simon, Anal. Chem., 58 (1986) 2585.
10 G.G. Guilbault, R.A. Durst, M.S. Frant, H. Freiser, E.H. Hansen, T.S. Light, E. Pungor, G. Rechnitz, N.M. Rice, T.J. Rohm, W. Simon and J.D.R. Thomas, Pure Appl. Chem., 48 (1976) 127.
11 P.C. Meier, D. Ammann, W.E. Morf and W. Simon, in J. Koryta (Ed.), Medical and Biological Application of Electrochemical Devices, Wiley, Chichester, 1980, p. 19.
12 P.C. Meier, Anal. Chim. Acta, 136 (1982) 363.
13 U. Schefer, D. Ammann, E. Pretsch, U. Oesch and W. Simon, Anal. Chem., 58 (1986) 2282.
14 O. Dinten, U.E. Spichiger, N. Chaniotakis, P. Gehrig, B. Rusterholz, W.E. Morf and W. Simon, Anal. Chem., 63 (1991) 596.
15 A. Bax and A.F. Summers, J. Am. Chem. Soc., 108 (1986) 2093.
16 P. Baudart, Bull. Soc. Chim. Fr., 11 (1944) 336.
17 G.A. Olah, S.C. Narang, B.G.B. Gupta and R. Malhotra, J. Org. Chem., 44 (1979) 1247.
18 R.A.W. Johnstone, D.W. Payling and C. Thomas, J. Chem. Soc. C, (1969) 2223.
19 U.E. Spichiger, in preparation.
20 L.A. Laplanche and M.T. Rogers, J. Am. Chem. Soc., 85 (1963) 3728.

Analytica Chimica Acta, 281 (1993) 135–152
Elsevier Science Publishers B.V., Amsterdam

Comparison of distillation with other current isolation methods for the determination of methyl mercury compounds in low level environmental samples

Part 1. Sediments

Milena Horvat [1]
"J. Stefan" Institute, Jamova 39, 61000 Ljubljana (Slovenia)

Nicolas S. Bloom
Frontier Geosciences, 8057 Corliss Av. NW, Seattle, WA 98107 (USA)

Lian Liang
Brooks Rand, Ltd., 3950 Sixth Avenue NW, Seattle, WA 98107 (USA)
(Received 15th January 1993)

Abstract

In the present study isolation of methyl mercury compounds (MeHg) from sediments by distillation, followed by aqueous phase ethylation, precollection on a Carbotrap, isothermal gas chromatography and cold vapour atomic fluorescence (CVAF) detection, was investigated. Results obtained by distillation were compared with those obtained by alkaline digestion and HCl leaching methods. A good agreement of the results for MeHg in sediments of various origins and wide concentration range (0.04–60.0 ng g^{-1}, dry weight) obtained by distillation and KOH–methanol digestion was found. The main advantage of the distillation method over alkaline digestion is avoidance of matrix effects during the ethylation process. Distillation gives consistent and high recoveries ($95 \pm 4\%$) and therefore provides more accurate results especially, at low MeHg concentrations. Detection limits as low as 0.001 ng MeHg g^{-1} as Hg for 100 mg sample weight were obtained. The HCl leaching method was found to be ineffective in releasing MeHg from sediment quantitatively. Even 8 M HCl could not release MeHg quantitatively; on the contrary, if the concentration of HCl was more than 4 M, decomposition of released MeHg occurred. Addition of Cu(II) ions increased the release of MeHg into solution, but not quantitatively. The difference in the results obtained by distillation and HCl leaching was in positive correlation with the concentration of MeHg ($r^2 = 0.92$) and the concentration of total organic carbon (TOC) ($r^2 = 0.88$). This suggests that the fraction of MeHg released from the sediment by HCl might be of certain interest in studies of the biogeochemical cycle of Hg. The results obtained in the present study clearly demonstrate the necessity for additional quality control exercises, particularly the establishment of certified reference materials such as sediment samples of various origin. The sediments currently certified for total Hg from NRCC (MESS-1, PACS-1), and NIES (Pond Sediment) were also analyzed for MeHg. Results obtained by three laboratories using different separation and detection systems showed good agreement. Additionally, the behaviour of MeHg under different storage conditions (deep frozen, refrigerated, dried) was also studied. No changes of MeHg concentration were found during a period of 8 months, if samples were deep frozen or refrigerated, while drying of sediments in an oven at 85°C resulted in a 15% decrease of total and 45% of MeHg.

Keywords: Acid leaching; Alkaline digestion; Cold vapour atomic fluorescence detection; Dimethyl mercury; Distillation; Methylmercury; Sediments

Correspondence to: M. Horvat, "J. Stefan" Institute, Jamova 39, 61000 Ljubljana (Slovenia).

[1] Current address: IAEA-MEL, Marine Environmental Studies Laboratory, 19 Av. des Castellans, MC-98000 (Monaco).

Under various natural conditions inorganic mercury may be converted to very toxic methylmercury (MeHg) compounds, which tend to bioaccumulate in the aquatic and terrestrial food chain. However, evidence for the methylation mechanisms is still largely circumstantial. Nearly all of the MeHg in the aquatic system resides in fish (85%). Usually, MeHg in sediments does not exceed 1.5% of the total Hg present. The concentration measured, however, represents the approximate equilibrium between concurrent methylation and demethylation processes [1]. The isolation and determination of MeHg in sediments is a well known problem. Compounds present in the sediment (sulphide, organic substances, especially humic substances, amino acids and proteins) are able to bind organomercury compounds. Acidifying the sediment with halogenic acids releases Hg compounds from binding sites. In general most analytical methods for MeHg are based on the acidification of the homogenized sample by a halogenic acid and extraction into an organic solvent (benzene or toluene). The organomercury compounds are then back extracted into an aqueous cysteine or thiosulphate solution. The aqueous phase is then acidified and organomercury compounds re-extracted into benzene, followed by gas chromatography with an electron capture detection (GC-ECD) [2,3]. The same method was also applied for the determination of MeHg in sediments, but with several modifications. In order to increase the release of MeHg from binding sites, Cu(II) bromide and sulphuric acid were used in the first extraction step [4,5].

Steam distillation has also been used in order to separate organic from inorganic Hg compounds in sediments. MeHg was subsequently measured by decomposition, reduction, and cold vapour atomic absorption spectrometry (CV-AAS) [6,7]. The method has later been modified in our laboratory in terms of using different apparatus for distillation and different reagents to release MeHg from the sample [8]. The method was also applied for separation of MeHg from biological samples. After separation MeHg was measured by CV-AAS or GC-ECD. Actually, the method developed by Zelenko and Kosta [9] and Gvadjancic et al. [10] which is based on isothermal volatilization of MeHg in a closed microdiffusion cell, gave us the idea of checking different reagents in order to increase the recovery of MeHg. Using sulphuric acid and sodium chloride resulted in good and reproducible recoveries (95 $\pm$ 5%). When the method is followed by measurement with nonspecific CV-AAS, the presence of a high concentration of inorganic Hg in the distillate may interfere. Therefore inorganic Hg should be removed with an ion exchanger [11].

However, it is difficult to estimate the recovery when speciation work has to be done with insoluble materials such as sediments and soils. Spiked MeHg is not equivalent to originally present MeHg in the sediment. The best way to establish an accurate value is the comparison of the results obtained by different isolation techniques. Once MeHg is separated from the sediment, it is advisable to use a sensitive and specific detection system. In most laboratories GC-ECD is used. Since the MeHg concentration in sediment is usually relatively low, there is always a suspicion that the small peaks that correspond to the retention time of MeHg may be due to some other compound in the extract, especially since the ECD measures halide (bromide or chloride) and not Hg. It would therefore be advantageous to use a more specific detector (microwave emission spectrometric detector) [12].

Alkaline digestion by KOH–methanol followed by aqueous phase ethylation, cryogenic gas chromatography and a cold vapour atomic fluorescence detector has also been applied for determination of MeHg in sediments [13]. Alkaline digestion released MeHg quantitatively, but serious problems were observed during aqueous phase ethylation, especially in the presence of sulphide ions. This increased the detection limit of the method.

The purpose of this work was to evaluate critically three isolation procedures (HCl leaching, alkaline digestion and distillation) in order to find the most suitable way of preseparating MeHg from sediment samples, particularly if followed by a sensitive analytical set-up based on aqueous phase ethylation, isothermal GC, and cold vapour atomic fluorescence (CV-AF) detection. Experiments performed on water samples (lake and sea

water samples) will be presented in our next publication, which is in preparation. This paper is therefore the first of two parts concerning determination of methyl mercury compounds in environmental samples (particularly sediment and water samples).

EXPERIMENTAL

Various approaches for separation of MeHg compounds from sediment samples were compared. Their principles are schematically shown in Fig. 1. Most of the separation techniques de-

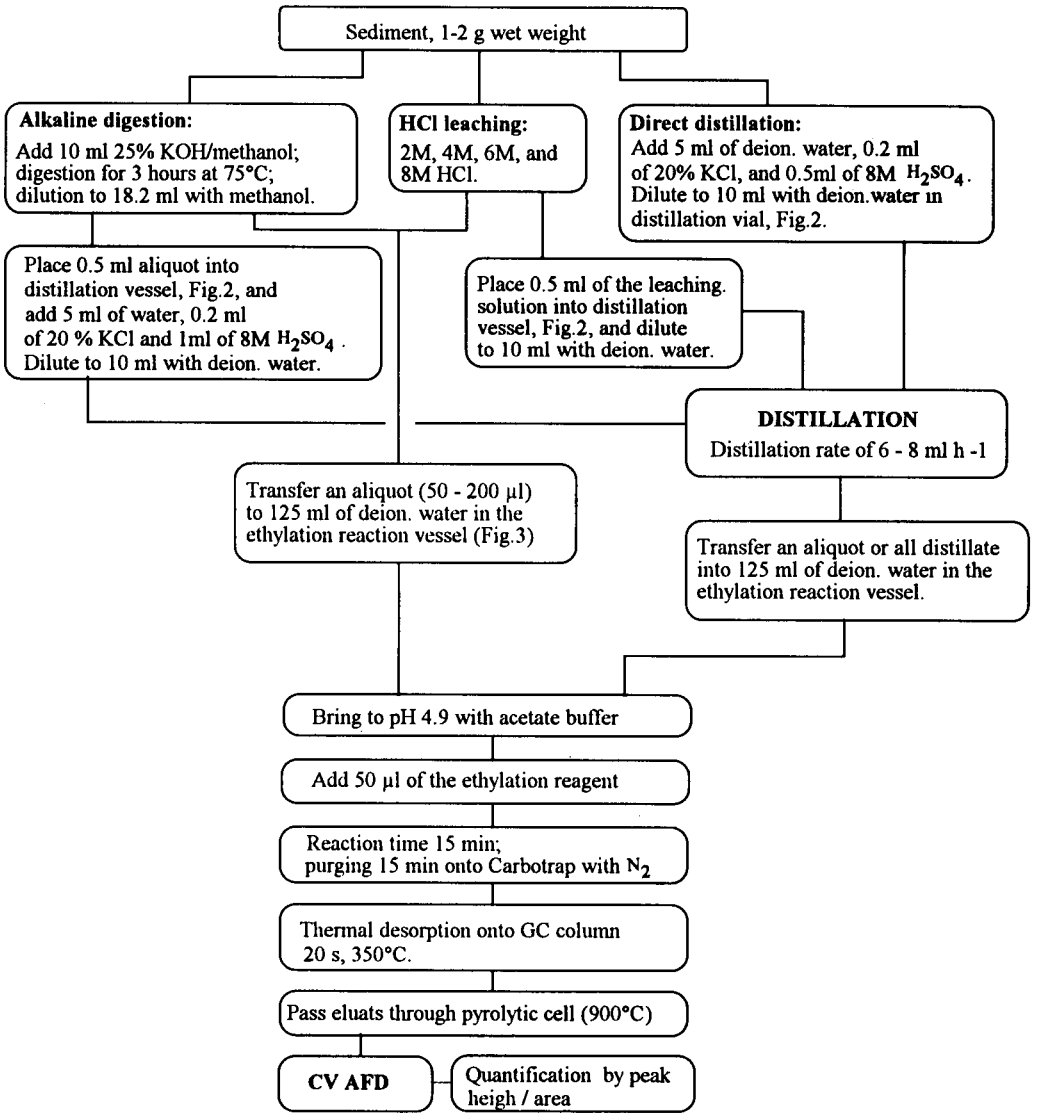

Fig. 1. Schematic flow chart of the isolation procedures followed by aqueous phase ethylation, isothermal GC, and CV-AF detection.

scribed in the present paper have already been compared for biological samples [8,14]. The main difference between previous studies and the present one is in the final determination of MeHg. In the previous study direct MeHg determination was performed by GC-ECD and indirectly by gold amalgamation atomic absorption spectrometry (CV-AAS). In the present study aqueous phase ethylation followed by isothermal GC and CV-AF detection was used, and therefore only this method is described in more detail.

Cleaning procedure

All glass and PTFE ware were thoroughly cleaned using the following procedure. New or used ware (vials and tubing) were placed into hot (90°C) concentrated HNO_3 for 24 h. After being thoroughly rinsed with deionized water, vials were filled with 1% HCl and heated at 70°C overnight and then kept in a clean place, preferably sealed in Hg-free plastic bags. Vials were emptied just before use for sample processing. Tubing was rinsed, dried and kept in Hg-free plastic bags.

Distillation

A distillation still for MeHg separation is shown in Fig. 2. Vials for distillation and distillate collection are made of PTFE obtained from the Savillex (USA). Instead of PTFE a glass distillation still might also be used [8].

Fresh sediment was accurately weighed (0.5–2.0 g) into a 30-ml (or 60-ml) PTFE vial followed by the addition of 5 ml of deionized water, 0.2 ml of 20% KCl, and 0.5 ml of 8 M H_2SO_4. The mixture was diluted to 10 ml with deionized water. It is important to start the distillation immediately after addition of the reagents at a nitrogen flow-rate of 60 ml min^{-1} and a heating block temperature of 145°C. This temperature was optimal for the analytical set-up in this laboratory. If the heating block is better insulated distillation can be done at lower temperature. It should be emphasized that it is more important to control the distillation rate rather than the temperature. Under the conditions described the distillation was finished in approximately 75–90 min when approximately 85% of the distillate was collected (approximately 7 ml h^{-1}). The distillate was collected in a 60-ml PTFE vial kept in an ice cooled water bath. Prior to distillation 5 ml of deionized water was placed in the collection vial. The distillate was then diluted with deionized water to 50 ml directly in the receiving vial. Only an aliquot of the distillate was taken for further analysis. The distillation time at constant block temperature and nitrogen flow varied with the type and the amount of sample. A higher distillation rate can be achieved by increasing the heating block temperature, but this resulted in lower recoveries. A higher flow-rate resulted in the breakthrough of the solution from the sample containing vial into the distillate collection tube. In prac-

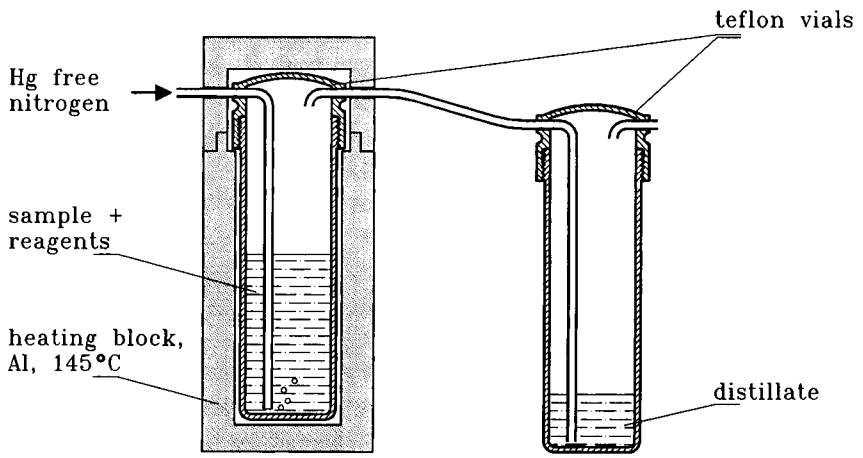

Fig. 2. Apparatus for distillation of MeHg from the sample.

tical terms distillation conditions should be adjusted to a distillation rate of not more than 7–8 ml h^{-1}. Distillates should be kept in darkness to avoid decomposition of MeHg by UV oxidation. MeHg in distillates is stable for at least two weeks, if stored in darkness. The volume of the aliquot of the distillate that was taken for further processing was dependent on the MeHg and inorganic Hg concentrations (see Results and Discussion). Under the optimum experimental conditions MeHg content in an aliquot should be in the range between 5 to 200 pg. The pH of the distillate usually varies between 3.9 to 4.2, and therefore addition of 0.2 ml of the acetate buffer to the ethylation reaction vessel is sufficient to achieve the optimum pH (4.5–4.9) necessary for the ethylation reaction.

Alkaline digestion

Approximately 1 g of the sediment sample was placed in the 22 ml PTFE vial, and 10.0 ml of 25% KOH in methanol solution was added. The vial was closed and the sample digested for 6 h at 90°C. The digest was cooled and diluted to 18.2 ml with methanol. MeHg in the alkaline digested sample was then determined (a) directly or (b) after separation by distillation (as shown in Fig. 1).

(a) An aliquot of 50–200 μl was added to 150 ml of deionized water in the aqueous phase reaction vessel. An appropriate amount of the acetate buffer (min. 0.2 and max. 2 ml) was added to reach pH 4.9 as necessary for the ethylation process. The sample was analyzed as described under the paragraph for MeHg determination below. Alkaline digested sediment samples should be analyzed within two days, otherwise losses due to readsorption of MeHg onto the undissolved particulate matter may occur. With longer storage time decomposition of MeHg also occurs.

(b) An aliquot of 0.5 ml of the alkaline digested sample was placed into the distillation vial. 5 ml of deionized water, 0.2 ml of 20% KCl, and 1 ml of 8 M H_2SO_4 were added. The mixture was then diluted to 10 ml with deionized water. The distillation was carried out as described above. An aliquot of the distillate and 0.2 ml of acetate buffer were added to 150 ml of deionized water in the ethylation reaction vessel and processed as described under the paragraph for the determination of MeHg below.

Leaching by hydrochloric acid

Various concentrations of HCl concentrations (2, 4, 6 and 8 M) were tested in order to find an optimal amount of HCl for releasing MeHg into solution. Approximately 1 g of sample was placed in a PTFE vial and 10 ml of HCl was added. The vial was closed and shaken for 2 h. The leachate was then diluted to 18.2 ml with the appropriate HCl solution. Vials with the sample and acid were always kept in the dark in order to avoid decomposition of MeHg by UV light. MeHg in the solution was determined (a) directly or (b) after additional separation by distillation (see Fig. 1).

(a) An aliquot of the leachate (50–200 μl) was analyzed as described for direct MeHg determination in alkaline digested sample.

(b) An aliquot of 0.5 ml of the HCl leachate was placed in the distillation vial and 9.5 ml of deionized water was added. Distillation was performed following the same procedure as described for distillation directly from the sample. The pH of the distillate was always checked before an aliquot was transferred in the ethylation reaction flask. The pH was adjusted to 4.9 with an appropriate amount of acetate buffer. However, if a very low pH (< 2) was measured and if larger volumes of the distillate had to be taken for further analyses, acetate buffer was not sufficient for adjustment of pH. In this case it was adjusted with KOH solution prior to addition of the acetate buffer.

Determination of MeHg

An improved method for mercury speciation by aqueous phase ethylation, and Carbotrap precollection, followed by isothermal GC with CV-AF detection was used. The method is described in more detail by Liang et al. [15,16]. Preparation of the reagents and the analytical set-up is also described by Bloom [13]. A schematic diagram illustrating the procedure is shown in Fig. 3. Briefly, the procedure is as follows: an aliquot of the sample (distillate, HCl leachate, or alkaline

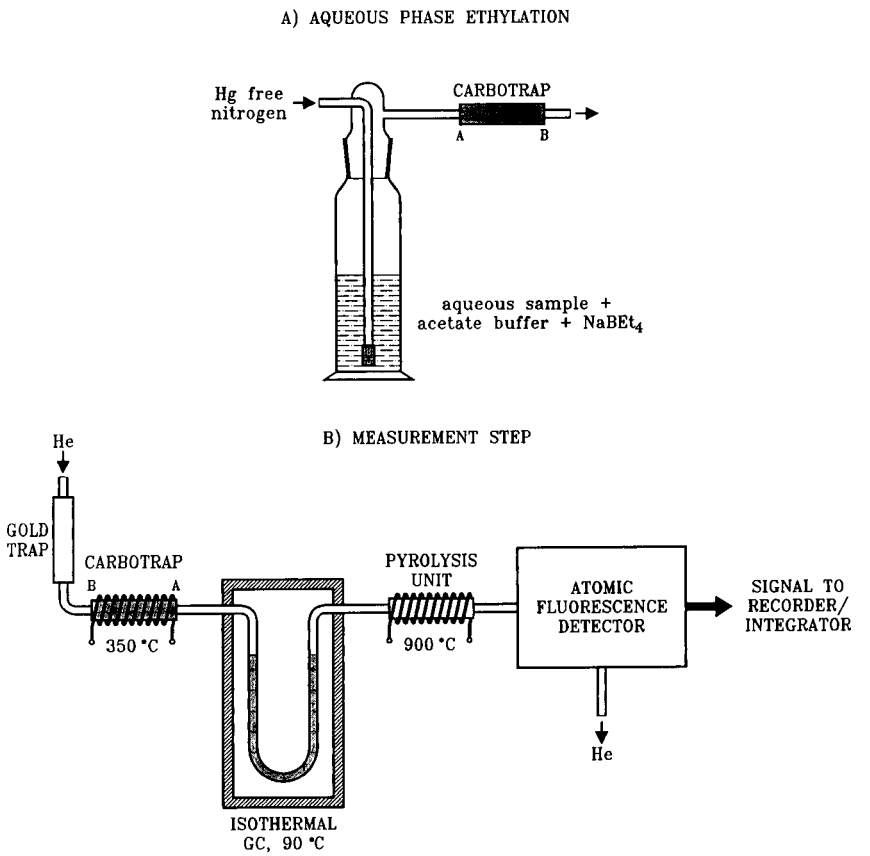

Fig. 3. Schematic diagram illustrating the procedure for MeHg determination by aqueous phase ethylation, isothermal GC, and CV-AF detection.

digestate) was added to 150 ml Hg-free deionized water (Millipore cleaned) in a 250-ml reaction flask. The sample was buffered to pH 4.9 with 2 M acetic acid–sodium acetate solution, and then 50 μl of 1% aqueous sodium tetraethyl borate solution was added. The flask was immediately closed, and the mixture allowed to react without bubbling for 15 min. The ethylation reaction results in the formation of ethylmethylmercury from reactive MeHg and diethylmercury from inorganic mercury [13,17]. After the reaction period, the solution was purged for 15 min at a flow-rate of 250 ml min^{-1} with Hg-free, high purity nitrogen. The outflowing gas stream was passed through a Carbotrap (a 6 mm id. silanized silica column containing 0.15 g of Carbotrap-graphitized carbon black, Supelco), which adsorbs the organomercury species. After the sample was purged, dry nitrogen is flushed through the Carbotrap to remove traces of condensed water vapour, a strong interference during chromatographic elution and CV-AF detection. The Hg species on the Carbotrap were released by thermal desorption [15] into the GC column which is a 60-cm long U shaped silanized glass column filled with 15% OV-3 on Chromosorb W, AW, DMCS at 90°C. It is important to keep the orientation of the Carbotrap as indicated in the Fig. 3. Under a flow of helium the eluted Hg species were converted into Hg° by thermal decomposition at 900°C and then detected by CV-AF. The output from the detector is quantified using a standard GC plotter/integrator. A CV AFD-2 mercury analyzer produced at Brooks Rand was used. Its operation is described in detail by Bloom and Fitzgerald [18]. Two typical chromatograms

obtained for distilled and alkaline digested sediment samples are shown in Figure 10.

Determination of total mercury

Sample aliquots of approximately 2 g were weighed into 30-ml PTFE vials and then 5 ml of conc. HNO_3 and 2 ml of conc. H_2SO_4 were added and the vials closed. The samples were allowed to digest overnight at room temperature, and then slowly brought to 90°C on a hot plate. A complete digestion of organic matter was achieved in 3 h. When cool the digestates were diluted to 25 ml with 0.002% BrCl solution. An aliquot (0.1–1.0 ml) of the digest was added to a purging flask containing 100 ml of water followed by the addition of 0.5 ml of 10% $SnCl_2$. Pre-reduction by hydroxylamine hydrochloride is not necessary, as the small quantity of bromine and chlorine in the aliquot are destroyed by $SnCl_2$. Hg vapour was purged from the solution and trapped on a gold trap, followed either by double amalgamation [19] or single amalgamation CV-AF detection [20]. Detection limits for total Hg determination in sediment, calculated as three times the standard deviation of the blank of the reagents was approximately 0.2 ng g^{-1} wet weight.

RESULTS AND DISCUSSION

Analytical quality control

Analytical quality control (AQC) of the results for total Hg and MeHg was performed by analysis of two certified reference materials (CRMs) (DORM-1 and TORT-1) for total and MeHg obtained from the National Research Council of Canada. These CRMs are of biological origin, and therefore they were used mainly to control the accuracy and the performance of the measurement step, that is aqueous phase ethylation, isothermal GC and AF detection. These materials were analyzed daily. Data were collected in the form of analytical quality control flow charts. Examples are shown in Fig. 4.

The accuracy of the results for total Hg in sediments was also checked by the analyses of sediment reference materials, certified for total Hg. Unfortunately, there are no CRMs certified

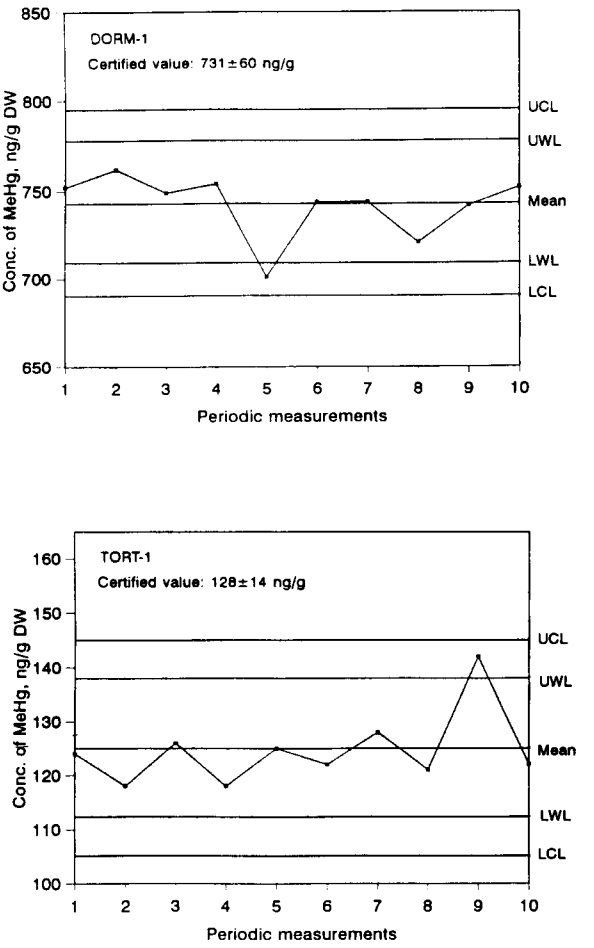

Fig. 4. Quality control flow charts for the analysis of MeHg in CRMs DORM-1 and TORT-1. Mean = arithmetic mean of the analyses; s = standard deviation; UWL = upper warning limit, mean + 2s; UCL = upper control limit, mean + 3s; LCL = lower control limit, mean − 3s; LWL = lower warning limit, mean − 2s.

for MeHg in matrices such as sediment. In our previous studies on MeHg determination in sediments [8,21], we concluded that samples such as sediment, soil and water deserve special attention. Serious matrix interferences, resulting in inaccurate results might occur during analysis of these samples, especially if nonspecific isolation or detection techniques are used. These conclusions were later confirmed by other authors [11]. Apart from the analysis of CRMs, the accuracy of the MeHg analyses may be evaluated by the stan-

dard addition method, intercalibration exercises, radiotracer methods, or comparison of the results obtained by various isolation and measurement procedures. Such an intercomparison has been performed for biological matrices [14]. However, the standard addition method, which is often used in many laboratories, might result in very good and reproducible recoveries of spiked MeHg, while only small percentage of MeHg bound to the sediment particles is recovered. This is particularly true for some sediment samples, which will be discussed later in this paper. Therefore, one of the primary objectives of the present work was to cross-check various isolation procedures in order to find out which give consistent recoveries for sediment samples of various origin.

Additionally, results for MeHg in three sediment samples (RMs certified for total Hg) were compared with results obtained by two other laboratories. Results are presented in Table 1. Relatively good agreement of the results obtained by the three laboratories was found. It would be of interest to analyze these samples additionally by an extraction procedure followed by GC-ECD, since this method is frequently used in many laboratories. Therefore the authors would appreciate receiving results from other laboratories for further comparison of the MeHg concentration in these sediment samples. There is an urgent need for the producers of the reference materials to certify MeHg in sediment samples, since many laboratories are able to analyze MeHg accurately even at very low concentration levels. A study of MeHg stability in RMs during long-term storage will be performed in future experiments.

HCl leaching

A correlation of the results for MeHg obtained by direct distillation and 4 M HCl leaching methods in 10 sediment samples with low TOC, is shown in Fig. 5. Even though the concentration of MeHg is relatively low, a good agreement between the results of these two isolation procedures was found. Such a comparison was also performed on 50 sediment samples collected from a Hg polluted freshwater bay (Montreal, Canada). Results are shown in Fig. 6. Evidently, the correlation between the results obtained by 4 M HCl leaching and the direct distillation method is good ($r^2 = 0.915$). However, the HCl leaching method gave much lower values. As shown in Fig. 7 the difference between these two methods is in very good correlation with the MeHg concentration in

TABLE 1

Comparison of the results for the determination of MeHg in sediment CRMs certified for total mercury obtained by different laboratories

[Results are given in ng g^{-1} as Hg ± S.D.; DW, of n determinations. Laboratory 1: Brooks Rand, Seattle, WA, USA (present work); laboratory 2: Academy of Natural Sciences, Benedict, MD, USA; laboratory 3: Applied Physical Chemistry, Research Centre, Jülich, Germany. Method A: distillation, followed by aqueous phase ethylation, GC and CV-AF detection; method B: alkaline digestion, followed by aqueous phase ethylation, GC and CV-AF detection; method C: distillation, ion exchange separation of Hg(II) and MeHg(II), UV irradiation, and CV-AA detection; method D: HCl leaching, ion exchange separation of Hg(II) and MeHg(II), UV irradiation and CV AA detection]

CRM	Laboratory 1 (methods A and B)	Laboratory 2 (method A)	Laboratory 3 (methods C and D)	Total Hg $\mu g\ g^{-1}$, dry weight Certified value ± 95% conf. limit
NRCC, PACS-1, Harbour marine sediment	8.47 ± 0.63, $n = 8$ (A) 7.99 ± 0.42, $n = 3$ (B)			4.57 ± 0.16
NRCC, BEST-1, Estaurine sediment	0.160 ± 0.054, $n = 3$ (A) 0.144 ± 0.023, $n = 3$ (B)	0.164 ± 0.051 (A) $n = 3$		not certified
NRCC, MESS-1, Estaurine sediment	0.348 ± 0.028, $n = 4$ (A) 0.384 ± 0.043, $n = 3$ (B)	0.506 ± 0.100 (A) $n = 4$		0.129 ± 0.012
NIES No. 2, Pond sediment	3.72 ± 0.26, $n = 4$ (A) 3.53 ± 0.18, $n = 3$ (B)	2.83 (A) $n = 1$	3.04 ± 0.32 (C) 3.76 ± 0.56 (D) n = not reported	1.3 (recommended value)

the sediments. This difference is also in statistically positive correlation with the percentage of TOC ($r^2 = 0.619$). Data on %TOC were given for 31 samples only. This clearly demonstrates that TOC affects the recovery of MeHg from sediment by the HCl leaching method. Lower MeHg recoveries might be the result of the decomposition of MeHg in HCl media or incomplete recovery from the sediment. In order to find the answer few experiments described below were performed.

A sandy sediment (low in TOC) was spiked with MeHg, so that the final MeHg concentration was about three times higher than in the original sample. 4 M HCl was added as described in the Experimental part. Independent triplicate analyses of spiked and unspiked sediments were performed. After 2 h of shaking samples were allowed to stand in the dark until the particles settled to the bottom. 10-ml aliquots of the clear solutions above the particles were then transferred into clean PTFE vials. So, the stability of

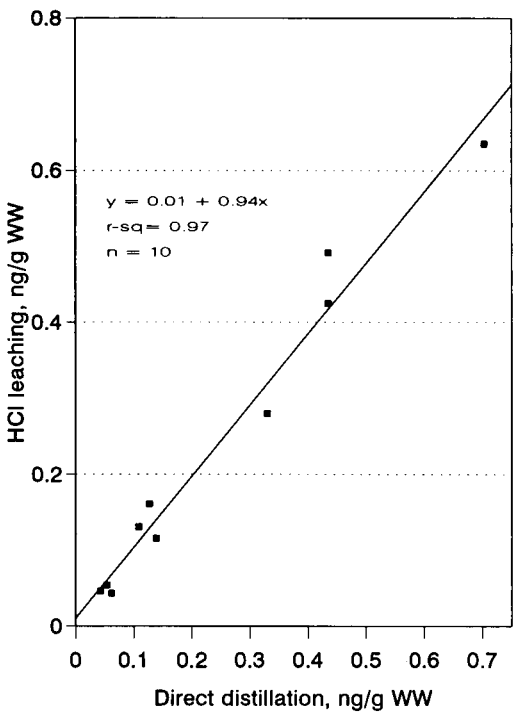

Fig. 5. Correlation of the results for MeHg obtained by direct distillation and HCl leaching methods in sediments with low content of TOC (< 0.1%).

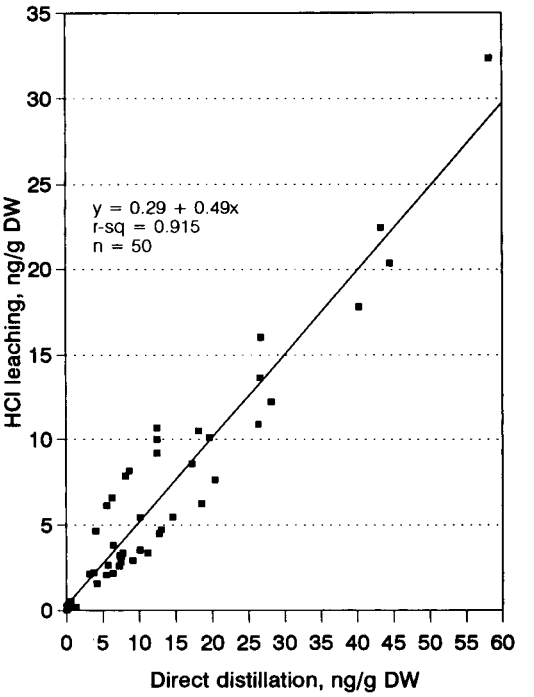

Fig. 6. Correlation of the results for MeHg obtained by direct distillation and HCl leaching methods in sediments from the mercury polluted freshwater bay.

MeHg (spiked and unspiked) was observed in HCl media containing particles and in solutions without the presence of particles. MeHg was then isolated by distillation of 0.5 ml aliquots, following the procedure described in the experimental part (Fig. 1). The pH of the distillates was always checked before the ethylation step in order to avoid low recoveries due to the interferences at lower pH. Results are shown in Fig. 8. Each point plotted in the figure is the average of three independent determinations. Evidently the presence of sediment particles does not affect the stability of MeHg in HCl sediment leachates. However, it was shown that the spiked MeHg is less stable than MeHg originally present in the sediment sample. If the recovery of the analytical procedure is calculated on the basis of the yield of spiked MeHg, care is necessary in terms of time after spiking.

In the next experiment three sediments were selected in which a significant disagreement between HCl leaching and direct distillation had

been observed. The percentage of TOC in these samples, labeled A, B and C, were 1.1, 3.9 and 4.2% respectively. The effect of various HCl concentrations (2, 4, 6 and 8 M) and equilibration times on the release of MeHg from sediment were observed. Various concentrations of HCl were added to a known amount of the wet sediment in a PTFE vial. Before an aliquot (0.5 ml) of the leachate was taken for distillation following the procedure described in the experimental part, the vials were shaken and then particles were allowed to settle to the bottom. Only the clear solution (without any particles) was further processed. From the results shown in Fig. 9a–c it is evident that none of the HCl concentrations could release MeHg quantitatively. Results were compared to those obtained by direct distillation from the sample. Each point in the figures is the result of two independent determinations. The release of MeHg from sediments in 2 M HCl increased with time. However, only half of the MeHg was released after 3–4 days. In the case of 4 M HCl the concentration of MeHg remained constant during a period of four days. If the HCl concentration was grater than 4 M, a decrease of MeHg concentration with time occurred.

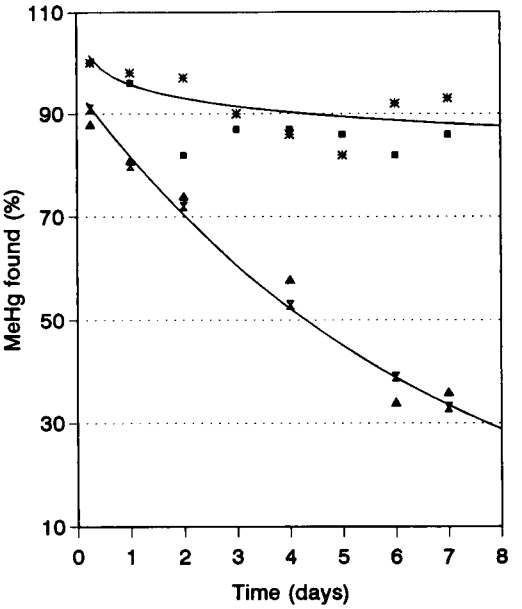

Fig. 8. Stability of spiked and originally present MeHg in 4 M hydrochloric acid sediment leachates. Sediment sample was low in TOC; concentration of MeHg obtained by direct distillation was 0.428 ± 0.044 ng g^{-1} wet weight. Key to symbols: ■ = unspiked, solution; * = unspiked, solution + particles; ▲ = spiked, solution; ⧖ = spiked, solution + particles.

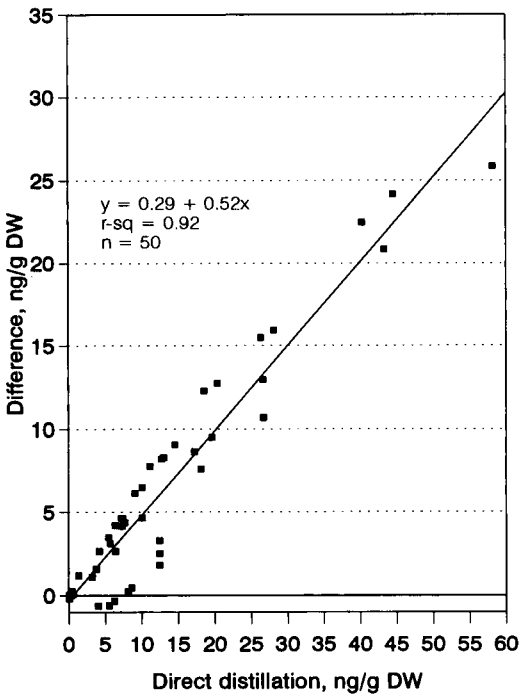

Fig. 7. The difference between MeHg concentrations obtained by direct distillation and HCl leaching methods vs. MeHg concentration obtained by direct distillation.

The last experiment was a continuation of the above experiment. Undissolved sediment particles after 4 M HCl leaching were rinsed three times with deionized water. The MeHg that remained bound to the particles was then further isolated by distillation. This experiment was performed for sediments A, B and C and also for three RMs certified for total Hg. The results are summarized in Table 2. The sum of MeHg concentration leached from the sediment into 4 M HCl solution and the amount of MeHg remaining bound the particles, corresponded to the MeHg concentrations obtained by direct distillation. This confirms the statement that MeHg remained bound to the particles rather than being decomposed in the HCl media.

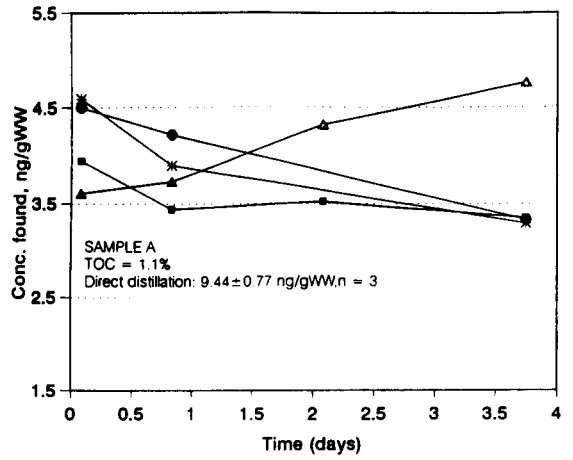

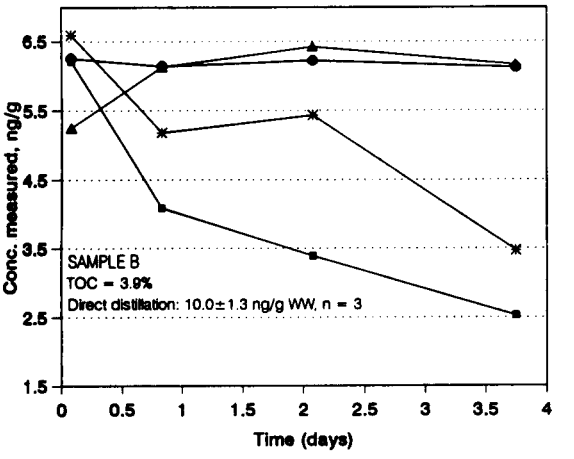

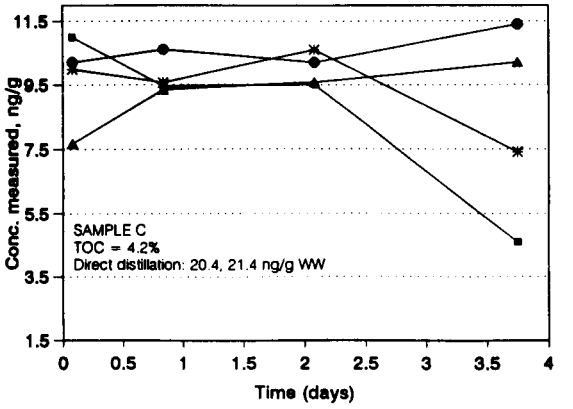

Fig. 9. Observation of MeHg concentration leached from sediments A, B, and C using various concentration of HCl vs. time. Key to symbols: ▲ = 2 M HCl; ● = 4 M HCl; * = 6 M HCl; ■ = 8 M HCl.

So, when HCl leaching was used two undesirable effects occurred: decomposition of MeHg in HCl solution and incomplete release of MeHg from the sediment sample (particularly those rich in TOC). These findings are not in agreement with conclusions published by other workers [22]. They concluded, on the basis of experiments with MeHg spiked on soil samples, that MeHg is quantitatively released from the sample using HCl.

In most conventional methods based on the extraction of MeHg into an organic solvent for subsequent GC determination, copper(II) ions are added to the sample in order to increase the release of MeHg from bounded sites. We have also checked the effect of Cu(II) on the release of MeHg from the sediments tested above (A, B and C). As evident from the results presented in Table 2, the addition of Cu(II) ions increased the release of MeHg from most sediments, but not quantitatively. However, in sediment sample C, which has the largest percentage of TOC, no increase was observed.

From these three experiments it is concluded that HCl leaching is insufficient to release MeHg from sediment samples. However, the fraction released by HCl is positively correlated with total organic carbon in the sediments, which might have a significant role in the interpretation of these data in the biogeochemical cycle of Hg. From the analytical point few of these experiments demonstrated that care is necessary when the recovery of the analytical procedure for MeHg is estimated by spiking. Particularly, the time of processing the analysis after spiking is important, since MeHg added to the sample is less stable with time in the acidic media than MeHg originally present in the sample.

Alkaline digestion

In Tables 1 and 3 results obtained by alkaline digestion are compared with those obtained by other methods. Results obtained by alkaline digestion are in good agreement with results obtained by direct distillation. This suggests that alkaline digestion releases MeHg quantitatively from the sediment. Results in Table 1 were obtained after an aliquot of the alkaline digested

TABLE 2

Concentration of MeHg leached from sediment by HCl and HCl ($CuSO_4$)
[Results are given in ng g^{-1} as Hg (arithmetic mean ± standard deviation) of n independent determinations. An aliquot of leaching solution was distilled following the procedure described in Fig. 1. Undissolved particles were rinsed with water and MeHg i-olated by distillation]

Samples code code	4 M HCl		4 M HCl (4 mg $CuSO_4$ ml^{-1})		Direct distillation
	Solution	Particles	Solution	Particles	
	ng g^{-1}, wet weight				
A (TOC 1.1%)	4.61, 4.94	4.02	7.64, 7.95	2.31	9.44 ± 0.77, $n = 3$
B (TOC 3.9%)	7.63, 6.98	3.95	7.28, 9.26	1.33	10.0 ± 1.27, $n = 3$
C (TOC 4.2%)	9.28, 9.58	7.94	12.4, 14.7	7.53	20.4, 21.4
	ng g^{-1}, dry weight				
NRCC PACS-1 Mar. sed.	4.73, 5.01	1.47	4.92, 5.18	1.02	8.47 ± 0.63, $n = 8$
NIES No.2 Pond sediment	2.37, 2.43	0.43	2.88, 2.94	0.13	3.72 ± 0.26, $n = 4$
NRCC MESS-1 Mar. sed.	0.31, 0.28	< 0.01	0.24, 0.34	0.012	0.348 ± 0.028, $n = 4$

sample was subjected to the ethylation reaction and analyzed following procedure (a) described in the Experimental part. Results in Table 3 were obtained by distillation of 0.5 ml of sediment alkaline digestate and subsequent measurement of MeHg in the distillate. A very good agreement of the results was found between these two methods, especially if the MeHg concentration was > 1 ng g^{-1}.

However, when an aliquot of the alkaline digest was transferred directly into the ethylation reaction vessel (procedure a), a serious matrix interference was observed with increasing volume of the alkaline digested sample taken for analyses. The pH of the mixture in the reaction vessel has to be adjusted to 4.9 with an appropriate volume of buffer. Due to the limited volume that can be taken for analysis, the detection limit was only 0.5 ng g^{-1}. It is well known that this detection limit is insufficient, since in many sediments lower values occur. Additionally, in sediment samples rich in sulphide, determination of MeHg

TABLE 3

Comparison of the results for the determination of MeHg in sediments obtained by different preseparation prior to distillation
[Results are given in ng g^{-1} as Hg, WW ± S.D. for n determinations. An aliquot of HCl leaching solution or alkaline digested sample was distilled as shown in Fig. 1]

Sample code	TOC (%)	4 M HCl leaching	Alkaline digestion	Direct distillation	Total Hg ($\mu g\ g^{-1}$, wet weight)
5	1.1	4.61, 4.94	8.06, 9.48	9.44 ± 0.77, $n = 3$	2.01
17	3.9	6.31 ± 0.42, $n = 8$	9.91, 9.81	10.5 ± 1.5, $n = 4$	0.52
34	4.4	12.1, 12.9	23.1, 22.8	20.4, 24.6	6.72
35	4.2	9.48 ± 0.71, $n = 6$	21.4, 22.8	20.4, 21.8	16.1
1	< 0.1	0.429 ± 0.060, $n = 3$	0.511, 0.435	0.435 ± 0.029, $n = 4$	0.012
4	< 0.1	0.425 ± 0.054, $n = 3$	0.421, 0.398	0.439 ± 0.049, $n = 6$	0.014
6	< 0.1	0.635 ± 0.073, $n = 3$	0.714, 0.674	0.703 ± 0.030, $n = 3$	0.021
Distillation efficiency (%)		88.6 ± 7.2, $n = 7$	95.9 ± 5.2, $n = 6$	99.5 ± 7.6, $n = 6$	

was not possible at all, since sulphide is the most serious interference for the ethylation reaction [13,16]. Even if the concentration of MeHg was higher, compounds that were also released from the alkaline digested sample during ethylation could gradually destroy the Carbotraps. However, not enough systematic experiments were performed to confirm this statement.

The second serious problem associated with procedure a is the presence of a high inorganic Hg concentration. It was observed that the ethylation reagent might induce MeHg from inorganic Hg if it is present at much higher concentrations. This would result in a positive systematic error in determination of MeHg. Induction of MeHg from inorganic Hg using two different ethylating reagent batches is shown in Table 4. Evidently, the amount of MeHg induced from inorganic Hg is dependent on the ethylating reagent quality. In the case of poor ethylation reagent, up to 1% of inorganic Hg could be transformed to MeHg. This is not acceptable, since under the natural conditions the percentage of MeHg in sediments is usually bellow 1.5%. Without taking this effect into account, high systematic errors for MeHg could be obtained. The induction of MeHg is correlated with the amount of inorganic Hg present during the ethylation process. However, the induction is not very reproducible, therefore it is not possible to use correction factors for final calculations. This interference represents a real limitation of using alkaline digestion, especially when samples from Hg contaminated areas are to be analyzed. In such samples inorganic Hg could exceed MeHg by a factor of 10–20 thousand. In order to overcome this problem it is suggested that each batch of the ethylating reagent be checked prior to its use for actual analyses. Distillation is very effective in separating MeHg from inorganic Hg. However, it was observed that in some sediment samples, a fraction of inorganic Hg was also distilled. It is interesting that in some cases inorganic Hg was not distilled even if present in 10000 fold excess, while in some sediment samples it was distilled even if present in much smaller concentration. This indicates that during distillation not only MeHg compounds but also some other "unknown" Hg compounds were distilled, which were later measured as inorganic Hg. It would be of interest to identify the Hg compounds that are also distilled under the conditions used. However, the concentration of inorganic Hg in the distillate was always much lower than before distillation, which provided conditions for accurate quantification of MeHg by aqueous phase ethylation.

Typical chromatograms are shown in Fig. 10. Peak a represents Hg° which is usually a breakdown product of diethyl mercury (derivative of inorganic mercury in the original sample). Breakdown of inorganic Hg to Hg° is mostly caused by the quality of the Carbotrap material. This is discussed in detail in two other publications [15,16]. Evidently the inorganic Hg peak (c) is always present. This peak represents the reagent blank value for inorganic Hg. Blanks for MeHg are very reproducible and very low. Chro-

TABLE 4

Induction of methyl mercury from inorganic mercury during aqueous ethylation phase as a function of different amount of Hg(II) and the ethylating reagent lot

Amount of Hg(II) added to the reaction cell (pg)	Amount of MeHg measured (pg)			
	Ethylation reagent 1		Ethylation reagent 2	
	$X \pm$ S.D. (n) [a]	% of Hg(II) transformed to MeHg	$X \pm$ S.D. (n)	% of Hg(II) transformed to MeHg
0	1.20 ± 0.04 (12)		< 0.3 (21)	
1000	6.36 ± 2.09 (8)	0.63 ± 0.21	0.80 ± 0.28 (4)	0.08 ± 0.03
2500	23.5 ± 5.73 (6)	0.94 ± 0.23	2.51 ± 0.44 (4)	0.10 ± 0.01
10000	33.1, 39.4	0.33, 0.39	8.10, 10.0	0.08, 0.10

[a] X = Mean value; n = number of determinations; S.D. = standard deviation.

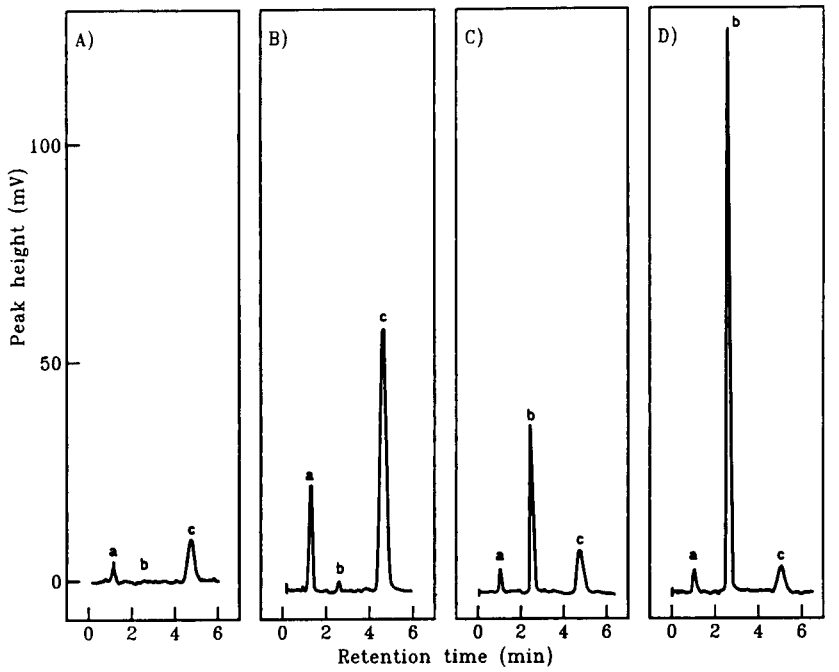

Fig. 10. Typical chromatograms obtained for alkaline digested and distilled sediment sample followed by aqueous phase ethylation, isothermal GC, and CV-AF detection (A) Distillation blank; (B) 50 μl of alkaline digested sample; 1.6 pg of MeHg as Hg; (C) an aliquot of the distillate; 30 pg MeHg as Hg; (D) MeHg standard solution; 100 pg MeHg as Hg. Peaks: a = Hg°; b = $CH_3HgCH_2CH_3$; c = $(CH_3CH_2)_2Hg$.

matogram B was obtained by direct measurement of MeHg in alkaline digested sediment. This sediment contained a relatively low amount of inorganic Hg. In many samples at the same MeHg peak height, inorganic Hg peak would be much higher. Chromatogram C was obtained for the same sediment sample after distillation. Quantification of the MeHg peak in the latter case is much more accurate.

The stability of MeHg in the alkaline digested samples (A, B and C) with time was also checked. Results are shown in Fig. 11. It is evident that the MeHg concentration decreased by 10–20% after 3 days. Its decrease is partly due to decomposition but more probably to readsorption of MeHg onto particles. If alkaline digestates are reheated almost no decrease of MeHg was found, which indicates that the lower MeHg concentration in the alkaline digestates is mostly due to readsorption on particles, rather than decomposition. It is interesting to note that the inorganic Hg peak height decreased significantly with time. After

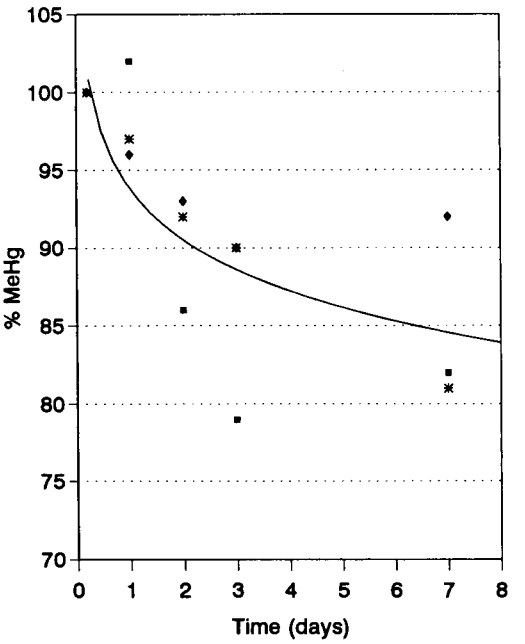

Fig. 11. Stability of MeHg in alkaline digested sediment samples A–C. Key to symbols: ■ = A; ◆ = B; * = C. Solid line = mean.

three days the inorganic Hg peak height decreased by a factor of four. So it would also be possible to overcome interference due to high inorganic Hg concentration during the ethylation phase by analyzing alkaline digested samples after two days. More experiments are certainly necessary before such an approach could be applied for routine analyses. However, we avoided this alternative due to the possible instability of MeHg in alkaline digested samples.

Distillation

Distillation was basically performed in the same way as described in a previous publication [9]. As presented in the scheme in Fig. 1 distillation of MeHg was performed directly from the sediment, from alkaline digested sample and HCl leachates. Comparison of the results is presented in Table 3.

In case when MeHg was distilled from HCl digested samples it was important to check the pH of the distillate before an aliquot is transferred into the ethylation reaction cell. Only 0.5-ml aliquots of the HCl leachates were taken for distillation. No other reagents were necessary for distillation. Larger volumes of the leachates resulted in a low pH (below 2) of the distillate and also in lower results. The pH should be adjusted prior to addition of the ethylating reagent to the reaction cell. Recoveries obtained by distillation of MeHg from HCl leachates were always lower ($88.6 \pm 7.2\%$) than by distillation from the alkaline digested samples or from the sediment directly.

Distillation of MeHg from alkaline digested samples without addition of acid and chloride ions gave very low recoveries ($< 10\%$). An aliquot (usually 0.5 ml) was diluted with deionized water, followed by the addition of sulphuric acid and chloride ions. Distillation of an aliquot of the alkaline digested samples is recommended in cases when the MeHg peak is too low to be measured accurately directly from the alkaline digested solution. Recoveries of spiked MeHg from alkaline digested samples using distillation was more than 90%, which is comparable to recoveries obtained by direct distillation of MeHg from the sample.

TABLE 5

Recovery of methyl mercury obtained by distillation as a function of sulphuric acid and KCl concentrations

Sulphuric acid (M)	KCl (M)	Results	
		ng MeHg g^{-1} as Hg (wet weight)	Spike recovery (%)
0.4	0.007	0.457, 0.420	98.1 ± 4.6, $n = 4$
0.4	0.013	0.412, 0.420	92.4 ± 3.6, $n = 3$
0.4	0.027	0.530, 0.394	94.8, 91.3
0.8	0.027	0.430, 0.375	92.3, 90.1
1.6	0.027	0.428, 0.366	84.5, 88.8
2.4	0.027	0.406, 0.372	83.4, 89.3

Recoveries of spiked MeHg using direct distillation from the sediment sample were consistent and high (more than 90%). It is important to note that spiking should be done just prior to distillation, since spiked MeHg is less stable in acidified sediment sample than MeHg originally present in the sediment. The lower recovery that might be obtained due to decomposition of spiked MeHg is not representative of the recovery of the originally present MeHg.

Recoveries of MeHg by distillation as a function of sulfuric acid and KCl concentration are shown in Table 5. A sediment sample with an MeHg concentration of 0.423 ± 0.044 ng g^{-1} as Hg (wet weight), was analyzed in two independent determinations. Spiked samples were also analyzed in two independent determinations. Recoveries slightly decreased with increased acid and KCl concentration. Concentrations of these two reagents were therefore kept at minimum.

The amount of sediment taken for direct distillation is basically dependent on the MeHg concentration and homogeneity of the sample. Under the analytical set-up in this laboratory 0.5 g of wet sediment was sufficient even for very low MeHg concentrations (< 50 pg g^{-1}). It is important to emphasize again (as with procedure a, Fig. 1, alkaline digestion) that with increased sample weight a larger proportion of inorganic Hg also distilled. In some sediments inorganic Hg was not distilled even if present at a 10000 fold excess, but in some sediments it distilled if present at only a 100 fold excess. The presence of a high

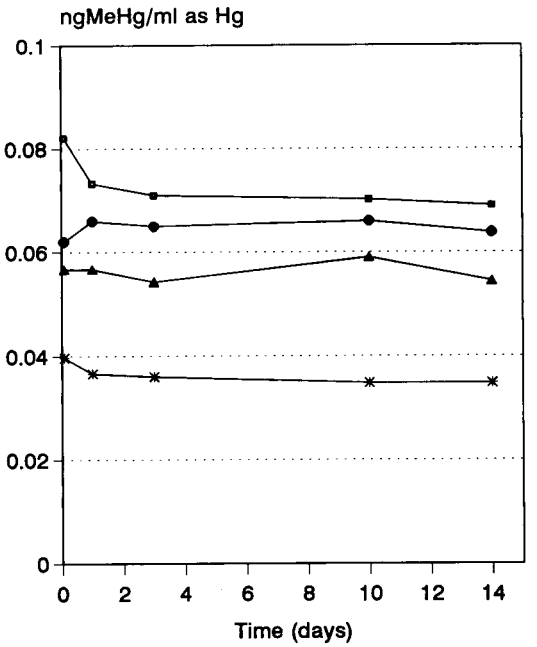

Fig. 12. Stability of MeHg in four different sediment distillates. Key to symbols: ● = 1; ▲ = 2; * = 3; □ = 4.

inorganic Hg concentration in the distillate induced an MeHg peak as described in the section on alkaline digestion. To overcome this problem it is suggested to distill MeHg from a lower sample weight and then take an appropriate aliquot for further processing.

It is also possible to separate inorganic MeHg by ion exchange as described elsewhere [11,23].

The stability of MeHg in the distillate was checked with four sediment distillates. Distillates were stored in the dark at room temperature without addition of any reagents. As evident from Fig. 12 the concentration of MeHg remained constant over a period of two weeks, even though its concentrations were relatively low.

Stability of MeHg in sediment

Total and MeHg in sediment are usually determined in wet samples. Wet/dry weight ratio is determined separately by drying the sediment at 85°C to constant weight. Then the results are expressed on a dry weight basis after correction for this factor. Drying of sediment at 85°C resulted in a 15% decrease of total Hg and a 45% decrease of MeHg, as shown in Table 6. Almost the same decrease was observed with spiked total Hg and MeHg.

Methyl and total Hg are stable in fresh sediments if stored in a refrigerator for up to 1.5 month, or deep frozen for half a year, as shown in Table 7. However, more experiments should be performed on the stability of MeHg under these storage conditions. Unfortunately, lyophilization of sediment samples was not investigated due to unavailability of the equipment. This will be investigated in future experiments.

Dimethyl mercury

Dimethyl mercury (DMM) is also a naturally formed Hg compound in the sediment. Once MeHg is formed, it can be further methylated under certain natural conditions to DMM. This is a very volatile compound, and may diffuse out of the sediment and through the water layer to the

TABLE 6

Losses of total and methyl mercury from sediment during oven drying at 90°C for 48 h
(Analyzes were performed by alkaline digestion. Results are given in ng g^{-1} as Hg)

Species	Wet weight	Dry weight	After drying	%Hg found
Unspiked sediment; 24.3% dry weight				
Total Hg				
Mean	54.2	223	191	85.7
S.D.	4.7	19	12	
n	3	3	2	
Methyl Hg				
Mean	0.42	1.71	0.94	55.3
S.D.	0.07	0.31	0.27	
n	3	3	4	
Spiked sediment; 22.9% dry weight				
Total Hg				
Mean	80.4	351	288	82.1
S.D.	3.05	13	3	
n	3	3	2	
Methyl Hg				
Mean	21.1	92.5	45.3	48.7
S.D.	0.3	1.3	2.6	
n	3	3	4	

Mean-arithmetic mean; SD-standard deviation; n = number of determinations.

atmosphere. DMM can be isolated from sediment simply by aeration. Recently, other analytical techniques for quantitative isolation of DMM have been published [24]. In this work possible presence of DMM was checked by aeration of the sediments and trapping of DMM on the Carbotrap and then measured using the procedure described in the present paper. DMM was not detected in any of the samples checked. However, some experiments were performed with spiked DMM in order to understand its behavior during the isolation procedures used in the present work.

DMM is relatively stable in alkaline media. However, during alkaline digestion at 90°C DMM is volatilized from the digestion vessels. After 6 h of digestion only about 20–30% of spiked DMM remained in the sample.

DMM spiked to the sediment sample was immediately converted to MeHg, if acidified by hydrochloric acid. If the sample was acidified with 2 M sulphuric acid, this conversion was much slower. In 2 h about 30% of DMM was converted to MeHg. In the case of the distillation isolation procedure, the sulphuric acid concentration used was much lower (0.4 M) and it was added just before the distillation. So, DMM was not converted to MeHg. It was aerated from the sample and the distillate solutions. In Table 8 it is shown that only 0.001–0.05% of spiked DMM was transformed to MeHg during the distillation process. Evidently, this conversion is dependent on the concentration of sulphuric acid. This experiment supports the conclusion that a low acid concentration should be used, additionally the use of sulphuric acid is also preferable to hydrochloric acid in order to prevent conversion of DMM in sediments (if present) to MeHg.

TABLE 7

Stability of methyl mercury in wet sediments stored in refrigerator or deep freezer
(Results are given in ng g^{-1} as Hg)

Deep freezer, −18 to −22°C		
Sample code	May, 1991 (alkaline digestion)	Dec., 1991 (distillation)
5A	7.06	7.05, 6.23
11A	15.7	16.6, 16.7
42A	7.01 ± 0.08, $n = 3$	7.18, 6.61
Refrigerator, 0 to 2°C		
Sample code	Dec. 17, 1991 (distillation)	Feb. 5, 1991 (distillation)
5	9.36 ± 0.72, $n = 3$	10.2 ± 1.19, $n = 3$
17	10.4, 9.88	11.2, 11.1
35	20.3, 21.3	22.2, 17.2

TABLE 8

Transformation of dimethyl mercury (DMM) to methyl mercury during the distillation

Sulphuric acid (M)	DMM transformed to methyl mercury (%)
0.04	0.001, 0.009
0.8	0.03, 0.02
1.6	0.05, 0.04

Conclusions

The results obtained in this study represent an important contribution toward better accuracy of results for MeHg in sediment, which is one of the most important compartments in the study of the origins of the MeHg in the natural environment. Distillation is a simple and specific isolation procedure for MeHg. As pointed out in previous studies, it can be followed by specific GC-ECD or by nonspecific CV-AAS. This study has shown that distillation is also a very suitable separation technique when followed by aqueous phase ethylation, isothermal chromatography and CV-AF detection. Its main advantage is avoidance of matrix interferences which often represent a limitation with other separation techniques, especially when low MeHg levels are to be determined. By implementation of the distillation technique more accurate results with better precision and detection limit could be obtained.

Leaching experiments with HCl have shown that HCl alone can not release MeHg from sediment quantitatively. The amount of the Hg released from the sediment is strongly correlated with %TOC. This suggests that the fraction released might have a certain significance in studies of the biogeochemical cycle of Hg. More studies should certainly be done in this respect.

On the other hand, experiments with HCl leaching have clearly demonstrated that standard addition experiments are not sufficient to ensure the accuracy of the analytical procedure. Very good and reproducible recoveries of spiked MeHg do not assure that the MeHg fraction bound to sediment will be released in the same way. This should be of particular concern to laboratories that still use HCl leaching followed by extraction of methyl mercury into an organic solvent.

This paper again stresses the urgent need for certifying sediment reference materials for MeHg. This would be of great importance for laboratories that have just started this kind of analysis, as well as those that have long-term experience in this matter. The time has come for the producers of reference materials to certify MeHg in any new material. It is also suggested that reference materials that have already been certified for total Hg should be recertified for MeHg, especially if they are still available in larger stocks. A step in this direction was recently taken [14].

Thanks are due to the Research Community of Slovenia for partial funding this work and EPRI through Contract No. RP-2020-10. Special thanks are also due to C. Gilmour and G. Riedl from the Academy of Natural Sciences, Benedict, USA and S. Padberg from KFA, Julich, Germany for providing data for intercomparison of the results for MeHg in RMs. Most of the experimental work presented in this paper done at Brooks Rand, Seattle, WA, USA special thanks are therefore also due to all co-workers at Brooks Rand. Thanks are also due to A.R. Byrne for useful suggestions and corrections of the present paper.

REFERENCES

1 P.J. Craig and P.D. Bartlett, Nature (London), 275 (1978) 635.
2 G. Westöö, Acta Chim. Scand., 21 (1967) 1790.
3 Y. Takizava and T. Kosaka, Acta Med. Biol. Niigata, 14 (1966) 153.
4 J.E. Longbottom, R.C. Dressman and J.C. Lichtenberg, J. Assoc. Off. Anal. Chem., 56 (1973) 1297.
5 J.F. Uthe, J. Solomon and B. Grift, J. Assoc. Off. Anal. Chem., 55 (1972) 583.
6 M. Floyd, L.E. Sommers, Anal. Lett., 8 (1975) 523.
7 H. Nagase, Y. Ose, T. Sato and T. Ishikawa, Interim. Environ. Anal. Chem., 13 (1987) 153.
8 M. Horvat, K. May, M. Stoeppler and A.R. Byrne, Appl. Organomet. Chem., 2 (1988) 515.
9 V. Zelenko and L. Kosta, Talanta, 20 (1973) 115.
10 I. Gvadjancic, L. Kosta and V. Zelenko, Zh. Anal. Khim., 32 (1978) 812.
11 S. Padberg and K. May, in Rossbach, Schladot and Ostapczuk (Eds.), Specimen Banking, Springer Verlag, Berlin, Heidelberg, 1992.
12 Y. Talmi, Anal. Chim. Acta, 74 (1975) 117.
13 N.S. Bloom, Can. J. Fish. Aquat. Sci., 46 (1989) 1131.
14 M. Horvat, Water, Air Soil Pollut., 56 (1991) 95.
15 L. Liang, M. Horvat and N.S. Bloom, Talanta, (1992) in press.
16 L. Liang, M. Horvat and N.S. Bloom, Clin. Chem., (1992) submitted for publication.
17 S. Rapsomanikis, O.X.F. Donard and J.H. Weber, Anal. Chem., 58 (1985) 35.
18 N.S. Bloom and W.F. Fitzgerald, Anal. Chim. Acta, 209 (1988) 151.
19 N.S. Bloom and E. Crecelius, Mar. Chem., 14 (1983) 49.
20 L. Liang and N.S. Bloom, Presentation at the Internatinal Conference on Mercury as a Global Pollutant, Monterey, June, 1992.
21 M. Horvat, A.R. Byrne and K. May, Talanta, 37 (1990) 207.
22 M. Hempel, H. Hintelman and R.D. Wilken, Analyst, 117 (1992) 669.
23 K. May, M. Stoeppler and K. Reisinger, Toxicol. Environ. Chem., 13 (1987) 153.
24 F. Baldi and M. Filippelli, Environ. Sci. Technol., 25 (1992) 302.

Analytica Chimica Acta, 281 (1993) 153–160
Elsevier Science Publishers B.V., Amsterdam

Investigation of extraction and back-extraction behaviour of platinum(IV) with rubeanic acid in tributyl phosphate, with tributyl phosphate and with thenoyltrifluoroacetone in *n*-butyl alcohol–acetophenone by means of platinum-191 radiotracer for platinum-enrichment purposes

M. Parent, R. Cornelis and R. Dams

Laboratory of Analytical Chemistry, Institute for Nuclear Sciences, University of Ghent, Proeftuinstraat 86, B-9000 Ghent (Belgium)

F. Alt

Institut für Spektrochemie und Angewandte Spektroskopie, Bunsen-Kirchoff-Strasse 11, D-4600 Dortmund (Germany)

(Received 17th December 1992; revised manuscript received 23rd February 1993)

Abstract

Using ^{191}Pt radiotracer, the liquid–liquid extraction behaviour of Pt(IV) from HCl medium with rubeanic acid in tributyl phosphate (TBP), with tributyl phosphate and with thenoyltrifluoroacetone (TTA) in *n*-butyl alcohol–acetophenone was examined. The effects of acidity, shaking time and Pt concentration were studied, in addition to the subsequent back-extraction. Optimum extraction recoveries were found when using 3 M HCl for TBP and 4 M HCl for TTA. Ammonia solution (2 M) yielded the best recovery for back-extraction. In order to evaluate the procedure in the presence of a matrix, some biological and environmental materials were spiked with ^{191}Pt and the recovery of the radiotracer in the different steps was investigated.

Keywords: Radiochemical methods; Extraction; Platinum

The determination of small amounts of Pt in biological and environmental samples has become a primary concern since the introduction of Pt-containing catalysts in automobile exhaust systems. Although there are strict requirements on durability, the emission of small amounts of Pt, estimated at 1 μg km^{-1} is unavoidable [1,2]. So far, dose–response relationships for platinum have remained unknown, but caution is recommended. To check the accumulation of Pt in the environment it is necessary to establish precise and accurate Pt background levels in a range of materials. These will probably occur at the ng kg^{-1} level.

Because the amount of Pt in environmental samples is extremely small, the development of procedures for its determination is a great challenge. The most effective way to obtain very low detection limits is to develop a procedure consisting of a digestion, isolation and preconcentration and detection of the Pt. Several techniques have

Correspondence to: R. Dams, Laboratory of Analytical Chemistry, Institute for Nuclear Sciences, University of Ghent, Proeftuinstraat 86, B-9000 Ghent (Belgium).

been applied to determine platinum, including neutron activation analysis (NAA) [3,4], x-ray fluorescence (XRF) [5], inductively coupled plasma mass spectrometry (ICP-MS) [6,7] and the most popular, graphite furnace atomic absorption spectrometry (GFAAS) [7–9]. The detection limits for these techniques are, however, insufficient to measure background levels of Pt, so preconcentration is necessary, which can be performed with extractions. A variety of extraction methods have been reported for the determination of platinum [9–14]. However, Wood and Vlassopoulos [7] investigated many different published extraction methods and concluded that none of them are as good or as reproducible as claimed. Radiotracer studies would be very helpful in optimizing extraction procedures owing to the ease of monitoring the ^{191}Pt activity during digestion and separation.

The first condition for a radiotracer is that it should behave in exactly the same way as the nuclides it characterizes. It should also possess an adequate half-life and, for ease of detection, be a γ-emitter.

Because the concentration of Pt is very low in most materials, a radiotracer with a high specific activity is required. Addition of large amounts of inactive platinum carrier would create non-representative conditions.

After digestion and subsequent treatment with aqua regia and HCl, Pt is present as Pt(IV) (H_2PtCl_6). It is preferable to extract this Pt(IV) without addition of reducing agents, which are liable to co-extract and interfere with the detection of the element.

In this work, Pt was extracted as Pt(IV) with rubeanic acid (dithiooxamide) in tributyl phosphate (TBP) [15], with tributyl phosphate [16] and with thenoyltrifluoroacetone (TTA) [17] in *n*-butyl alcohol–acetophenone from HCl followed by subsequent back-extraction with ammonia solution (hereafter referred to as NH_3). Losses during the extraction could be corrected for by means of isotope dilution mass spectrometry. In order to evaluate the procedure in the presence of a matrix, the extraction behaviour of Pt in ^{191}Pt-spiked materials (liver, leek and soil) was also investigated.

EXPERIMENTAL

Reagents

All reagents were of analytical-reagent grade unless indicated otherwise. Water purified using a Milli-Q system (Millipore) was used throughout.

^{191}Pt ($t_{1/2}$ = 71.04 h) was prepared by neutron activation of Pt enriched in ^{190}Pt to 4.19% (purchased from Oak Ridge National Laboratory). A 1-μg amount was irradiated as H_2PtCl_6 at a flux of 2×10^{14} n cm^{-2} s^{-1} in the BR2 reactor in Mol for 4 days. The compound was dissolved in aqua regia and, after evaporation of HNO_3, the solution was diluted with 3 M HCl to give a ^{191}Pt tracer solution containing 10 μg Pt l^{-1}.

TBP (UCB, 98%) was pre-equilibrated with 3 M HCl (equal volumes) for 30 min. Rubeanic acid (UCB) was dissolved in ethanol to give a 0.1% (w/v) solution.

A 0.15 M TTA (Fluka, purum) solution in *n*-butyl alcohol (UCB) was prepared, with addition of HCl so the overall concentration was 1 M. Acetophenone was purchased from Merck.

Apparatus

The activity of the 539-keV peak of ^{191}Pt in the aqueous and organic phases was measured with a Ge(Li) detector (efficiency = 25%, FWHM = 1.9 keV), coupled to a 4000-channel analyser.

Extraction

In each experiment 10 ml of aqueous and 10 ml of organic phase were used, unless stated otherwise. Both phases were shaken for 15 min with a motor-driven whirl stirrer.

To a Pt(IV) solution in HCl, 1 ml of rubeanic acid was added and stirred for 1 min to allow formation of the complex, which was then extracted into 10 ml TBP. Pt(IV) was extracted with 100% TBP solution. The Pt(IV) solution was made up to 4 M HCl and extracted with a mixture of 6.5 ml of 0.15 M TTA in *n*-butyl alcohol and 3.5 ml of acetophenone.

Back-extraction

A 10-ml volume of an aqueous solution was added to the organic phase and shaken for 15 min.

Sample decomposition

Acid digestion in open vessels was applied to all three matrices.

Soil. About 200 mg of sandy soil were weighed in a PTFE beaker. The sample was heated with 10 ml of HNO_3 at about 70°C for ca. 3 h, 5 ml of $HClO_4$ were added and the solution was heated at 120°C overnight. Volumes of 5 ml each of HNO_3, $HClO_4$ and HF were added, heating was continued at 70°C for 24 h and the solution was evaporated nearly to dryness. The residue was dissolved by adding 5 ml each of HNO_3, HCl and HF followed by heating at 70°C for 24 h. The solution was evaporated nearly to dryness several times to remove HF and HNO_3, with dissolution of the residue in HCl, until a clear solution was obtained. The contents of the vessel were transferred quantitatively into the extraction vessel and diluted to 10 ml so the required molarity of HCl for extraction was obtained.

Liver and dried leek. About 200 mg were weighed in a quartz vessel (liver) or in a PTFE beaker (leek), 1 ml of HNO_3 and 0.1 ml of $HClO_4$ were added and the solution was gradually heated to 140°C over a period of 1 h. After addition of 1 ml of HNO_3 and 0.2 ml $HClO_4$, the temperature was increased to 170°C. Again, 1 ml HNO_3 and 0.2 ml of $HClO_4$ were added and the solution was heated to 200°C and evaporated nearly to dryness. Dried leek needed a subsequent treatment with concentrated HF. The residue was dissolved in aqua regia and the solution was evaporated nearly to near dryness several times to remove HF and HNO_3, with dissolution of the residue in HCl, until a clear solution was obtained. The contents of the vessel were transferred quantitatively into the extraction vessel and diluted to 10 ml so that the required molarity of HCl for extraction was obtained.

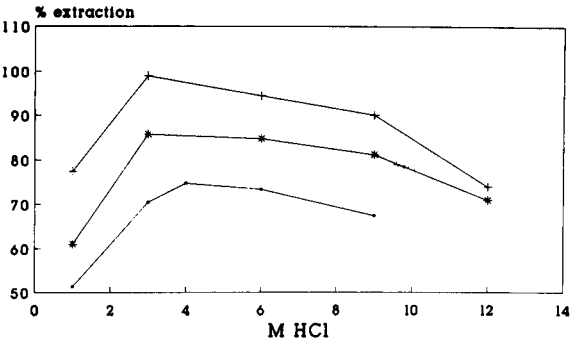

Fig. 1. Extraction of Pt (∗) with rubeanic acid in TBP, (+) with TBP and (●) and TTA as a function of hydrochloric acid concentration.

RESULTS AND DISCUSSION

Influence of the acidity of the aqueous phase on the extraction yield

Each experiment was performed in triplicate. The organic and aqueous phases were both measured in order to determine the total recovery of ^{191}Pt. Acidities of 1, 3, 6, 9 and 12 M HCl were investigated for TBP and TBP + rubeanic acid; for TTA, 4 M HCl was also examined, but not 12 M, because of the total miscibility of the two phases. With 9 M HCl the phases separated very slowly, so > 6 M HCl is not recommended.

TABLE 1

Influence of shaking time on the ^{191}Pt recovery [recovery in the organic phase (O) and total recovery (Σ)] with rubeanic acid in TBP, with TBP and with TTA ($n = 3$)

Shaking time (min)	TBP + rubeanic acid (3 M HCl)		TBP (3 M HCl)		TTA (4 M HCl)	
	$O \pm$ S.D. (%)	$\Sigma \pm$ S.D. (%)	$O \pm$ S.D. (%)	$\Sigma \pm$ S.D. (%)	$O \pm$ S.D. (%)	$\Sigma \pm$ S.D. (%)
5	87.5 ± 0.4	101.9 ± 0.7	90.8 ± 1.6	100.9 ± 2.3	77.6 ± 1.7	95.6 ± 1.2
10	86.0 ± 0.7	100.0 ± 1.1	91.6 ± 1.6	102.3 ± 1.7	73.1 ± 3.0	99.0 ± 1.0
15	87.6 ± 1.0	100.9 ± 0.4	91.6 ± 1.0	101.0 ± 1.0	74.8 ± 1.5	100.3 ± 1.2
30	87.0 ± 4.6	96.8 ± 3.5	91.7 ± 1.2	102.1 ± 0.3	74.4 ± 2.1	98.9 ± 1.7
60	84.3 ± 0.9	95.0 ± 3.2	90.7 ± 0.9	100.6 ± 0.6	77.3 ± 2.3	101.4 ± 2.4

The mean results for the three media are shown in Fig. 1; 3 M HCl is considered the optimum acidity because of the high extraction yield of Pt for TBP and TBP + rubeanic acid, whereas 4 M HCl gives the best Pt recovery for TTA extraction. In all instances the total recovery of ^{191}Pt for both phases appears to be about 100%.

Influence of shaking time

The shaking time was varied between 5 min and 1 h. Each experiment was performed in triplicate. In each instance the organic and aqueous phases were measured and the total recovery was calculated. The mean values of the ^{191}Pt recovery in the organic phase (O) and the total recovery (Σ) for the three media are given in Table 1. The shaking time appears to exert no influence on the ^{191}Pt extraction yield. The recovery of Pt is very reproducible and the total recovery is nearly 100%.

Influence of the TTA / acetophenone ratio on the ^{191}Pt recovery

Volume ratios of 0.15 M TTA (n-butyl alcohol) to acetophenone between 9:1 and 1:9 were investigated. Pure TTA solution and acetophenone were not considered, because in the former instance the two phases were totally miscible, and in the latter the complexing agent is absent. Each experiment was performed in triplicate and the means of the results are plotted in Fig. 2. As can be seen, a ratio of 3:7 for 0.15 M TTA to acetophenone gives the best recovery (89%).

Influence of the Pt concentration on the extraction yield

The influence of the Pt carrier concentration on the extraction yield was investigated in the three different media. Amounts of 10, 1 and 0.1 ng of radiolabelled Pt were added to the aqueous phase. Each experiment was performed in triplicate. Because the ^{191}Pt activity was very low with 0.1 ng of Pt, gamma counting was performed with an NaI detector. The mean values of these experiments are plotted in Fig. 3. No significant influence was observed. The results of the three different concentrations were reproducible within a range of 10% and a Pt recovery > 90% in TBP was obtained.

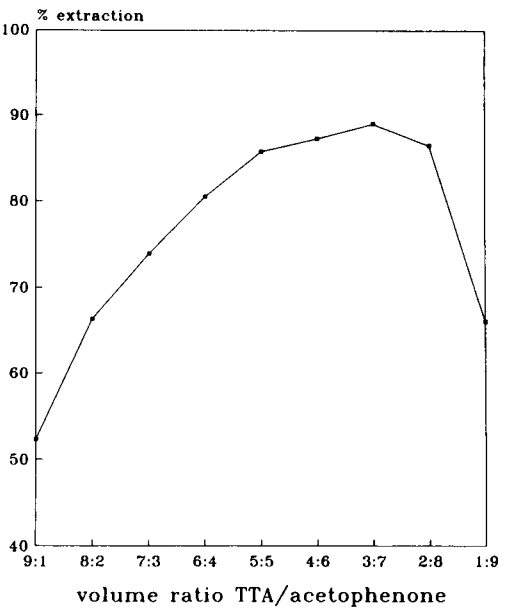

Fig. 2. Influence of TTA/acetophenone ratio on the ^{191}Pt recovery.

Experimental determination of the extraction coefficient by varying the volume of the organic phase

The extractions were very reproducible and the total recovery was almost always 100%. An

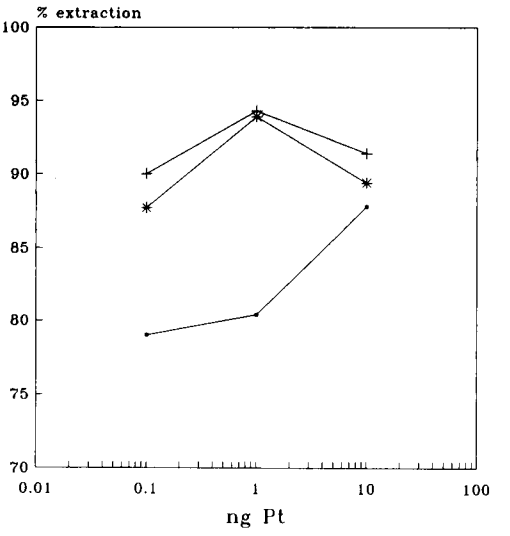

Fig. 3. Influence of Pt carrier concentration on the extraction yield. ■ = TTA; + = TBP; * = TBP + rubeanic acid.

TABLE 2

Experimental determination of the extraction coefficient (E) for TBP by varying the volume of the organic phase (v_0) ($n = 3$) [a]

v_0	$O \pm$S.D. (%)	$A \pm$S.D. (%)	$\Sigma \pm$S.D. (%)	$E \pm$S.D.
2	75.0±3.1	20.9±1.9	95.8±2.4	17.9±0.1
4	86.2±2.2	11.8±0.2	97.9±2.4	18.2±0.1
6	91.2±1.5	8.4±0.8	99.5±1.4	18.1±0.1
8	91.7±1.8	6.9±0.4	98.6±1.6	16.6±0.1
10	91.4±2.2	5.6±0.3	97.0±2.4	16.3±0.1

[a] Recoveries in the organic phase (O) and aqueous phase (A) and total recovery (Σ). The aqueous phase is 3 M HCl.

TABLE 3

Experimental determination of the extraction coefficient (E) for TTA by varying the volume of the organic phase (v_0) ($n = 3$) [a]

v_0	$O \pm$S.D. (%)	$A \pm$S.D. (%)	$\Sigma \pm$S.D. (%)	$E \pm$S.D.
2	47.8±2.9	54.3±0.9	102.1±3.1	4.0±0.1
4	61.6±1.2	41.2±1.3	102.8±1.7	3.7±0.1
6	69.7±3.4	34.7±1.0	104.5±3.1	3.4±0.1
8	74.4±1.0	26.9±0.6	101.3±1.5	3.5±0.1
10	75.9±2.3	23.0±1.3	98.9±1.4	3.3±0.1

[a] Recoveries in the organic phase (O) and aqueous phase (A) and total recovery (Σ). The aqueous phase is 4 M HCl.

attempt was made to determine the extraction coefficient (E) of Pt with TTA and TBP by varying the volume of the organic phase between 2 and 10 ml, increasing in increments of 2 ml. For the TTA extraction the volume ratio of 0.15 M TTA to acetophenone was held at 1.0. Each experiment was performed in triplicate. Each time the sum of the activities in the aqueous and organic phases was checked. The mean values with standard deviations for Pt in the organic phase (O) and for the total recovery (Σ) are given together with the extraction coefficient in Tables 2 and 3 for TBP and TTA respectively.

The value of E was calculated using the following extraction equation:

$$Y = \left\{1 - \left[\frac{1}{1 + (v_0/v_a)E}\right]^n\right\} \times 100\%$$

where Y = extraction yield (experimental percentage recovery in the organic phase), v_0 = volume of the organic phase, v_a = volume of the aqueous phase and n = number of extractions, on the basis of the experimental value for Y (mean of three replicates). Resolving this equation for E (with $n = 1$) leads to

$$E = \frac{Y}{100 - Y} \cdot \frac{v_a}{v_0}$$

The percentage of ^{191}Pt as measured in the aqueous phase was used to describe the factor $100 - Y$.

The mean value for the extraction coefficient of Pt in TBP is $E = 17.4 \pm 0.9$, which yields an acceptable recovery. The extraction coefficient for TTA is much lower ($E = 3.7 \pm 0.4$), although after two successive extractions a recovery of ca. 94% could be obtained.

TABLE 4

Back-extraction of ^{191}Pt from TBP + rubeanic acid in different media ($n = 1$) [a]

Original HCl concentration (M)	Back-extraction					
	1.4 M HNO_3		5% $HClO_4$		3 M NaOH	
	A (%)	Σ (%)	A (%)	Σ (%)	A (%)	Σ (%)
1	32.3	100.7	29.9	96.5	87.2	100.8
3	46.7	100.0	3.0	93.5	84.6	100.6
9	48.3	98.7	55.6	102.1	24.3	97.9
12	61.8	100.8	64.5	103.8	82.8	93.9
	2% $HClO_4$		3 M NH_3		6 M NH_3	
	A (%)	Σ (%)	A (%)	Σ (%)	A (%)	Σ (%)
6	31.9	99.1	53.1	102.6	48.2	105.3

[a] Recovery in aqueous phase (A) and total recovery (Σ).

Back-extraction of Pt

Because a variety of detection methods require aqueous solutions (e.g., ICP-MS), Pt must be "stripped" from the organic phase. This is possible either by evaporation of the organic phase in presence of a small volume of acid or by back-extraction into an aqueous phase. For the latter several possibilities can be considered: acidification of the aqueous phase; addition of a complexing agent, which forms charged unextractable complexes; or destruction of the chelate by addition of HNO_3 or $HClO_4$.

Because the complex had already been extracted from an acidic medium, two possibilities were explored: a first attempt consisted in destroying the complex with oxidizing agents and a second in re-extracting Pt in alkaline medium. In each instance the organic (O) and aqueous (A) phase recoveries were measured and the total recovery (Σ) calculated.

Back-extraction from TBP + rubeanic acid. Back-extraction was performed with oxidizing acids in order to decompose the complex. A 1.4 M HNO_3 and a 2% $HClO_4$ solution were used. The results are given in Table 4. As the back-extractions are not quantitative, other medium was investigated (see Table 4); 3 M NaOH gave the best results, but is not suitable for ICP-MS because of the large input of unwanted Na^+ ions. As the ultimate detection will be done with this technique, the amount of salts should be reduced as much as possible. These results, however, indicate that an alkaline solution is suitable. Ammonia solution is preferred because no interfering elements are introduced for the Pt measurement. In this extraction Pt(IV) is reduced to Pt(II) by rubeanic acid and the much more stable Pt(II) complex is extracted to TBP. The high stability of the Pt(II) complex hinders the back-extraction into NH_3. An additional factor for the less successful back-extraction recoveries when using NH_3 may be that this weak base does not sufficiently neutralize the organic phase.

Back-extraction from TTA. Again different media (1.4 M HNO_3, 2% $HClO_4$ and 2 M NH_3) were investigated in order to find the optimum parameters for back-extraction. The results of these experiments are given in Table 5. The yield

TABLE 5

Back-extraction of ^{191}Pt from TTA in different media ($n = 1$) [a]

Original HCl concentration (M)	Back-extraction					
	1.4 M HNO_3		2% $HClO_4$		2 M NH_3	
	A (%)	Σ (%)	A (%)	Σ (%)	A (%)	Σ (%)
0.5	67.7	91.4	84.5	96.6	63.8	97.4
1	71.4	96.1	84.1	95.1	63.9	99.8
3	64.6	91.7	79.0	94.7	74.4	93.8
4	62.3	96.3	72.0	97.6	79.1	94.0
6	57.6	104.3	65.1	95.1	60.2	94.7
9	58.9	104.4	54.3	111.0	26.6	125.4

of the back-extraction depends on the original HCl acidity from which Pt was extracted, as can be seen in Table 5. NH_3 is preferred because the recovery of Pt is highest when considering 4 M HCl. These results can be improved by a second extraction of the organic phase. It appeared, however, that some of the organic material, presumably from TTA, is also extracted into 2 M NH_3. This showed up later during ICP-MS measurements of in-active Pt, where the organic residue present in the NH_3 solution drastically reduced the detection signal.

The influence of the molarity of the NH_3 solution was also investigated. The recovery was found to be greatest when extracting with 1 M NH_3.

Back-extraction from TBP. The influence of the molarity of NH_3 solution and the addition of a complexing agent to the aqueous phase to enhance the back-extraction was investigated. Five series were prepared with 2, 3 and 4 M NH_3 and 2 and 3 M NH_3 containing 10 mg l^{-1} EDTA. The back-extraction was performed twice and for each series three replicates were carried out. The results are given in Table 6. The molarity of NH_3 solution has virtually no influence on the back-extraction. No enhancement could be observed after addition of a complexing agent.

Extraction and back-extraction in the presence of a matrix. Because the destruction is performed in open vessels, possible losses due to spattering or adsorption on the vessel may occur. Therefore, the Pt content of the digested material was checked before extraction. The vessel was always cleaned with several portions of HCl. The loss of

TABLE 6

Influence of the molarity of NH_3 solution and the addition of a complexing agent on the back-extraction of Pt from TBP ($n = 3$) [a]

NH_3 (M)	$A \pm$S.D. (%)	$\Sigma \pm$S.D. (%)
2	87.3 ± 0.9	99.1 ± 0.8
3	89.1 ± 2.3	102.0 ± 2.9
4	90.3 ± 1.3	103.0 ± 1.5
2 + EDTA	87.3 ± 2.3	100.0 ± 3.1
3 + EDTA	93.2 ± 7.1	107.0 ± 8.3

[a] Recovery in aqueous phase (A) after two successive extractions and total recovery (Σ). Original concentration HCl = 3 M.

Pt during digestion and through adsorption on the walls of the vessel (glass, quartz or PTFE) was measured and appeared to be less than 1%. The actual loss is, probably even lower, however, because the counting geometry of the vessels and the ^{191}Pt reference in a counting vial were different.

To check whether the recoveries remain the same in presence of a matrix, soil, liver and plant materials were spiked with ^{191}Pt solution, mineralized and extracted. The overall recovery of Pt after this procedure was examined. The results of the extraction and back-extraction for the three media and the three matrices are given in Table 7. Every experiment was performed in triplicate. Each extraction and each back-extraction consisted of two repetitions. As can be seen from Table 7, the overall recovery was 75–81% with extraction from TBP and back-extraction with 2 M NH_3. For TTA, the overall recovery was less satisfactory, but acceptable when correction was possible with isotope dilution. Those recoveries are similar to those obtained without a matrix. Because of the poor back-extraction from TBP + rubeanic acid, this medium is not suitable for the determination of Pt at very low levels.

Conclusion

The overall recovery increases when extraction and back-extraction are performed twice. Extraction with TBP and back-extraction with 2 M NH_3 gave recoveries of almost 90% for solutions with and without a matrix. The molarity of NH_3 solution does not seem to influence the back-extraction from TBP. This recovery is acceptable when isotope dilution is applied, as possible losses during the procedure are accounted for.

The overall recovery with TBP + rubeanic acid is not suitable for the determination of Pt at trace or ultratrace levels, because of the very poor back-extraction with NH_3.

The residue of the acids used for the digestion of soil decreases the recovery of Pt with TBP. The same decrease is found when adding $HClO_4$ and/or HF to solutions without a matrix. This is probably due to extraction of those acids with TBP, with an adverse effect on the Pt complexation [18].

The authors are grateful to Professor G. Tölg (Institut für Spektrochemie und angewandte Spektroskopie, Dortmund, Germany) for promot-

TABLE 7

Total recovery of ^{191}Pt after extraction with TBP, TTA and TBP + rubeanic acid and back-extraction with 2 M NH_3 in the presence of a matrix

Medium	Matrix	Extraction ± S.D. (%)	Back-extraction ± S.D. (%)	Overall recovery ± S.D. (%)
TBP (3 M HCl)	Liver	83.6 ± 5.4	96.6 ± 5.4	81.0 ± 9.4
	Plant	89.7 ± 0.4	83.8 ± 2.2	75.2 ± 1.7
	Soil	29.9 ± 12.5	87.9 ± 13.3	26.9 ± 13.2
TTA (4 M HCl)	Liver	69.4 ± 5.6	66.7 ± 1.1	58.0 ± 2.4
	Plant	87.2 ± 3.2	80.7 ± 1.2	70.4 ± 1.7
	Soil	70.6 ± 2.2	89.5 ± 4.8	63.2 ± 4.5
TBP + rubeanic acid (3 M HCl)	Liver	86.4 ± 2.1	67.2 ± 4.4	58.0 ± 2.4
	Plant	86.7 ± 1.3	47.1 ± 7.5	40.7 ± 5.9
	Soil	92.0 ± 0.8	13.7 ± 5.9	12.3 ± 5.4

ing this work. They also acknowledge with gratitude the financial support of the National Fund for Scientific Research and of the German Ministry of Research and Technology (scientific project "Edelmetallemissionen").

REFERENCES

1 V.F. Hodge and M.O. Stallard, Environ. Sci. Technol., 20 (1986) 1058.
2 H.P. König, R.F. Hertel, W. Koch and G. Rosner, Atmos. Environ., 26A (1992) 741.
3 R. Zeisler and R.R. Greenberg, J. Radioanal. Chem., 75 (1982) 27.
4 P.S. Tjioe, K.J. Volkers, J.J. Kroon and J.J.M. De Goeij, Int. J. Environ. Anal. Chem., 17 (1984) 13.
5 Yu. A. Zolotov, O.M. Petrukhin, G.I. Malofeeva and E.V. Marcheva, Anal. Chim. Acta, 148 (1983) 135.
6 O. Nygren and G.T. Vaughan, Anal. Chem., 62 (1990) 1637.
7 S.A. Wood and D. Vlassopoulos, Anal. Chim. Acta, 229 (1990) 227.
8 F. Alt, U. Jerono, J. Messerschmidt and G. Tölg, Microchim. Acta, III (1988) 299.
9 A. Simonsen, Anal. Chim. Acta, 49 (1970) 368.
10 M.A. Khattak and R.J. Magee, Talanta, 12 (1965) 733.
11 P. Vest and M. Schuster, Fresenius' Z. Anal. Chem., 339 (1991) 142.
12 S.J. Al-Bazi and A. Chow, Talanta, 31 (1984) 815.
13 Z. Marczenko, S. Kús and M. Mojski, Talanta, 31 (1984) 959.
14 M. Mojski, Talanta, 25 (1978) 163.
15 K. Brajter and U. Kozicka, Talanta, 26 (1979) 417.
16 T. Ishimori, K. Watanabe and E. Nakamura, Bull. Chem. Soc. Jpn., 33 (1960) 636.
17 A.K. Dé and M.S. Rahaman, Analyst, 89 (1964) 795.
18 A.K. Dé and S.M. Khopkar, in R.A. Chalmers (Ed.), in Solvent Extraction of Metals, Van Nostrand Reinhold, London, 1970, p. 172.

Analytica Chimica Acta, 281 (1993) 161–171
Elsevier Science Publishers B.V., Amsterdam

Qualitative and quantitative mixture analysis by library search: infrared analysis of mixtures of carbohydrates

K. Meyer, M. Meyer, H. Hobert and I. Weber

Institut für Physikalische Chemie, Friedrich-Schiller-Universität Jena, Lessingstr. 10, O-6900 Jena (Germany)

(Received 22nd September 1992; revised manuscript received 1st March 1993)

Abstract

A method for automatic qualitative mixture analysis and the evaluation of the relative composition of the mixtures using the library search system SUSY is described. The method makes use of a library of reference spectra and their peak tables. The components in a mixture are identified and quantified by a combination of a special comparison of peak tables and a linear regression. The method was developed to analyse solid mixtures prepared as KBr pellets containing only a few compounds from a great number of possible constituents. It was tested with 91 two- and three-component mixtures of nine different carbohydrates. Using a corresponding library of reference spectra, the method can be applied to any kind of mixture spectra if there are only small differences between the band positions of the pure and the mixed components.

Keywords: Infrared spectrometry; Carbohydrates; Library search systems

The rapid and automatic qualitative and quantitative analysis of complex mixtures with variable constituents is of increasing interest in infrared spectrometry. There are several approaches for computer-assisted mixture analysis, e.g., methods based on linear regression, principal component analysis, pattern recognition procedures, knowledge-based or expert systems and library search methods. If the number of constituents is constant and every mixture is composed of the same components, a quantitative analysis is relatively simple and can be performed with the classical least-squares procedure, principal component regression or partial least-squares analysis [1–5].

Correspondence to: K. Meyer, Institut für Physikalische Chemie, Friedrich-Schiller-Universität Jena, Lessingstr. 10, O-6900 Jena (Germany).

However, these methods fail if there are more reference spectra than real components of the mixture and the spectra of the mixtures are impaired by background, interactions between the components and effects of particle size and sample preparation. Osten and Kowalski [6] reported that in such instances additional (false-positive) compounds are detected in the mixture with non-negligible amounts and the quantitative analysis becomes erroneous. These problems should be considered especially if solid samples are analysed using the KBr pellet technique [7,8]. In the more difficult case of an unknown qualitative composition, the components are identified incorrectly because their presence is derived from the analysed amount for each of the components. The tendency of the regression methods to identify false-positive components can be decreased

by constraining non-negative concentrations and residual spectra. Hong-kui et al. [9] proposed two iterative least-squares fitting procedures for the identification and quantification of organic vapour mixtures. However, the successful application of such methods requires that the Beer–Lambert law is followed and a correct baseline model is assumed.

On the other hand, knowledge-based systems are used not only for structural interpretation of infrared spectra but also for qualitative mixture analysis [10–15]. Hesse et al. [10] proposed an expert system for the identification and quantification of urinary calculi prepared as KBr pellets. Using a rule base that is specific only for the components of urinary calculi, the components in 64% of the samples were identified correctly. After identification the components are quantified by comparing the mixture spectrum with a library of mixture spectra. Levine and co-workers [11–13] and Wythoff and Tomellini [14,15] developed systems for the identification of liquid organic mixtures. These systems can work with a large number of reference spectra by an indirect use of spectra libraries. Tests with different spectra sets showed that 80–100% of all components were identified correctly. It is advantageous that these expert systems can tolerate the deviations from the Beer–Lambert law in liquid mixtures caused by interactions between the components because the identification procedures performed by evaluation of the peak tables of the spectra also consider band shifts. The disadvantage of knowledge-based systems is their limited transferability to other substance systems and the time-consuming development of the system and the knowledge base.

In order to analyse the infrared spectra of mixtures of different qualitative compositions without strong interactions between the components rapidly and automatically, it is desirable to use a spectral library containing the spectra of all possible constituents directly. However, only a few studies have involved mixture analysis using library search systems [16–18]. The interactive subtraction method of some commercial library search systems allows only a qualitative mixture analysis. This method fails if the bands of the components are broad and strongly overlapped because the estimation of the factor for subtraction becomes fortuitous and impairs the evaluation of the difference spectrum and also the identification of several components. The usual search algorithms and measures of similarity [19,20] have proved to be unsuitable for automatic qualitative mixture analysis without subjective control by the user.

The purpose of this work was to develop a simple and efficient method for the qualitative and quantitative analysis of solid mixtures prepared as KBr pellets, which should supplement the library search system SUSY [21]. This method should quickly identify mixtures prepared under routine conditions. Deviations from the Beer–Lambert law should not impair the result for the qualitative composition. The spectra of solid mixtures rarely show band shifts caused by interactions between the components. The exclusion of band shifts allows the direct use of a library of reference spectra of the pure compounds. However, deviations from the Beer–Lambert law appear as variations of band widths, intensity ratios and background, which are essentially caused by dispersion effects depending on the grain size and the absorption coefficient of the samples [7,22]. This means that a robust method for mixture analysis is required. The identification of the components should be independent of band widths, intensity ratios and background. Hence the qualitative analysis is performed by a backward peak table comparison. Instead of the usual measure of similarity, the probability of the presence of a reference compound in the mixture is evaluated. Linear regression is applied to check the qualitative composition and to quantify the components.

For the evaluation of the efficiency of the method under routine conditions, a test set of 91 spectra of two- and three-component mixtures of nine carbohydrates was used because the spectra of the selected carbohydrates are very similar and give strong overlapping of the bands in the mixture spectra. The same spectra set was analysed by use of the method of iterative spectra exhaustion (ISE) developed by Hobert et al. [23] for the analysis of solid mixtures.

EXPERIMENTAL

Method

Using the library generation routine of SUSY, the reference library is built up with the absorbance spectra of the pure compounds for an amount of substance of 1 mg. Because the reference spectra in the library are normalized to unit maximum absorbance, the spectral library is extended by a weighting factor for each reference which establishes the connection between the library spectra and the original spectra of the compounds for 1 mg. This is necessary for the quantification of the compounds. Further, the spectral library can contain several model spectra for the baseline without any weighting factor which distinguish them from the spectra of the compounds. The library spectra are interpolated to 512 points per spectrum. The peak tables are automatically generated from these spectra using an absorbance threshold and a noise level of 0.02.

For qualitative mixture analysis a backward comparison of peak tables is the best search method because as many as possible peaks of the reference should be found in the unknown mixture spectrum. The absence of peaks of a reference in the mixture spectrum decreases the probability value of this reference, but a greater number of peaks in the mixture spectrum has no influence on the probability value. The whole mixture analysis is performed in the following stages:

1. Survey comparison of peak tables using the actual peak window: preselection of the references, whose five most intensive peaks were found in the mixture spectrum.

2. Detailed comparison of peak tables of the preselected references and the mixture spectrum using the actual peak window: the comparison of peak tables results in a measure of the probability p of the presence of a reference in the unknown mixture for each of the preselected references which is calculated by

$$p = \frac{\sum_{i=1}^{n} \delta_i \cdot \frac{I_i f(\tilde{\nu}_i)}{H_i}}{\sum_{i=1}^{n} \frac{I_i f(\tilde{\nu}_i)}{H_i}} \cdot F(H_{\min}) \cdot 100\%$$

with $f(\tilde{\nu}_i \leqslant 3200\ \mathrm{cm}^{-1}) = 1$, $f(\tilde{\nu}_i > 3200\ \mathrm{cm}^{-1}) = 0.5$ and $F(H_{\min} = 1) = 1$, $F(H_{\min} \geqslant 2) = 0.5$.

Only the n peak positions of a reference are compared with that of the unknown because the peak intensities in the mixture spectrum depend on the composition of the mixture. If a peak of the unknown mixture lies within a Boolean peak window around the location of the reference peak i, the parameter δ_i is set to 1, otherwise it is zero. Each peak i of the reference is weighted by its intensity I_i. From the higher contribution of the strong bands to the probability value, minor compounds can also be identified, even if the mixture spectrum shows only their main bands. Because water, especially water adsorbed on KBr, disturbs peak detection above 3200 cm^{-1}, the peaks above 3200 cm^{-1} are only weighted with half the intensity. The frequency H_i of peak i of the reference is the number of all peaks of the references preselected in step 1 in the peak window of peak i. The introduction of the frequency parameter H_i results in a lower weighting factor for all peaks, which could be overlaid by peaks of other preselected references. If none of the peaks of the reference certainly occurs as single peak with a minimum frequency value of $1(H_{\min} = 1)$, the presence of the reference in the mixture is uncertain. Therefore, the probability value is decreased to half. The probability values of all preselected references depend on the size of the peak window because the parameters δ_i, H_i and $F(H_{\min})$ vary with the window size. A first suggestion for the qualitative composition of the mixture is derived from the probability values sorted by their magnitude:

first component: p = maximum
second and third components: p_2 and $p_3 > 30\%$
further components: $p_4, \cdots, p_i > 40\%$

These limits for the probability values guarantee that the set of the suggested components contains two or three references at least, but at most five or six references. The following steps 3–6 are necessary to check the set of selected components by means of a linear regression, to eliminate the false positives and to supplement the set by the false negatives. In addition to the check and the

correction of the set of the components, steps 3–6 also give the relative composition of the mixture.

3. Quantification of the components in the mixture spectrum **a** by classical least-squares regression:

$$\mathbf{c} = (\mathbf{K}^T\mathbf{K})^{-1}\mathbf{K}^T\mathbf{a}$$

The calibration matrix **K** is built up from the absorbance values of the selected reference spectra scaled with the weighting factors from the normalization of the reference spectra and from the absorbance values of the model spectra for the baselines at all peak positions. By evaluation of the intensity values at the peak positions, the elements of vector **c** for the components are independent of variations of the band widths and also of variations of the baseline if the reference library contains the appropriate baseline models. All elements of vector **c** except that for the baselines should be positive values. References with negative values in **c** are eliminated from the calibration matrix. Then the linear regression is repeated until no negative values for the components are present in vector **c**.

4. Generation of the peak table for the difference spectrum **d**:

$$\mathbf{d} = \mathbf{a} - \mathbf{Kc}$$

and library search (step 2) for additional components with $p > 30\%$. If an additional component is found, the linear regression (step 3) is repeated.

5. Calculation of the total standard deviation for the quantitative analysis:

$$\sigma = \sqrt{\frac{\sum_{i=1}^{r}\left(a_i - \sum_{j=1}^{m} k_{ij}c_j\right)^2}{r-1}}$$

where r = number of peak positions, m = number of components and a_i, k_{ij}, c_j = elements of **a**, **K** and **c**, respectively. In the case of an unknown qualitative composition, the total standard deviation is only the measure of the quality of the adjustment to the mixture spectrum at the peak positions by the selected reference spectra and the baseline models. Therefore, the total standard deviation is used to characterize the correctness of the set of the selected components.

6. Verification of the composition if $\sigma > 0.01$. For the verification one of the components is always eliminated from the calibration matrix, then the linear regression (step 3) is repeated and a new difference spectrum and its peak table are computed, which has to undergo a library search with the calculation of new p values (step 4). If the references with the highest probability (greater than 30%) are not among the components, these references are entered into the set of the components. Only if the eliminated component is not among the references selected for the actual difference spectrum is this component finally deleted from the set of components, otherwise it will be considered again in the next cycle of verification. This procedure is repeated for each component.

7. When all the components have been checked, the percentage of each component in relation to the total weight of the sample, the total standard deviation, the theoretical spectrum of the mixture for the computed composition and the difference spectrum are calculated.

The peak window can be set by the user. However, the standard peak window is defined as the threefold point distance of the reference spectra. In the automatic mode the standard peak window is used first. If the total standard deviation in step 7 is larger than 0.01, the whole procedure from step 1 to step 7 will be automatically repeated using different peak windows between the twofold and the sixfold point distance of the reference spectra. The calculation of the final result requires no actions by the user. In most instances the peak window with a minimum total standard deviation gives the correct qualitative composition of the analysed mixtures.

The computer program for mixture analysis was written in PASCAL as a subroutine of SUSY running on a PC under MS-DOS. For the analysis of a single mixture with the standard peak window a computing time of about 1 min is necessary using a 386 DX system with 20 MHz. The determination of the peak window with the minimum total standard deviation for a single mixture takes about 5 min. The computing time is

proportional to the number of preselected references (in step 1), but not to the number of reference spectra in the library.

Samples and implementation

To test the method under routine conditions, 35 two-component mixtures and 56 three-component mixtures of the nine carbohydrates, lactose (la), saccharose (sa), starch (st), glycogen (gl), fructose (fru), maltose (ma), galactose (ga), sorbose (sor) and xylose (xy), were prepared by weighing. The compositions of the mixtures are given as a percentage of the total weight of the samples and are listed in Table 1. All samples were prepared as KBr pellets of 20 mm diameter by grinding 1–3 mg of the sample and 800 mg

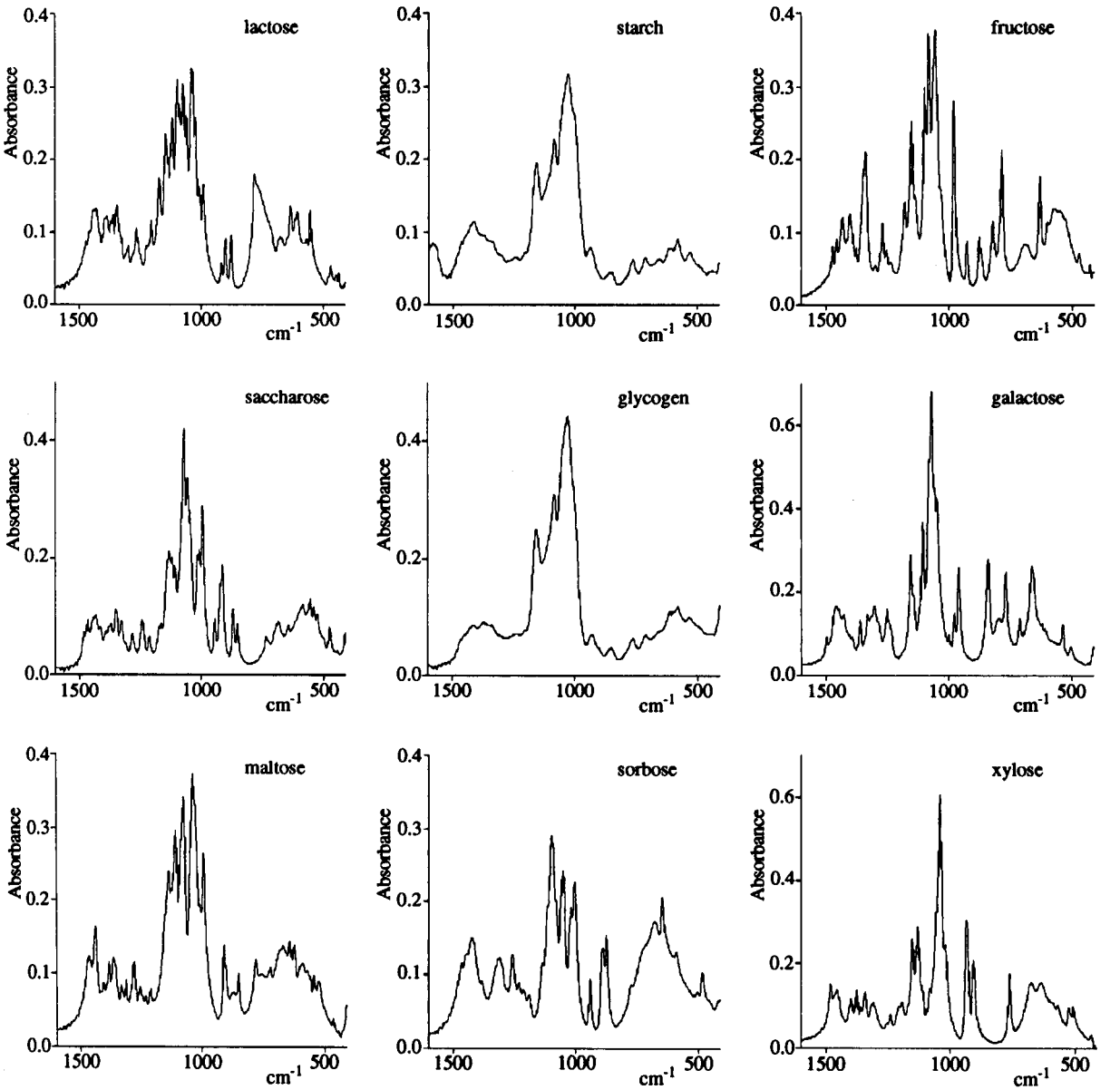

Fig. 1. Absorbance spectra of the carbohydrates for an amount of 1 mg.

TABLE 1

Compositions of the mixtures

Two-component systems	Compositions for each two-component	Three-component systems system (%)	Compositions for each three-component system (%)
fru–st	10:90	sor–la–gl	33:33:33
ma–st	20:80	xy–sa–la	20:40:40
xy–st	40:60	fru–ma–st	40:20:40
xy–fru	60:40	ma–la–ga	40:40:20
xy–ma	80:20	sa–ma–ga	12.5:37.5:50
ga–la	90:10	sor–ga–fru	37.5:12.5:50
		xy–ga–gl	37.5:50:12.5
		sor–ma–st	

KBr in a vibration mill and compressing the mixture at 20 MPa under vacuum corresponding to an exactly defined preparation instruction. After extensive investigations this optimized preparation instruction for KBr pellets was given [7] which guarantees the linear dependence of the absorbance values from the substance weight with a relative error of less than 1% if the samples show a small and constant grain size. However, when analysing carefully pulverized samples of different prehistory, their different grain sizes can lead to deviations of up to 10% between the measured and the given percentage [7]. Therefore, the precision of the analysis cannot be better than 10% and the calibration can be simply performed as univariate linear regression.

The absorbance spectra were recorded with an IRF 180 Fourier transform IR spectrometer (Zentralinstitut für Wissenschaftlichen Gerätebau, Akademie der Wissenschaften, Berlin) with a TGS detector in the region from 3945 to 400 cm^{-1} using 50 scans and a resolution of 4 cm^{-1}. The evaluation of the spectra was restricted to the region from 1600 to 410 cm^{-1}. The spectra were interpolated to 512 points per spectrum and a point distance of 2.33 cm^{-1}. The reference spectra of the pure components were calculated by linear regression from the absorbance spectra of three different amounts of the pure substances after a correction of the baseline using the spectrum of the pure KBr and a linear constant baseline. In addition to these reference spectra the reference library also includes the spectrum of KBr, the linear constant baseline and a linear baseline increasing to higher wavenumbers. These baseline models describe all variations of background in the spectra of carefully prepared KBr pellets. Therefore, all mixtures can be analysed without any baseline correction of their spectra.

Because of a point distance of 2.33 cm^{-1}, the standard peak window for the comparison of the peak tables was set to 7 cm^{-1} and the peak window was varied between 5 and 15 cm^{-1} to obtain the analysis with the minimum total standard deviation.

RESULTS AND DISCUSSION

The spectra of the nine pure carbohydrates are presented in Fig. 1. There is a high similarity between the spectra of starch and glycogen. The spectra of the other compounds are characterized by many, mostly narrow, bands, which are strongly overlapped in the spectra of the mixtures. For example, the three spectra of mixtures of lactose, sorbose and glycogen in Fig. 2 demonstrate that the determination of the qualitative composition of such mixtures is a difficult task.

For the evaluation of the efficiency of the proposed method, all 91 mixture spectra were

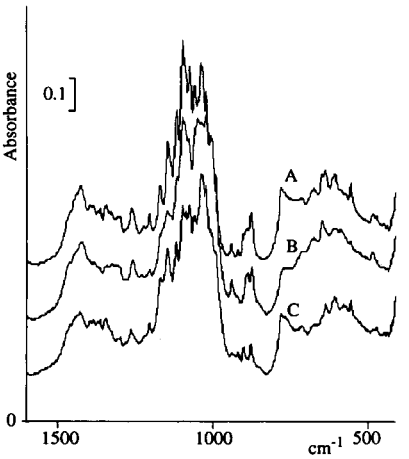

Fig. 2. Absorbance spectra of mixtures of sorbose, lactose and glycogen. (A) 37.5% sorbose, 50.0% lactose, 12.5% glycogen; (B) 37.5% sorbose, 12.5% lactose, 50.0% glycogen; (C) 12.5% sorbose, 37.5% lactose, 50.0% glycogen.

automatically analysed with determination of the optimum peak window. Further, two fixed peak windows (7 and 10 cm^{-1}) were applied to demonstrate that a statistical evaluation of the results by means of the total standard deviation is necessary to obtain the correct composition. The components were considered to be identified with certainty if their analysed percentage was larger than 5%. Because of the preparation of the samples as KBr pellets the analyses were assessed to be correct if the deviation between the measured and the given percentage for each of the components was less than 10%. The results of the mixture analyses are divided into five categories:

Category I: correct analysis. The compounds present are detected with a precision of better than 10%. The percentage of additional components which are not present in the mixture is less than 5%.

Category II: qualitatively correct analysis. The compounds present are determined with a precision worse than 10%, but additional components are not found to more than 5%.

Category III: qualitatively incorrect analysis with one false-positive component only. All compounds present but also an additional compound with more than 5% are detected.

Category IV: qualitatively incorrect analysis with only one false-negative component. One of the components could not be determined. False-positive components are possible.

Category V: qualitatively incorrect analysis with more false-negative components.

Table 2 shows all the results obtained with the the optimum peak window and the two fixed windows. The application of the fixed windows yields altogether worse results than the determination of the optimum peak window by means of the minimum total standard deviation which was only carried out if the total standard deviation using the standard peak window was larger than 0.01. The results in Table 2 demonstrate that an individually optimum peak window exists for each mixture spectrum. This behaviour is characteristic for all library search procedures based on a comparison of peak tables. In the case of mixture spectra the influence of the window size is essentially stronger than in the case of pure compounds. The size of the optimum peak window depends on the similarity of the spectra of the pure compounds contained in the mixture and the degree of overlap of their bands. Because the components are unknown at the stage of identification of the mixture the total standard deviation is the only measure for the correctness of the qualitative composition.

TABLE 2

Results of mixture analyses

Category	Total number of mixtures		
	Optimum peak window	Peak window of 7 cm^{-1}	Peak window of 10 cm^{-1}
I	56	33	34
II	25	15	18
III	3	1	2
IV	7	41	35
V	–	1	2

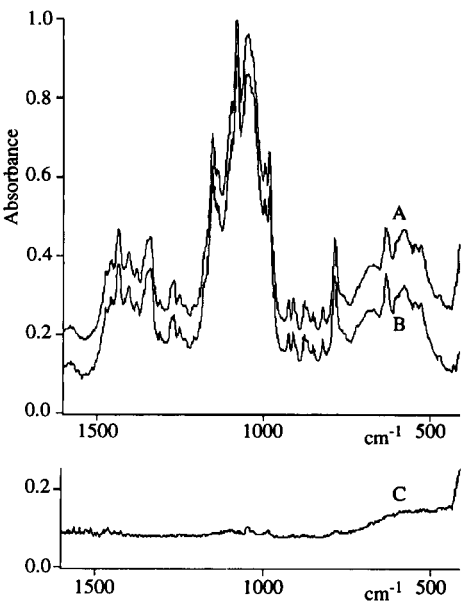

Fig. 3. Analysis results for category I. (A) Spectrum of a mixture of 33.3% fructose, 33.3% maltose and 33.3% starch; (B) synthetic spectrum; (C) difference spectrum.

In the following the results are discussed by some selected examples. An example of a correct analysis is presented in Fig. 3. Spectrum A, the measured spectrum of a three-component mix-

ture with the same content of starch, fructose and maltose, was analysed with the same total standard deviation of 0.0047 using peak windows of 7 and 10 cm^{-1}. Spectrum B was calculated from the analysed composition of 37.1% starch, 32.9% fructose and 30.0% maltose. The absolute deviation from the given composition is less than 4%. Spectrum C, the difference between A and B, consists mainly of background. However, often the use of different peak windows led to different results, which also fell in different categories. Among the mixtures in category I, only 25 mixtures gave the same result with several peak windows. The introduction of the total standard deviation as a criterion for the correctness of the qualitative analysis results in 56 correct analyses. In order to characterize the quality of the analysed compositions within category I, the arithmetic mean and the standard deviation of the differences between the given and measured percentages of the components of all mixtures in category I were calculated. The distribution of the differences corresponds to a Gaussian function with a mean value of 0.3% and a standard deviation of 4.6%.

In 25 of the 91 mixtures the components were detected with a deviation of more than 10% from the given composition if the optimum peak window was used. In contrast to the use of optimum peak windows, the application of fixed peak windows also decreased the number of mixtures in category II. For example, the components of a mixture of 37.5% xylose, 12.5% saccharose and 50% lactose were correctly identified with a peak window of 7 cm^{-1}. This peak window is also the optimum peak window and the total standard deviation is less than 0.01. Using a peak window of 10 cm^{-1} the result of the analysis would fall into category IV with a total standard deviation of 0.024 because saccharose is not found.

TABLE 3

Given and measured compositions for the example of category II

Given composition	Measured composition	
	Optimum peak window of 7 cm^{-1}	Peak window of 10 cm^{-1}
37.5% xy	41.7% xy	42.2% xy
12.5% sa	24.6% sa	33.6% la
50.0% la	33.7% la	22.9% ma
	σ = 0.0047	1.3% sor
		σ = 0.0240

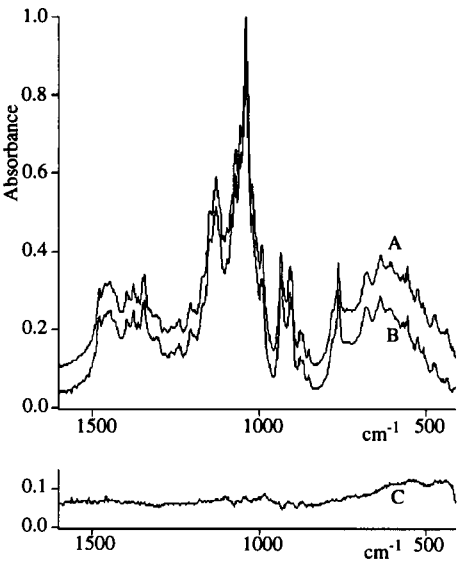

Fig. 4. Analysis results for category II. (A) Spectrum of a mixture of 37.5% xylose, 12.5% saccharose and 50.0% starch; (B) synthetic spectrum; (C) difference spectrum.

Table 3 shows the composition of the mixture analysed with peak windows of 7 and 10 cm^{-1}. Figure 4 shows the result for this mixture obtained with the optimum peak window of 7 cm^{-1}. Because the standard deviation is low and the difference spectrum C in Fig. 4 shows almost no spectral information, the deviation from the given composition is caused by errors in the preparation of the sample under routine conditions. However, the efficiency of the method is determined by a correct identification of the components present especially because a quantitatively correct analysis requires first a correct identification of the components. The distribution function of the differences between given and measured percentages of the components of the mixtures in category II is characterized by an arithmetic mean of 0.0% and a standard deviation of 11.8%.

Among the 81 mixtures in categories I and II there are 40 mixtures containing one minor com-

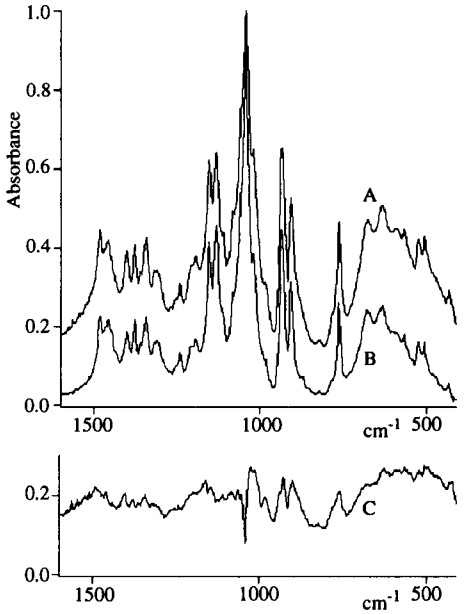

Fig. 5. Analysis results for category III. (A) Spectrum of a mixture of 80% xylose and 20% fructose; (B) synthetic spectrum; (C) difference spectrum.

ponent with a percentage up to 20%. This indicates that the determination of the optimum peak window by the minimum total standard deviation is a useful method also for the detection of minor components in the case of strongly overlapped bands.

The tendency of the method to find false-positive components in a mixture is very low in contrast to the approaches of classical least-squares or principal component regression. Only three of the 91 mixtures fall into category III when analysing them with the optimum peak window. In these three cases always one additional component was detected with a percentage of less than 15%. For example, the spectra of a mixture containing 80% xylose and 20% fructose are shown in Fig. 5. Using the optimum peak window of 9 cm^{-1} the analysis of the mixture spectrum A gave a composition of 83.1% xylose, 7.6% fructose and 9.3% saccharose and a minimum total standard deviation of 0.0271. The percentage of fructose is too low and saccharose was found as an additional component.

A detailed inspection of the difference spectrum in Fig. 5 shows that it still contains all bands of the components fructose and xylose, except for the most intense bands of both components. At the position of the maximum peak of xylose at 1042 cm^{-1} the difference spectrum has a minimum. Different intensity ratios between strong and weak bands in the reference and sample spectra are the reason for this minimum in the difference spectrum. These different intensity ratios are a typical symptom of variations in the grain sizes in the reference and the mixture sample which could easily arise from small differences in sample preparation. The variation of the grain size for xylose also affects the result for fructose because the maximum band of fructose is located at 1054 cm^{-1} beside the maximum band of xylose. Using the optimum peak window of 9 cm^{-1} the too low percentage of fructose is compensated for by 9.3% saccharose and therefore the minimum of the total standard deviation is reached. The application of the standard peak window of 7 cm^{-1} yielded a result which would fall into category IV with a slightly larger total standard deviation of 0.0297. The measured compositions are given in Table 4. However, using a peak window of 10 cm^{-1} a composition of 86.7% xylose, 11.9% fructose and only 1.4% maltose and a total standard deviation of 0.0296 were obtained. This result would still fall into category I, but its total standard deviation is greater than that for a peak window of 9 cm^{-1}.

In the case of false-positive components (results of category III) the selection of the result with the minimum total standard deviation often leads to a wrong analysis because false-positive

TABLE 4

Given and measured compositions for the example of category III

Given composition	Measured composition		
	Peak window of 7 cm^{-1}	Peak window of 10 cm^{-1}	Optimum peak window of 9 cm^{-1}
80.0% xy	88.1% xy	86.6% xy	83.1% xy
20.0% fru	11.6% la	12.0% fru	7.6% fru
	$\sigma = 0.0297$	1.4% ma	9.3% sa
		$\sigma = 0.0296$	$\sigma = 0.0271$

components decrease the total standard deviation in general. However, this can be neglected because of the low tendency for false-positive components.

Using the optimum peak window, seven of the 91 mixtures had to be allocated to category IV, but none of the mixtures fell into category V. In six of these cases the minor component with a percentage up to 20% could not be detected and in one case starch with a percentage of 40% was exchanged for glycogen because their spectra are very similar. However, the use of fixed peak windows led to large numbers of 41 and 35 mixtures in category IV, respectively, and one and two mixtures, respectively, fell into category V. However, there are not only minor components among the false negatives. The selection of the result by means of the minimum of the total standard deviation gave a decrease in the number of false-negative components. Only for seven of these mixtures was no better result reached with the peak window for the minimum total standard deviation. These mixtures show an unchangeably bad result and a constant total standard deviation for all peak windows between 5 and 15 cm^{-1}.

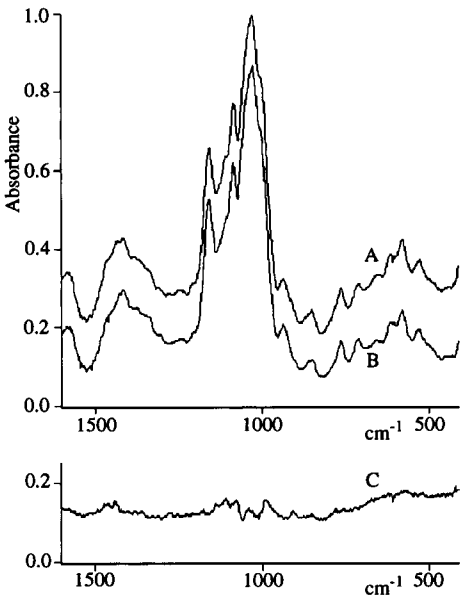

Fig. 6. Analysis results for category IV. (A) Spectrum of a mixture of 90% starch and 10% maltose; (B) synthetic spectrum; (C) difference spectrum.

As an example of category IV, the spectra of a mixture of 10% maltose and 90% starch are presented in Fig. 6. Using various peak windows, 90.0% starch, 9.7% glycogen and 0.3% xylose and a constant total standard deviation of 0.0071 were obtained. The minor component maltose could not be detected. A comparison of the spectra of maltose and starch in Fig. 1 shows that the most intense bands of both substances are located between 1000 and 1200 cm^{-1}. In the measured spectrum A of the mixture in Fig. 6, only the broad bands of starch are evident and the narrow bands of maltose are not noticeable in the region between 1000 and 1200 cm^{-1}. This is why maltose at a level of 10% cannot be identified in the presence of 90% starch. This example demonstrates the limits of an identification procedure based on a comparison of peak tables.

Conclusions

A method for qualitative and quantitative mixture analysis based on a comparison of peak tables was developed as a subroutine of the library search system SUSY. The unsatisfactory results of common library search systems for the identification of mixtures were overcome by the definition of the probability of the presence of a reference in a mixture as measure of similarity. The detection of the most probable references requires no assumption about the linearity of the system. Even in the case of non-linearities (variations of background and variations of intensity ratios and band widths in the component spectra) the identification procedure works correctly if there are no variations in the band positions caused by strong interactions between the components of the mixtures. Whereas the approaches to quantitative mixture analysis based on regression procedures using the full spectra often yield false-positive components if the constituents of the mixture are unknown, the proposed method shows in general only a slight tendency to detect false-positives. The problem of different results using different peak windows can be controlled by means of the total standard deviation. Because of the slight tendency of the method to find false-positives, the minimum of total standard deviation can be exploited successfully to de-

crease the number of false-negative components to a minimum. The limits for the identification of minor components are determined by the peak detection procedure. The method has no properties of an expert system, but the completely automated, correct identification of 89% of all mixtures is comparable to the results given by knowledge-based systems.

The method was not developed for quantitative mixture analyses of high precision. Only the relative compositions of the mixtures are calculated. The quantitative results of the method always have to be assessed in connection with the attainable precision determined by the kind of samples and the preparation technique. Using the KBr technique under routine conditions the quality of the analysed compositions is satisfactory. The method allows a rapid and automatic identification of mixtures and a rapid calculation of their relative compositions. It is applicable to any kind of mixtures if the following four conditions are fulfilled: the components do not show variations in the band positions caused by interactions between the components in the mixture, a library of corresponding reference spectra of the pure compounds exists, this library includes the appropriate models for the baselines and the point distance of the reference spectra guarantees the clear differentiation of the components.

REFERENCES

1 H. Martens and T. Naes, Multivariate Calibration, Wiley, Chichester, 1989.
2 D.L. Massart, B.G.M. Vandeginste, S.N. Deming, Y. Michotte and L. Kaufmann, Chemometrics: a Textbook, Elsevier, Amsterdam, 1987.
3 E.R. Malinowski and D.G. Howery, Factor Analysis in Chemistry, J Wiley, New York, 1980.
4 D.M. Haaland, R.G. Easterling and D.A. Vopicka, Appl. Spectrosc., 38 (1984) 73.
5 E.V. Thomas and D.M. Haaland, Anal. Chem., 62 (1990) 1091.
6 D.W. Osten and B.R. Kowalski, Anal. Chem., 57 (1985) 908.
7 K. Meyer, Thesis, Friedrich-Schiller-Universität Jena, 1992.
8 H. Hobert and K. Meyer, Fresenius' J. Anal. Chem., 344 (1992) 178.
9 X. Hong-kui, S.P. Levine and J.B. D'Arcy, Anal. Chem., 61 (1989) 2708.
10 A. Hesse, M. Gergeleit, P. Schneller and K. Moeller, J. Clin. Chem. Clin. Biochem., 27 (1989) 639.
11 M.A. Puskar, S.P. Levine and S.R. Lowry, Anal. Chem., 58 (1986) 1981.
12 M.A. Puskar, S.P. Levine and S.R. Lowry, Anal. Chem., 58 (1986) 1156.
13 L.S. Ying, S.P. Levine, S.A. Tomellini and S.R. Lowry, Anal. Chem., 59 (1987) 2197.
14 B.H. Wythoff and S.A. Tomellini, Anal. Chim. Acta, 227 (1989) 343.
15 B.J. Wythoff and S.A. Tomellini, Anal. Chim. Acta, 227 (1989) 359.
16 W. Herres, Comput. Anwend. Labor, 2 (1984) 93.
17 M.F. Delaney and D.M. Mauro, Anal. Chim. Acta, 172 (1985) 193.
18 T.M. Rossy and I.M. Warner, Appl. Spectrosc., 39 (1985) 949.
19 J.T. Clerc, M. Zuercher and A.L. Terkovics, Wiss. Z. Tech. Hochsch. Chem. "Carl Schorlemmer" Leuna-Merseburg, 31 (1989) 28.
20 K. Varmuza, Pattern Recognition in Chemistry, Springer, Berlin, 1980.
21 M. Meyer, I. Weber, R. Sieler and H. Hobert, Jena Rev., 35 (1990) 16.
22 G. Kortüm, Reflexionsspektroskopie, Springer, Berlin, 1969.
23 H. Hobert, K. Meyer and I. Weber, Vib. Spectrosc., 4 (1993) 207.

Analytica Chimica Acta, 281 (1993) 173–177
Elsevier Science Publishers B.V., Amsterdam

Indicator for the titrimetric determination of calcium and total calcium plus magnesium with ethylenediaminetetraacetate in water

D.P.S. Rathore, P.K. Bhargava, Manjeet Kumar and R.K. Talra

Chemical Laboratory, Atomic Minerals Division, Department of Atomic Energy, West Block-VII, R.K. Puram, New Delhi 110 066 (India)

(Received 19th January 1993; revised manuscript received 9th March 1993)

Abstract

The use of 2-[(4-phenylthioacetic acid)azo]-1,8-dihydroxynaphthalene-3,6-disulphonic acid as an indicator for the titrimetric determination of both calcium and total calcium plus magnesium is reported. The variables affecting the colour change at the end-point were optimized. The method is free from most metal interferences without the need for potassium cyanide and other masking agents. The method was applied to water samples and the results obtained compared favourably with those given by standard methods.

Keywords: Titrimetry; Azo dyes; Calcium; Indicators; Magnesium; Waters

Calcium and magnesium determinations in water are of importance in hydrogeochemical surveys [1,2] and for determining total hardness, potability and suitability for irrigation [3].

Complexometric determination of calcium and magnesium has been thoroughly investigated and is widely accepted [4,5]. Eriochrome Black T [6], murexide [7], calcon [8,9], the indicator of Patton and Reeder [10], Arsenazo I [11] and other indicators [12] change colour slowly at the end-point. Moreover, traces of iron, copper, nickel and other metal ions dissolved in water "block" these indicators, thereby preventing a sharp-end point or seriously reducing its sharpness unless potassium cyanide and other masking agents are used. Potassium cyanide is a potential safety hazard [11] and has to be handled with the utmost care.

Correspondence to: D.P.S. Rathore, Chemical Laboratory, Atomic Minerals Division, Department of Atomic Energy, West Block-VII, R.K. Puram, New Delhi 110 066 (India).

Recently, *p*-aminophenylmercaptoacetic acid was used as a diazotizable amine for the spectrophotometric determination of nitrite [13–16], the detection and determination of cerium [17], the indirect determination of chromium [18] based on azo dye formation, the identification of vanadium [19] as its schiff base using 2-furfuraldehyde and the rapid detection of vanadium [20] via its azo dye derived from chromotropic acid as coupling agent.

In this work, 2-[(4-phenylthioacetic acid)azo]-1,8-dihydroxynaphthalene-3,6-disulphonic acid (PTAADNDA), an azo dye [15,20], was used for the titrimetric determination of both calcium and total calcium plus magnesium using disodium EDTA as titrant.

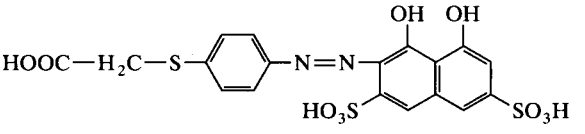

PTAADNDA

EXPERIMENTAL

Apparatus

Spectral measurements were made with a Varian 634-S double-beam spectrophotometer with 1.0-cm quartz cuvettes.

Reagents

p-Aminophenylmercaptoacetic acid of 98.1% purity (Evans Chemetics, New York) was used as received. All other chemicals were of analytical-reagent grade and standard solutions were prepared by the usual methods [4].

The azo dye indicator PTAADNDA [15,20] was prepared by diazotization of *p*-aminophenylmercaptoacetic acid and coupling with chromotropic acid in alkaline media, as follows. A 5.5-g amount of *p*-aminophenylmercaptoacetic acid was dissolved in 50 ml of hydrochloric acid 1 + 1 and 3.0 g of sodium nitrite were added with constant stirring at 0–5°C. Excess nitrite was destroyed by adding a pinch of sulphamic acid. The resulting salt was coupled by adding a solution of chromotropic acid disodium salt dihydrate (10.70 g in 10% sodium hydroxide), with stirring, while keeping the temperature at 0–5°C. When the addition was complete, stirring and cooling were continued for 30 min, then 40 ml of concentrated hydrochloric acid were added and the mixture was stored in a refrigerator overnight. The precipitate was filtered and washed with dilute hydrochloric acid and absolute ethanol, then dried for 6 h at 105°C (yield 4–5 g).

Azo dye (indicator) solution (0.1%, w/v) was prepared by dissolving 0.1 g of the azo dye in distilled water containing a pellet of sodium hydroxide. This solution is stable for at least 3 months.

Analytical procedures

The procedures for the determination of calcium and total calcium plus magnesium were carried out as described [4], using PTAADNDA as indicator for both titrations. The difference between the two titrations gave the magnesium content in the sample.

RESULTS AND DISCUSSION

Preliminary experiments were conducted using known aliquots of standard calcium and magnesium solutions diluted to 50 ml with distilled water. Titrations were performed by adding 0.01 M EDTA solution from a 10-ml burette.

Calcium

The basis of the calcium determination is that magnesium is precipitated as magnesium hydroxide by addition of potassium hydroxide (pH 12–13) and calcium forms a stronger complex with EDTA than does magnesium [6], hence calcium remaining in solution is then selectively titrated. A 4–5-ml volume of 4 M potassium hydroxide solution per 50 ml final volume was the optimum to bring the desired pH to between 12 and 13 and to precipitate magnesium hydroxide virtually completely. After adding potassium hydroxide, the sample solution should be titrated within 3–5 min, otherwise there may be a loss of calcium as calcium carbonate at high alkalinity owing to atmospheric carbon dioxide, thereby resulting in a slightly lower titre for calcium. Any error in the calcium determination will result in an incorrect result for the magnesium content of the sample, although the total calcium and magnesium content remains the same. It was found that 5–7 drops of the 0.1% aqueous solution of the indicator per 50 ml final volume were optimum for the visual observation of the end-point. Near the end-point, a bluish tinge appears first, and then sharply changes to reddish violet at the end-point. Hence the colour change is from orange to reddish violet.

If the calcium concentration is more than 10 mg per 50 ml final volume, then after adding potassium hydroxide some calcium is precipitated as the hydroxide [9]. Vigorous stirring is necessary to dissolve the $Ca(OH)_2$ as the titration progresses. If the stirring is slow, false end-points are obtained. The return of the colour after each change as the stirring is continued might be due to a slow change of $Ca(OH)_2$ to free Ca^{2+}, responsible for the colour change. A smaller aliquot of the sample should then be taken and diluted with distilled water.

Total calcium and magnesium

At pH ≈ 10 both calcium and magnesium are titrated with EDTA solution. The colour change at the end-point is from reddish to bluish violet. The end-point is sharper for the magnesium titration. An azo dye indicator concentration of 5–7 drops of 0.1% aqueous solution per 50 ml final volume was the optimum for visual observation of the end-point. A volume of 5 ml of buffer solution, pH ≈ 10, was optimum for a 50-ml final volume.

Absorption spectra of the free azo dye, calcium–azo dye complex and magnesium–azo dye complex are illustrated in Fig. 1.

End-point

The visual end-points in both titrations were compared with spectrophotometric titration curves for calcium or magnesium at pH ≈ 10 and calcium at pH 12–13 by titration with 0.1 M EDTA using the azo dye as indicator. The titration curve shows that the sharp colour change occurs near to the equivalence point (Fig. 2).

Effects of foreign ions

The effects of various foreign ions that generally accompany calcium and magnesium in water were studied using 5 ml of 1 mg ml^{-1} each of

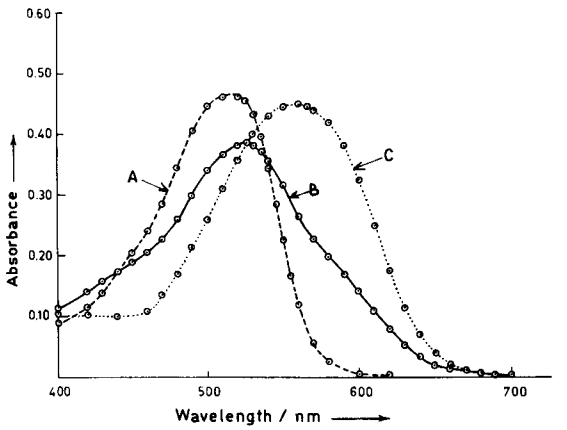

Fig. 1. Absorption spectra for (A) magnesium–azo dye complex; (B) calcium–azo dye complex and (C) azo dye indicator. Conditions: calcium (1 mg ml^{-1}), 5 ml; magnesium (1 mg ml^{-1}), 5 ml; buffer, pH ≈ 10, 5 ml; PTAADNDA azo dye (0.1%), 1 ml; total volume, 50 ml.

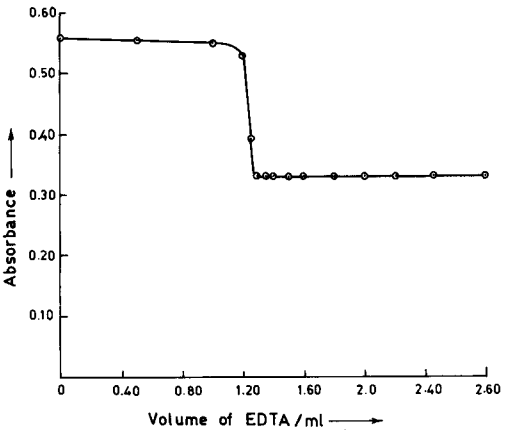

Fig. 2. Spectrophotometric titration curve of calcium by EDTA using PTAADNDA azo dye as indicator against distilled water at 495 mn. Conditions: calcium, 5 mg per 50 ml total volume; EDTA solution, 0.1 M; indicator (0.1%), 1 ml; potassium hydroxide (4 M), 4–5 ml; pH, 12–13.

TABLE 1

Effects of interfering ions (50 ml of sample)

Interferent	Tolerated amount (μg) [a]
Copper(II)	10
Iron(III)	500
Cobalt(II)	20
Nickel(II)	100
Manganese(II)	100
Barium(II)	500
Aluminium(III)	500
Strontium(II)	1000
Zinc(II)	500
Cadmium(II)	500
Lead(II)	500
Mercury(II)	1000
Chromate(II)	1000
Silicate	2500
Uranyl(II)	500
Vanadium(V)	40
Carbonate	2000
Hydrogencarbonate	5000
Sulphate	10000
Chloride	10000
Nitrite	5000
Nitrate	1500
Fluoride	500
Phosphate	2000
Sulphite	5000
Sodium salts	No interference
Potassium salts	No interference

[a] Amount of foreign ions causing a sharp end-point with a drop of titrant.

TABLE 2

Standard addition for the determination of calcium contents in tap water (means of five analyses, 50-ml samples)

Sample No.	Calcium added per 50 ml (mg)	Calcium found (mg)	Recovery (%)	Magnesium added per 50 ml (mg)	Calcium (mg)	Recovery (%)
1	0	1.6	–	0	1.6	100
2	5	6.5	98	5	1.6	100
3	10	11.2	96	10	1.6	100

calcium and magnesium per 50 ml final volume at pH 12–13 and 10, respectively, by titration with 0.01 M EDTA solution. Unlike the common interferences due to Co(II), Ni(II), Cu(II), Fe(III), Mn(II), Ba(II), Sr(II), Pb(II) and Zn(II) in complexometric methods [6–11], these ions are tolerated to a great extent with the present procedure without the need for potassium cyanide and other masking agents (as is evident from Table 1). This high tolerance can be attributed to the presence of the thio and carboxylic groups, which probably facilitate chelate formation of these ions. This results in a decreased availability of these ions in solution to interfere in the determination of calcium and magnesium. The concentrations of interfering ions are almost same at pH ≈ 10 and 12–13.

Application of the method

In order to check the validity of the method for the determination of calcium and magnesium in water, two sets of experiments were done. In

TABLE 3

Standard addition for the determination of magnesium content in tap water (means of five analyses, 50-ml samples)

Sample No.	Calcium added per 50 ml (mg)	Calcium found (mg)	Magnesium added per 50 ml (mg)	Magnesium found by difference (mg)	Recovery (%)
1	0	1.6	0	1.1	
2	5	6.5	0	1.1	98
3	10	11.2	0	1.2	96
4	0	1.6	5	6.1	100
5	0	1.6	10	11.0	99
6	0	1.7	20	21.3	101

TABLE 4

Determination of calcium and magnesium in water samples (means of five analyses, 50-ml samples)

Sample No.	Proposed method		Conventional method	
	Calcium (μg ml^{-1}) (direct method)	Magnesium (μg ml^{-1}) (by difference)	Calcium (μg ml^{-1}) (direct method Using Patton and Reeder's indicator)	Magnesium (μg ml^{-1}) (by difference using Eriochrome Black-T indicator)
1	28	51	28	52
2	24	24	23	25
3	53	25	51	24
4	24	15	20	18
5	26	11	25	11

TABLE 5

Comparison of the proposed method with other complexometric determinations of calcium and magnesium

Indicator	Potential interferents [a]	Ref.
Eriochrome Black T	Ba^{2+}, Sr^{2+}, Pb^{2+}, Zn^{2+}, Cu^{2+}, Co^{2+}, Ni^{2+}, Mn^{2+}, Fe^{3+}, Al^{3+}	6
Murexide	Ni^{2+}, Co^{2+}, Cu^{2+}, Zn^{2+}, Ba^{2+}, Sr^{2+}, Pb^{2+}	7
Calcon	Cu^{2+}, Fe^{3+}, Sr^{2+}, Ba^{2+}	8, 9
Patton and Reeder's indicator	Ba^{2+}, Sr^{2+}, Pb^{2+}, Zn^{2+}, Cu^{2+}, Co^{2+}, Ni^{2+}, Mn^{2+}, Fe^{3+}	10
Arsenazo I	Mn^{2+}, Co^{2+}, Ni^{2+}, Zn^{2+}, Cd^{2+}	11
PTAADNDA azo dye	None	This work

[a] Without the use of potassium cyanide and other masking agents.

the first, the recoveries of calcium and magnesium were checked by adding varying concentrations of calcium and magnesium to tap water. In the other, various amounts of sample solutions were taken and diluted to constant volume with distilled water. For all samples accurate results were obtained. The results are summarized in Tables 2–4 and show that the proposed method is comparable to the conventional complexometric methods employing Eriochrome Black T and the Patton and Reeder indicator.

The proposed method is a variant of the conventional complexometric method. Unlike other indicators, the same azo dye indicator is recommended for the determination of both calcium and magnesium. The sharp end-points and high tolerance to many foreign ions are the advantages of the proposed method.

Table 5 shows the comparative performances of the complexometric methods for the determination of calcium and magnesium. The simplicity and selectivity of the proposed procedure allows the routine on-site determination of calcium and magnesium over a wide range of concentrations.

The authors are grateful to Evans Chemetics, New York, for the gift of *p*-aminophenylmercaptoacetic acid. Thanks are due to Shri K.P. Cheria, Head of the Chemistry Group, Dr. S. Viswanathan, Director of the Atomic Minerals Division, and Shri Jagmer Singh, Regional Director, for providing the necessary facilities.

REFERENCES

1 J.C. Robbins, CIM Bull., 71 (1978) 61.
2 S.W. Reeder, B. Hilton and A.A. Levinson, Geochim. Cosmochim. Acta, 36 (1972) 825.
3 P.L. Jaiswal (Ed.), Handbook of Agriculture, Indian Council of Agricultural Research, New Delhi, 1984, p. 158.
4 A.I., Vogel, A Textbook of Quantitative Inorganic Analysis, Longman, London, 4th edn., 1985, pp. 257–278, 325–327.
5 Standard Methods for the Examination of Water and Waste Water, American Public Health Association, Washington, DC, 15th edn., 1981.
6 G. Schwarzenbach and W. Biedermann, Helv. Chim. Acta, 31 (1948) 678.
7 L. Aconskey and M. Mori, Anal. Chem., 27 (1955) 1001.
8 G.P. Hildebrand and C.N. Reilley, Anal. Chem., 29 (1957) 258.
9 H. Diehl and J.L. Ellingboe, Anal. Chem., 28 (1956) 882.
10 J. Patton and W. Reeder, Anal. Chem., 28 (1956) 1026.
11 J.S. Fritz, J.P. Sickafoose and M.A. Schmitt, Anal. Chem., 41 (1969) 1954.
12 H. Diehl and J.L. Ellingboe, Anal. Chem., 32 (1960) 1120.
13 P.K. Tarafder and D.P.S. Rathore, Analyst, 113 (1988) 1073.
14 D.P.S. Rathore and P.K. Tarafder, J. Indian Chem. Soc., 66 (1989) 185.
15 D.P.S. Rathore and P.K. Tarafder, J. Indian Chem. Soc., 67 (1990) 231.
16 D.P.S. Rathore and P.K. Tarafder, Acta Cienc. Indica (Physics section), 16 (P) (1990) 21.
17 D.P.S. Rathore and P.K. Tarafder, J. Indian Chem. Soc., 68 (1991) 179.
18 D.P.S. Rathore and P.K. Tarafder, Anal. Chim. Acta, 257 (1992) 129.
19 R.K. Chugh, M. Kumar and D.P.S. Rathore, J. Indian Chem. Soc., (1993) Jan. issue.
20 M. Kumar and D.P.S. Rathore, J. Indian Chem. Soc., submitted for publication.

Analytica Chimica Acta, 281 (1993) 179–183
Elsevier Science Publishers B.V., Amsterdam

Resolution of acid strength in non-aqueous acid–base titrations

A. Gustavo González, M. Angeles Herrador and Agustín G. Asuero

Department of Analytical Chemistry, University of Seville, 41012 Seville (Spain)

(Received 18th January 1992; revised manuscript received 23rd February 1993)

Abstract

The equivalence between the resolution of the acid strength in a given solvent and the ratio (ρ^*/ρ) of Hammett's reaction constants for the solvent and water was obtained on the basis of empirical linear free energy relationships (LFER). The resolution for benzoic acids in a number of solvents from reported data was calculated by regression techniques. Fair correlations between the resolution and some solvent parameters such as the Mayer–Gutman acceptor number and the normalized Dimroth polarity parameter were observed.

Keywords: Titrimetry; Acid strength; Benzoic acids

The resolution of acid mixtures in a given medium depends on the nature of the acidic solutes and of the solvent. Each solvent possesses to a certain extent differentiating properties that permit the successive titration of components of acid mixtures [1]. A first attempt to evaluate such differentiating effect was made by Kreshkov et al. [2], who studied the relationship between the pK_a values of some substituted benzoic acids in several alcohols and in water and showed it to be linear. More recently, Chantooni and Kolthoff [3–6] studied this dependence for benzoic acids in a variety of aprotic and protophilic solvents. They defined the resolution of acid strength in a given medium for acids belonging to the same chemical family as the slope of the straight line obtained by plotting the pK_a^* for these acids in the given medium against pK_a in water, (see also [7]) that is,

$$pK_a^* = m\ pK_a + n \qquad (1)$$

Correspondence to: A. Gustavo González, Department of analytical Chemistry, University of Seville, 41012 Seville (Spain).

THEORETICAL BACKGROUND

Equation 1 is the general form of the correlation between the logarithm of the rate or equilibrium constant belonging to two reaction series or reaction media [8]. The linear free energy relationship (LFER) approach attempts to express reaction rates and equilibrium constants for a series of structurally related compounds (the chemical family) in terms of properties of the substituent groups and the reaction media [9] such as the well known Hammett relationships:

$$(pK_a)_{sub} = (pK_a)_0 - \rho \sum_i \sigma_i \qquad (2)$$

where the subscripts 0 and sub refer to the parent molecule (e.g., benzoic acid) and the *meta*- or *para*-substituted molecule, respectively, ρ is a reaction medium constant that is independent of the substituents and σ_i is a constituent constant that is independent of the reaction medium. The parameter ρ depends on the solvent, temperature and the nature of the acidic group in the aromatic nucleus (–COOH for benzoic acids, –OH

for phenols, $-NH_3^+$ for anilinium ions, etc.). The reaction constant expresses the sensitivity of the acidic group to inductive and resonant effects. This constant is assumed to be the same whether the compounds contain *meta* or *para* substituents, but it fails to account for *ortho* derivatives owing to steric and other short-range effects. This common approach is the general rule. However, recent studies [10] have given evidence that the effects of *meta* and *para* substituents are different in nature. According to Ludwig et al. [10], the classical Hammett equation, treating *meta* and *para* derivatives together is strictly valid only in the simplest cases ("similarity models") or when the small number of data prevent a more correct treatment. For our purposes, the classical approach is adequate enough. The substituent constant σ_i measures the ability of the substituent i (*meta* or *para*) either to withdraw electrons from the ring or to donate them by induction or resonance.

RESULTS AND DISCUSSION

Consider a set of fourteen benzoic acids (Table 1) in the following solvents: water, methanol, ethanol, *N*,*N*-dimethylformamide (DMF), acetonitrile (ACN) and dimethyl sulphoxide (DMSO). When the corresponding pK_a data were subjected to factor analysis (FA), two primary factors emerged. The technique of target factor analysis (TFA) according to Malinowski [9] was utilized for testing two possible target solute factors: unity to account for the unity coefficient multiplier of the $(pK_a)_0$ term and the Hammett σ constant, obtained from previous studies involving only *meta* and *para* groups. As can be observed in Table 1, the agreement is satisfactory, considering the experimental errors and the dispersion due to the different sources of data.

TABLE 1

Target factor analysis for the pK_a data for fourteen *meta*- and *para*-substituted benzoic acids [a]

Solute substituent	Unity		Hammett σ constant	
	Test	Prediction	Test [b]	Prediction
H	1	1.00	0.00	0.05
m-$COCH_3$	1	0.99	0.36	0.29
p-$COCH_3$	1	1.00	0.47	0.42
p-NH_2	1	1.00	−0.57	−0.55
m-Br	1	0.99	0.39	0.43
p-Br	1	1.00	0.22	0.28
m-Cl	1	1.01	0.37	0.42
p-Cl	1	1.00	0.24	0.27
m-CN	1	1.00	0.62	0.60
p-CN	1	0.99	0.70	0.64
m-OH	1	0.98	0.13	0.03
p-OH	1	0.98	−0.38	−0.37
m-NO_2	1	0.99	0.74	0.68
p-NO_2	1	0.99	0.78	0.72

[a] pK_a data taken from [11] for all solvents except DMSO [13].
[b] Values taken from [12].

This shows that although completely empirical, LFER may be directed by some theoretical concepts. Returning to the Hammett relationships, and taking into account that $\sum_i \sigma_i$ is independent of the solvent, one can write

$$[(pK_a)_{sub} - (pK_a)_0]/\rho = [(pK_a^*)_{sub} - (pK_a^*)_0]/\rho^* \quad (3)$$

where the asterisks indicate another solvent different from water. Rearrangement gives

$$(pK_a^*)_{sub} = (\rho^*/\rho)(pK_a)_{sub} + [(pK_a^*)_0 - (\rho^*/\rho)(pK_a)_0] \quad (4)$$

As can be observed, Eqns. 1 and 4 are essentially the same (disregarding the subscript sub) and from them one obtains

$$m = \rho^*/\rho \quad (5)$$

Equation 5 is very interesting because it shows that for the ionization of *meta*- and *para*-substituted benzoic acids (characterized by $\rho = 1$ at 25°C) the resolution, m, is equal to the reaction medium constant in the solvent studied, ρ^*.

The reaction medium constant for any solvent can be obtained by fitting Eqn. 2 from the pK_a values of a number of *meta*- and *para*-substituted parent acids (benzoic acids, phenols, anilinium ions, etc.) and the Hammett substituent constants σ (*meta* and *para*) [11]. Alternatively, this could be also attained by regression of eqn. 1. From Eqn. 5 the fitted value of m is converted into ρ^* taking into account the tabulated values of the reaction medium constant for water [ρ(benzoic

TABLE 2

Resolution of acid strength, m, with reference to water

Solvent [a]	$m \pm$S.D. [b]	$r(n)$ [c]	Ref.
MeOH	1.48±0.03	0.994 (37)	11
EtOH	1.66±0.06	0.978 (37)	11
IPA	1.83±0.12	0.993 (5)	6
TBA	3.27±0.25	0.988 (6)	6
ExOH	1.76±0.14	0.990 (5)	6
DMF	2.29±0.11	0.965 (38)	11
ACN	2.10±0.08	0.981 (32)	11
SL	2.10±0.12	0.959 (34)	11
Acetone	2.29±0.11	0.961 (33)	11
DMSO	2.61±0.16	0.978 (14)	13
THF	4.46±0.17	0.995 (8)	7

[a] Abbreviations: MeOH, methanol; EtOH, ethanol; IPA, isopropyl alcohol; TBA, *tert*-butyl alcohol; ExOH, *n*-hexanol; DMF, *N,N*-dimethylformamide; ACN, acetonitrile; SL, sulpholane; DMSO, dimethyl sulphoxide; THF, tetrahydrofuran. [b] Standard deviation of the slope m of the fitted straight line (with n as in the next column). [c] Correlation coefficient, r, with number of observations, n, in parentheses.

acids) = 1, ρ(phenols) = 2.23, ρ(anilinium ions) = 2.88, etc.] [12]. Thus, from the pK_a values reported by several workers [6,7,11,13] for the ionization of *meta*- and *para*- substituted benzoic acids in several solvents, the resolution $m = \rho^*$ was evaluated by regression analysis of Eqn. 1. The results are given in Table 2.

At first glance, tetrahydrofuran (THF) seems to be optimum for titration of acid mixtures. However, THF exhibits a low relative permittivity of 7.6 and, accordingly, proton transfer equilibria are greatly complicated by ion association leading to ion pairs of various types [7]. Therefore, THF is a less suitable solvent for acid–base titration. DMSO, with a high relative permittivity of 46.6, and still with a high resolution value, would then be considered as the optimum solvent. Moreover, its relatively large break at the end-point of the titration [14,15] and other features (low toxicity, suitable viscosity, very good solvent for organic and inorganic substances) indicate that DMSO [or better a water–DMSO (3 + 97) mixture] is an excellent medium for non-aqueous titrations [16].

The occurrence of a high resolution value in a given solvent may be explained on the basis of dispersion interactions [17]. Electronegative non-*ortho* substituents markedly increase the dispersion interaction of the aromatic conjugate base ($Ar-COO^-$) with the solvent:

$$Ar-COOH \rightleftharpoons Ar-COO^- + H^+$$

If the solvent is a strong hydrogen bond donor (HBD), the negative charge of the aromatic anion becomes localized on the oxygen atom and it is hardly dispersed by the substituents. Conversely, if the solvent is a weak HBD, the electronegative substituents can disperse the negative charge over the aromatic ring. The large resolution of benzoic acids in diprotic apolar solvents can be attributed to a marked increase in dispersion interaction of the aromatic anion $Ar-COO^-$ with the solvent. Hence the solvatochromic parameter α (HBD scale) [18] would be a suitable indicator of the resolution in a given solvent. However, aprotic dipolar media are characterized by a value of $\alpha = 0$ and consequently it would be advisable to use another indicator. The Mayer–Gutmann acceptor number (MGAN), which is a measure of the electron acceptor strength of the solvent based on the ^{31}P chemical shift of triethylphosphine oxide in the solvent [19,20], is suggested as a good indicator of the resolution. When the MGAN decreases, the resolution in the solvent increases. THF shows the lowest MGAN value, 8, and the greatest resolution, 4.46, and conversely water exhibits the highest MGAN value, 54.8, and the lowest resolution, unity. The following empirical relationship was found by using the MGAN values available [19,20]:

$$m = 0.77 + 27.08(1/\mathrm{MGAN}) \quad r = 0.939\ (n = 9) \tag{6}$$

A better solvent parameter would be the Dimroth-Reichardt solvatochromic parameter $E_T(30)$ [21], which is related to the α and π^* (Kamlet–Taft dipolarity–polarizability solvent parameter) scales according to [22]

$$E_T(30) = 30.31 + 14.6\pi^* + 15.53\alpha$$

Nowadays, a normalized $E_T(30)$ parameter (E_T^N) referred to tetramethylsilane ($E_T^N = 0$) and water ($E_T^N = 1$) is preferred [23]. It can easily be obtained:

$$E_T^N = [E_T(30) - 30.7]/32.4$$

TABLE 3

Values of MGAN and E_T^N for various solvents

Solvent [a]	MGAN [b]	E_T^N [c]
MeOH	41.3	0.762
EtOH	37.1	0.722
IPA	33.5	0.546
TBA	–	0.387
DMF	16.0	0.404
ACN	18.9	0.460
Acetone	12.5	0.355
DMSO	19.3	0.444
THF	8.0	0.207
Water	54.8	1.000

[a] Abbreviations as in Table 2. [b] Values taken from [19] and [20]. [c] Values taken from [23].

The E_T^N parameter is another good indicator of the resolution of the acid strength. Similarly to MGAN, THF shows the lowest E_T^N value, 0.207 and the greatest resolution, 4.46, and water exhibits the highest E_T^N value, 1.00 and the lowest resolution, unity. The following empirical equation relating m and E_T^N was found:

$$m = 0.989/E_T^N \quad r = 0.931 \ (n = 10) \qquad (7)$$

Taking into account that the E_T^N parameter has been determined for a wide variety of solvents, it will be preferred for prediction purposes. The values of the MGAN and E_T^N parameters are given in Table 3.

When *ortho*-substituted benzoic acids are fitted according to Eqn. 1 the resolution values obtained are lower than for *meta* and *para* substitutions. Thus, for instance, the resolution in THF for ortho-substituted benzoic acids is 2.75 and for di-*ortho*-substituted benzoic acids 1.25 compared with the value of 4.46 for the corresponding *meta* and *para* derivatives. This has been explained by Barbosa et al. [7] on the basis of solute–solvent interactions on the *ortho*-substituted benzoic acid. They stated that one or more water molecules (or other solvent molecules such as *n*-alkanols) are fixed by ion–dipole, ion-quadrupole and especially hydrogen bond interactions by forming a ring among the molecule of water, the *ortho* substituent and the carboxylate residue. This ring stabilizes the anion and increases the dissociation of the acid in water or HBD solvents but not in dipolar aprotic solvents and some other than cannot form such a ring. Thus, by solute–solvent interactions that occur selectively depending on the HBD character of the medium, a decrease in the resolution values for *ortho* and di-*ortho*-substituted benzoic acids is expected.

Conclusion

The equivalence between the resolution of acid strength in a given solvent with respect to water and the ratio ρ^*/ρ has been established. The resolution observed for the benzoic acids in different solvents is explained according to the Hammett relationships (for *meta* and *para* derivatives) and on the basis of differential solute–solvent interactions (for *ortho* substitutions). Resolution seems to be fairly well correlated with the reciprocal of the MGAN and E_T^N parameters.

The financial support of the Dirección General de Investigación Científica y Técnica de España (Project PB 89-0630) is gratefully acknowledged.

REFERENCES

1 A.P. Kreshkov, Talanta, 17 (1970), 1029.
2 A.P. Kreshkov, N.S. Aldarova and N.T. Smolova, Zh. Obshch. Khim., 39 (1969) 1390.
3 M.K. Chantooni and I.M. Kolthoff J. Phys. Chem., 80 (1976) 1306.
4 M.K. Chantooni and I.M. Kolthoff J. Am. Chem. Soc., 92 (1970) 7025.
5 M.K. Chantooni and I.M. Kolthoff, Anal. Chem., 51 (1979) 133.
6 I.M. Kolthoff and M.K. Chantooni, J. Am. Chem. Soc., 93 (1971) 3843.
7 J. Barbosa, D. Barrón, E. Bosch and M. Rosés, Anal. Chim. Acta, 265 (1992) 157.
8 P.R. Wells, Linear Free Energy Relationships, Academic, London, 1968, Chap. 1 and 4.
9 E.R. Malinowski, Factor Analysis in Chemistry, Wiley, New York, 1991, Chap. 10.
10 M. Ludwig, S. Wold and O. Exner, Acta Chem. Scand., 46 (1992) 549.
11 M. Ludwig, W. Baron, K. Kalfus, O. Pitela and M. Vecera, Collect. Czech. Chem. Commun., 51 (1986) 2135.
12 D.D. Perrin, B. Dempsey and E.P. Serjeant, pK_a Prediction for Organic Acids and Bases, Chapman and Hall, London, 1981.

13 K. Isutzu, Acid–Base Dissociation Constants in Diprotic Apolar Solvents, Blackwell, Oxford, 1990, pp. 64–100.
14 L. Sucha, and S. Kotrly, Solution Equilibria in Analytical Chemistry, Van Nostrand-Reinhold, Princenton, NJ, 1972.
15 A.G. Gonzalez, M.A. Herrador and A.G. Asuero, Microchem. J., 44 (1991) 243.
16 O. Budevsky, Talanta, 36 (1989) 1209.
17 E. Grunwald and E. Price, J. Am. Chem. Soc., 86 (1964) 4517.
18 R.W. Taft and M.J. Kamlet, J. Am. Chem. Soc., 98 (1976) 2886.
19 J.F. Coetzee, B.K. Deshmukh and C.C. Liao, Chem. Rev., 90 (1990) 827.
20 V. Gutman, The Donor–Acceptor Approach to Molecular Interactions. Plenum, New York, 1978.
21 K. Dimroth, C. Reichardt, T. Siepmann and F. Bohlmann, Justus Liebigs Ann. Chem., 661 (1963) 1.
22 M.J. Kamlet, J.M. Abboud, M.H. Abraham and R.W. Taft, J. Org. Chem., 48 (1983) 2877.
23 E. Bosch and M. Rosés, J. Chem. Soc., Faraday Trans., 88 (1992) 3541.

Analytica Chimica Acta, 281 (1993) 185–190
Elsevier Science Publishers B.V., Amsterdam

Automatic on-line preconcentration system for graphite furnace atomic absorption spectrometry for the determination of trace metals in sea water

Zhen-Shan Liu and Shang-Da Huang

Department of Chemistry, National Tsing Hua University, Hsinchu 30043 (Taiwan)

(Received 8th December 1992; revised manuscript received 22nd February 1993)

Abstract

An automatic on-line preconcentration system for graphite furnace atomic absorption spectrometry (GFAAS) for the determination of trace metals in sea water was developed. This system was modified from a Perkin-Elmer AS-40 autosampler by mounting a silica gel C_{18} microcolumn near the tip of the automsampler capillary. The preconcentration procedure was performed by using the pumps of the AS-40 autosampler and a four-way valve and controlled by a programmable controller. The chelating agent ammonium tetramethylenedithiocarbamate [ammonium pyrrolidinedithiocarbamate (APDC)] was added to the sample solution and only 0.2–2 ml of sample was required to determine cadmium and copper in sea water. The calibration graph method was used and the detection limits of cadmium and copper were 1.26 and 6.5 ng l^{-1}, respectively.

Keywords: Atomic absorption spectrometry; Cadmium; Copper; Preconcentration; Sea water; Trace metals; Waters

In general, the concentration range of the trace metals in sea water is $\mu g\ l^{-1}$ to ng l^{-1} so that the method used for the determination must be highly sensitive, such as inductively coupled plasma mass spectrometry, graphite furnace atomic absorption spectrometry (GFAAS) and anodic stripping voltammetry [1]. GFAAS has been used to determine trace metals in sea water directly [2], but this technique has some limitations. Direct determination by GFAAS is difficult not only because of the presence of many trace metals in sea water near or even below the detection limits, but also the matrix of sea water may cause serious interference.

Preconcentration steps not only concentrate the analyte but can also simplify the matrix of the sample. Many kinds of preconcentration methods have been reported, such as coprecipitation, ion exchange, liquid–liquid extraction and solid-phase extraction [3]. It seems that the solid-phase extraction is better than liquid–liquid extraction, because it is more efficient, reproducible and simpler in sample handling and transfer [4]. The solid-phase extraction technique has been used over 10 years ago to preconcentrate trace metals in sea water followed by determination by GFAAS [5]. Traditional off-line solid-phase extraction required very large sample volumes (500–1000 ml) for preconcentration, and only a small part of the eluate was used. Sometimes, the eluate from a solid-phase extraction must be digested with concentrated acid to destroy the metal complexes and to transfer the analyte to the aqueous phase for the feasibility of the instrument.

Correspondence to: S.D. Huang, Department of Chemistry, National Tsing Hua University, Hsinchu 30043 (Taiwan).

These drawbacks were solved by using an on-line flow-injection column preconcentration in atomic spectrometry which has been reviewed by Fang [6,7]. Fang et al. [8] and Sperling et al. [9–11] modified the on-line flow-injection mode of a flame atomic absorption spectrometer to achieve feasibility of determination by GFAAS. Porta et al. [12] used different materials in a preconcentration column. The above systems had the problem that the eluate volume of the micro-column was larger than the capacity of the injection sample of the graphite furnace. Fang et al. [8] and Sperling et al. [9–11] solved this problem by using the sub-sampling technique. Porta et al. [12], on the other hand, eluted the microcolumn twice and evaporated the solvent of the eluate twice in the graphite furnace.

It has recently been reported [13] that by using a smaller amount of C_{18} material in the microcolumn and using an ammonium tetramethylenedithiocarbamate [ammonium pyrrolidinedithiocarbamate (APDC)] complex, the analyte (copper and cadmium) in sea water can be recovered quantitatively from the microcolumn with only 40 μl of methanol, and that all the eluate can be injected directly into the graphite furnace. The drawback of that work was the need for manual manipulation in the preconcentration procedure. This paper describes the improvement of this manual system and its conversion into an automatic on-line preconcentration system by using a modified Perkin-Elmer AS-40 autosampler, a four-way distribution valve and a programmable controller. The accuracy of this automatic method was examined by the analysis of certified reference sea water.

EXPERIMENTAL

Chemical and reagents

All the chemicals used and the purification methods were the same as reported earlier [13]. The chelating agent, 5% (w/v) APDC (Fluka), was prepared weekly. The buffer solution used was 5 M ammonium acetate (Fluka) solution. The washing solution was prepared by adding 1 ml of buffer solution to 1.25 ml of APDC solution, diluted to 25 ml and purified by passing through a Sep-Pak C_{18} cartridge. Methanol and nitric acid were purified by means of sub-boiling distillation and deionized water was obtained from a Milli-Q purification system (Millipore). NASS-2 and SLEW-1 sea-water reference standards were obtained from the Marine Analytical Chemistry Standards Program of National Research Council of Canada. Merck standard solution (1000 μg ml^{-1}) was used to prepare the standard solution to establish a calibration graph [13]. The temperature programmes for GFAAS for cadmium and copper are presented in Table 1. A Perkin-Elmer Zeemam 5100PC atomic absorption spectrometer equipped with an HGA-600 graphite furnace was used throughout. The graphite tube used was pyrolytically coated with a platform in it.

Sample and reference standard solution preparation

A sample aliquot (200–2000 μl) was accurately pipetted into a sample cup, followed by addition of 10–20 μl of 5% APDC solution and 20–50 μl of the buffer solution to adjust the pH of the solution within the range 6–8. The flow-rate of sample loading was ca. 5 $\mu l\ s^{-1}$, which was faster than that used previously [13]. Standard aliquots

TABLE 1

Temperature programme of graphite furnace

Step	Cu			Cd		
	Temperature (°C)	Ramp (s)	Hold (s)	Temperature (°C)	Ramp (s)	Hold (s)
Drying	120	5	20	120	5	20
Ashing	300	5	35	300	5	35
Cooling	20	1	15	20	1	15
Atomization	2400	0	6	1200	0	5
Clean-out	2650	1	5	2600	1	5

(Cd 0–1.0 $\mu g\ l^{-1}$, 20 μl; Cu 0–2 $\mu g\ l^{-1}$, 200 μl) were treated in the same way as the sample aliquots.

Automatic on-line preconcentration system

The C_{18} microcolumn was prepared using a PTFE capillary tube of the AS-40 autosampler (2.5 cm × 0.94 mm i.d.) (Perkin-Elmer), packed with 5 mg (ca. 7 μl) of silica gel C_{18} (particle size 50–105 μm). In both ends of microcolumn polyethylene frits (porosity 0.5 μm) were fixed. The materials of the C_{18} microcolumn except the capillary tubing were taken from a Sep-Pak C_{18} cartridge (Waters). The C_{18} microcolumn was mounted near the tip of the capillary sampler. The four-way distribution valve (Omnifit) was switched pneumatically.

A diagram of the automatic on-line preconcentration system modified from the AS-40 autosampler is presented in Fig. 1. Pump 1 (g) was used to suck the solutions sequentially from the sample cups in the sample tray (c). Pump 1 was connected to the sampler capillary (b) and the microcolumn (a) through the four-way distribution valve (f). Pump 2 (d) was used to suck methanol in the bottle (h) and to push methanol eluate into the graphite tube (i). Pump 2 (d) was connected to the methanol bottle (h) or the sampler capillary (a) through the delay tubing (e) and the four-way distribution valve (f). The on-line preconcentration system was operated automatically and controlled digitally by a programmable controller (Sysmac C120; Omoron, Tokyo, Japan).

Procedure

Methanol, deionized water, a sample aliquot (or standard solution) and washing solution were placed sequentially into the sample cups in the sample tray; the volumes of sample aliquots (or standards) must be transferred accurately into

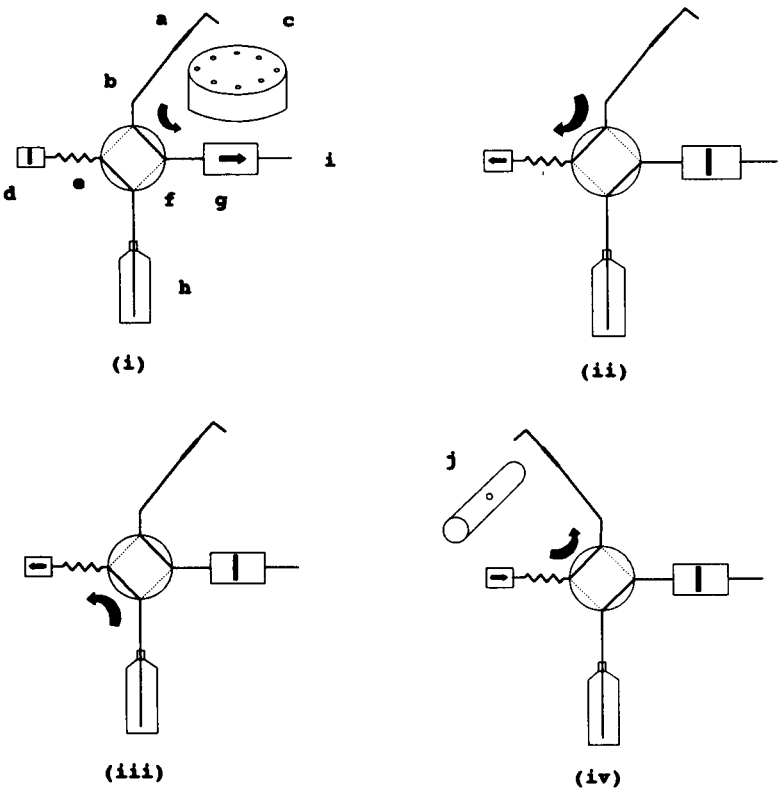

Fig. 1. On-line preconcentration system. (a) C_{18} microcolumn; (b) sampler capillary; (c) sample tray; (d) pump 2; (e) delay tubing; (f) four-way distribution valve; (g) pump 1; (h) methanol in bottle; (i) to waste; (j) graphite furnace.

TABLE 2

Preconcentration steps

Step	Fig. 1	Time (s)	Pump 1	Pump 2	Sampler capillary position	Purpose
1	(i)	16	On	Off	Methanol cup	Wash column
2	(i)	11	On	Off	Deionized water	Change mobile phase
3	(i)	104 [a]	On	Off	Sample cup	Load sample
4	(i)	14	On	Off	Washing solution cup	Wash matrix of sample in column
5	(i)	16	On	Off	Empty cup	Dry tubing and column
6	(ii)	20	Off	Pull	Up	Draw air into tubing
7	(iii)	9	Off	Pull	Up	Draw methanol into tubing
8	(iv)	58	Off	Push	Graphite tube	Elute analyte

[a] Depends on sample volume. Here it is 500 μl.

the sample cups with a micropipette. After inputting the parameters of the Sysmac C120, the system will execute all the preconcentration steps automatically. The procedures are described as follows and are outlined in Table 2 and Fig. 1.

The sampler capillary (b) was connected to pump 1 (g) and the sampler capillary sucked the methanol in the first sample cup to wet the C_{18} microcolumn, then the sample tray was rotated and the sampler capillary sucked the deionized water in the second sample cup to change the mobile phase of the microcolumn. The sampler capillary then sucked the sample or standard aliquot (these aliquots should be sucked completely). After the washing solution in the fourth sample cup had been sucked, the sample capillary sucked air in order to dry the C_{18} microcolumn. The above actions are shown in Fig. 1 (i) and Table 2 (steps 1–5).

When a series of suctions of liquid in sample tray had been completed, the four-way valve turned clockwise and connected the sampler capillary with pump 2 (d), then pump 2 began to suck some air in order to transfer all the methanol eluate into the graphite tube (i) in the elution step (step 8 in Table 2). This action is shown in Fig. 1 (ii) and Table 2 (step 6).

The four-way valve turned counterclockwise to suck the methanol in the bottle [see Fig. 1 (iii) and step 7 in Table 2] and turned clockwise again to connect the sampler capillary with pump 2 [see Fig. 1 (iv)]. Pump 2 transferred all the methanol eluate into the graphite tube (step 8 in Table 2). When elution procedure was completed, the four-way valve turned counterclockwise to the starting position in Fig. 1 (i).

When GFAAS was executed with temperature programming, the on-line preconcentration sys-

TABLE 3

Results of examination of the accuracy of the method

Standard sea water	Cu		Cd	
	This method ($\mu g\,l^{-1}$) [a]	Certified value ($\mu g\,l^{-1}$)	This method ($\mu g\,l^{-1}$) [a]	Certified value ($\mu g\,l^{-1}$)
NASS-2	0.104 ± 0.004 (100) [b]	0.109 ± 0.011	0.0309 ± 0.0005 (25) [b]	0.029 ± 0.004
SLEW-1	1.80 ± 0.04 (10) [b]	1.76 ± 0.09	0.0156 ± 0.0002 (25) [b]	0.018 ± 0.003

[a] Averages and standard deviations for seven runs. [b] Concentration factor.

tem also proceeded simultaneously with the preconcentration procedure for the next sample.

RESULTS AND DISCUSSION

The accuracy and precision of the method using this automatic on-line preconcentration system were examined by the determination of copper and cadmium concentrations in the open-ocean standard NASS-2 and the estuarine water standard SLEW-1. The results in Table 3 show that this automatic system provides analytical data within the ranges of the certified values. The average values of the absolute blanks for copper and cadmium are 19 and 1.19 pg, respectively. The detection limits for copper and cadmium are 6.5 and 1.26 ng l^{-1}, respectively. The absolute blank values were obtained by using the preconcentration and determination procedures with 20 μl of deionized water; the detection limit was obtained by dividing three times the standard deviation of the blank values (copper and cadmium concentration) by the concentration factor (copper 100; cadmium 25).

It was very difficult to control the rate of liquid suction or volume of liquid sucked very precisely, not only because pull-and-push pumps are used in this preconcentration system, but also because the microcolumn is located near the tip of the sampler capillary. Even though the action of the pumps can be controlled precisely by the digital controller, the back-pressure inside the tubing causes the flow-rate of the liquid to vary to some extent. The effects of small variations in the volumes of methanol, deionized water and washing solution transferred may not be significant, but precise control of the amount of sample solution is extremely important in order to obtain highly accurate and precise analytical results. To solve this problem, the precise amounts of sample aliquots or standard solutions are transferred to the sample cups with a micropipette (APDC solution and buffer solution are also added to the sample cups with sea-water samples) and all the solution is sucked out from the sea-water sample cups by the pump.

The time required to concentrate 500 μl of sample using this automatic system was 251 s, which is shorter than that using the manual system [13]. As the analytes (copper and cadmium) in sea-water samples can be recovered quantitatively from the microcolumn with only 40 μl of methanol, and all the eluate can be injected directly into the graphite furnace, there is no need for a sub-sampling technique as in other methods [8–11]; also, the sensitivity of the analysis is increased by a factor of two or more. Further, standard solutions are used with much higher concentrations and smaller volumes (e.g., 20 μl of 0.5–1.0 μg l^{-1} Cd compared with 3 ml of 0.01–0.03 μl^{-1} Cd) to obtain the calibration graph. The risk of errors caused by the contamination of the standard solution is reduced using standard solutions with higher concentrations. The precision and accuracy of the results of this work are comparable to those of other methods [8–13]. The drawback of this preconcentration system is that owing to the use of the pull-and-push pumps of the AS-40 autosampler, only half of the time is available for suction of sample liquid. This drawback could probably be improved if the pumps were to be replaced with peristaltic pumps. Another drawback of this system is that exact amounts of sample aliquots must be placed in the sample cups manually with a micropipette.

In conclusion, the precision and accuracy of the results of this work are comparable to those of other methods [8–13]. As there is no need to use a sub-sampling technique, the disadvantage caused by such techniques [8–11] are avoided, and the sensitivity of the analysis is increased by a factor of two or more.

The authors are indebted to the National Science Council of the Republic of China for a grant (NSC 82-0421-M-007-095-Z) in support of this work. They are also indebted to Mr. Jiann-Chang Chen for his help in writing the program for the preconcentration system.

REFERENCES

1 T.R. Crompton, Analysis of Seawater, Butterworths, Guildford, 1989.
2 D.L. Tsalev, V.I. Slaveykova and P.B. Mandjukov, Spectrochim. Acta Rev., 13 (1990) 225.

3 Y.A. Zolotov and N.M. Kuz'min, Comprehensive Analytical Chemistry, Vol. XXV, Elsevier, Amsterdam, 1990.
4 M. Zief and R. Kiser, Am. Lab., 20 (1990) 70.
5 H. Watanabe, K. Goto, S. Taguchi, J.W. McLaren, S.S. Berman and D.S. Russell, Anal. Chem., 53 (1981) 738.
6 Z.-L. Fang, Spectrochim. Acta Rev., 14 (1991) 235.
7 J.L. Burguera (Ed.), Flow Injection Atomic Spectroscopy, Dekker, New York, 1989.
8 Z.-L. Fang, M. Sperling and B.J. Welz, J. Anal. At. Spectrom., 5 (1990) 639.
9 M. Sperling, X. Yin and B.J. Welz, J. Anal. At. Spectrom., 6 (1991) 295.
10 M. Sperling, X. Yin and B.J. Welz, J. Anal. At. Spectrom., 6 (1991) 615.
11 M. Sperling, X. Yin and B. Welz, Spectrochim. Acta, Part B, 46 (1991) 1789.
12 V. Porta, O. Abollino, E. Mentasti and C. Sarzanini, J. Anal. At. Spectrom., 6 (1991) 119.
13 Z.-S. Liu and S.-D. Huang, Anal. Chim. Acta, 267 (1992) 31.

Analytica Chimica Acta, 281 (1993) 191–195
Elsevier Science Publishers B.V., Amsterdam

Quantitative desorption of humic substances from Amberlite XAD resins with an alkaline solution of sodium dodecyl sulfate

Mohammad-Hussein Sorouradin [1], Masataka Hiraide, Young-Sang Kim [2] and Hiroshi Kawaguchi

Department of Materials Science and Engineering, Nagoya University, Nagoya 464 (Japan)

(Received 28th January 1993; revised manuscript received 12th March 1993)

Abstract

Microgram quantities of humic or fulvic acid are quantitatively adsorbed on a small amount (ca. 1 ml) of pulverized Amberlite XAD-2 and XAD-8 resins. A sodium hydroxide solution, aqueous ammonia, or a mixture of methanol and aqueous ammonia leads to very low desorption recoveries of the humic substance, however. Pre-saturation of strong adsorption sites of the resin with some surfactants increases the desorption recovery, but it is not quantitative. The desorption efficiency is tremendously improved with the aid of an anionic surfactant. Humic and fulvic acids retained on the XAD resins are completely desorbed with 200 mg of sodium dodecyl sulfate in 10 ml of 0.1 M sodium hydroxide solution. The surfactant does not interfere with the spectrophotometric determination of humic substances. Further, it can be removed from the solution as a precipitate by increasing the alkalinity to 0.25 M.

Keywords: Spectrophotometry; Adsorption; Desorption; Fulvic acids; Humic acids; Waters

Naturally occurring humic and fulvic acids, the major organic constituents of fresh water, interact with various heavy metals to form negatively charged humic complexes [1–3]. For example, 50–70% of dissolved iron and copper in river water were found to be humic complexes [4–6]. These humic substances are also considered to be precursors of organic halogenated compounds formed during chlorination of water [7]. Therefore, determination and characterization of humic substances are essential for a better understanding of the environmental and geochemical role of these compounds.

Correspondence to: M. Hiraide, Department of Materials Science and Engineering, Nagoya University, Nagoya 464 (Japan).
[1] Present address: Faculty of Chemistry, University of Tabriz, Tabriz (Iran).
[2] Department of Chemistry, College of Natural Sciences, Korea University, Jochiwon, Choong-nam 339-700 (Korea).

Generally, the concentration of humic substances in fresh water is too low for direct analysis, hence a preconcentration step is required. The most common preconcentration technique seems to be adsorption on macroreticular adsorbents, especially on Amberlite XAD resins [2,8]. The adsorbents collect humic substances more selectively than anion exchangers such as diethylaminoethyl (DEAE)–cellulose [9] and DEAE–Sephadex A-25 [10]. Variety of reagents such as sodium hydroxide, aqueous ammonia and alkaline solution of methanol have been used for the desorption of milligram quantities of humic substances from XAD resins, with recoveries of 83–96% [11]. However, we experienced that none of these reagents proved to be useful for the desorption of microgram quantities of humic substances because of the presence of irreversible sorption sites.

The present paper describes the significant

enhancement of desorption recovery from XAD resins with the aid of an alkaline solution of sodium dodecyl sulfate. The humic or fulvic acid is completely desorbed with a minimum volume of the eluant. The surfactant has also advantages of negligible absorbance at 400 nm (commonly used for the spectrophotometric determination of humic substances) and the ease of removal from the humic substances.

EXPERIMENTAL

Apparatus

A Retsch Model MM vibrating pulverizer was used for pulverizing XAD resins with an agate grinding vial (18 mm inner diameter, 50 mm height) containing two agate balls (12 mm diameter). A Shimadzu UV-180 spectrophotometer was used with 5-cm cells for the measurement of absorbances at 400 nm to determine humic and fulvic acids. An Iwaki Model AP-220ZN air pump was used for suction through the XAD resin column.

Reagents

A humic acid solution (200 μg ml^{-1}) was prepared by dissolving humic acid powder (Nakarai Chemicals, extracted from peat soil) in 0.1 M sodium hydroxide solution and filtering through 0.45-μm Millipore filters. A fulvic acid solution (1.0 mg ml^{-1}) was prepared by dissolving fulvic acid powder (extracted from brown forest soil [12]) in water.

Amberlite XAD-2 or XAD-8 resin (200–800 μm in diameter) was pulverized to particles of 10–100 μm and washed ultrasonically in ethanol followed by water. The resin was then packed into a column (5 mm $\times$ 15 mm i.d.), which was supported by a sintered-glass disk. A 0.45-μm Millipore filter was inserted between the packed resin and sintered-glass disk to prevent the disk from clogging.

Surfactants used include sodium dodecyl sulfate (SDS, anionic), sodium dodecylbenzene sulfonate (ABS, anionic), benzalkonium chloride (BC, cationic) and Brij-35 [non-ionic, $C_{12}H_{25}$-$(OCH_2CH_2)_{23}OH$].

Procedure

A water sample (50 ml, pH 7) containing microgram quantities of humic or fulvic acid was acidified to pH 1.5 with 4 M hydrochloric acid and passed through the XAD resin column at a flow-rate of 4 ml min^{-1}. The humic substance retained on the column was desorbed with 10 ml of eluant at a flow-rate of 1 ml min^{-1}. To obtain the humic recovery, the absorbance of the effluent was measured at 400 nm and compared with that of the original sample solution at the same pH.

RESULTS AND DISCUSSION

Adsorption of humic substances on XAD resins

Amberlite XAD resins are generally divided into two groups: styrene–divinylbenzene copolymers and polymethacrylate-based materials [13]. In the present work, typically XAD-2 (the former type) and XAD-8 (the latter type) were used in pulverized form, because the pulverization had enhanced the adsorption efficiency [4].

The adsorption behavior was first examined by using humic substances at μg ml^{-1} levels, because those concentrations provided the sufficient absorbance in spectrophotometry. Water (50 ml, pH 1.5) containing humic or fulvic acid was passed through the XAD resin column at a flow-rate of 4 ml min^{-1}. The extent of adsorption was determined by directly comparing the absorbance of the original sample and the column effluent. As shown in Table 1, humic and fulvic acids are recovered in greater than 96% yields with the small volume (ca. 1 ml) of pulverized XAD resin. Humic acid precipitates in acidic solutions, but visible precipitates were not observed with such a tiny amount of humic acid.

Desorption of humic substances with conventional eluants

A sample solution (50 ml, pH 1.5) containing 50 μg of humic acid or 100 μg of fulvic acid was introduced on the XAD-2 or XAD-8 column and then desorption was carried out by passing 10 ml of eluants used in the literature [11] at a flow-rate of 1 ml min^{-1}. As shown in Table 2, none of

TABLE 1

Adsorption efficiency of humic substances on XAD-2 and XAD-8 columns

Resin	Humic substance	Amount (μg in 50 ml water)	Adsorbed at pH 1.5 (%)
XAD-2	Humic acid	50	98, 100
	Humic acid	250	99, 99
	Humic acid	500	99, 100
	Fulvic acid	100	98, 99
	Fulvic acid	250	98, 100
	Fulvic acid	500	98, 99
XAD-8	Humic acid	50	99, 100
	Humic acid	250	98, 99
	Humic acid	500	99, 100
	Fulvic acid	100	96, 98
	Fulvic acid	250	97, 99
	Fulvic acid	500	98, 99

these eluants proved to be useful for quantitative recovery of humic substances, although a better recovery was obtained from XAD-8. Considerable difference was not observed between the desorption efficiency of humic and fulvic acids.

The desorption efficiency was also examined using samples containing varying amounts of humic substances. Table 3 shows that desorption recovery is affected by the amount of the loaded humic substances on the resin. This indicates that there is a limited number of strong sorption sites on both types of resins on which humic substances are retained and cannot be desorbed.

TABLE 2

Desorption efficiency of humic substances from XAD-2 and XAD-8 columns with conventional eluants

Resin	Eluant (10 ml)	Total recovery [a] (%)	
		Humic acid	Fulvic acid
XAD-2	0.1 M NaOH	10	13
	0.2 M NaOH	12	14
	1 M aq. NH_3	4	5
	CH_3OH+2 M aq. NH_3 (1:1)	12	15
XAD-8	0.1 M NaOH	58	65
	0.2 M NaOH	64	68
	1 M aq. NH_3	57	60
	CH_3OH+2 M aq. NH_3 (1:1)	67	70

[a] Including adsorption and desorption steps.

TABLE 3

Effect of humic substance quantity in the sample solution on its desorption from XAD columns [a]

Humic substance	Amount (μg in 50 ml solution)	Total recovery [b] (%)	
		XAD-2	XAD-8
Humic acid	50	10 (14)	58 (67)
	100	18 (22)	62 (71)
	500	42 (56)	69 (79)
	1000	51 (67)	74 (82)
	2000	63 (75)	78 (87)
Fulvic acid	100	18 (24)	65 (74)
	250	34 (42)	71 (82)
	500	46 (63)	75 (85)
	1000	54 (70)	78 (89)
	2000	65 (77)	82 (93)

[a] Desorbed with 10 ml (or 50 ml in parentheses) of 0.2 M sodium hydroxide solution. [b] Including adsorption and desorption steps.

Saturation of strong sorption sites of XAD resins

Pre-saturation of irreversible adsorption sites was tried by using ABS, because it has high affinity towards XAD-2 resin [13]. Pulverized XAD-2 resin, 1 g, was soaked in 50 ml of water containing ABS (5 mg ml^{-1}, pH 2) for 3 h, with gentle stirring, and packed into a column (5 mm $\times$ 15 mm i.d.). The column was then washed with 50 ml of 0.01 M hydrochloric acid.

Humic acid, 50 μg, in 50 ml of water was completely adsorbed on the pre-treated resin column. About 70% of the humic acid was then recovered with 10 ml of 0.2 M sodium hydroxide solution. Similarly, other surfactants were also examined for the pre-saturation. The recovery was 70 and 50% with SDS and Brij-35, respectively. Since our aim was quantitative recovery of humic substances, we moved on to other possible ways, such as searching for more effective eluants.

Effective desorption of humic substances with alkaline solutions of surfactants

It is known that surfactants enhance the water-solubility of sparingly soluble organic compounds, as a result of a partitioning of the solute into the interior of the micelle. Surfactants also

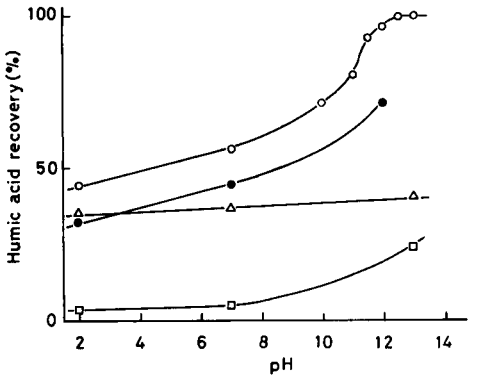

Fig. 1. Effect of pH on desorption of humic acid from XAD-2. Desorption was carried out with 10 ml of surfactant solution (20 mg ml^{-1}): (○) SDS, (●) ABS, (□) BC and (△) Brij-35.

form aggregates on solid surfaces and their interior is capable of solubilizing hydrophobic organic compounds [14,15].

In the present work, we used surfactants at relatively high concentrations to enhance the desorption of humic substances from XAD resins. After the adsorption of 50 μg of humic acid from 50 ml of water, the humic acid was desorbed with an anionic, cationic, or non-ionic surfactant at different pH's.

As it is shown in Fig. 1, alkaline solutions containing anionic surfactants, especially SDS, enhanced tremendously the humic acid desorption. The ABS solution went cloudy at pH higher than 12. Desorption efficiency was also dependent on the concentration of SDS, as shown in Fig. 2. Similar results were obtained for XAD-8 resin (see Table 4). Optimum conditions for maximum desorption were found to be pH 13 and an SDS concentration of 20 mg ml^{-1}.

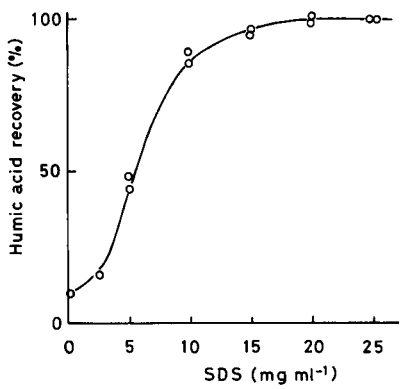

Fig. 2. Effect of SDS concentration on the desorption of humic acid from XAD-2. Desorption was carried out with 10 ml of 0.1 M sodium hydroxide solution containing SDS.

TABLE 4

Desorption of humic acid from XAD-8 with 10 ml of alkaline solution of surfactants

Surfactant (20 mg ml^{-1})	Desorption pH	Total recovery [a] (%)
SDS	13	98, 100
ABS	12	73, 75
BC	13	61, 62
Brij-35	13	66, 69

[a] 50 μg of humic acid was adsorbed and then desorbed.

Under the optimal conditions, fulvic acid (100 μg) desorption from both XAD-2 and XAD-8 resins was also quantitative ($\geq$ 98%).

Removal of SDS from humic substances

Presence of SDS did not affect the spectrophotometric determination of humic or fulvic acid. The absorbance of SDS solution (20 mg ml^{-1} in a 0.1 M sodoum hydroxide solution) was 0.015 at 400 nm in a 5-cm cell.

In characterization studies, however, SDS (200 mg used for desorption) should be removed from the solution. This was effectively achieved with a minimum effort such as precipitation by increasing sodium hydroxide concentration to 0.25 M or higher, refrigerating overnight, and filtration through a 0.45-μm filter without any loss of humic substances. The SDS remaining in the filtered solution was determined by colloidal titration with toluidine blue and found to be ca. 1 mg. This indicates that more than 99% of SDS can be removed by the above simple method.

Since the XAD resins adsorb humic substances at mg l^{-1}–μg l^{-1} levels in water, the proposed preconcentration method can be applicable to the characterization and quantitative determination of aquatic humic substances. This will be investigated in future work.

REFERENCES

1 S. Boggs, D.G. Livermore and M.G. Seitz, J. Macromol. Sci. Rev. Macromol. Chem. Phys. Part C, 25 (1985) 599.
2 R.F. Christman and E.T. Gjessing (Eds.), Aquatic and Terrestrial Humic Materials, Ann Arbor Sci. Publ., Ann Arbor, MI, 1983.
3 M. Hiraide, Anal. Sci., 8 (1992) 453.
4 M. Hiraide, Y. Arima and A. Mizuike, Anal. Chim. Acta, 200 (1987) 171.
5 M. Hiraide, M. Ishii and A. Mizuike, Anal. Sci., 4 (1988) 605.
6 M. Hiraide, T. Ueda and A. Mizuike, Anal. Chim. Acta, 227 (1989) 421.
7 K. Urano, H. Wada and T. Takemasa, Water Res., 17 (1983) 1797.
8 K.L. Cheng, Mikrochim. Acta (Wien), II (1977) 389.
9 C.J. Miles, J.R. Tuschall and P.L. Brezonik, Anal. Chem., 55 (1983) 410.
10 M. Hiraide, S.P. Tillekeratne, K. Otsuka and A. Mizuike, Anal. Chim. Acta, 172 (1985) 215.
11 R.F.C. Mantoura and J.P. Riley, Anal. Chim. Acta, 76 (1975) 97.
12 S. Kuwatsuka, A. Watanabe, K. Itoh and S. Arai, Soil Sci. Plant Nutr., 38 (1992) 23.
13 R.L. Gustafson and J. Paleos, in S.J. Faust and J.V. Hunter (Eds.), Organic Compounds in Aquatic Environments, Marcel Dekker, New York, 1971, p. 213.
14 T.M. Holsen, E.R. Taylor, Y.C. Seo and P.R. Anderson, Environ. Sci. Technol., 25 (1991) 1585.
15 K.T. Valsaraj, Sep. Sci. Technol., 27 (1992) 1633.

Analytica Chimica Acta, 281 (1993) 197–206
Elsevier Science Publishers B.V., Amsterdam

Reliability of the parameters in the resolution of overlapped Gaussian peaks

Guido Crisponi, Franco Cristiani and Valeria Nurchi

Dipartimento di Chimica e Tecnologie Inorganiche e Metallorganiche, Università di Cagliari, Via Ospedale 72, 09124 Cagliari (Italy)

(Received 7th September 1992; revised manuscript received 22nd February 1993)

Abstract

The reliability of the parameters obtained in the decomposition of two overlapped Gaussian peaks has been studied both as a function of the degree of overlapping between them and of the height and halfband width ratios. To do this a method based on the examination of the elements of dispersion matrix, obtained in a Gauss Newton non linear least squares procedure has been adopted. This is a potent tool for pointing out the functional dependence of the parameter errors on the set of numerical values defining the model and on the choice of experimental conditions. It has been shown that the ratio between halfband widths and the degree of overlapping of the bands are the leading factors affecting the reliability of results in this kind of curve decomposition.

Keywords: Gaussian peaks; Least squares; Optimal design

The resolution of a composite function in the constituent peaks and the estimation of the relative parameters is valuable in many fields of science, in particular in analytical chemistry for handling chromatographic and spectrophotometric data. Since the availability of computing facilities, various methods of analysis have been proposed [1–7]; at the same time different studies on the sources of errors affecting the fitting procedure have been carried out [8–14].

In this paper we propose an approach to the study of the factors affecting the precision of the parameters, based on the analysis of the elements of the dispersion matrix.

This kind of study has been already proposed in order to obtain an optimal experimental design [15], and also to observe how some particular sets of the parameters can lead to unreliable results, even with the highest experimental precision and accuracy [16].

Correspondence to: G. Crisponi, Dipartimento di Chimica e Tecnologie Inorganiche e Metallorganiche, Università di Cagliari, Via Ospedale 72, 09124 Cagliari (Italy).

It allows to gain information on the precision which can be obtained both using different experimental designs and as a function of the degree of peak overlapping.

CURVE FITTING

The Gaussian density function for a random variable is defined in statistics [17,18] as follows:

$$\Phi(x) = \frac{1}{\sigma(2\pi)^{1/2}} \exp\left[-\frac{(x-\mu)^2}{2\sigma^2}\right]$$

in which μ and σ are the expectation value and the standard deviation respectively.

When this mathematical formula is used to describe an experimental signal (for example a spectral band or a chromatographic peak) the easily handled form is used:

$$Y = H \exp\left[-k\frac{(X-X')^2}{2W^2}\right] \quad (1)$$

where H is the height of the peak, X' is the abscissa of maximum, W is the width of the band at half height (halfbandwidth) and $k = 8 \ln 2 = 5.545$ is the proportionality factor for the substitution of σ with W. In order to obtain the parameters H, X', W of a peak from N measurements of X_i, Y_i, the sum of the squares of residuals $S^2 = \Sigma_{i=1,N}[Y_i - Y_{ci}(H, X', W, X_i)]^2$ has to be minimized. This sum being non-linear with respect to the parameters, the non-linear least squares procedure of Gauss-Newton [19,20] is used. Knowing the estimates H^0, X'^0, W^0 of the parameters to be determined, the Y_c term can be expanded as a Taylor series truncated to the first term

$$Y_{ci} = Y_c^0(H^0, X'^0, W^0, X_i) + (\delta Y/\delta H) \cdot \Delta H + (\delta Y/\delta X') \cdot \Delta X' + (\delta Y/\delta W) \cdot \Delta W \quad (2)$$

A linear function in the correction terms $\Delta H = H - H^0$, $\Delta X' = X' - X'^0$ and $\Delta W = W - W^0$ is thus obtained. Then a linear least squares procedure can be applied. In this way the vector $\mathbf{\Delta}$ of the correction terms can be calculated as

$$\mathbf{\Delta} = (\mathbf{Z}^T \cdot \mathbf{Z})^{-1} \cdot \mathbf{Z}^T \cdot (\mathbf{Y}_c - \mathbf{Y}) \quad (3)$$

where $\mathbf{Z}$ is the matrix of derivatives, $\mathbf{Z}^T$ its transpose matrix, $\mathbf{Y}_c$ and $\mathbf{Y}$ the vectors of the calculated and experimental signal intensities, respectively.

The matrix $\mathbf{C} = (\mathbf{Z}^T \cdot \mathbf{Z})^{-1}$ called dispersion matrix, is furthermore useful in estimating the variances of the parameter as

$$V_{jj} = C_{jj} \cdot [S^2/(N - N_P)] \quad (4)$$

N_P being the number of optimized parameters, and the correlation coefficients between each pair of parameters as

$$r_{j1j2} = C_{j1j2}/(C_{j1j1} \cdot C_{j2j2})^{1/2} \quad (5)$$

From Eqn. 4 it is clear that the error variances are the product of two independent terms: one $S^2/(N - N_P)$ is a measure of the error involved in the experimental measurements, the other C_{jj}, which does not depend on the Y values, is a function of the way in which the values of the independent variable X are chosen, i.e. a function of the experimental design.

In order to gain the best estimates of the parameters (those affected by the minimum V_{jj} values), S^2 has to be minimized by a proper choice of experimental apparatus and procedures. Then the experiments have to be planned for obtaining the least values of the C_{jj} terms in the limits of their experimental restraints (working time, number of measurements, etc.).

Knowledge of the behaviour of the dispersion matrix in the actual system studied is therefore necessary. In the following section we will first present a study on the dispersion matrix for a single Gaussian peak, and then for two overlapped Gaussian peaks.

This could give a clear measure of the precision which can be achieved in the determination of the peak parameters in a representative sample of possible real situations (i.e., in a wide variability of ratios between heights, widths and distances of the peaks).

SINGLE GAUSSIAN PEAK

The Gaussian peak described by Eqn. 1, and plotted in Fig. 1A, can be normalized to give a single presentation of each possible real Gaussian peak and to obtain general results which can be applied whenever a single peak is examined.

To achieve this the new variables $\eta = Y/H$ and $\xi = (X - X')/W$ are introduced. Thus Eqn. 1 assumes the normalized form plotted in Fig. 1B

$$\eta = \exp(-\kappa\xi^2) \quad (6)$$

It is equivalent and simpler to consider a Gaussian peak in the primitive form with $H = 1$, $X' = 0$ and $W = 1$. Any result can thus be generalized for each experimental case, provided that the latter is represented in a scale in which its height and halfband width are the ordinate and abscissa units respectively. To obtain some knowledge on the variability of the three derivatives, which are the real independent variables of the system,

$$Z_H = \delta Y/\delta H = \exp[-k(X - X')^2/2W^2] = Y/H$$
$$Z_X = \delta Y/\delta X' = Y \cdot k \cdot [(X - X')/W^2] \quad (7)$$
$$Z_W = \delta Y/\delta W = Y \cdot k \cdot [(X - X')^2/W^3]$$

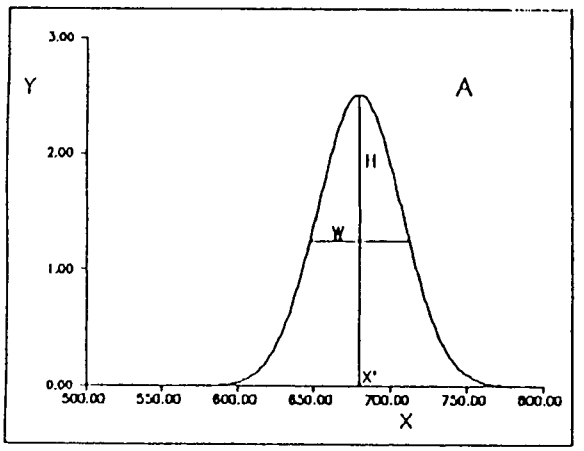

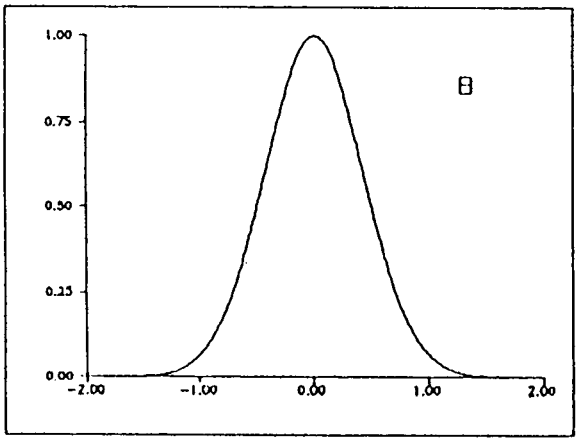

Fig. 1. (A) A Gaussian peak is reported, centred at $X = X'$, with height H and halfband width W. (B) The same Gaussian peak as in (A) is reported in the normalized variables χ and η.

the derivatives are plotted in Fig. 2. Z_H looks like the parent function Y; Z_W is equal to zero for $X = X'$ and has two maxima at $X = 0.61\ W$ and $X = -0.61\ W$ respectively, while Z_X is also zero at $X = X'$, is positive for $X > X'$ with a maximum at $X = 0.42\ W$, and negative for $X < X'$ with a minimum at $X = -0.42\ W$.

In the study of a Gaussian peak a certain range of the X variable is usually explored by picking up measurements at equally spaced ΔX intervals. If this range varies roughly between -1.5 and 1.5, we consider this a correct experimental approach because each portion of the X range is in turn important for the determination of one of the three parameters, as can be seen from Fig. 2. Nevertheless some aspects are to be settled, concerning the influence of certain factors on the errors affecting the final estimates of the parameters; these are (a) the size of the symmetrical range of X, around X', explored; (b) the size of the step ΔX, i.e., the number of experimental points; (c) the analysis limited to an asymmetrical portion of the whole curve.

To clarify point (a) the square roots of the diagonal elements of the dispersion matrix $E_j = C_{jj}^{1/2}$ have been calculated, together with the partial correlation coefficients, for different sets of data. These elements, multiplied by the experimental standard deviation, tell us how a certain experimental error is reflected on the standard deviations of the parameters.

Different sets were taken in the range $-X_m < X < X_m$ with a very little constant step $\Delta X = 0.015$ and X_m variable from 2 to 0.2 (at $X = 2$ the terms Y, Z_H, Z_X and Z_W are almost zero). It can be clearly seen in Fig. 3 that as far as $X_m = 1$, the E_j values for the three parameters do not vary significantly, while for $X_m < 1$ there is an increase of elements E_j in the order $E_W \gg E_X > E_H$; this can be easily understood from the trends of derivatives in Fig. 2: in fact going from $|1|$ to 0, Z_W is the first derivative to assume significantly positive values, then Z_X and at last Z_H.

The cut of the X range beneath $|1|$ obviously affects above all Z_W, then Z_X and only to a little extent Z_H.

The second point was the influence of the number of points, i.e. the size of the ΔX step used in scanning the X axis. In Fig. 4 the square roots of the diagonal elements of the dispersion matrix E_j are reported as the function of the number of points. These terms are of the order of 0.1 for E_X and 0.2 for E_H and E_W when 200 points are studied (a value $[S^2/(N - N_p)]^{1/2} = 0.01$, corresponding to an error of 1% on the signal intensity, because of the normalization on the intensity, causes a standard deviation $\sigma_x = 0.1 \cdot 0.01 = 0.001$ of 0.1% for X', and a standard deviation of H and W, $\sigma_H = \sigma_W = 0.002$ expressed in W units). These standard deviations increase in a quasi-linear fashion when the number of points decreases to 50, where the E_j terms

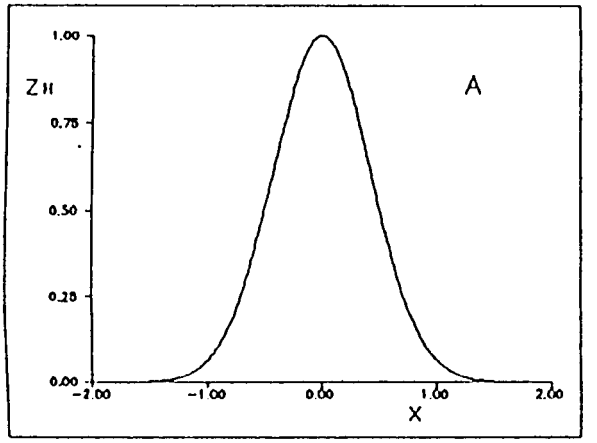

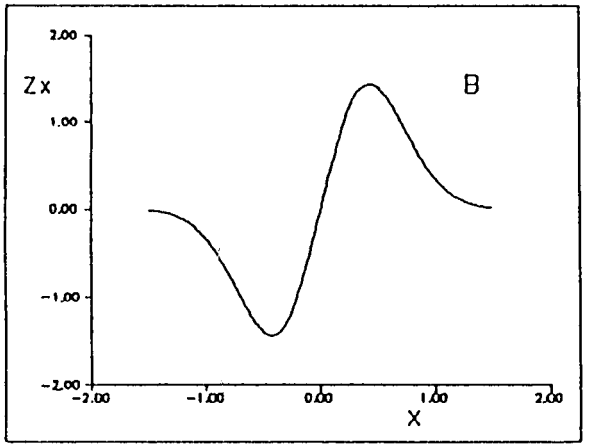

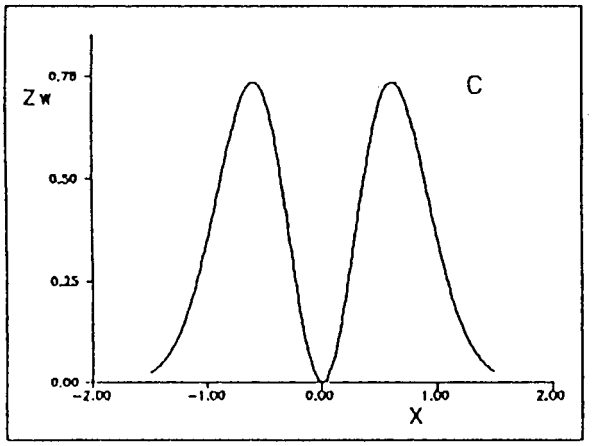

Fig. 2. The derivatives Z_H, Z_X, Z_W of a Gaussian peak centred at $X = 0$, with height 1 and halfband width 1 are reported in A, B and C, respectively.

are practically doubled with respect to the valued at 200 points. When less than 50 points are used, the E_j terms increase rapidly, reaching about 1 for E_W and E_H and 0.5 for E_X at 7–8 points; nevertheless they can still be considered acceptable values.

To examine point (c), different fractions of the entire curve, in the range $-1 \div 1$, were explored always with a $\Delta X = 0.03$ step: i.e., the ranges $-0.9 \div 1$; $-0.8 \div 1$; ... $0 \div 1$ were studied. The corresponding elements E_j and the partial correlation coefficients are reported in Fig. 5, as a function of the absolute value of the initial point on the left: the fact that one side of the Gaussian curve is lacking leads to completely correlated parameters, with a complete unreliability of the final estimates.

TWO GAUSSIAN PEAK

When the experimental curve is the sum of two individual overlapped Gaussian peaks, the precision with which the parameters of the first peak are determined can be influenced by the second peak, according to its relative position, width and height, and vice versa. In order to give a clear quantitative picture of these mutual influ-

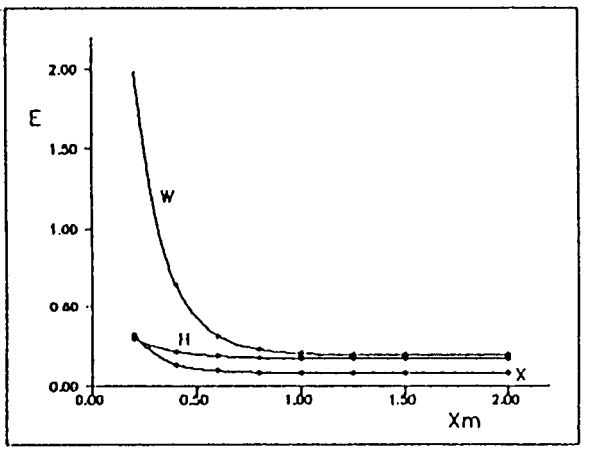

Fig. 3. The values E_j of the square roots of the diagonal elements of the dispersion matrix, calculated in different X ranges $-X_m \div X_m$ for the Gaussian peak [$X' = 0$, $H = 1$, $W = 1$] are reported as a function of the X_m value.

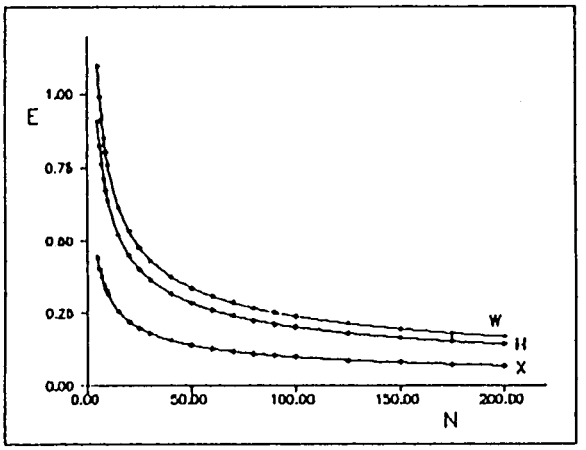

Fig. 4. The values E_j of the square roots of the diagonal elements of the dispersion matrix, calculated in the X range $-1 \div 1$ for the Gaussian peak [$X' = 0$, $H = 1$, $W = 1$], with a variable number of points N are reported as a function of N.

ences, the E_j elements have been calculated for a representative set of relative widths, positions and heights of the second peak. Also in this case a normalization procedure was adopted. For the two peaks I and II, the signal is given by the sum

$$Y = H_1 \cdot \exp\left[-k(X - X_1')^2/2W_1^2\right] + H_2 \cdot \exp\left[-k(X - X_2')^2/2W_2^2\right] \quad (8)$$

Assuming the new variables $\eta = Y/H_1$ and $\xi = (X - X_1')/W_1$ with respect to peak I, Eqn. 8 takes the form

$$\eta = \exp(-\kappa\xi^2) + (H_2/H_1) \times \exp\left[-k(\xi - X_2'')^2/2W_2^2\right] \quad (9)$$

where $X_2'' = (X_2' - X_1')/W_1$ and $W_2' = W_2/W_1$. Peak I on the left is therefore the leading one in the normalization procedure, and its height and

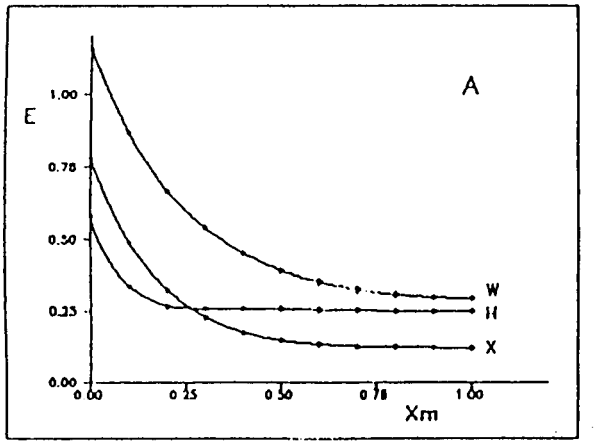

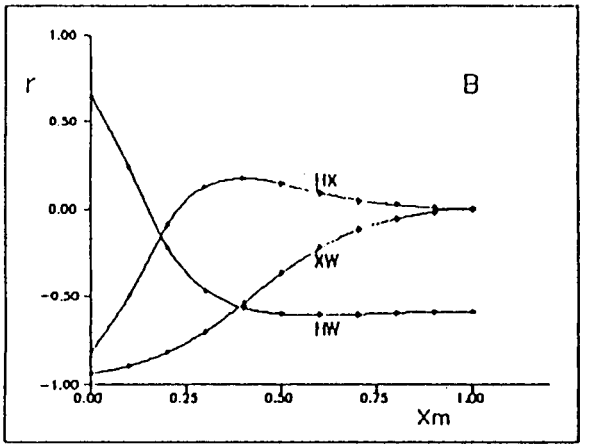

Fig. 5. The values E_j of the square roots of the diagonal elements of the dispersion matrix, calculated in the X range $-X_m \div 1$ for the Gaussian peak [$X' = 0$, $H = 1$, $W = 1$] are reported as a function of X_m in (A). The corresponding partial correlation coefficients r are reported in (B).

width are the units of vertical and horizontal axis respectively.

To obtain a representative set of experimental

TABLE 1

The marks used to distinguish the fifteen studied cases of two overlapped Gaussian peaks reported vs. height and width of peak II. Height and width of peak I have unitary values

W_2	H_2				
	4	2	1	0.5	0.25
1	$M(1, 4)$	$M(1, 2)$	$M(1, 1)$	$M(1, 0.5)$	$M(1, 0.25)$
0.5	$M(0.5, 4)$	$M(0.5, 2)$	$M(0.5, 1)$	$M(0.5, 0.5)$	$M(0.5, 0.25)$
0.25	$M(0.25, 4)$	$M(0.25, 2)$	$M(0.25, 1)$	$M(0.25, 0.5)$	$M(0.25, 0.25)$

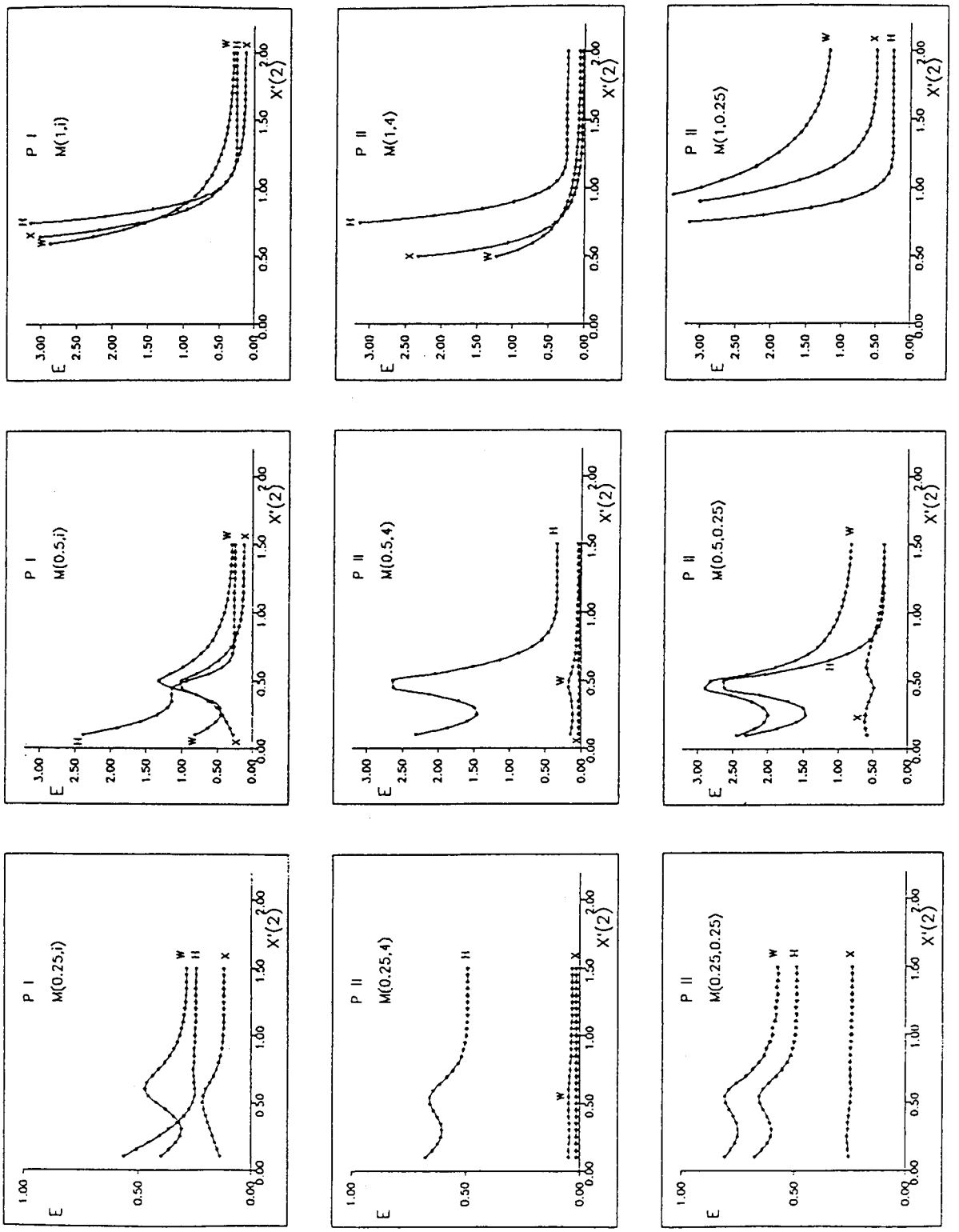

Fig. 6. The values E_j of the square roots of the diagonal elements of the dispersion matrix for two Gaussian peaks are reported as a function of the position of the second peak. The index of the peak and the case according to Table 1, are shown in the figures.

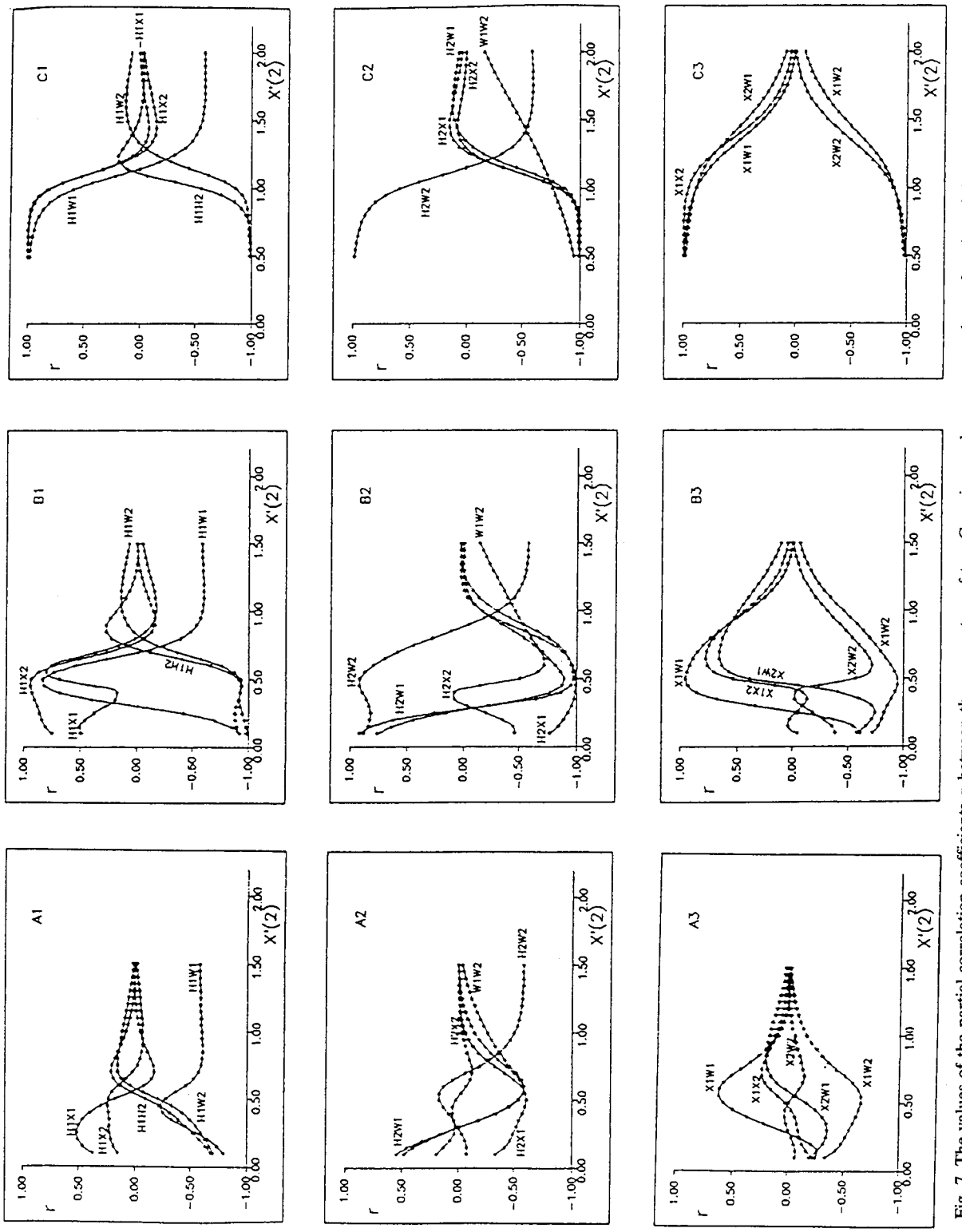

Fig. 7. The values of the partial correlation coefficients r between the parameters of two Gaussian peaks are reported as a function of the position of the second peak. A, B, C are relating to W_2 equal to 0.25, 0.5 and 1.0, respectively.

situations, the parameters of peak II were allowed to vary according to the scheme reported in Table 1. To obtain a fixed precision of the parameters of peak I, a ΔX step 0.03 was always used. In this way a width of 0.25 for peak II was chosen as the smallest, otherwise too few representative points for peak II would have been scanned, and 1.0 was the biggest because the effect of a larger peak could be inferred by reversing the results for peak I and peak II. The relative positions vary from one in which the two peaks do not overlap (this is chosen according to the width of peak II) to a distance between maxima of 0.1 in which the two peaks can be considered completely overlapping. The ratio H_2/H_1 was varied from 1/4 to 4 in order to have a large set of situations. Considering for example a spectrophotometric determination with an available range of absorbances $0 \div 4$, both peaks can be measured with a fairly good precision; moreover the distribution of errors can be considered homoscedastic and then the term $S^2/(N - N_P)$ can be assumed constant for all the set of measurements.

For a clearer discussion the results for the situations of no overlapping have to be analyzed first. In Table 2 the elements E_j relating to the two peaks in condition of no overlapping are reported.

The results relating to peak I do not change at all in this situation; this is correct, this being a case of orthogonality in which the independent variables of one peak vary totally independently of those of the other. On the other hand a variation of the parameters of peak II on varying both its height and its width is observed. Nevertheless this variability is not in contrast with the orthogonality between peaks and can be explained easily.

The E_{H_2} values in Table 2 depend only on the width of peak II and not on H_2; this implies that, $S^2/(N - N_P)$ being constant, as peak II is higher its relative precision increases; on the other hand E_{H_2} terms increase as peak II becomes narrower, but this can be explained by taking into account that as the width of peak II decreases, also the number of points with which it is explored decreases, leading to an increase in E_{H_2} elements.

As far as E_{W_2} and E_{X_2} are concerned, we can see that, for a given halfband width, they decrease linearly with H_2, i.e., the higher the peak, the higher the precision with which it is determined. For the same H_2 value, the relative errors E_{W_2}/W_2 and E_{X_2}/W_2 decrease with the W_2 val-

TABLE 2

The square roots of the diagonal elements of the dispersion matrix reported for the fifteen studied cases of two overlapped Gaussian peaks

Case	E_{H_1}	E_{X_1}	E_{W_1}	E_{H_2}	E_{X_2}	E_{W_2}
$M(1, 4)$	0.2462	0.1208	0.2918	0.2462	0.0302	0.0729
$M(1, 2)$	0.2462	0.1208	0.2918	0.2462	0.0604	0.1459
$M(1, 1)$	0.2462	0.1208	0.2818	0.2462	0.1208	0.2918
$M(1, 0.5)$	0.2462	0.1208	0.2918	0.2462	0.2415	0.5836
$M(1, 0.25)$	0.2462	0.1208	0.2918	0.2462	0.4830	1.167
$M(0.5, 4)$	0.2462	0.1208	0.2918	0.3470	0.0214	0.0512
$M(0.5, 2)$	0.2452	0.1208	0.2918	0.3470	0.0428	0.1024
$M(0.5, 1)$	0.2462	0.1208	0.2918	0.3470	0.0855	0.2048
$M(0.5, 0.5)$	0.2462	0.1208	0.2918	0.3470	0.1711	0.4096
$M(0.5, 0.25)$	0.2462	0.1208	0.2918	0.3470	0.3421	0.8191
$M(0.25, 4)$	0.2462	0.1208	0.2918	0.4912	0.0150	0.0360
$M(0.25, 2)$	0.2462	0.1208	0.2918	0.4912	0.0301	0.0720
$M(0.25, 1)$	0.2462	0.1208	0.2918	0.4912	0.0602	0.1439
$M(0.25, 0.5)$	0.2462	0.1208	0.2918	0.4912	0.1204	0.2879
$M(0.25, 0.25)$	0.2462	0.1208	0.2918	0.4912	0.2407	0.5757

ues and again this can be explained with the fact that the points are fewer. We can therefore attest that in an homoscedastic situation higher peaks are determined with better precision.

As peak II approaches peak I, there is a large variability in all E_j and r_{j1j2} values. The results are reported in Figs. 6 and 7. As a first point some illustrative remarks can be made: (i) the trends of E_j relating to peak I and those of the correlation coefficients do not depend on the H_2 but only on the W_2 values; therefore the plots in Figs. 6 and 7 are representative of all the cases in Table 1; (ii) the trends of E_j relating to peak II instead depend both on H_2 and W_2 values. Therefore in Fig. 6 for each W_2 value two cases are reported as an example for the extreme H_2 values 0.25 and 4.0.

As regards the behaviour of peak I parameters with the three different halfband widths of peak II, the following considerations can be made. $W_2 = 0.25$. As X_2' is about equal to 1 we are in an orthogonal case, the E_j values being the same as those of a pure single Gaussian peak; as X_2' becomes less than 1, the derivatives, first Z_{W_1}, then Z_{X_1} and last Z_{H_1} begin to overlap with those of the second peak. Therefore a progressive increase in E_{W_1}, E_{X_1} and E_{H_1} is observed in the plots, which goes through a maximum when Z_{H_2} superimposes Z_{W_1} and Z_{X_1} respectively, followed by a decrease in E_{W_1} and E_{X_1} terms for lower X_2' values, when the overlapping of Z_{X_1} and Z_{W_1} derivatives is reduced. The loss of precision of the peak I parameters due to the superimposition of the second peak is not as important and till allows a correct determination of all the six parameters with high reliability, not open to compensations. $W_2 = 0.50$. The trend is very similar to the above for the lower $W_2 = 0.25$ value, but the increase in E_1 terms is much higher and can lead to remarkable compensations between parameters, which will be exemplified in the following. $W_2 = 1.00$. In this case, when the X_2' value approaches 1, there is a dramatic increase of all the E_1 values, leading to the disappearance of any possibility of determining the parameters of the two peaks separately.

Analogous behaviour can be observed in Fig. 7 in the plots of partial correlation coefficients: the fact that the two bands get nearer leads to a succession of overlaps of the various derivatives. This raises the partial correlation coefficients, followed by inversions when they no longer overlap. At the minimum in the E_1 plots, many of the partial correlation coefficients are near zero for the cases $W_2 = 0.25$ and $W_2 = 0.50$. On the other hand, for the case $W_2 = 1$, from $X_2' < 1.25$ there is a drastic increase (or decrease) in all the partial correlation coefficients leading to 1 (or -1) at $X_2' = 1$, i.e., to a complete correlation between parameters.

The same observations can be made on the plots relating to the parameters of the second peak in Fig. 6. It is to be remarked, as with the examination of the results in Table 2, that the E_{H_2} terms are constant on varying H_2 (constant relative error of heights) and E_{W_2} and E_{X_2} decrease on varying H_2. Some differences are to be pointed out when observing the behaviour of peak II parameters; in the actual case we are looking at the approach of a peak larger than that under observation. In this case Z_{H_2} superimposes Z_{X_1} and Z_{W_1}, and then E_{H_2} passes through a maximum; Z_{X_2} is not perturbed by superimposition with Z_{H_1}. Furthermore it overlaps Z_{X_1} and Z_{W_1} with both negative and positive sides. Therefore an almost complete insensitivity of E_{X_2} is observed. Moreover E_{W_2} values feel these effects to a lesser extent than E_{W_1}: this happens because Z_{W_2} is superimposed only by Z_{W_1} and Z_{X_1}, but not by Z_{H_1}.

Following this analysis it can be pointed out that the relevant factors in determining the reliability of the parameters are the ratio between the halfband widths and the degree of overlapping between peaks. It will be useful to illustrate these things with a simulated example, in order to emphasize the practical significance of the partial correlation coefficients.

Let us consider the two simulated peaks reported in Fig. 8, defined by the values

set 0 $H_1 = 1.40$, $X_1' = 510.0$, $W_1 = 78.0$
$H_2 = 0.70$, $X_2' = 549.0$, $W_2 = 39.0$

This case is similar to the model $M(0.5, 0.5)$ in Table 1, with a superimposition corresponding to the maxima in Fig. 6. The limits of error for a

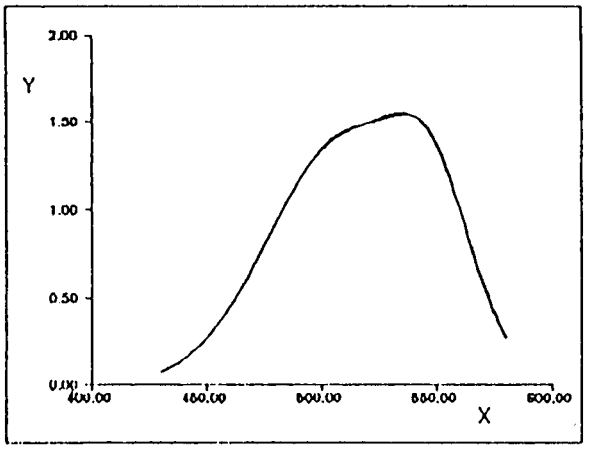

Fig. 8. The simulated sum of the two Gaussian peaks for sets 0, 1, 2 are shown, and are practically indistinguishable.

value $S^2/(N-N_P)=0.01$ can therefore be estimated at 99%, using the relation $P=P^* \pm t_\alpha \cdot \sigma_p$ (where t_α is the value of the t distribution for $N-N_P$ degrees of freedom at a $(1-2\alpha)\cdot 100$ confidence level), as

$t\cdot\sigma_{H_1}=0.04$, $t\cdot\sigma_{X_1}=2.2$, $t\cdot\sigma_{W_1}=3$

$t\cdot\sigma_{H_2}=0.1$, $t\cdot\sigma_{X_2'}=0.9$, $t\cdot\sigma_{W_2}=3$

Considering these error limits and the correlation coefficients of Fig. 7 the curves for the two sets of parameters,

set 1 $H_1=1.44$, $X_1'=512.3$, $W_1=80.4$
$H_2=0.60$, $X_2'=549.3$, $W_2=35.1$

set 2 $H_1=1.35$, $X_1'=507.8$, $W_1=76.0$
$H_2=0.79$, $X_2'=548.3$, $W_2=43.0$

have been calculated and are reported in Fig. 8. From these it is possible to observe that changes of the order of 10% on one parameter can be internally compensated by a proper change on the correlated parameters. In this case therefore the reliability of the results and the error limits have to be properly evaluated.

To sum up, some practical suggestions to obtain reliable results are remembered: (i) the ΔX step has to be chosen according to the halfband width of the narrowest peak in order to examine the curve with a sufficient number of points; (ii) the peaks have to be as high as possible without any loss of precision; (iii) the initial guesses of the parameters have to be estimated accurately by taking into account the various methods available; (iv) the final results must always be accompanied by the proper estimates of errors and correlations.

It is to be stressed once more that a good reproduction of the experimental data is not on its own a criterion of reliability of the parameters, but always has to be followed by low standard deviations and low correlation coefficients.

REFERENCES

1 J. Pitha and R.N. Jones, Can. Spectrosc., 11 (1966) 14.
2 J. Pitha and R.N. Jones, Can. J. Chem., 44 (1966) 3031.
3 J.R. Morrey, Anal. Chem., 40 (1968) 905.
4 A.W. Westerberg, Anal. Chem., 41 (1969) 1770.
5 R.D.B. Fraser and E. Suzuki, Anal. Chem., 41 (1969) 37.
6 F.C. Strong, Appl. Spectrosc., 23 (1969) 593.
7 R.P. Young and R.N. Jones, Chem. Rev., 71 (1971) 219.
8 J. Pitha and R.N. Jones, Can. J. Chem., 45 (1967) 2347.
9 J.W. Perram, J. Chem. Phys., 49 (1968) 4245.
10 A.H. Anderson, T.C. Gibb and A.B. Littlewood, Chromatographia, 2 (1969) 466.
11 J.R. Beacham and K.L. Andrew, J. Opt. Soc. Am., 61 (1971) 231.
12 A.R. Davis, D.E. Irish, R.B. Roden and A.J. Weerheim, Appl. Spectrosc., 26 (1972) 384.
13 B.G.M. Vandeginste and L. De Galan, Anal. Chem., 47 (1975) 2124.
14 P. Gans and J.B. Gill, Anal. Chem., 42 (1980) 351.
15 G. Carta and G. Crisponi, J. Chem. Soc., Perkin Trans. II, (1986) 37.
16 G. Crisponi, V. Nurchi and M.L. Ganadu, J. Chemometr., 4 (1990) 123.
17 W.C. Hamilton, Statistics in Physical Science, Ronald Press, New York, 1964.
18 E. Lloyd, in W. Ledermann (Ed.), Handbook of Applicable Mathematics, Vol. II, Wiley, Chichester, 1980.
19 F.R. Bevington, Data Reduction and Error Analysis for the Physical Sciences, McGraw-Hill, New York, 1969.
20 N. Draper and H. Smith, Applied Regression Analysis, Wiley, New York, 2nd edn., 1981.

Analytica Chimica Acta, 281 (1993) 207–218
Elsevier Science Publishers B.V., Amsterdam

Background bilinearization by the use of generalized standard addition method on two-dimensional data

Yulong Xie, Jihong Wang, Yizeng Liang, Kai Ge and Ruqin Yu

Department of Chemistry and Chemical Engineering, Hunan University, Changsha 410012 (China)

(Received 30th September 1992; revised manuscript received 3rd March 1993)

Abstract

The capability of the standard addition method to correct the matrix effects and the advantage of two-dimensional bilinear analytical data were utilized in a hybrid method combining the generalized standard addition method (GSAM) and constrained background bilinearization. The proposed method can effectively compensate for both matrix effects and the influence of unexpected interferents in multivariate calibration. First, GSAM was extended to two-dimensional bilinear data. In the process of standard additions, the background is fixed and the standard responses of the sought-for components in actual samples could be thus acquired even with the existence of unexpected interferents in the sample. The quantification of the sought-for analytes was then completed by use of background bilinearization. In the optimization process of background bilinearization, a global optimization technique, generalized simulated annealing (GSA), was adopted to guarantee the global minimum. The characteristic performance of the proposed method was tested by a series of simulations and experimental fluorescence excitation–emission data with organic dye mixtures.

Keywords: Multivariate calibration; Background bilinearization; Background correction; Generalized standard addition method; Generalized simulated annealing; Two-dimensional bilinear data

With the widespread availability of various modern analytical instruments, it is more and more challenging to handle the huge amounts of experimental data efficiently in order to solve complicated analytical problems. A commonly encountered problem in the calibration of modern analytical instruments is the difficulty of access to the actual standard responses for the sought-for analytes and the correction of the matrix effect for a complicated multi-component sample. The actual standard response for a given analyte in a real sample might be radically different from that measured in pure solutions owing to matrix effects and other factors. The generalized standard addition method (GSAM) provided a useful tool for compensating for both the matrix effect and the influence caused by the interaction between co-existing components in the sample [1]. Very often, unfortunately, the sample also contained some unexpected interferents (background constituents), and GSAM could not eliminate their influence. Search methods for obtaining quantitative results from samples with background constituents without time-consuming separation is of considerable interest. Osten and Kowalski [2] proposed a method based on curve resolution and calibration techniques for solving this kind of problems. A hybrid method combining GSAM and iterative target factor analysis was developed in this laboratory [3]. These methods, unfortunately, cannot provide a unique solution, because they are applied to one-dimensional analytical signals (the data for each sample will be a vector) which have the intrinsic limitation of lacking

Correspondence to: Ruqin Yu, Department of Chemistry and Chemical Engineering, Hunan University, Changsha 410012 (China).

enough information necessary for the data interpretation. The situation changed dramatically when two-dimensional analytical data were adopted to attack this kind of problem. Rank annihilation factor analysis (RAFA), proposed by Ho et al. [4], was the first chemometric procedure treating two-dimensional bilinear data. The iterative RAFA method was later modified to a direct approach by Lorber [5] and extended by Sanchez and Kowalski [6] to a more universal procedure called generalized rank annihilation factor analysis (GRAFA). More recently, the residual background bilinerization (RBL) method was presented by Ohman et al. [7,8], and the constrained background bilinearization (CBBL) method by Liang et al. [9]. These methods were claimed to be able to provide better results than GRAFA. These methods, based on two-dimensional bilinear data, tried to remove the influence of unmodelled background constituents in the quantification of the sought-for analytes, but still required the actual standard response of the pure sought-for analytes or a set of their standard mixtures, which might not be available for samples with a complicated matrix. Therefore, for the quantification of the sought-for analytes in a sample containing some unexpected interferents with a complicated matrix, neither the GSAM- nor RBL-type methods used individually would be successful. In this paper, an algorithm is proposed for tackling this extremely complex problem. First, GSAM is extended to two-dimensional bilinear data and the actual standard response of the sought-for analytes in the actual sample environment is obtained by the use of GSAM with the background fixed in the process of standard additions. The sought-for analytes are then quantified in the presence of unexpected interferents with the bilinearization of the background under certain constraints. A global optimum search algorithm, generalized simulated annealing (GSA), was used for the bilinearization.

THEORY AND COMPUTATION STRATEGY

Throughout the text, normal letters signify scalars, bold lower-case letters represent column vectors and bold capital letters denote matrices. Italic bold capital letters refer to third-order tensors. For the sake of clarification, a list of symbols is given in the Appendix.

One-dimensional GSAM

The standard addition method (SAM) is a well known procedure for correcting for so-called matrix effects. Saxberg and Kowalski [1] extended SAM to multi-component systems by using standard additions of more than one analyte and called it generalized SAM (GSAM), which is able to detect and correct for the matrix effects and spectral interferences among components simultaneously. The details of GSAM have been extensively studied and described elsewhere [1,10,11] and only a brief discussion is presented here for the purpose of clarification of the proposed procedure. For one-dimensional data obtained by techniques such as UV–visible spectrophotometry or a sensor array with which each sample yields a data vector in a single measurement, GSAM can be formulated as

$$\mathbf{z}^{\mathrm{T}} = \mathbf{n}^{\mathrm{T}}\mathbf{B} + \mathbf{e}^{\mathrm{T}} = \sum_{l=1}^{L} n_l \mathbf{b}_l^{\mathrm{T}} + \mathbf{e}^{\mathrm{T}} \quad (1a)$$

$$\mathbf{Z} = (\delta\mathbf{N} + \mathbf{l}\mathbf{n}^{\mathrm{T}})\mathbf{B} + \mathbf{E} \quad (1b)$$

where $\mathbf{z}$ is the response vector of the original sample measured with J sensors; $\mathbf{n}$ is the sought-for concentration vector of all the L analytes in the original sample; $\mathbf{l}$ is a column vector of I elements, all of them are ones; and $\mathbf{B}$ is an $L \times J$ sensitivity matrix which also remains unknown because of the matrix effects. Equation 1a reflects the relationship among these three quantities. In order to obtain the sensitivity matrix $\mathbf{B}$ in a certain sample matrix, I ($I \geq L$) standard additions for all the L analytes are made, and one will obtain an $I \times J$ response matrix $\mathbf{Z}$ and an $I \times L$ concentration increment matrix $\delta\mathbf{N}$. A similar linear relationship between concentration and response will be hold for the sample after standard additions (Eqn. 1b); $\mathbf{e}$ and $\mathbf{E}$ refer to measurement noise and the superscript T signifies the transpose of a matrix or a vector. All the responses and concentrations are assumed to be volume-corrected.

Subtracting Eqn. 1a from each row of matrix **Z** in Eqn. 1b, one obtains

$$\delta\mathbf{Z} = (\delta\mathbf{N})\mathbf{B} + \mathbf{E} \quad (2)$$

where $\delta\mathbf{Z}$ is an $I \times J$ response increment matrix obtained after standard additions. The estimate of **B** is thus obtained:

$$\mathbf{B} = (\delta\mathbf{N})^{+}(\delta\mathbf{Z}) = \left[(\delta\mathbf{N})^{\mathrm{T}}(\delta\mathbf{N})\right]^{-1}(\delta\mathbf{N})^{\mathrm{T}}(\delta\mathbf{Z}) \quad (3)$$

and consequently the sought-for concentrations **n** is

$$\mathbf{n}^{\mathrm{T}} = \mathbf{z}^{\mathrm{T}}\mathbf{B}^{+} = \mathbf{z}^{\mathrm{T}}\mathbf{B}^{\mathrm{T}}(\mathbf{B}\mathbf{B}^{\mathrm{T}})^{-1} \quad (4)$$

where the superscript -1 represents the inverse of a matrix and the superscript $+$ denotes the generalized inverse, and the least-squares inverse is adopted in this context.

Two-dimensional GSAM

A certain type of instrument, including chromatography with a multi-channel detector (e.g., liquid chromatography with ultraviolet diode array detection (LC–UV), gas chromatography–mass spectrometry (GC–MS)) and excitation–emission spectrofluorimetry (EX–EM), possesses the important characteristics that (i) each sample yields a response data matrix (as opposed to a single scalar or a data vector); in the case of LC–UV, for instance, the signal from each sample is a chromatographic profile times a UV spectrum; and (ii) the rank of a response matrix for a pure chemical component is unity in the absence of noise. The bilinear response can be expressed as a product of two independent responses. In LC–UV, the elution profile and the UV spectrum are independent of each other. Instruments and the data thereby generated meeting these two requirements are called two-dimensional bilinear [4]. These characteristics are very useful for data interpretation. For a pure component, its response data matrix **Q** produced by a two-dimensional bilinear instrument can be expressed as the product of two vectors:

$$\mathbf{Q} = \mathbf{d}\mathbf{g}^{\mathrm{T}} \quad (5)$$

where **d** may represent, for example, an excitation spectrum in two-dimensional spectrofluorimetry or the chromatographic profile in coupled chromatography (e.g., LC–UV), and **g** may be the corresponding emission spectra or standard spectrum, respectively.

For a mixture sample, the number of components, L, can be determined from the rank of the corresponding two-dimensional bilinear data matrix **Q**, which is not possible in one-dimensional data interpretation. Also, **Q** can be expressed as the summation of the products of vector pairs as follows:

$$\mathbf{Q} = \sum_{l=1}^{L} \mathbf{d}_l \mathbf{g}_l^{\mathrm{T}} \quad (6)$$

GSAM can be applied to the two-dimensional bilinear data in a similar way as in the one-dimensional case:

$$\mathbf{Q} = \mathbf{n}^{\mathrm{T}}\boldsymbol{S} + \mathbf{E} = \sum_{l=1}^{L} n_l \mathbf{S}_l + \mathbf{E} \quad (7a)$$

$$\boldsymbol{Q} = (\delta\mathbf{N} + \mathbf{l}\mathbf{n}^{\mathrm{T}})\boldsymbol{S} + \boldsymbol{E} \quad (7b)$$

where **Q** refers to the $J \times K$ response matrix of the original sample, J and K denoting the numbers of the measurement points in both directions of the two-dimensional bilinear instrument, e.g., J excitation wavelengths and K emission wavelengths in EX–EM fluorimetry, $\boldsymbol{S}$ refers to the unknown $L \times J \times K$ response sensitivity tensor consisting of L response sensitivity matrices $\mathbf{S}_l$ ($l = 1, 2, \ldots, L$) of L components, $\boldsymbol{Q}$ is also a third-order response tensor constructed by $IJ \times K$ data matrices after I standard additions on the original sample, and the concentration vector, **n**, and the concentration increment matrix, $\delta\mathbf{N}$, remain the same as before. Following the method of treatment in one-dimensional GSAM, one can therefore write

$$\delta\boldsymbol{Q} = \delta\mathbf{N}\boldsymbol{S} + \boldsymbol{E} \quad (8)$$

$$\boldsymbol{S} = (\delta\mathbf{N})^{+}(\delta\boldsymbol{Q}) = \left[(\delta\mathbf{N})^{\mathrm{T}}(\delta\mathbf{N})\right]^{-1}(\delta\mathbf{N})^{\mathrm{T}}(\delta\boldsymbol{Q}) \quad (9)$$

and

$$\mathbf{n}^{\mathrm{T}} = \mathbf{Q}\boldsymbol{S}^{+} = \mathbf{Q}\boldsymbol{S}^{\mathrm{T}}(\boldsymbol{S}\boldsymbol{S}^{\mathrm{T}})^{-1} \quad (10)$$

An inverse operation of the third-order tensor $\boldsymbol{S}$ is included in Eqn. 10. Equivalently, the inverse

of the third-order tensor can be transferred into the inverse of a large matrix. For doing this, the cube S can be broken up into L $(J \times K)$ planes (matrices) and an $L \times (J \times K)$ large plane (matrix) will be formed by putting the L planes of S end to end. Correspondingly, the $J \times K$ matrix $\mathbf{Q}$ should be changed into an $1 \times (J \times K)$ vector by linking rows of $\mathbf{Q}$ into a large row (vector).

GSAM with a fixed background in the presence of unexpected interferents

Up to now, we have only discussed the direct extension of GSAM to a two-dimensional bilinear data version without considering the presence of unexpected background interferents. If some unexpected background interferents exist in the sample, the corresponding response models of the original sample for one- and two-dimensional data (Eqns. 1a and 7a, respectively) should be changed to

$$\mathbf{z}^{\mathrm{T}} = \sum_{l=1}^{L} n_l \mathbf{b}_l^{\mathrm{T}} + \sum_{m=1}^{M} n_m \mathbf{r}_m^{\mathrm{T}} + \mathbf{e}^{\mathrm{T}} = \mathbf{n}^{\mathrm{T}}\mathbf{B} + \mathbf{r}^{\mathrm{T}} \tag{11a}$$

$$\mathbf{Q} = \sum_{l=1}^{L} n_l \mathbf{S}_l + \sum_{m=1}^{M} n_m \mathbf{R}_m + \mathbf{E} = \mathbf{n}^{\mathrm{T}}S + \mathbf{R} \tag{11b}$$

where M is the number of the unexpected interferents and $\mathbf{R}_m$ (or $\mathbf{r}_m$) is the corresponding response sensitivity matrix (or vector). The overall contribution of M unmodelled interferents together with the random noise $\mathbf{E}$ (or $\mathbf{e}$) can be expressed by an overall background response matrix $\mathbf{R}$ (or vector $\mathbf{r}$).

If one conducts standard additions of L sought-for analytes under the constraint of a fixed overall background (this can easily be done by fixing the volume of the original sample taken and the ultimate volume after addition), the overall background response $\mathbf{R}$ (or $\mathbf{r}$) will remain constant in the responses of both the original sample and samples after standard additions. It will be subtracted in the computation of the response increment and Eqn. 8 (or Eqn. 2) will still hold on this occasion. Hence the response sensitivity tensor S (or matrix $\mathbf{B}$) of L sought-for analytes can also be obtained from the response and concentration increment tensors (or matrices) from Eqn. 9 (or Eqn. 3). However, the quantification of the L sought-for components in the original sample is still impossible because the term $\mathbf{R}$ (or $\mathbf{r}$) in Eqn. 11b (or Eqn. 11a) is not known. Obviously, in order to estimate $\mathbf{n}$ in Eqn. 11, the term $\mathbf{R}$ (or $\mathbf{r}$) should be estimated in advance or during the computation process.

For the one-dimensional case, we tried to search for an approximate estimate of $\mathbf{r}$ by use of iterative target factor analysis, partially alleviating the aforementioned difficulty [3].

For two-dimensional bilinear data, the situation changed dramatically. The total number of chemical species (including the sought-for analytes and the unexpected interferents) of the original sample can be determined by the use of a factor-analytical technique treating the response matrix, $\mathbf{Q}$, of the original sample. Consequently, the number of unexpected interferents, M, can be obtained by simply subtracting the number of sought-for analytes, L, from the rank of matrix $\mathbf{Q}$. The information about the number of unmodelled background interferents is crucial. In spite of the lack of the knowledge of the response features of these M background constituents, one does know that the overall background concerns with M independent factors. Therefore, according to the bilinear structure of the response, one can factor analyse the overall background and reconstructed it with the M leading principal components. This process is called the bilinearization of background and can be formulated as follows:

$$\mathbf{R} = \sum_{m=1}^{M} \mathbf{t}_m \mathbf{u}_m^{\mathrm{T}} + \mathbf{E} = \mathbf{T}\mathbf{U}^{\mathrm{T}} + \mathbf{E} \tag{12}$$

where $\mathbf{t}_m$ is the mth orthonormal factor score vector and $\mathbf{u}_m$ is the corresponding orthogonal factor loading vector. $\mathbf{T}$ is a $J \times M$ matrix consisting of the M leading score vectors and $\mathbf{U}$ is a $K \times M$ matrix consisting of the M leading loading vectors. The product $\mathbf{T}\mathbf{U}^{\mathrm{T}}$ represents the bilinear part in $\mathbf{R}$ and $\mathbf{E}$ is the residual. In this way, Eqn. 11b can be rewritten as

$$\mathbf{Q} = \mathbf{n}^{\mathrm{T}}S + \mathbf{R} = \sum_{l=1}^{L} n_l \mathbf{S}_l + \sum_{m=1}^{M} \mathbf{t}_m \mathbf{u}_m^{\mathrm{T}} + \mathbf{E} \tag{13a}$$

or

$$Q_{jk} = \sum_{l=1}^{L} n_l S_{ljk} + \sum_{m=1}^{M} \mathbf{t}_m \mathbf{u}_m^{\mathrm{T}} + E_{jk} \qquad (13b)$$

Through the bilinearization of overall background, the concentration vector of the sought-for analytes can be obtained by an optimization procedure according to following reasoning.

Given an estimate of **n**, an estimate of overall background matrix **R** could be obtained from the difference of **Q** and $\Sigma n_l \mathbf{S}_l$. If the estimate of **n** is a correct one, the difference matrix $\mathbf{Q} - \Sigma n_l^{\mathrm{true}} \mathbf{S}_l$ should be a good estimate of **R** and could be expressed in the form of Eqn. 12. Hence, with the constraint of rank (**R**) being equal to M, the leading M principal components of the difference matrix should reconstruct the background matrix fairly well and the residual part of the background matrix, $\mathbf{E} = \mathbf{Q} - \Sigma n_l^{\mathrm{true}} \mathbf{S}_l - \Sigma \mathbf{t}_m \mathbf{u}_m^{\mathrm{T}}$, should be at the same level as the measurement noise. Here the first summation taking from 1 to L and the second summation from 1 to M. On the other hand, if **n** is misestimated, the information about the sought-for analytes would be subtracted incorrectly, and consequently the difference matrix $\mathbf{Q} - \Sigma n_l \mathbf{S}_l$ is not a suitable estimate of the background matrix **R** and could not be regenerated accurately with M leading principal components of the current difference matrix during the computation process. Hence the residual matrix $\mathbf{E} = \mathbf{Q} - \Sigma n_l \mathbf{S}_l - \Sigma \mathbf{t}_m \mathbf{u}_m^{\mathrm{T}}$ would be significantly different from the measurement noise. Obviously, the sum of the squares of the elements of the residual matrix **E** could be used as a suitable objective function $\mathscr{F}$ for the optimization problem of searching **n**:

$$\mathscr{F} = \sum_{j=1}^{J} \sum_{k=1}^{K} E_{jk}^2 \qquad \begin{matrix} j = 1, \ldots, J \\ k = 1, \ldots, K \end{matrix} \qquad (14)$$

Therefore, the best estimate of **n** should correspond to the minimum of the response surface of $\mathscr{F}$.

Computation strategy

According to the discussion above, the following computation strategy is proposed:

Solving the sensitivity tensor S. The response matrix **Q** (Eqn. 7a) is subtracted form each of I planes (matrices) in the response tensor $\boldsymbol{Q}$ (Eqn. 7b) obtained after I ($I \geq L$) standard additions for L sought-for analytes with fixed amount of unexpected interferents (see above), the increment response tensor $\delta \boldsymbol{Q}$ is computed. The estimate of the sensitivity tensor $\boldsymbol{S}$ is calculated from Eqn. 9 by the use of $\delta \boldsymbol{Q}$ and the real concentration increment matrix $\delta \mathbf{N}$.

Estimating the number of unexpected interferents. The number of the unexpected interferents, M, is obtained by subtracting L from the rank of the original sample response matrix **Q**:

$$M = \mathrm{Rank}(\mathbf{Q}) - L \qquad (15)$$

The rank of matrix **Q** may be estimated by using a factor-analytical method. If M equals zero, complete the quantification of L sought-for analytes directly by using Eqn. 10; otherwise, turn to the next step.

Defining the search region. In order to improve the efficiency of optimization, a relatively small search region is defined with some constraints [9].

The reasonable requirement of non-negative spectral intensity can be expressed as follows with consideration of the experimental error:

$$R_{jk} = Q_{jk} - \sum_{l=1}^{L} n_l S_{ljk} \geq -\epsilon \qquad l = 1, \ldots, L \qquad (16a)$$

or

$$\sum_{l=1}^{L} n_l S_{ljk} \leq Q_{jk} + \epsilon \qquad (16b)$$

where ϵ is an error bound associated with the instruments adopted.

This constraint can be used to define the upper limits of the sought-for concentrations [9]:

$$n_{l(\max)} = n_{l(\max)} \frac{S_{ljk}}{S_{ljk}} \leq \frac{\sum_{l=1}^{L} n_l S_{ljk}}{S_{ljk}} \leq \frac{(Q_{jk} + \epsilon)}{S_{ljk}}$$

$$\leq \mathrm{Min}\left[\frac{(Q_{jk} + \epsilon)}{S_{ljk}}\right] \qquad l = 1, \ldots, L \qquad (17)$$

Together with another reasonable requirement of non-negative concentration, the sought-for concentrations could be limited in a relatively small region as follows:

$$0 \le n_l \le n_{l(\max)} \qquad l = 1, 2, \ldots, L \tag{18}$$

Calculating $\boldsymbol{n}$. One can calculate $\mathbf{n}$ by the use of the background bilinearization with generalized simulated annealing (GSA) as a global optimization procedure.

(a) GSA is started by selecting a random initial guess $\mathbf{n}$ as the current state and the objective function is computed:

$$\phi = \phi(\mathbf{n}) = \sum_{j=1}^{J} \sum_{k=1}^{K} E_{jk}^2 \tag{19}$$

(b) A new random state $\mathbf{n}'$ is generated in the neighbourhood of the current state according to following equation:

$$\mathbf{n}' = \mathbf{n} + \Delta r \mathbf{v} \tag{20}$$

where Δr is the step size, which should be preset in advance together with other parameters mentioned below; $\mathbf{v}$ is a random direction with elements v_l determined by L random numbers u_l ($l = 1, \ldots, L$) from $N(0, 1)$ according to

$$v_l = \frac{u_l}{\left(\sum_{l=1}^{L} u_l^2 \right)^{1/2}} \tag{21}$$

(c) The perturbed state $\mathbf{n}'$ is checked to see whether it satisfies the constraints formulated in

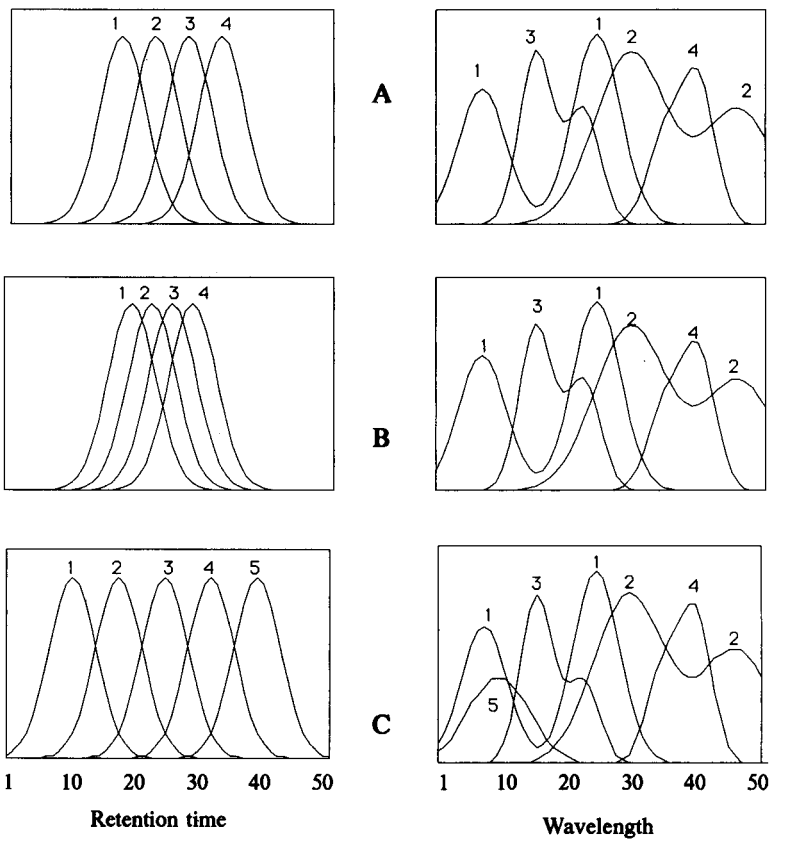

Fig. 1. Simulated chromatographic bilinear data. Left: chromatographic profiles. Right: standard spectra. The numbers denote the components. From top to bottom: A, B and C represent three analytical systems with varied chromatographic and spectral overlapping.

Eqn. 18. If not, the process is returned to step (b) and a new random state is generated again with Eqn. 20. Otherwise, the objective function of the perturbed state, $\phi' = \phi(\mathbf{n}')$, is calculated together with its difference from ϕ, $\delta\phi = \phi - \phi'$. If $\delta\phi \leq 0$, the perturbed state is accepted as the next current state unconditionally. If $\delta\phi > 0$, an acceptance probability p is defined:

$$p = \exp[-\beta\delta\phi/(\phi - \phi_0)] \quad (22)$$

where β is a controlling parameter and ϕ_0 is the value of the objective function in the global optimum (see below).

The calculated probability p is compared with a random number, P, drawn from a uniform distribution at the interval [0,1]. If $p \geq P$, the detrimental perturbed new state is accepted as the current state; otherwise, the process is returned to step (b) and another random perturbation on the current state $\mathbf{n}$ is executed for computing another new state. The process is repeated until some termination criteria defined by the analytical precision are satisfied. The result satisfying the stopping criterion is taken as the best estimate of the sought-for concentrations.

EXPERIMENTAL

Apparatus

Spectrofluorimetric measurements were done with a Hitachi 850 spectrofluorimeter. All computations were carried out on a Macintosh II microcomputer and an IBM 386 compatible microcomputer.

Numerical simulation

Three 50×50 two-dimensional bilinear coupled chromatographic systems with various spectra and chromatographic profiles were simulated by use of Gaussian bands and their combinations

TABLE 1

Results for simulated chromatographic data in Fig. 1

System	Analytes	Interferents	Concentration of analytes (arb. units)	
			Taken	Estimated
A	1,2	3,4	0.5000, 0.5000	0.4981, 0.5038
	1,3	2,4	0.5000, 0.5000	0.5054, 0.4971
	1,4	2,3	0.5000, 0.5000	0.4956, 0.5049
	2,3	1,4	0.5000, 0.5000	0.5026, 0.5119
	2,4	1,3	0.5000, 0.5000	0.5048, 0.5008
	3,4	1,2	0.5000, 0.5000	0.5050, 0.5033
B	1,2	3,4	0.5000, 1.0000	0.4996, 1.0043
	1,3	2,4	0.5000, 1.0000	0.4953, 0.9988
	1,4	2,3	0.5000, 1.0000	0.4965, 0.9925
	2,3	1,4	1.0000, 0.5000	1.0101, 0.4977
	2,4	1,3	1.0000, 0.5000	0.9933, 0.5018
	3,4	1,2	1.0000, 0.5000	1.0185, 0.4957
C	1,2,3	4,5	0.5000, 0.5000, 0.5000	0.4798, 0.5108, 0.4955
	1,2,4	3,5	0.5000, 0.5000, 0.5000	0.4907, 0.5103, 0.4983
	1,2,5	3,4	0.5000, 0.5000, 0.5000	0.4989, 0.5010, 0.4849
	1,3,4	2,5	0.5000, 0.5000, 0.5000	0.4835, 0.4902, 0.4878
	1,3,5	2,4	0.5000, 0.5000, 0.5000	0.5012, 0.5005, 0.4980
	1,4,5	2,3	0.5000, 0.5000, 0.5000	0.4951, 0.4973, 0.5107
	2,3,4	1,5	0.5000, 0.5000, 0.5000	0.4966, 0.5095, 0.5021
	2,3,5	1,4	0.5000, 0.5000, 0.5000	0.5024, 0.5056, 0.4967
	2,4,5	1,3	0.5000, 0.5000, 0.5000	0.4961, 0.5004, 0.5013
	3,4,5	1,2	0.5000, 0.5000, 0.5000	0.4972, 0.4977, 0.4898

TABLE 2

Results for simulated system B with different concentration profiles (the sought-for analytes are 1 and 2 and the interferents are 3 and 4 arb. conc. units)

Real concentration	Estimated concentration
1.0000, 1.0000	1.0018, 0.9971
0.1000, 1.0000	0.1026, 0.9985
1.8000, 0.1000	1.8030, 0.0982
0.2000, 0.7000	0.1965, 0.7161
5.0000, 0.0500	5.0039, 0.0544

(see Fig. 1). Each time two components of these four- and five-component systems were taken in turn as the unexpected interferents, and the remaining constituents were regarded as the sought-for analytes. A total of 22 cases were formulated, each one corresponding to an original unknown sample (see Table 1). For each case, several additions of the sougth-for species were made by simply increasing their coefficients in the synthetic data with constant coefficient(s) of the assumed unknown interferent(s). To simulate different concentrations of analytes and interferents, the spectra of these species were multiplied by different numbers (Table 2). The data were processed with the proposed method and the concentrations of the sought-for analytes were estimated. All simulations were carried out on the noise-free condition except in the experiments for studying the influence of noise.

Fluorimetric measurements

Three organic dyes, Rhodamine B, fluorescein and Eosin Y, were of analytical-reagent grade and standard solutions of each and their mixtures were prepared with 2.5×10^{-3} mol l^{-1} NaOH. Eight mixtures with various concentration ratios were taken as the original unknown samples. One or two of these three dyes in each sample were treated as the sought-for analyte(s) and standard additions were made on them and thus eight sets of solutions were prepared. The fluorescence measurement was made with each set of solutions including the original unknown sample and samples with additions. The fluorescence intensities were recorded every 4 nm in the range 484–600 nm of the emission spectra for a fixed excitation wavelength and the excitation wavelength was varied in the range of 454–570 nm with a 4-nm increment. Thus, a two-dimensional EM–EX matrix of size 30×30 was obtained for each solution. The data were acquired on-line by an IBM 386 compatible microcomputer interfaced with the spectrofluorimeter. The communication program was written in BASICA. All measurement data were corrected for the reagent blanks before processing. All computing programs were written in MATLAB.

RESULTS AND DISCUSSION

The experimental design of GSAM has been extensively studied [10,11] and the present experiments followed the published conclusions without further explanation. Both in simulation and real experiments, the additions were conducted for the sought-for analyte one after another. As random noise would be predominant source of error, the total difference calculation (TDC) method [10] was used for the computation of the increment matrix (tensor) of concentrations and responses.

In the *Calculating* $\boldsymbol{n}$ step of the proposed computation method (see above), $\mathbf{n}$ can be calculated by the use of GRAFA or by the iterative method for minimizing $\mathcal{F}$ with alternative fixing $\mathbf{n}$ and $\mathbf{R}$ as described by Ohman et al. [7,8]. Liang et al. [9] suggested a direct optimization procedure with the Powell algorithm and the constraints of positive concentrations and spectral intensities to narrow the search region. In order to reduce further the possibility of sinking into local optima, GSA was adopted for the optimization step in this work with the same constraints as used in the literature [9]. Simulated annealing (SA) is a category of stochastic optimization algorithms applied first by Kirkpatrick et al. [12] to the solution of combinatorial optimization problem and later generalized by Bohachevsky et al. [13] for searching the global optimum on a continuous multi-dimensional response surface. GSA was used for analytical calibration [14,15]. GSA was chosen as the optimization algorithm in this work owing to

TABLE 3

Results for simulated system B with different initial values (the sought-for analytes are 1 and 2 and the interferents are 3 and 4 arb. conc. units)

Initial state	Real concentration	Estimated concentration
0.0000, 0.0000	0.5000, 1.0000	0.4996, 1.0043
1.0000, 1.0000	0.5000, 1.0000	0.4978, 1.0139
1.0000, 0.0000	0.5000, 1.0000	0.5032, 0.9903
0.0000, 1.0000	0.5000, 1.0000	0.5067, 1.0063
0.5000, 0.5000	0.5000, 1.0000	0.4975, 0.9955
0.2000, 2.0000	0.5000, 1.0000	0.5063, 0.9946

its excellent mechanism of walking across local optima.

The influences of the parameters of GSA have been extensively discussed [12–15]. According to Bohachevsky et al. [13], β was chosen and adjusted automatically in the process of computation so that the inequality $0.5 < p < 0.9$ is satisfied. In order to search the whole space of states, a relatively large initial step size, say 10% of the size of the constrained region, is adopted. The objective function of the global optimum, ϕ_0, is not always known a priori. A reasonable initial value of zero was used in this paper.

TABLE 4

Results for simulated system B with different noise levels (the sought-for analytes are 1 and 2 and the interferents are 3 and 4 arb. conc. units)

Standard deviation of noise (σ)	Real concentration	Estimated concentration
0.001	0.5000, 1.0000	0.5035, 0.9879
0.005	0.5000, 1.0000	0.4999, 0.9963
0.010	0.5000, 1.0000	0.5057, 0.9841
0.030	0.5000, 1.0000	0.5097, 0.9878

Some modifications of GSA were adopted [16]. First, the step size Δr is a constant in the GSA, which limits the precision of the optimization results. Therefore, an additional cycle for reducing Δr is introduced in this algorithm. Second, as GSA accepted detrimental states with non-zero probability, which makes GSA not sink into local optima, the ultimate state in one cycle of GSA is usually not the best state produced in this cycle. In order to improve the efficiency of the algorithm, the best state appearing in the cycle of the computation is stored and taken as the initial state of the successive cycle or the ultimate result if the algorithm is terminated. In this way, GSA can operate more efficiently.

TABLE 5

Interpretation of two-dimensional fluorescence data

No.	Concentration of analytes (taken) [a]	Concentration of interferent(s) [a]	Concentration of analytes (estimated) [a]	Relative error (%)
1	A(0.2080)	C(0.2052)	A(0.2254)	8.4
	B(0.2088)		B(0.2134)	2.2
2	A(0.2080)	B(0.2088)	A(0.2162)	3.9
		C(0.2052)		
3	A(0.3130)	C(0.2052)	A(0.3426)	9.5
	B(0.2088)		B(0.2217)	6.2
4	A(0.4160)	C(0.2052)	A(0.4560)	9.6
	B(0.2088)		B(0.2023)	−3.1
5	B(0.2088)	A(0.5200)	B(0.2077)	−0.5
		C(0.2052)		
6	B(0.3132)	A(0.5200)	B(0.2945)	−6.0
		C(0.2052)		
7	A(0.2006)	B(0.4320)	A(0.1966)	−2.0
	C(0.4372)		C(0.4686)	7.2
8	B(0.5400)	A(0.1003)	B(0.5311)	−1.6
	C(0.2187)		C(0.2303)	5.3

[a] A = Fluorescein; B = Eosin Y; C = Rhodamine B; concentrations in ppm.

Table 1 shows the quantification results for the sought-for species of the simulation systems. It is clear that for all 22 cases the global optima have been found. As GSA played the central role in this procedure, its performance was tested in some detail. Table 2 presents the results for the first case of simulated system B of Table 1 with different concentration profiles. Although the estimates were less precise for the minor components when the difference in concentrations between species was large, they were still acceptable. Table 3 lists the results for the same case of simulated system B of Table 1 with different initial values. It demonstrates that the positions of initial states had no influence on the performance of GSA owing to its intrinsic randomness. The influence of noise was also investigated. Normal random numbers with zero-mean and four different standard deviations, $\sigma = 0.001$, 0.005, 0.010 and 0.030, were generated and added to the mixture response matrices after multiplying the absolute value of the largest element in each mixture response matrix to simulate the experimental error. The results in Table 4 show that a moderate level of noise did not degrade the analytical results very much.

Two-dimensional fluorescence data

Eight mixtures of three dyes were prepared according to the GSAM experimental design and the measured fluorescence excitation–emission data sets were treated by using the proposed method. The error bound, ϵ, was taken as ten times the fluorescence intensity unit of the Hitachi 850 instrument. One or two of these three components were taken as unknown interferents and the concentration of the remaining components was estimated. The initial estimates of concentrations were set to zero. The true concentrations and their estimates are given in Table 5. If one remembers that the proposed method did not require the standard spectra of analytes in the environment of real samples or any a priori information concerning the background interferents, the estimated results should be considered to be reasonably acceptable.

It must be pointed out that the computation of GSA is generally more time consuming than that of generally used local optimization algorithms such as the Powell algorithm [9] owing to its intrinsic randomness. However, there are two advantages with the adoption of GSA. First, the response surface of background bilinearization would be complicated owing to its complex relationship with **n** and **R**. Some local optima may exist. GSA has the ability to walk across them. Also, GSA is only slightly influenced by the initial values owing to its intrinsic randomness. This may not be the case with the Powell algorithm and algorithms of this type. Second, the concentration constraints (Eqn. 18) can be exerted more easily in the process of computation of GSA just by checking directly the availability of the perturbed state, but in the algorithms associated with a one-dimensional search, as in the Powell algorithm, the troublesome transfer of the multidimensional constraints to the one-dimensional search boundary is inevitable.

From the results of simulation and processing of real EX–EM data, it seems that the proposed method can work satisfactority.

This work was supported by Natural Science Foundation of China and partially by the Laboratory of Electroanalytical Chemistry, Changchun Institute of Applied Chemistry, Chinese Academy of Science.

APPENDIX

List of symbols

- $\mathbf{b}_l^T$ a row vector of response sensitivity for the lth analyte (size $1 \times J$)
- $\mathbf{B}$ the matrix of response sensitivity (size $L \times J$)
- $\mathbf{d}$ a column vector of one direction variable in a two-dimensional instrument (size $J \times 1$)
- $\mathbf{e}^T$ a row vector of experimental error for the original sample (size $1 \times J$)
- E_{jk} the (j,k)th element of experimental error matrix
- $\mathbf{E}$ a matrix of experimental error after additions in the one-dimensional case (size $I \times J$) or a matrix of experimental error for the original sample in the two-dimensional case (size $J \times K$)

$\boldsymbol{E}$ the third-order tensor of experimental error after additions in the two-dimensional case (size $I \times J \times K$)
$\mathcal{F}$ the objective function
$\mathbf{g}^T$ a row vector of another direction variable in a two-dimensional instrument (size $1 \times K$)
i a dummy index for counting standard additions
I the number of standard additions
j a dummy index for counting variable of a one-dimensional instrument or for counting one direction variable of a two-dimensional instrument
J the number of measurement variable
k a dummy index for counting another direction variable of a two-dimensional instrument
K the number of measurement variable
l a dummy index for counting sought-for analytes
L the number of sought-for-analytes
m a dummy index for counting unexpected interferents or principal components
M the number of unexpected interferents or the number of principal components
n_l the concentration of the lth analyte
n_m the concentration of the mth unexpected interferent
$\mathbf{n}^T$ a row vector of concentration (size $1 \times L$)
p the calculated acceptance probability
P a random number drawn from uniform distribution at the interval [0,1].
Q_{jk} the (j,k)th element of original response matrix
$\mathbf{Q}$ a matrix of response yielded in the original sample (size $J \times K$)
$\boldsymbol{Q}$ the third-order tensor of response after standard additions (size $I \times J \times K$)
$\mathbf{r}_m^T$ a row vector of response sensitivity for the mth unexpected interferent (size $1 \times J$)
$\mathbf{r}^T$ a row vector of overall response for M unexpected interferents (size $1 \times J$)
R_{jk} the (j, k)th element of overall response matrix
$\mathbf{R}_m$ a matrix of response sensitivity for the mth unexpected interferent (size $J \times K$)
$\mathbf{R}$ a matrix of overall response for M unexpected interferents (size $J \times K$)
S_{ljk} the (l, j, k)th element of response sensitivity tensor
S_l a matrix of response sensitivity for the lth analyte (size $J \times K$)
$\boldsymbol{S}$ the third-order tensor of response sensitivity (size $L \times J \times K$)
$\mathbf{t}_m$ a column vector of factor score for $\mathbf{R}$, factor m (size $J \times 1$)
$\mathbf{T}$ the matrix of $\mathbf{R}$ scores (size $J \times M$)
u_l a random number for $N(0, 1)$
$\mathbf{u}_m^T$ a row vector of factor loading for $\mathbf{R}$, factor m (size $1 \times K$)
$\mathbf{U}^T$ the matrix of $\mathbf{R}$ loadings (size $M \times K$)
v_l the lth element in $\mathbf{v}$
$\mathbf{v}$ a column vector representing a random direction in GSA optimization (size $L \times 1$)
$\mathbf{z}^T$ a row vector of response yielded in the original sample (size $1 \times J$)
$\mathbf{Z}$ the matrix of response after standard additions (size $I \times J$)
β controlling parameter in GSA
$\delta\mathbf{N}$ the matrix of concentration increment (size $I \times L$)
$\delta\boldsymbol{Q}$ the third-order tensor of response increment (size $I \times J \times K$)
$\delta\mathbf{Z}$ the matrix of response increment (size $I \times J$)
$\delta\phi$ the difference of objective function between the current state $\mathbf{n}$ and the perturbed state $\mathbf{n}'$
Δr step size
ϵ error bound
ϕ the value of objective function
ϕ_0 the value of objective function at the global optimum

REFERENCES

1 D.E. Saxberg and B.R. Kowalski, Anal. Chem., 57 (1985) 908.
2 D.W. Osten and B.R. Kowalski, Anal. Chem., 57 (1985) 908.
3 Y.-Z. Liang, Y.-L. Xie and R.-Q. Yu, Chin. Sci. Bull. (Engl. Ed.), 34 (1989) 1533.
4 C.N. Ho, G.D. Christian and E.R. Davidson, Anal. Chem., 50 (1978) 1108.
5 A. Lorber, Anal. Chim. Acta, 164 (1984) 293.
6 E. Sanchez and B.R. Kowalski, Anal. Chem., 58 (1986) 496.

7 J. Ohman, P. Geladi and S. Wold, J. Chemometr., 4 (1990) 79.
8 J. Ohman, P. Geladi and S. Wold, J. Chemometr., 4 (1990) 135.
9 Y. Liang, R. Manne and O.M. Kvalheim, Chemometr. Intell. Lab. Syst., 14 (1992) 175.
10 M.G. Moran and B.R. Kowalski, Anal. Chem., 56 (1984) 562.
11 C. Jochum, P. Jochum and B.R. Kowalski, Anal. Chem., 53 (1981) 85.
12 S. Kirkpatrick, C.D. Gelatt and M.P. Vecchi, Jr., Science, 220 (1983) 671.
13 I.O. Bohachevsky, M.E. Johnson and M.L. Stein, Technometrics, 28 (1986) 209.
14 J.H. Kalivas, N. Roberts and J.M. Sutter, Anal. Chem., 61 (1989) 2024.
15 J.H. Kalivas, J. Chemometr., 5 (1991) 37.
16 X.-L. Xie, J.-H. Wang, Y.-Z. Liang, K. Ge and R.-Q. Yu, J. Chemometr., in press.

Analytica Chimica Acta, 281 (1993) 219–220
Elsevier Science Publishers B.V., Amsterdam

Obituary

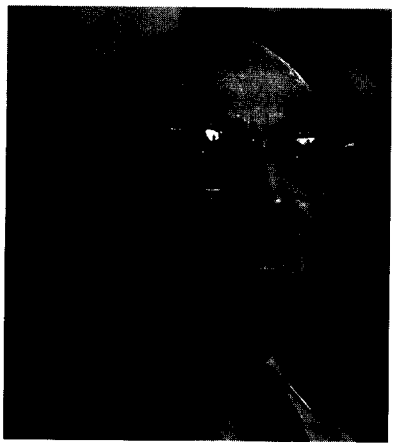

I.M. Kolthoff
Scientist and humanitarian

Izaak Maurits Kolthoff died, 99 years old, on Thursday, March 4, at Bethesda Lutheran Hospital and Rehabilitation Center in St. Paul, Minnesota. He was once described by the late Professor Herbert Laitenen as "the person most influential to the modern discipline of analytical chemistry" [1]. For many years he was the only analytical chemist who was a member of the US National Academy of Sciences. Although enthusiastic about the significant advances in instrumentation made in his lifetime, Kolthoff was well aware of the potential drawbacks in an approach to analytical problems in which too much emphasis is placed on apparatus and data processing and not enough on the chemical principles behind the measurement being made [2].

Kolthoff was born in 1894, in Almelo, Netherlands. He studied pharmacy at the University of Utrecht. His first paper on acid–base titrations appeared in 1915. By the time he received his PhD degree in 1918, Kolthoff had already published 33 papers. He remained at Utrecht as a lecturer for nine years. In 1927 he began his long association with the University of Minnesota, serving as Professor and Chief of the Division of Analytical Chemistry until 1962 and then as Professor Emeritus.

In 1942, Kolthoff participated in US efforts to initiate a synthetic rubber capability by organizing one of several academic research groups which co-operated with an industrial R&D program. Besides their analytical contributions, his team carried out extensive studies of the mechanism of emulsion polymerization. One area of investigation during the synthetic rubber program was the amperometric determination of sulfhydryl and disulfide. Numerous papers concerned with these groups, especially in proteins, appeared in ensuing years.

In the late 1970s, the behaviour of macrocyclic compounds, such as the crown ethers, became the focus of his attention. He undertook a study of their analytical behaviour. After a thorough literature study, he wrote a review article containing 207 references, in which he noted that he had actually read every publication!

Kolthoff actively campaigned throughout his career to have analytical chemistry recognized as a truly scientific discipline in its own right, both by his fellow chemists and by the ruling bodies of

science. As an official of IUPAC, he was commissioned in 1951 to establish the Analytical Chemistry Division.

On the social front he was politically active, and helped German scientists persecuted by Hitler to find jobs at the University of Minnesota. He publically criticised the investigations carried out by Senator Joseph R. McCarthy and the congressional Un-American Activities Committee. He also led protests against nuclear weapons.

Kolthoff was recognized for his work in modern analytical chemistry by the American Chemical Society, which accorded him the William H. Nichols Medal in 1949. He was knighted in the Netherlands and received many other honors including the Charles Medal of the Charles University in Prague and the Fisher Award of the American Chemical Society. Six universities presented him with honorary doctorates. He is said to have considered as his greatest honor the 1983 award for teaching excellence in Analytical Chemistry from the Division of Analytical Chemistry of the American Chemical Society. Kolthoff was its first recipient. In 1972, Kolthoff Hall on the University's Minneapolis campus was dedicated in his honor.

He was a member of the United States National Academy of Sciences, a foreign member of the Royal Flemish Academy of Sciences and of a number of other learned Societies throughout the world.

He left no survivors in the United States, but has relatives in the Netherlands and Israel.

REFERENCES

1 H.A. Laitenen, Trends Anal. Chem., 1 (1981) 4.
2 P.T. Shepherd, Trends Anal. Chem., 1 (1981) 1.

Analytica Chimica Acta, 281 (1993) 221–228
Elsevier Science Publishers B.V., Amsterdam

BOOK REVIEWS

J. Yinon and S. Zitrin, *Modern Methods and Applications in Analysis of Explosives*, Wiley, Chichester, 1993 (ISBN 0-471-93894-7). x + 305 pp. Price £ 60.00.

Since the publication of the authors' earlier book *The Analysis of Explosives* in 1981, there has been much progress in the field of explosives analysis both at the macro and trace levels as well as an increased public interest in such matters. The first chapter concerns "Explosive compounds and their mixtures" and gives up-to-date information (obtained by a questionnaire sent to laboratories dealing with explosives analysis) on explosives used, manufactured or encountered during the last few years. The rest of the text is divided into methodological and application chapters. The chapters on "Chromatographic Methods" and "Mass Spectrometric Methods" include current practice, recent developments and instrumentation. It is regretted that other possibly important techniques such as NMR and ESR were not reviewed because of their current limited application. The applications chapters deal with "Analysis of Explosive Residues", "Environmental Analysis of Explosives" and the "Detection of Hidden Explosives". A deal of attention is given to recovery and to clean up procedures, crucial steps in schemes for trace and residue analysis. The inclusion of material on the measurement of explosives and their degradation products in soil and water via disposal or manufacture is timely and relevant to the growing public concern on environmental chemical issues. The detection of hidden explosives remains as a particular analytical challenge. Herein only published work could be dealt with since much in this area is classified or restricted information to national forensic laboratories. The literature, post 1980, is dealt with comprehensively, and most usefully the titles of papers are included with each reference.

This authoritative monograph is a worthy follow up to the authors' earlier volume. It will be of great interest to both those with specialist and those with more general forensic interests.

D. Thorburn Burns

H.H. Hill and D.G. McMinn, *Detectors for Capillary Chromatography*, Wiley, New York, 1992 (ISBN 0-471-50645-1). xvii + 444 pp. Price £ 67.00.

An excellent compilation is provided on basic knowledge about detectors for GC and, rather as an addendum, for SFC and microcolumn LC. It consists of 15 chapters, written by highly qualified authors. It makes the reader aware of the fact that there are many more detectors than are routinely used.

The first detector described (by the editors of the book) is the flame ionisation detector (FID). Although designated as the most common detector, the subject is covered in about 10 pages, dealing with the probable mechanisms of ion formation, optimum gas flow rates and relative detector responses.

The helium ionisation detector (HID), described by Ramsey and Andrawes in a lively style, is more adventurous, and provides excellent sensitivity for components not detected by the ECD (to which it is somewhat related).

The description of the photo-ionization detector (PID) by Driscoll, *the* expert in this field, is concise and complete, covering the principles, the technology and some applications.

Reading the part on the electron capture detector (ECD) by Grimsrud, the dilemma of the authors seemed obvious, either writing an interesting contribution to experts or to help the practitioner to get his analysis done. Grimsrud has chosen the first approach. The chapter provides highly competent information, but anyone who bought the book to learn about practical work with an ECD finds little more than references.

Hall provides the information about the electrolytic conductivity (Hall) detector in such a manner that the reader has the feeling of having had a look backstage. The description of the nitrogen-phosphorus detector (NPD) by Patterson, certainly *the* expert in the field, seems complete and deep in background. It leaves the impression once more that a device works and nobody really understads why. The AFID might, however, be disqualified too rapidly: a somewhat more complex optimization is easily balanced by more robust performance, particularly in work involving large amounts of solvent. The treatment of the sulphur-selective detectors in one chapter (Hutte and Ray) provides interesting comparative information and reminds one that the most widely used flame photometric detector (FPD) is not necessarily and always the best for sulphur-selective detection.

As is also true for the other 7 chapters, I enjoyed reading them and they provided many new insights. The book seems to be written for scientists with a fair background of physics and chemistry. A technician might find it hard to follow some descriptions. Texts concentrate on principles, an outline of the detector design, and some examples of application, but provide little help to those struggling with every-day problems in the laboratory. For instance, curves on optimum flow rates for a particular FID are given, but no information is provided on how to optimize detector gases in practice, on the importance of the column position at the jet orifice, on problems, such as spikes, falling baselines due to contamination of the jet, and valleys after major peaks. This would be a subject for another book.

Konrad Grob

Bernd Wenclawiak (Ed.), *Analysis with Supercritical Fluids: Extraction and Analysis*, Springer Verlag, New York, 1992 (ISBN 0-387-55420-3). xi + 213 pp. Price DM 148.00.

Supercritical-fluid chromatography (SFC) and extraction (SFE) are relatively new analytical techniques. Hence it is clear that the number of books on these subjects is still limited. Including this book the SFC/SFE bookshelf comprises only some five books that help prospective users learn what SFC and SFE offer and how these techniques can be used to advantage. The new book contains 11 chapters, all written by recognized experts in the field, covering the physico-chemical principles of SFC and SFE, injection techniques and stationary phases for SFC and describing a number of more exotic detection methods.

After a very brief introduction for novices by the editor, the book starts with a chapter on physico-chemical principles of supercritical fluid separation techniques by Schneider. This chapter could be looked upon as a second introduction as it contains a wealth of information on the solvating and transport properties of supercritical fluids, relevant both for SFC and SFE. Chapter 3 is excellent and focuses on the basic principles of analytical SFE. It elegantly describes the principles involved in applying this technique for sample preparation and opens the analyst's eyes as to the selectivity that can be obtained and how to optimize supercritical fluid extractions. The on-line combination of SFE with GC is discussed in Chapter 4. Two interfacing methods are discussed in detail: split SFE–GC and on-column SFE–GC. A good, exhaustive comparison of the two approaches is presented.

Chapter 5, by Klesper and Schmitz, treats the use of gradient elution techniques in packed and open-tubular SFC and briefly discusses the plate heights and the Van Deemter curves of chromatographic columns in GC, SFC and LC. In Chapter 6 an interesting comparison of the various techniques available for sample introduction in SFC is given. Special emphasis is on sampling techniques for the introduction of relatively large sample volumes in capillary SFC. Chapter 7 concerns stationary phases for packed column work. Various stationary phases, including chemically deactivated and polymer encapsulated packings, are compared with both neat CO_2 and modified fluids as the mobile phase. The conclusion reached is that even the most chemically inert materials will fail in some critical cases; improvements of existing materials and new materials created especially for SFC are needed in order to

meet the required inertness requirements. Enantiomer separations by capillary SFC are the subject of Chapter 8. The influence of temperature and mobile phase composition on the resolution obtained is discussed. Column loadability, efficiency, the nature and properties of the stationary phase and the speed of analysis are all considered. Many impressive examples are given.

The last three chapters concern the combination of SFC with some identification techniques. In Chapter 9 Pinkston reviews SFC–MS with both packed- and open-tubular columns. Information is given regarding several types of interfaces for application in the EI as well as in the CI mode. In the conclusions section of this chapter emphasis is placed on the unique advantages of packed and open-tubular SFC for certain types of applications. The focus of Chapter 10 is SFC/FT-IR. Taylor and Calvey present an in-depth discussion of the pros and cons of the flow cell and the solvent elimination interface in coupled SFC/FT-IR. Sensitivity, spectral resolution, chromatographic peak shapes and ease of use of the two interfacing methods are discussed with a large number of examples of actual analyses. The last chapter pertains to the coupling of supersonic jet spectroscopy to SFC. After a brief description of the principle of supersonic expansion, the practical aspects of supercritical fluid injection are discussed. Finally, the hardware required for on-line SFC-supersonic jet spectroscopy is examined.

In summary, the book is a useful addition to the SFC and SFE literature. Although not all aspects of SFC and SFE are discussed, it contains without any doubt a large amount of useful information in a condensed form. I am surprised by the extensive lists of references given in the various chapters. Unfortunately it appears that some three years elapsed between the preparation of the first version of the manuscript and the actual publication. In most of the chapters no references are given to literature after 1989. This is the more regrettable since new techniques like SFE and SFC are in general characterized by an extremely rapid development. Indeed, many major improvements have occurred in the last two to three years. The summary of recommented literature presented in the last 5 pages helps to relieve this omission.

Hans-Gerd Janssen

T.R. Crompton, *Comprehensive Water Analysis*, Vols. 1 and 2, Elsevier Applied Science, London, 1992 [ISBN 1-851-66750-4 (set), 1-851-66751-2 (Vol 1), 1-851-66752-0 (Vol 2)]. xii + 524 pp. (Vol. 1), viii + 418 pp. (Vol. 2). Price £ 325.00 (set).

Volume 1 of this set covers natural waters which include surface waters, groundwaters, aqueous precipitation and estuarine waters. The first two categories are considered together in great detail, with separate chapters on anions, cations, elemental analysis, organics, organometallics, oxygen demand parameters, dissolved gases, radioactive elements and miscellaneous determinands. Precipitation and estuary waters are covered much more briefly under the same headings.

Volume 2 covers treated waters which include potable waters, waste waters, sewage effluents, trade effluents, and miscellaneous waters (mineral, high purity, boiler feed, swimming pool and nuclear reactor coolant). The breakdown in terms of species is the same as for Volume 1.

Both Volumes are therefore logically arranged, with extensive references throughout (mainly citing primary journals from the 1970s and 1980s) and a good index for each volume. It has clearly been a major undertaking to collate such a vast amount of information in a coherent manner and it is a useful reference source. The text is written in the style of a review with considerable factual information but very little critical discussion.

The book is intended for a wide range of people concerned with monitoring (and control of) the environmental, social and political impact of water pollutants. It is therefore surprising that there is no general introduction to the book or to any of the individual chapters that provides a framework within which the analytical detail can be placed. Details of national and international water quality legislation, for example, would en-

able the reader better to assess the relative merits of the various analytical approaches. Given the scope of the two titles and the thousands of references included, it is not suprising that there are omissions and errors, e.g., in Volume 1 on page 146 much better detection limits for the spectrophotometric determination of iron can be achieved than those quoted, and on page 501 the same paper is discussed in consecutive but independent paragraphs with separate reference numbers.

In summary this is a useful but expensive compendium of approaches to the analysis of natural and treated waters and is therefore a worthwhile source book for analytical chemists. However it does not include critical discussion of the various approaches or set the analytical methods in a wider environmental context.

Paul J. Worsfold

I. Nagy, *Introduction to Chemical Process Instrumentation*, Elsevier, Amsterdam, 1992 (ISBN 0-444-98712-6). xx + 448 pp. Price US$ 177.00/Dfl. 345.00.

This book is the third volume in the series *Process Measurement and Control*. It presents a well-structured comprehensible introduction to chemical process instrumentation. In three parts the fundamentals of metrology, process control theory and design methods of process instrumentation, the automatic control of unit operations and processes, and process plant instrumentation are discussed. The book gives a transparent presentation of the field. Because it is not specifically written for analytical chemists but rather aims at chemical engineers and control engineers, its scope is much wider than purely process analytical chemistry. Nevertheless analytical chemists coming in contact with aspects of process control will find several sections of particular interest highlighted with numerous illustrations.

In the cover text it is claimed that the "most recent advances in the field have been treated". This seems not to be entirely true: it gives the state-of-the-art of the 1980s. For instance, artificial intelligence in process control is only briefly mentioned in connection with the development of knowledge-based expert systems. Nothing is said about the use of neural networks in this respect.

In conclusion, this is a rather classical, easy to read book written for newcomers in the field. Its nice format as well as the many illustrations and examples makes it good value for money.

Willem E. van der Linden

A. Montaser and D.W. Golightly (Eds.), *Inductively Coupled Plasmas in Analytical Atomic Spectrometry*, 2nd edn., VCH, Weinheim, 1992 (ISBN 3-527-28339-0). 1017 pp. Price £ 111.00.

This is a timely update of a well respected and useful book. The basic aims of the book remain unchanged, i.e., to provide a comprehensive reference on the theory and practice of ICPs aimed at both the student and established researcher. However the revised text includes five new chapters and much updating of the chapters from the first edition to reflect advances since 1987. The basic format of the book has been retained and again calls on contributions from internationally known scientists for each of the twenty heavily referenced chapters. The book itself may be split into four principal sections covering the potentials and limitations of plasma sources compared to ICP discharges for analytical spectrometry; basic concepts and analytical applications of ICP-AES; complementary techniques such as the analytical applications of ICP as an atomization cell for atomic fluorescence spectrometry and the fundamentals, instrumentation and applications of ICP-MS; and finally modified sample introduction systems, mixed gases and the use of mathematical models. The most important revision in this second edition is the expansion of the coverage given to ICP-MS which now extends to three chapters. This book is presented to a high standard and is highly recommended to all ICP spectroscopists.

S.J. Hill

F.D. Garfield, *Quality Assurance Principles for Analytical Laboratories*, 2nd edn., AOAC, Washington, DC, 1991 (ISBN 0-935584-46-3). v + 195 pp. Price US$ 63.00 (N. America), US$ 69.00 (rest of the world).

In the introduction the author explains that this book was "designed to provide useful guidelines for initiating a QA program". What is not said is that this "program" is almost entirely focused to domestic US needs and heavily biased towards FDA compliance at that! Perhaps this is not surprising as the author has had a career in the FDA and US regulatory area.

Questions are therefore inevitable about the relevance of such a targeted work to the European chemist. One of the problems is that Quality Assurance is defined in the first chapter as "planned activities designed to ensure that the quality control activities [*in the analytical laboratory*] are properly implemented". Many European chemists would choose Quality Control to define these activities. Not withstanding these limitations there are within the 10 chapters and 6 appendices much useful guidance.

Chapter 1, QA planning, is a generic overview with suggestions for organisational and procedural controls. It is very basic but for those starting from scratch provides a useful checklist of points to consider. The next chapter on statistical applications and control charts is poor. It is far too short and basic to be useful and distinctly old fashioned in its sole reliance on Shewart control charts. Cusum charts do get one paragraph.

Chapter 3, personnel considerations, looks at roles and responsibilities of staff together with training and performance appraisal. It is somewhat brief but gives much more generally applicable recommendations. Chapter 4, management of equipment and supplies, is very USA in detail but the overall approach to supply management is sound and the relationship to recognised standards of excellence commendable. Sample and record handling is dealt with in Chapter 5 and in a highly stylised FDA manner. It is not very useful unless you are in the pharmaceutical business for the USA! Chapter 6 is arguably the best in the book and deals with sampling and sample analysis. Topics include sampling plans and subsampling for analysis, sample preparation, method selection and method validation considerations. It gives a very good introduction to the topic. Proficiency and check samples, Chapter 7, covers intra and interlaboratory testing programmes. Regrettably all the references are domestic USA. Chapter 8, 9 and 10 cover audit procedures, design and safety of facilities and laboratory accreditation which are limited to American perspectives. That things are different "over there" is evident from the comment that "beards [*in laboratories*] should be discouraged or shortened". The six appendices are not very relevant to European laboratories with the exception of C on Instrument Performance Checks. Here are listed by equipment type a check set of proposed frequencies, parameters to be checked, and the appropriate standard with general procedures. There if much here for debate but it is a very useful starting point. Interestingly the standard for photometric accuracy for UV–visible spectrometry is that of the *Pharm. Eur.* Perhaps it is not a coincidence that this appendix was derived from the Canadian authorities.

All in all it is difficult to identify a market for this book within Europe. Laboratories covered by the regulatory umbrella of the USA may find it of use but otherwise it will be of limited interest.

C. Burgess

P.M. Gy, *Sampling of Heterogeneous and Dynamic Material Systems. Theories of heterogeneity, sampling and homogenizing*, Elsevier, Amsterdam, 1992 (ISBN 0-444-89601-5). xxx + 654 pp. Price US$ 266.00/Dfl. 425.00.

This book is to be considered as a follow-up to previous books by the same author, who is certainly one of the world's best experts in this field. In this book he has collected 40 years of experience in sampling. The book consists of 35 chapters, clustered in 10 parts. Each chapter is subdivided into sections and sub-sections. All possible aspects are apparently treated and those who face problems in sampling will certainly find some valuable hints how to deal with them.

Having given full credit to this opus magnum of Gy, some comments have to be made. The book cannot be read as a textbook; it is more an extensive compilation of definitions, short statements and examples in an over-structured presentation which do not make it easily accessible for someone who is just interested in a specific subject. Also there is hardly any distinction between matters of primary, secondary and minor importance. This is strengthened by the unattractive lay-out of the text.

In conclusion this book should be present in all analytical libraries for consultation but it is less suitable for learning the "art" of sampling.

Willem E. van der Linden

J.A. Marinsky and Y. Marcus (Eds.), Ion Exchange and Solvent Extraction. A Series of Advances, Vol. II, Marcel Dekker, New York, 1993 (ISBN 0-8247-8472-3). xiv + 375 pp. Price US$ 195.00.

This volume aims to provide an interested reader with the opportunity for examination, comparison and evaluation of state-of-the-art ion-exchange theory.

Chapter I (S.A. Grant and P. Fletcher, 108 pages, 106 refs.) reviews the chemical thermodynamics of cation-exchange reactions highlighting recent theoretical and practical developments. The correlation of ion-exchange phenomena via a simple but non-predictive three-parameter model is outlined in Chapter II (E. Hogfeldt, 42 pages, 31 refs.).

Chapter III (W.H. Höll, M. Franzreb, J. Horst and S.H. Eberle, 58 pages, 67 refs.) comprises a description of the developments and applications of surface complexation theory to ion-exchange phenomena and links with, and is complemented by, Chapter IV (G. Sposito, 22 pages, 53 refs.), an account of metal-natural colloid surface reactions. A Gibbs-Donnan based analysis of ion-exchange and related phenomena is expounded in Chapter V (J.A. Marinsky, 98 pages, 67 refs.). The volume concludes with a topic of environmental chemical interest, namely the influence of humic substances on the uptake of metal ions by naturally occurring materials (J.H. Ephraim and B. Allard, 33 pages, 107 refs.).

Overall this is a series of scholarly reviews of particular interest to those working in, or wishing to enter, the fascinating world of ion-exchange phenomena.

D. Thorburn Burns

James H. Clark, Adrian P. Kybett and Duncan J. Macquarrie, *Supported Reagents. Preparation, Analysis and Applications*, VCH, New York, 1992 (ISBN 1-56083-010-6). xi + 152 pp. Price US$ 108.00.

Supported reagents, i.e., reagents bound in some way to a solid support, are finding considerable use in analytical chemistry, especially in flow systems. Immobilized enzymes and antibodies are two popular examples, but there are many more. This book, however, deals with such reagents in the context of organic synthesis, a subject that has a shorter history and, as yet, a smaller range of applications. Nevertheless, the analytical chemist will learn from the present monograph. A range of procedures, both physical and chemical, is described for preparation of the supported reagents and there is a useful chapter detailing the use of various analytical techniques for studying the immobilised reagents. The book concludes with some case studies in organic synthesis, and a tabulation of a wide range of other syntheses.

Alan Townshend

F. Rouessac, *Analyse Chimique*, Masson, Paris, 1992 (ISBN 2-225-83919-0). xi + 291 pp. Price FF. 160.00.

Ce livre, en français, sera certainement très apprécié par les étudiants et par les enseignants car, bien fait, il répond à une attente de tous less analystes.

Toutes les méthodes et techniques instrumentales sont présentées de manière attrayante. Après un rappel des principes et des fondements l'auteur a largement utilisé des schémas clairs qui aident beaucoup à la lecture et à la compréhension. On remarquera que ce livre répond pour chaque technique à la question: "oui, mais comment?". En effet la forme de l'échantillon aussi bien que son mode d'introduction sont décrits comme pour rappeler que la Chimie Analytique est d'abord une science expérimentale.

Les huit premiers chapitres, consacrés à la chromatographie et à ses derniers développements, se terminent par l'electrophorèse capillaire et son couplage avec la spectrométrie de masse. Les méthodes spectrales sont également très complètes et par exemple la correction de bruit de fond par effet Zeeman en spectrométrie d'absorption atomique est expliquée. Les techniques radiochimiques ne sont pas oubliées et on appréciera que le dosage Karl Fischer ou la préparation des échantillons fassent l'objet de chapitres. L'idée de quelques "hors textes" consacrés au contrôles de l'environnement et antidopage, ainsi qu'aux Bonnes Pratiques de Laboratoire, est excellente.

M. Leroy

G.M. Crean, R. Stuck and J.A. Wollam (Eds.), *Semiconductor Materials. Analysis and Fabrication Process Control. Proceedings of Symposium D of the 1992 E-MRS Spring Conference, Strasbourg, France, June 2–5 1992*, Elsevier, Amsterdam, 1993 (ISBN 0-444-89908-1). xiv + 338 pp. Price US$ 215.50/Dfl. 345.00.

The contents, a collection of the majority of the papers and posters delivered at the above conference, are reproduced from Vol. 63 of *Applied Surface Science*. They are classified under spectroscopic ellipsometry (10 papers), SIMS (3), contamination monitoring (3), epiotic characterization techniques (4), photoreflectance of III–V materials (6), photoluminescence (PL) of photonic material systems (6), characterization of electronic properties (4), FTIR and PL of silicon material systems (6) and other topics (4), and 14 poster presentations. There is an index to the authors of the papers, and a reasonable subject index.

TrAC – Trends in Analytical Chemistry: Reference Edition. Volume 11: (1992), Elsevier, Amsterdam, 1993 (ISBN 0-444-89926-X). vi + 402 pp. Price US$ 387.50/Dfl. 620.00.

The annual Reference Edition of TrAC is an integral part of the subscription of the library edition of the journal, but is also available for individual purchase. In either instance, it discusses an amazing range of topics of current interest in analytical science, written at the level at which a competent scientist is readily informed. Capillary electrophoresis, biosensors, determination of mercury speciation, diode laser-induced fluorescence, microdialysis for on-line brain analysis, expert systems and image analysis are but a sample of the extensive contents. There is currently "raging" an argument as to the definition of analytical chemistry – one suggestion might be "those topics described in TrAC"!

R. Bruce Holman, Alan J. Cross and Michael H. Joseph (Eds.), *High Performance Liquid Chromatography in Neuroscience Research*, Wiley, Chichester, 1993 (ISBN 0-471-93813-0). xvii + 369 pp. Price £ 49.95.

This ring-bound volume begins with two short chapters on basic aspects of the theory and practice of liquid chromatography (LC). There follows a series of detailed chapters, written by different authors, on analysis by LC of amines and metabolites, amino acids, nucleotides and related compounds, inositol phosphate, proteins and peptides, and psychotropic and related drugs, all directed towards their function in the nervous system. Taken together, they show how powerful a technique LC is proving to be in elucidating the very complex processes occurring in nervous function. There is an extensive subject index.

R.J.H. Clark and R.E. Hester (Eds.), *Biomolecular Spectroscopy Part A* (*Advances in Spectroscopy*, Vol. 20), Wiley, Chichester, 1993 (ISBN 0-471-93806-8). xxi + 383 pp. Price £ 120.00.

This is the first of two volumes which describe the power of modern spectroscopic techniques in determining structure, bonding and dynamics in molecular biology. Eight chapters, written by authorities from a range of countries describe aspects of IR and Raman (including resonance and surface enhanced Raman) spectroscopies in studies of proteins, of conformational disorder, and of interactions between enzymes and substrates, and between nucleic acids and anti-tumour drugs, often in living cells. Fluorimetry and fluorine NMR are also used to probe protein structure.

B. Siefert, H.J. van de Wiel, B. Dodet and I.K. O'Neill (Eds.), *Environmental Carcinogens. Methods of Analysis and Exposure Measurement. Vol. 12, Indoor Air* (*IARC Scientific Publications*, No. 109), IARC, Lyon, 1993 (ISBN 92-832-2109-5). xii + 384 pp.

This book continues the well-known and useful series organised by the IARC, and concentrates on carcinogens and mutagens found in indoor air (i.e., that in homes and other non-industrial indoor environments). Chapters 2–6 give an excellent, detailed account of these indoor pollutants and their effect on human health. The next four chapters cover analytical sampling and measurement (including radon and its daughters), followed by two chapters on exposure assessment. The remainder of the text (225 pp.) gives 25 detailed methods for determination of a range of analytes (asbestos, formaldehyde, nicotine, metals, mutagens generally, pesticides, etc.) in indoor air, in the usual format.

Multivariate Pattern Recognition in Chemometrics, Illustrated by Case Studies

edited by **R.G. Brereton**, University of Bristol, Bristol, UK

Data Handling in Science and Technology Volume 9

Chemometrics originated from multivariate statistics in chemistry, and this field is still the core of the subject. The increasing availability of user-friendly software in the laboratory has prompted the need to optimize it safely. This work comprises material presented in courses organized from 1987-1992, aimed mainly at professionals in industry.

The book covers approaches for pattern recognition as applied, primarily, to multivariate chemical data. These include data reduction and display techniques, principal components analysis and methods for classification and clustering. Comprehensive case studies illustrate the book, including numerical examples, and extensive problems are interspersed throughout the text. The book contains extensive cross-referencing between various chapters, comparing different notations and approaches, enabling readers from different backgrounds to benefit from it and to move around chapters at will. Worked examples and exercises are given, making the volume valuable for courses.

Tutorial versions of SPECTRAMAP and SIRIUS are optionally available as a Software Supplement, at a low price, to accompany the text.

Contents:

ELSEVIER

SCIENCE PUBLISHERS

1992 xii + 326 pages

Hardbound
Price: US $ 174.50 / Dfl. 305.00
ISBN 0-444-89783-6

Paperback
Price: US $ 85.50 / Dfl. 150.00
ISBN 0-444-89784-4

5 Pack Paperback + Software Supplement
Price: US $ 428.50 / Dfl. 750.00
ISBN 0-444-89786-0

Software Supplement
Price: US $ 100.00 / Dfl. 175.00
ISBN 0-444-89785-2

TO ORDER

Contact your regular supplier or:

ELSEVIER SCIENCE PUBLISHERS
P.O. Box 211
1000 AE Amsterdam
The Netherlands

Customers in the USA & Canada:

ELSEVIER SCIENCE PUBLISHERS
Attn. Judy Weislogel
P.O. Box 945
Madison Square Station
New York, NY 10160-0757, USA

No postage will be added to prepaid book orders. US $ book prices are valid only in the USA and Canada. In all other countries the Dutch guilder (Dfl.) price is definitive. Customers in The Netherlands please add 6% BTW. In New York State please add applicable sales tax. All prices are subject to change without prior notice.

414\143\0036

Hyphenated Techniques in Supercritical Fluid Chromatography and Extraction

edited by **K. Jinno,** Toyohashi University of Technology, Toyohashi, Japan

Journal of Chromatography Library Volume 53

This is the first book to focus on the latest developments in hyphenated techniques using supercritical fluids. The advantages of SFC in hyphenation with various detection modes, such as, FTIR, MS, MPD and ICP and others are clearly featured throughout the book. Special attention is paid to coupling of SFE with GC or SFC.

In this edited volume, chapters are written by leading experts in the field. The book will be of interest to professionals in academia, as well as to those researchers working in an industrial environment, such as analytical instrumentation, pharmaceuticals, agriculture, food, petrochemicals and environmental.

Contents:

1992 x + 334 pages
Price: US $ 157.00/ Dfl. 275.00
ISBN 0-444-88794-6

ELSEVIER
SCIENCE PUBLISHERS

ORDER INFORMATION
For USA and Canada
ELSEVIER SCIENCE PUBLISHERS
Judy Weislogel
P.O. Box 945
Madison Square Station,
New York, NY 10160-0757
Tel: (212) 989 5800
Fax: (212) 633 3880

In all other countries
ELSEVIER SCIENCE PUBLISHERS
P.O. Box 211
1000 AE Amsterdam
The Netherlands
Tel: (+31-20) 5803 753
Fax: (+31-20) 5803 705

US$ prices are valid only for the USA & Canada and are subject to exchange fluctuations; in all other countries the Dutch guilder price (Dfl.), is definitive. Books are sent postfree if prepaid.

711/414\141\0001-00

PUBLICATION SCHEDULE FOR 1994

	S'93	O'93	N'93	D'93	J	F						
Analytica Chimica Acta	281/1 281/2 281/3	282/1 282/2 282/3	283/1 283/2	283/3 284/1 284/2	284/3 285/1 285/2	285/3 286/1 286/2						
Vibrational Spectroscopy		6/1			6/2							

INFORMATION FOR AUTHORS

Detailed "Instructions to Authors" for *Analytica Chimica Acta* was published in Volume 256, No. 2, pp. 373–376. Free reprints of the "Instructions to Authors" of *Analytica Chimica Acta* and *Vibrational Spectroscopy* are available from the Editors or from: Elsevier Science Publishers B.V., P.O. Box 330, 1000 AH Amsterdam, The Netherlands. Telefax: (+31-20) 5862845.

Manuscripts. The language of the journal is English. English linguistic improvement is provided as part of the normal editorial processing. Authors should submit three copies of the manuscript in clear double-spaced typing on one side of the paper only. *Vibrational Spectroscopy* also accepts papers in English only.

Abstract. All papers and reviews begin with an Abstract (50–250 words) which should comprise a factual account of the contents of the paper, with emphasis on new information.

Figures. Figures should be prepared in black waterproof drawing ink on drawing or tracing paper of the same size as that on which the manuscript is typed. One original (or sharp glossy print) and two photostat (or other) copies are required. Attention should be given to line thickness, lettering (which should be kept to a minimum) and spacing on axes of graphs, to ensure suitability for reduction in size on printing. Axes of a graph should be clearly labelled, along the axes, outside the graph itself. All figures should be numbered with Arabic numerals, and require descriptive legends which should be typed on a separate sheet of paper. Simple straight-line graphs are not acceptable, because they can readily be described in the text by means of an equation or a sentence. Claims of linearity should be supported by regression data that include slope, intercept, standard deviations of the slope and intercept, standard error and the number of data points; correlation coefficients are optional.

Photographs should be glossy prints and be as rich in contrast as possible; colour photographs cannot be accepted. Line diagrams are generally preferred to photographs of equipment.

Computer outputs for reproduction as figures must be good quality on blank paper, and should preferably be submitted as glossy prints.

Nomenclature, abbreviations and symbols. In general, the recommendations of the International Union of Pure and Applied Chemistry (IUPAC) should be followed, and attention should be given to the recommendations of the Analytical Chemistry Division in the journal *Pure and Applied Chemistry* (see also *IUPAC Compendium of Analytical Nomenclature, Definitive Rules* 1987).

References. The references should be collected at the end of the paper, numbered in the order of their appearance in the te> (*not* alphabetically) and typed on a separate sheet.

Reprints. Fifty reprints will be supplied free of charge. Additional reprints (minimum 100) can be ordered. An order form containing price quotations will be sent to the authors together with the proofs of their article.

Papers dealing with vibrational spectroscopy should be sent to: Dr J.G. Grasselli, 150 Greentree Road, Chagrin Falls, OH 44022, U.S.A. Telefax: (+1-216) 2473360 (Americas, Canada, Australia and New Zealand) or Dr J.H. van der Maas, Department of Analytical Molecule Spectrometry, Faculty of Chemistry, University of Utrecht, P.O. Box 80083, 3508 TB Utrecht, The Netherlands. Telefax: (+31-30) 518219 (all other countries).

0003-2670/93/$06.00

This issue is printed on acid-free paper.

PRINTED IN THE NETHERLANDS

Intelligent Software for Chemical Analysis

Edited by **L.M.C. Buydens** and **P.J. Schoenmakers**

Data Handling in Science and Technology Volume 13

Various emerging techniques for automating intelligent functions in the laboratory are described in this book. Explanations on how systems work are given and possible application areas are suggested. The main part of the book is devoted to providing data which will enable the reader to develop and test his own systems. The emphasis is on expert systems; however, promising developments such as self-adaptive systems, neural networks and genetic algorithms are also described.

Contents:

1. Introduction. Automation and intelligent software. Expert systems. Neural networks and genetic algorithms. Reader's guide. Concepts. Conclusions.

2. Knowledge-based Systems in Chemical Analysis (P. Schoenmakers). Computers in analytical chemistry. Sample preparation. Method selection. Method development. Instrument control and error diagnosis. Data handling and calibration. Data interpretation. Validation. Laboratory management. Concluding remarks. Concepts. Conclusions. Bibliography.

3. Developing Expert Systems (H. van Leeuwen). Introduction. Prerequisites. Knowledge acquisition. Knowledge engineering. Inferencing. Explanation facilities. The integration of separate systems. Expert-system testing validation and evaluation. Concepts. Conclusions. Bibliography.

4. Expert-System-Development Tools (L. Buydens, H. van Leeuwen, R. Wehrens). Tools for implementing expert systems. Tool selection. Knowledge-acquisition tools. Concepts. Conclusions. Bibliography. **5. Validation and Evaluation of Expert Systems for HPLC Method Development - Case Studies** (F. Maris, R. Hindriks). Introduction. Case study I: Expert systems for method selection and selectivity optimization. Case study II: System-optimization expert system. Case study III: Expert system for repeatability testing, applied for trouble-shooting in HPLC. Case study IV: Ruggedness-testing expert system. General comments on the evaluations. Concepts. Conclusions. Bibliography.

6. Self-adaptive Expert Systems (R. Wehrens). Introduction - maintaining expert systems. Self-adaptive expert systems: Methods and approaches. The refinement approach of SEEK. Examples from analytical chemistry. Concluding remarks. Concepts. Conclusions. Bibliography.

7. Inductive Expert Systems (R. Wehrens, L. Buydens). Introduction. Inductive classification by ID3. Applications of ID3 in analytical chemistry. Concluding remarks. Concepts. Conclusions. Bibliography. **8. Genetic Algorithms and Neural Networks** (G. Kateman). Introduction. Genetic algorithms. Artificial neural networks. Concepts. Conclusions. Bibliography. **9. Perspectives.** Limitations of Intelligent Software. Dealing with intelligent software. Potential of intelligent software. **Index.**

© 1993 366 pages Hardbound
Price: Dfl. 350.00 (US $ 200.00)
ISBN 0-444-89207-9

ELSEVIER
SCIENCE PUBLISHERS

ORDER INFORMATION

For USA and Canada
ELSEVIER SCIENCE PUBLISHERS
Judy Weislogel, P.O. Box 945
Madison Square Station
New York, NY 10160-0757
Fax: (212) 633 3880

In all other countries
ELSEVIER SCIENCE PUBLISHERS
P.O. Box 330
1000 AH Amsterdam
The Netherlands
Fax: (+31-20) 5862 845

US$ prices are valid only for the USA & Canada and are subject to exchange rate fluctuations; in all other countries the Dutch guilder price (Dfl.) is definitive. Customers in the European Community should add the appropriate VAT rate applicable in their country to the price(s). Books are sent postfree if prepaid.

0003-2670(19930901)281:1;1-G